Do Helium Monolayer Films Melt by Unbinding of Dislocations?

Thesis by

Jeffrey Mark Greif

In Partial Fulfillment of the Requirements

for the Degree of

Doctor of Philosophy

California Institute of Technology

Pasadena, California

1982

(Submitted November 19, 1981)

Acknowledgments

The variety of experimental and phenomenological work that led to this thesis (much of it not discussed here) spanned a longer time than most such projects, and was helped in many ways by colleagues and friends at Caltech and elsewhere. Discussions and suggestions from colleagues I have tried to cite elsewhere in the thesis. My friends, who encouraged, supported and diverted me during some of the gloomier phases of this work, and provided links to the rejuvenating powers of music and mountains, will know my gratitude in other ways.

However, special thanks are owed to my advisor, David Goodstein, from whom I learned much physics, who patiently and encouragingly bore the various reverses, periods of confusion and slow progress in this seemingly endless job, and whose scientific standards, insight and thoughtful criticism contribute to every page of this thesis in one way or another.

Finally, to my wife, Margaret Thornhill, who succored and inspired me in this work despite the many quiet, solitary evenings she was forced to endure, I give my deepest thanks for her love and patient support.

Abstract

The Kosterlitz-Thouless-Nelson-Halperin-Young theory of melting in two dimensions by unbinding of thermally excited dislocation pairs is tested against thermodynamic data on monolayer films of ^{3}He and ^{4}He on graphite. It is shown using a new analysis of the theory in the asymptotic region that a definitive test is not possible with these data because the theory is expected to be most accurate in a regime very close to the melting transition which is inaccessible to experiments that are not performed on extremely long time and length scales.

One of the two unknown parameters of the theory, that which measures the resistance to twist of the monolayer with respect to the periodic substrate, is calculated, along with the equilibrium angle, to moderate accuracy using the most recent information about the helium graphite potential from atomic scattering experiments. The other parameter, which characterizes the energy of a dislocation core, is provisionally determined by finding what values make the heat capacity of the film, computed from the theory and elastic data on the film, are consistent with experimental results.

These computations are carried out using the full renormalization group equations, crossing the transition from the solid into into the region where those equations break down, by cutting off the integration at a finite value characteristic of the size of a graphite platelet, which works until the mean distance between free dislocations decreases to approximately the size of the patch. The core parameter falls in a range considerably larger than previously estimated for classical Lennard-Jones solids and other materials. Only at large values can the dislocation heat capacity be suppressed enough not to be inconsistent with experiment.

Non-rigorous interpolation methods were developed to try to include some quantum effects in the heat capacity calculations, but these improved the agreement between the theory and the experiments only slightly.

Also appearing for the first time are extensive tables of the thermodynamic functions of ^{3}He for coverages ranging from .001 to 1 layer and temperatures from 50mK to 10K.

Contents

Chapter 1. Introduction

Melting may be the least-understood of everyday phenomena. The physicist's intuitive concept of melting as the vibration of atoms (or molecules) out of the cages formed by their neighbors when the solid is heated is as good as any theory of bulk melting that has been proposed, and yet does not provide a mechanism for a phase transition.

There is, however, a recent theory [1,2,3] of melting in two dimensions which can, in principle, be used to predict the thermodynamic and dynamic behavior of the solid and the fluid phases. In particular, it predicts that the melting transition is a critical transition which takes place when thermally excited dislocation dipoles first weaken the solid (which lowers their energy and allows more to be created at larger separations as the temperature is increased), and then unbind, allowing the material to flow under slow shear stresses.

The theory is elegant and attractive because its central idea that order is broken up by a kind of topological excitation (the dislocation) finds application in theories of other two-dimensional phase transitions, e.g. superfluids, magnetic systems, and possibly liquid crystals. Of course, it is hoped that it also may lead to an explanation of bulk three-dimensional melting, but little progress has been made in this area.

However, it is not yet established that the theory is correct. The question treated in this thesis is whether it applies to the particular experimental systems for which enough data may exist to test it, the helium monolayer films on graphite, in which the two-dimensional solid was first observed.

Crystalline order (in the sense of the existence of sharp Bragg diffraction peaks) was rigorously proven by Mermin in 1968 not to occur at any finite temperature in two dimensions,[4] owing to smearing out by low frequency vibrations, although Landau and Peierls had made this point many years earlier. However, experiments [5] with helium monolayers on Grafoil, a commercial graphite product, established that at sufficiently high density and low temperature, the heat capacity of the films was proportional to T^2, characteristic of a two-dimensional system whose low-lying excitations are phonons. Independent measurements [6] of the compressibility of the monolayers showed that transverse as well as longitudinal phonons were present and the material had a non-zero shear modulus, and hence, exhibited the most important characteristic of a solid, even though translational crystalline order might not be present. Soon after this, Bretz, *et al.* [5] found sharp, cusplike peaks in the heat capacity at constant coverage of these monolayers, peaks which were thought to mark the melting transition. Figure 1.1 shows these heat capacity peaks for ^{4}He and figure 1.2 is the data of Hering, *et al.* [8] for ^{3}He. Elgin and Goodstein[7] added overlapping adsorption isotherms and heat capacity measurements to the earlier data on ^{4}He. They showed how the combined results could be used to produce detailed thermodynamic tables for the film and to disentangle the contributions to the heat capacity and other thermodynamic quantities owing to such deviations from ideal 2-D behavior as promotion into a second adsorbed layer and desorption into the bulk gas in equilibrium with the monolayer films. Similar analysis has been performed on ^{3}He.[9]

The elastic properties of the solid were shown by Stewart[10] to be similar to the properties of bulk helium solids at the same interatomic spacing, and the heat capacity peak temperatures were likewise comparable to bulk melting temperatures. The solid is known to be incommensurate with the substrate from

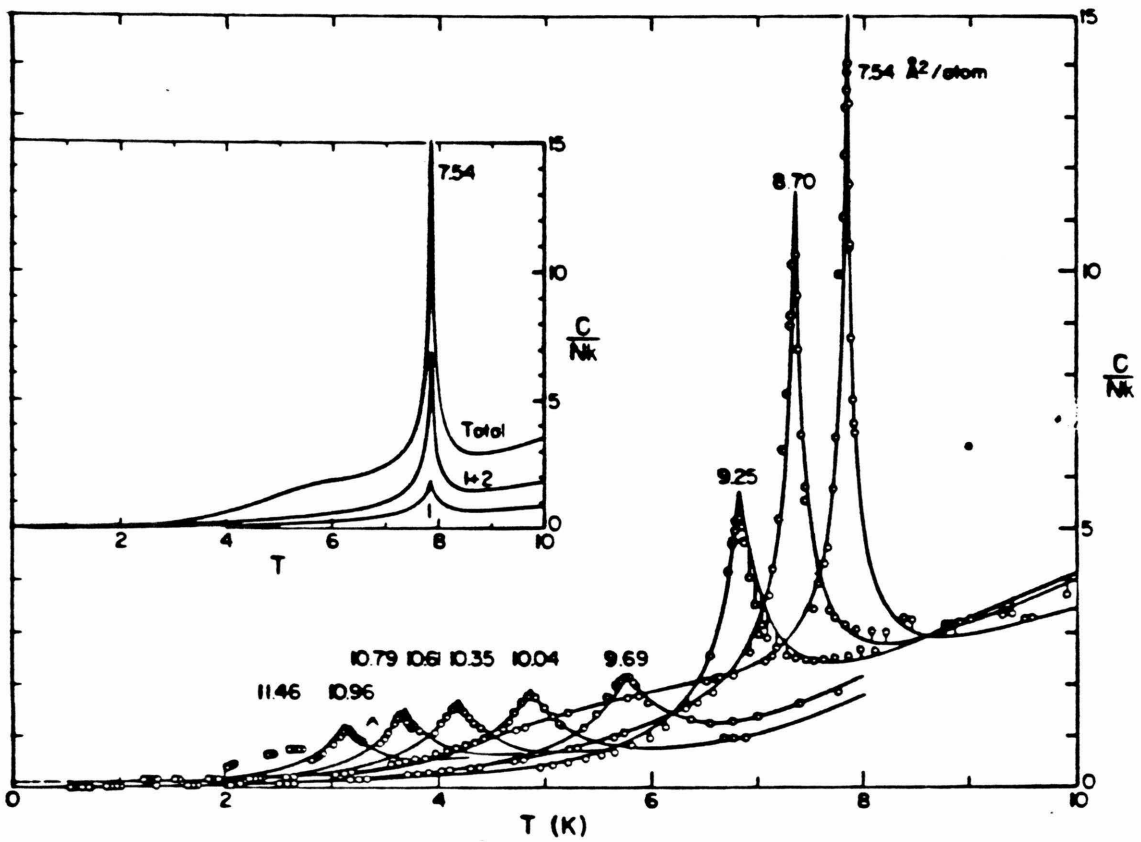

Figure 1.1. Heat capacity of ^{4}He films at several densities for which the films are solid at low temperature. Reprinted from Elgin and Goodstein.[7]

Figure 1.2. Heat capacity of ^{3}He films which are solid at low temperature. Reprinted from Hering, *et. al.*[8]

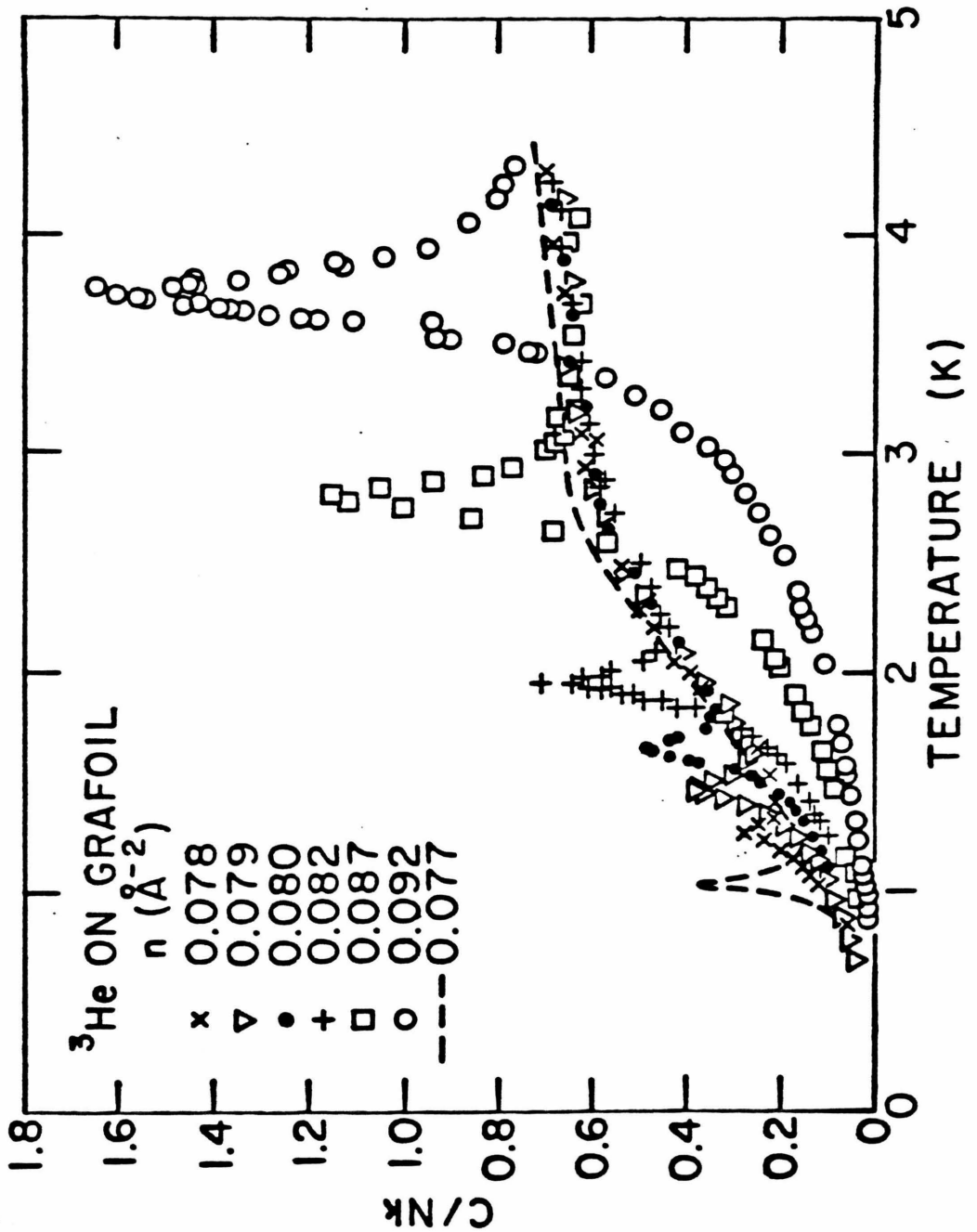

neutron scattering measurements of the lattice parameter.

This experimental work makes the helium monolayers the best-characterized of all 2-D systems; nonetheless, the task of verifying the predictions of the theory for these films is extremely difficult, for several reasons.

The most easily extracted predictions of the theory are of the behavior of equilibrium and non-equilibrium properties of the system in the asymptotic critical region around the phase transition. These predictions are, in summary, that no quantity measurable by thermodynamic techniques exhibits singular behavior at the phase transition, except of the type of the infinitely smooth essential singularity of the form $1+be^{|t|^{-\nu}}$ where t is reduced temperature and ν is positive. That means the critical behavior is undetectable in these experiments and, in addition, that the transition cannot even be found, because the transition temperature depends upon two parameters which can only be estimated for helium films. These parameters are the dislocation core energy, which measures the energy of the strongly distorted central region of a dislocation and acts as a kind of chemical potential governing the average density of dislocations, and the strength of the restoring torque opposing twist of the substrate with respect to the film arising from the effect of the periodic lateral variation of the substrate-adatom potential.

Thus, thermodynamic measurements, which have been used in the past to map out phase diagrams of 2D and 3D systems, and without which very few dynamical measurements can be correctly interpreted, cannot be used to locate phase transitions in several of the most important and interesting 2D cases, if the theory is correct. Furthermore, if phase boundaries (such as that deduced from the heat capacity peaks, and displayed in figure 2.2) are found, the theory tells us they must be other transitions than melting, superfluid-normal, or ferromagnetic-paramagnetic.

Since the thermodynamic experiments can give little or no information about the phase transition itself, the major effort of this thesis was to extend the theory to give useful comparisons with experiment away from the critical region, at temperatures below and above melting. Those efforts have been along several lines.

First, some success has been achieved in determining a parameter characterizing the strength of the distortions of the helium lattice by the underlying periodic potential of the substrate. This parameter, called γ, can be calculated only as a function of the distance from the substrate to the helium overlayer, which is not known precisely enough to give accurate answers, but we are able to use recent neutron scattering results to determine that it is usually too small to affect other calculations significantly.

The corrections to the elastic theory of a triangular lattice in the presence of finite equilibrium pressure and substrate interactions have been worked out, including their effect on the dislocations which break up the solid.

The effect of dislocations in softening the elastic response of the crystal and has been calculated directly from the theory and also from non-rigorous techniques designed to take into account quantum mechanical effects.

For future experimental studies, we have derived more rigorously than had previously been done the characteristic critical behavior above the melting transition. The method reveals that the region over which the asymptotic formulae are accurate approximations to the actual behavior of the system. has never been probed in an experiment, nor it is likely to be with currently used techniques.

The succeeding chapters develop these themes in more detail. Chapter II briefly surveys the experiments on 2-D melting and the information gleaned from them. Chapter III contains the theory of helium monolayers treated as

compressed elastic continua subject to a 2-D periodic external potential. Chapter IV reviews the renomalization group calculation of dislocation unbinding, discusses the problems of testing it, and displays calculations of the effect of this mechanism on the heat capacity of the films above and below the transition. Chapter V is a calculation of the substrate effects on the elastic properties of the films and a speculation on the origin of the heat capacity peaks. Chapter VI discusses the behavior of the theory in the critical region and the extent of that region.

References

1. J. M. Kosterlitz and D. J. Thouless, *J. Phys.* **C6**, 1181(1973).
2. D. R. Nelson and B. I. Halperin, *Phys. Rev.* **B19**, 2457(1979).
3. A. P. Young, *Phys. Rev.* **B19**, 1855(1979).
4. N. Mermin, *Phys. Rev.* **176**, 250(1968).
5. M. Bretz, J. G. Dash, D. C. Hickernell, E. O. McLean, and O. E. Vilches, *Phys. Rev.* **A8**, 1589(1973).
6. G. A. Stewart, S. Siegel, and D. L. Goodstein, in *Proceedings of the 13th International Conference on Low Temperature Physics, Boulder, Colorado, 1972*, (Plenum, New York,).
7. R. L. Elgin and D. L. Goodstein, *Phys. Rev.* **A9**, 2657(1974).
8. S. V. Hering, S. W. van Sciver, and O. E. Vilches, *J. Low Temp. Phys.* **25**, 793(1976).
9. R.L. Elgin, J.M. Greif and D. L. Goodstein, unpublished; see appendix A.
10. G. A. Stewart, *Phys. Rev.* **A10**, 671(1974).

Chapter 2

Experimental Data on 2-D Melting

1. Overview of Available Information

The study of 2-D behavior in physisorbed monolayers has come of age since 1969, when Thomy and Duval [1] discovered phase transitions in submonolayer rare gas films on exfoliated graphite which seemed little influenced by substrate inhomogeneity. Soon after, Grafoil [2] was found by Bretz[3] to have a surface homogeneous enough that the properties of the monolayer could be disentangled from the interaction with the substrate. The surface area of about 20 m^2/gm for Grafoil means that signals of, e.g. heat capacity, could be comfortably extracted from the background (at least at low temperature) to make accurate measurements. The fact that more than 90% of the Grafoil surface is basal-plane crystal face means that once the tighter binding sites (at platelet edges, junctions of two platelets, steps in the crystal surface, impurities, etc.) are filled up the rest of the surface appears to the adsorbed atoms as a uniform weakly corrugated surface over very large distances. The corrugation arises because the adsorbing van der Waals potential is most strongly attracting at the center of the graphite hexagons and weakest near carbon atoms.

This means that mobile phases of adsorbed atoms can be formed. At low temperatures, the mobility arises from tunneling through the corrugation barriers. These mobile phases behave (after corrections for band structure effects of the periodicity of the potential in the plane) like 2-D gases and liquids. A rich

range of solid behavior is also observed, depending upon whether or not the corrugation amplitude and period cause that energy to dominate the adsorbate-adsorbate interactions, or vice versa. Prior to this, the closest thing to a 2-D material that could be made in the laboratory was a monolayer of large organic molecules (stearates) on some immiscible liquid (e.g. water), and there the dynamics of the monolayer was strongly coupled to the dynamics of the base material.

The helium monolayers were the first and most completely studied systems on Grafoil, and will be discussed in the succeeding section and chapters. It is necessary to view that work with some knowledge of parallel research on other monolayers, using a wide variety of techniques. There is essentially only one other known substrate (made from compressed MgO smoke)[4] which has the same degree of homogeneity as the best Grafoil (there are several varieties with slightly different properties), and a somewhat smaller surface to volume ratio. Very little work has been done with it, so a summary of the results on Grafoil is essentially a summary of the most useful results in the field.

The techniques for studying phase transitions of adsorbed films can be divided into three categories based on the kind of information they provide, although there is actually considerable overlap of one technique into more than one area. The three kinds of information are thermodynamic, structural and dynamic, the first two usually pertaining to the equilibrium properties, and the last to a large class of effects both microscopic and macroscopic.

1.1. Thermodynamic Measurements

The thermodynamic experiments consist of measurements of the chemical potential of the film as a function of coverage and temperature, and the heat capacity of the film. The latter is obtained by standard calorimetric methods, with some care taken to understand and calibrate the background effects from

the calorimeter, the gas in equilibrium with the film, and the dynamic balance of adsorption, desorption (which changes the coverage as a function of temperature if a fixed amount of adsorbate is introduced into the sample chamber) and promotion of adsorbate atoms into the second and higher layers which may occur as the adsorbate approaches monolayer density at moderate temperatures. The chemical potential is equal to the value in the gas in equilibrium with the film, and is thus measured by measuring the pressure of the gas. This gas is always dilute enough that an ideal or one-term virial gas relation between pressure and chemical potential is sufficiently accurate. As is discussed in Elgin and Goodstein, [5] and in the appendix to this thesis, if heat capacity and chemical potential are each measured wherever possible in the temperature-coverage plane, and the measurements overlap in some region extending down to very low coverage, the thermodynamic functions can be found at all temperatures for which the heat capacity can be measured for the region of coverage spanned by the overlapping measurements, and at all coverages where pressure can be measured for the region of temperature spanned by the overlapping measurements, if the measurements are sufficiently dense in the plane.

For most cases, heat capacity measurements, together with the other thermodynamic functions, are the most direct way of studying phase transitions. In fact, heat capacity measurements are the most common way phase boundaries are discovered, or mapped out if they are discovered in some other measurement. The transitions are almost always marked by some sort of anomaly or singularity in the heat capacity, and the shape of these anomalies is often predicted by theories or models of the phase transition, so direct tests of the theories can be performed if the data are accurate enough. It should be noted that according to the theory of 2-D melting discussed in this thesis, the heat capacity, while showing non-ideal behavior near the transition, does not exhibit

any singularity right at the melting point.

In one-phase regions, certain shapes of the heat capacity are indicators of the type of phase present. For instance,a behavior $C=AT^2$ at low temperature with A proportional only to the bulk modulus (determined from the coverage variation of the chemical potential) indicates the phase is a liquid (since there is no shear modulus). The solid also has a T^2 heat capacity signature, but it cannot be accounted for by longitudinal sound waves alone -- there must be a non-zero shear modulus. The gas phase is marked by a high-temperature heat capacity approaching the ideal 2-D gas value for the particular substance, with quantum virial corrections that should be predictable using known interatomic or intermolecular potentials, plus possible effects from substrate-mediated interactions. It is also possible, using the thermodynamic measurements, to investigate the effects of the inhomogeneity and periodicity of the grafoil substrate on the behavior of adsorbates. For example, the registered overlayer of various gases at $\sqrt{3}$ times the graphite lattice spacing was found first in heat capacity measurements.[6] The band structure effects of substrate periodicity have an observable signature in the heat capacity of the 2-D gas at low coverage.[7] The extrapolation of the chemical potential to zero Kelvin yields the distribution of inhomogeneous adsorption sites as a function of energy.[8] Where first-order phase transitions are known to occur, the slope of the chemical potential vs. coverage in the regime of two-phase coexistence is determined by the inhomogeneities of the substrate.[9] The finite binding energy of the substrate implies that excited states of single atoms in the substrate potential exist, and the energy of these can be deduced from the heat capacity of low-density 2-D gases at high temperatures.[5]

At high temperatures and coverages, the heat capacity is affected by the desorption of atoms into the bulk gas and promotion into higher layers. Meas-

urement of the 3-D gas pressure and assumption of a virial equation of state in the second layer allows this effect to be removed in a consistent fashion.[5]

While measurements of the heat capacity near a phase boundary often accurately locate the phase transition point and help characterize it (as a first-order or critical transition, and if the latter, according to the strength of the singularity), the real power of the thermodynamic measurements in studying adsorbed films is that all of the thermodynamic equilibrium properties can be obtained if an experimenter is willing to engage in the long-term and somewhat tedious work needed to collect the necessary data, and to take considerable care in reducing that data. This sort of work results in an integrated knowledge of the behavior of the film and a large database against which to test predictions made from analysis of particularly "interesting" regions of the phase diagram. Only for helium films has this type of program been carried out.

1.2. Structural Techniques

The techniques aimed at eliciting the structure of adsorbed systems are necessarily microscopic, and usually involve scattering of some probe from the adsorbed atoms. Among the techniques so far used are neutron scattering,[10] X-ray scattering, most recently using synchrotron radiation,[11] low-energy electron scattering,[12] Mössbauer spectroscopy (limited to adsorbates containing a gamma emitter). Recently, a new technique involving a second gas species used as a two-dimensional piston to compress a solid has been developed.[13] Research applying modern surface science tools as Auger electron spectroscopy to physisorbed monolayers is just beginning.

Because scattering occurs at particular angles dependent upon lattice constant, the scattering experiments yield information mainly about adsorbed solid phases, the location of lines and satellite peaks marking lattice spacings, modulation of those spacings by substrate periodicity, coexistence of two or more

solid phases, superlattices of domains of registered material.[11] Changes of the spacings with temperature is related to structural phase transitions, and melting. The relative and absolute intensity of the lines gives information about the quantity of material in the various phases and the amount in possibly unobservable or hard-to-resolve coexisting gas or liquid phases. The line shapes provide information about the size of homogeneous regions, if the lines are not limited by instrumental resolution, and also about dynamical properties of the system (Debye-Waller factors), especially if inelastic scattering experiments can be done. The lineshapes also contain information about position correlation functions, and hence about the degree of order in the adsorbed systems.

One other recent application of neutron scattering has been, by measuring the interference of the scattering from helium and Grafoil at a particular Bragg peak of the substrate, to determine the distance of a helium monolayer from the substrate to within about 2%.[14] Since the corrugation of the potential seen by the adsorbed atoms varies strongly with that distance, this result is important for understanding the density waves in incommensurate solid films (see chapter 5) and in the transformation between registered and incommensurate phases.

It is also possible to use nuclear magnetic resonance measurements to deduce structural information when the lines are not significantly narrowed by molecular motion and not broadened by substrate-induced local magnetic field gradients, but in practice, this is nearly impossible on Grafoil.

1.3. Dynamical Techniques

Dynamical properties of the adsorbed system are elicited from all the experimental techniques mentioned so far, and additionally from some extremely revealing atomic scattering experiments. From the thermodynamic measurements, it is possible to deduce elastic properties. From scattering

lineshapes, related information is available, and in principle, inelastic neutron scattering could directly be used to measure the phonon spectrum of adsorbed materials, although current beam intensity limitations make this extremely difficult. . NMR lineshapes and intensities also lead to dynamical information, within the context of some model for the motions of the system, presumably justified by some theory or other experimental evidence. Some results of NMR experiments, with delicate interpretation, may be extremely important to understanding melting transitions. [15,16,17] The atomic scattering experiments [18] provide direct measurement of bound-state energies of single adsorbate molecules to the substrate and diffraction by different substrate corrugation components. Thus they allow the adsorbate-substrate potential to be derived in detail, including effects from the dielectric anisotropy of graphite.

Finally, under the rubric of dynamic techniques, we should mention computer experiments, done either by molecular dynamics or Monte Carlo methods, the latter being usually used to study phase transitions. Essentially, configurations of a few hundred or a few thousand atoms are chosen randomly and accepted or rejected according to a thermodynamic weighting function. Time averages over the time steps provide equilibrium or dynamical properties.

These techniques suffer from finiteness and inefficiency of computing resources. Typically, even for moderate size samples, runs "heating" the sample through a phase transition go at a rate of 10^9K/sec, which is probably far too fast to assure that the sample reaches equilibrium at any temperature along the way, especially near possible critical phase transitions at which critical slowing down may occur. Practitioners of these experiments[19] are as yet unable to determine the order of the melting transition with certainty in their systems, because it is difficult to untangle the problems of finite time intervals and relatively small samples. (This is not to say that physical experimentalists do not

have similar problems. Dash and Puff[9] argue that the helium melting transition may be a first-order phase transition smeared out by substrate inhomogeneity, in which case it cannot be caused by the dislocation unbinding mechanism alone. See also chapter 6.) The computer experiments have produced tantalizing indications that defects, particularly dislocations and combinations of them, are important constituents in these systems near melting.

The rapid improvement in computer technology and development of better schemes for parallel processing even using conventional microcomputers will undoubtedly produce new classes of computer experiments which may shed more light on phase transitions.

1.4. Experimental Systems and What is Known About Them

With this background, we will try to discuss what is known about 2-D melting in various simple adsorbates (except helium treated in the next section). The literature of experiments done with various physisorbed monolayers on Grafoil in the past 10 years or so has grown so large and has addressed so many separate problems that trying to tabulate it here would be of little use to anyone. References to most of these problems can be found in recent review articles in conference proceedings edited by Dash and Ruvalds, and by Sinha.(see references this chapter.) Dash[20] provides a book-length review. We will just mention that spin conversion of ortho- and para-hydrogen, and amongst various spin states of methane, conformational changes of non-spherical molecules (standing up or lying down) on the substrate, different forms of registered-incommensurate transitions, have all been or are being studied. Inclusion of thicker films in a survey would reveal a large body of experiments on the onset of superfluidity in helium films, which seem to give strong evidence in favor of a theory of that phenomena very similar to the theory of 2-D melting examined here. All of this work will be ignored here, and we will discuss only a modest

selection from the extant research on melting.

Most of the systems discussed here are mentioned in review articles of Nielsen, McTague and Passell, [10] and Vilches[21]

Argon has been studied by X-ray and neutron scattering, both elastic and inelastic, and there are sketchy heat capacity measurements. It forms an incommensurate solid, since it is too small to self condense at the 1/3 density.

Krypton has been studied by neutron diffraction, heat capacity measurements, X-ray scattering, and LEED and forms registered solid at 1/3 density up to monolayer completion, since it is just barely too small to choose that density for itself in the absence of a substrate lateral field. A denser solid can be made by compressing the first layer slightly with a second. Renormalization group calculations of the phase diagram of Kr assuming 3-D Lennard Jones potentials give reasonable agreement with experiment.

Xenon is too large an atom to form the registered solid and is incommensurate everywhere. It has been studied by heat capacity techniques, X-ray and neutron scattering. The triple point of solid-liquid-vapor coexistence has been observed, and produces an extremely sharp heat capacity signature.

Nitrogen has been studied by heat capacity measurements and neutron scattering. It has an incommensurate structure and a small set of data near melting has been taken.

One of the most promising candidates for experimental work is methane, because it is one of the few materials accessible by nearly all the techniques. It has been observed in several neutron scattering experiments (in the isotopic form CD_4), some rudimentary heat capacity studies, some preliminary NMR studies by this author, and infrared spectroscopy of its rotational transitions on the surface. The closely related compound CF_4 is also accessible and being studied

by some of these techniques. A detailed set of heat capacity measurements on methane is now being taken at Caltech, of the sort that have been made on both helium isotopes, and a pulsed NMR experiment is being set up to study dynamical properties near melting. It is hoped that this classical material will provide a better test of the theory than helium films do.

Neon films have had moderately detailed heat capacity studies done, and have been probed by LEED. They have a complicated collection of registered and incommensurate solid phases.

Hydrogen and mixed hydrogen isotopes have also been studied, not as systematically as some of the other systems, mainly by neutron diffraction, but at least one NMR experiment at low temperatures has been performed. Hydrogen seems to form both commensurate and incommensurate structures.

The magnetic properties of Oxygen make it an extremely interesting candidate for study, and it exhibits 3 different incommensurate phases, some of which may be magnetically ordered (antiferromagnetic). It has been studied mainly by neutron scattering.

Finally, it is possible to perform experiments on lattices of electrons crystallized into states above a liquid helium surface or helium film at very low densities, and held in place by image forces and external electrostatic potential. These are non-degenerate electrons on a smooth substrate and can be studied using various electronic and microelectronic techniques. It is also possible to properly compute the energy of dislocations and other defects in the electron solid, which gives hints as to possible values of such things as the core parameter.[22]

2. Measurements on Helium Monolayers

The thermodynamic measurements on helium monolayers have been reviewed in chapter 1 as they pertain to melting, but to orient the reader better, figure 2.1 shows a contour map of the heat capacity of ^{4}He films, and figure 2.2, the conjectured phase diagram of ^{4}He below the monolayer coverage.

At extremely low coverage, most of the adsorbed helium is frozen onto the most tightly binding sites of the substrate. Once these sites are filled, the material forms a gas whose behavior is well accounted for by a 2-D quantum virial gas moving in a periodic potential (which induces band-structure effects).

At around 2/3 layer coverage, there is a registered solid corresponding to one atom per 3 graphite hexagons, with a transition at 3K to a fluid. At nearby densities, vacancies or interstitials must form to preserve the overall registry. This costs energy, so the order is broken up at lower temperature, explaining at least qualitatively the curvature of the phase boundary. At lower coverage there seems to be a coexistence with a dilute gas, and at higher coverage, with a dense fluid. This phase boundary has not been completely mapped out, but presumably, at high coverage, runs into a poorly understood phase boundary at around 1K which connects registered phase to the low-temperature, low coverage end of what was once thought to be the melting line. These 1K heat capacity peaks, discovered by Hering, *et al.* [23] are extremely sharp, occur in both isotopes, and as yet are not explained, although they probably mark a coexistence region between registered and higher-density incommensurate solid.

The line of heat capacity peaks at higher temperature and coverage was originally identified as the melting line, but the theory may make us reconsider that conclusion, since according to the dislocation unbinding theory, the solid is unstable to formation of free dislocations at a temperature substantially below the peak temperature at any coverage. This criterion is essentially a

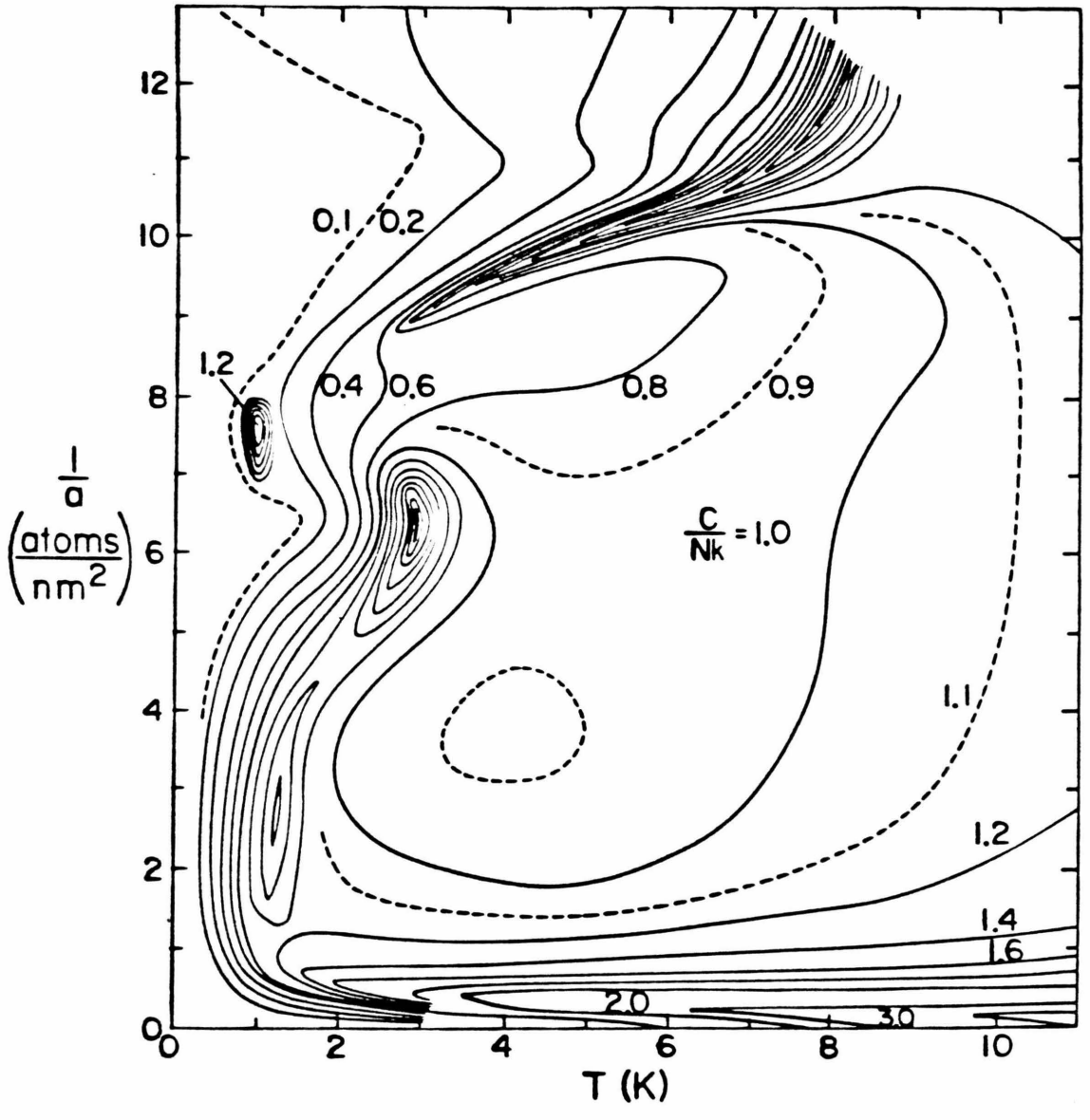

Figure 2.1 Contours of heat capacity per atom of ^{4}He as function of coverage and temperature. Adapted from Elgin and Goodstein.[5]

Figure 2.2. Phases of ^{4}He monolayers on Grafoil indicated on a heat capacity contour plot. The ^{3}He phase diagram is similar, but the line of heat capacity peaks near the monolayer runs down to lower coverage and temperature to intersect the short band of peaks near 1K, whose origin is not understood.

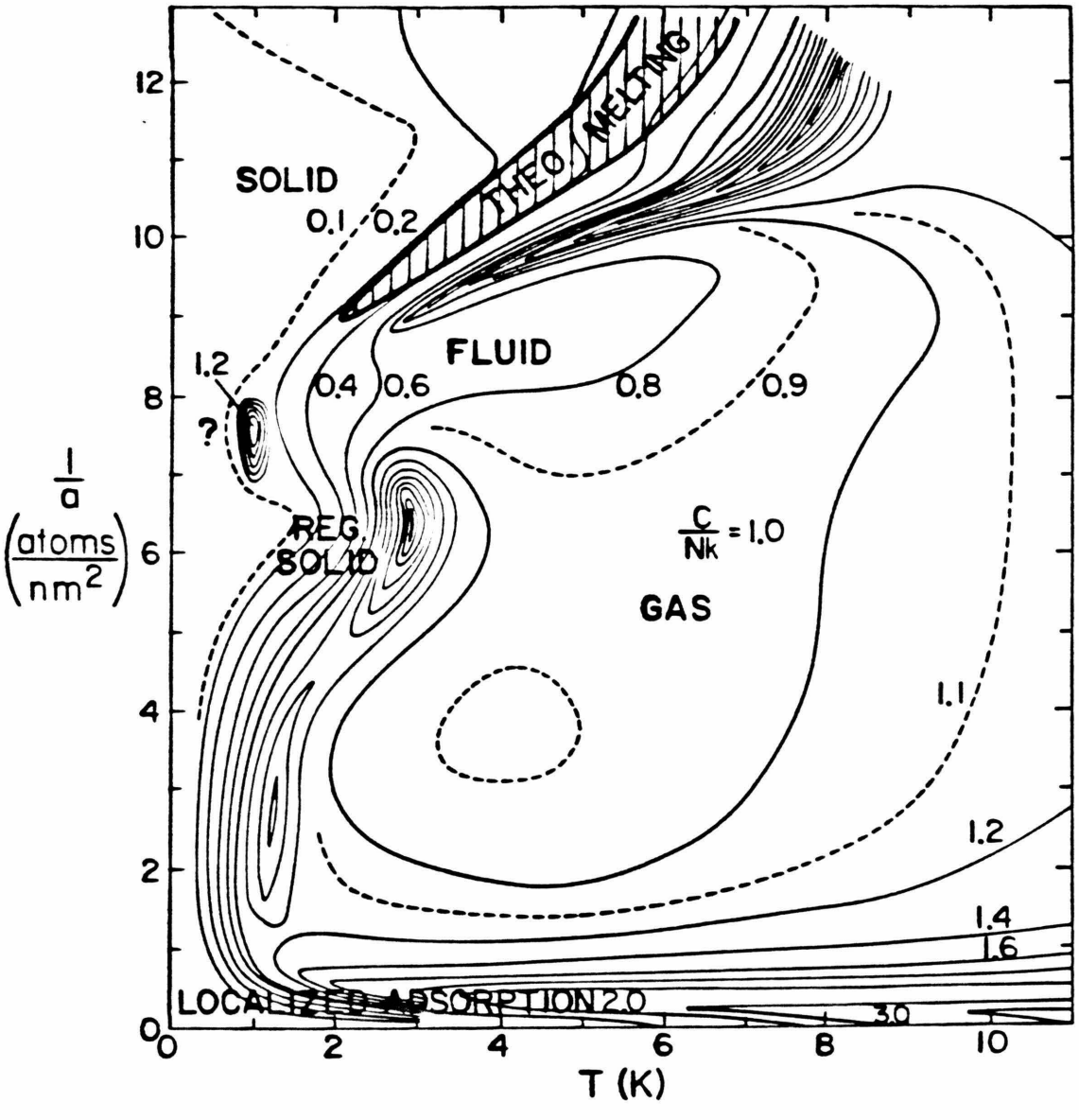

mechanical stability criterion – it does not guarantee that melting is caused by dislocation unbinding, but that in order to be observed, any other mechanism causing melting must produce a transition at a lower temperature than that predicted by the dislocation unbinding theory. Several speculations on the origin of the line of high-density heat capacity peaks are briefly presented in chapter 4.

Just below 1 monolayer, this line of peaks turns rather sharply upward, and the qualitative shape of the peaks change. At lower coverages, the peaks resemble low flat cusps, but at higher density, they appear to become much larger, narrower and steeper. Elgin and Goodstein [5] have shown that this amplification and sharpening of the peaks is explained by the effects of desorption into the bulk gas and promotion into the second layer, and the part of the heat capacity owing to the atoms still in the first layer has roughly the same shape as that at lower coverages. The slope of the line of heat capacity peaks gets steeper because, as the coverage reaches one layer and continues to increase, the atoms in the first layer can be only slightly compressed, and the second layer atoms form a 2-D gas and does not participate in the transition. Thus the temperature of the first-layer transition is roughly constant as the overall coverage changes, since the density in that layer is almost constant.

As was pointed out in the introduction, the thermodynamic measurements were able to show that a solid existed at low temperature. Unfortunately, the method of deducing this result depends upon being able to deduce the shear modulus from the Debye temperature and the compressibility, as explained in chapter 3. Since the Debye temperature characterizes the behavior of the heat capacity only at low temperature, there is no known way to extract the shear modulus from thermodynamic data at higher temperatures in precisely the region where it should be driven to zero by dislocation unbinding, if the theory is

correct. Since the theory predicts no striking singularity in the heat capacity at melting, and no pressure discontinuity, etc., it is not possible to identify the transition from these measurements. The next question is, how much further information can be gotten from dynamical and structural probes?

Helium monolayers are the most weakly bound of any, to graphite or any other substrate. This makes the usual dynamic probes like X-ray and electron scattering, which have rather high energies if they have high resolution, difficult to use on helium monolayers, because they disturb significantly or even desorb them. Neutron scattering is a usable technique, but is hindered by the low coherent scattering cross section of both the helium isotopes, and lack of high beam currents at the low momenta needed. Many interesting problems that in principle could be very profitably studied by neutron diffraction await the development of higher-intensity monochromatic slow-neutron beams, but the technique has produced some results on melting that are not fully understood.[24,14,25] Some very similar experiments using NMR on He3 [16] have also not been explained properly, since they involve properties of the system at finite frequency, and as such are a province of dynamical theories. The dynamics of dislocations are treated by Zippelius, Halperin and Nelson [26] but their work has not yet been applied to the NMR results.

The main piece of information that can be drawn from the neutron scattering results on He3 is that for coverages sufficiently below the monolayer that second-layer promotion is unimportant, in the neighborhood of the dislocation unbinding temperature (which is not known precisely), the nearest neighbor distance in the solid portion of the adsorbate decreases as the temperature is raised, so the solid must be compressed somehow even though the overall density is not changing.[24] (The liquid, if one coexists with the solid, cannot be resolved.) This can occur by converting some of the solid to a less dense fluid, or

by creating defects (point defects or dislocations) which cause imperfect spacefilling as the temperature is raised. The intensity of the line also decreases above this onset of compression, which may be a signal that fewer and fewer atoms remain solid and scatter coherently with their neighbors.

The NMR results are rather similar, although they are talked about in other language.[16] There is a change in the behavior of the spin-spin relaxation time near the predicted melting temperature, which may indicate the onset of significant diffusion in the material, and perhaps imply that it has melted. An anomaly in the spin-lattice relaxation time near the heat capacity peak temperatures is conceivably caused by the loss of orientational order that is supposed to remain above the transition, since when it disappears, the local correlations between atoms disappear and the full disorder of the liquid, with relaxation induced by collisions, markedly changes the relaxation mechanisms.

This sort of interpretation of the NMR and neutron scattering results is tentative at best.

Helium monolayers, which exhibit strong quantum effects in all thermodynamic phases, seem to be the least likely ones to quantitatively obey the predictions of a dislocation unbinding theory formulated for classical systems (although that mechanism may still govern the process). Nonetheless, it is worth making the comparison of the theory and experiment using the data on these films simply because a set of data complete enough for the necessary comparison does not exist for other substances. The effort currently underway at Caltech to obtain thermodynamic and NMR data on methane films will, it is hoped, allow more rigorous comparison with the classical theory.

References

1. A. Thomy and X. Duval, *J. Chim. Phys.* **66**, 1966(1967).

2. A commercial product manufactured by Union Carbide

3. M. Bretz, Midwinter Solid State Physics Conference, Newport Beach, CA, 1972; unpublished.

4. J. G. Dash preprint.

5. R. L. Elgin and D. L. Goodstein, *Phys. Rev.* **A9**, 2657(1974).

6. M. Bretz and J. G. Dash, *Phys. Rev. Lett.* **27**, 647(1971).

7. A. F. Silva-Moreira, J. Codona, and D. L. Goodstein, *Phys. Lett.* **76A**, 324(1980).

8. R. L. Elgin, J. M. Greif, and D. L. Goodstein, *Phys. Rev. Lett.* **41**, 1723(1978).

9. J. G. Dash and R. D. Puff, *Phys. Rev.* **B24**, 295(1981).

10. M. Nielsen, J. P. McTague, and L. Passell, in *Phase Transitions in Surface Films*, ed. J. G. Dash and J. Ruvalds, (Plenum, New York, 1980) gives a review..

11. R. J. Birgenau, E. M. Hammons, P. Heiney, P. W. Stephens, and P. M. Horn, in *Ordering in Two Dimensions*, ed. S. Sinha, (North-Holland, New York, 1980) contains a review..

12. C. G. Shaw, S. C. Fain, Jr., and M. D. Chinn, *Phys. Rev. Lett.* **41**, 955(1978).

13. M. Nielsen, J. Als-Nielsen, J. Bohr, and J. P. McTague, to be published in Physical Review B.

14. K. Carneiro, L. Passell, W. Thomlinson, and H. Taub, to be published, Physical Review B.

15. M. G. Richards, in *Phase Transitions in Surface Films*, ed. J. G. Dash and J. Ruvalds, (Plenum, New York, 1980) gives a review..

16. A. Widom, J. R. Owers-Bradley, and M. G. Richards, *Phys. Rev. Lett.* **43**, 1340(1979).

17. R. J. Rollefson, *Phys. Rev. Lett.* **29**, 410(1972).

18. M. W. Cole, D. R. Frankl, and D. L. Goodstein, *Rev. Mod. Phys.* **53**, (2)(April 1981).

19. S. Toxvaerd, *Phys. Rev.* **A24**, 2735(1981).

20. J. G. Dash, *Films on Solid Surfaces* (Academic Press, New York, 1975).

21. O. E. Vilches, in *Ordering in Two Dimensions*, ed. S. Sinha, (North-Holland, New York, 1980).

22. D. S. Fisher, in *Ordering in Two Dimensions*, ed. S. Sinha, (North-Holland, New York, 1980) and references cited therein..

23. S. V. Hering, S. W. van Sciver, and O. E. Vilches, *J. Low Temp. Phys.* **25**, 793(1976).

24. H. J. Lauter, H. Wiechert, and R. Feile, in *Ordering in Two Dimensions*, ed. S. Sinha, (North-Holland, New York, 1980).

25. L. Passell private communication.

26. A. Zippelius, B. I. Halperin, and D. R. Nelson, *Phys. Rev.* **B22**, 2514(1980).

Chapter 3.

Elastic Theory of Helium Monolayers

1. Fundamentals

In this section, the elastic theory of helium monolayers is derived by an unusual method suggested by Feynman[1] although the general technique is used in other problems.[2] The unusual derivation is designed to display explicitly the importance of quantum mechanical quantities in the classical elastic parameters.

The basic idea is to express the ground state energy of an elastically deformed system at T=0 (or the free energy at finite T) as a perturbation to that of the undistorted system. The correction terms are expectation values in the undistorted ground state at T=0 or statistical averages over the unperturbed density matrix at finite T.

The distortions considered are homogeneous deformations produced by external stresses on the boundary of the crystal. There are two contributions to the energy shift -- a change in the potential energy of the new equilibrium positions (this is the entire shift in classical elasticity) and a change in the kinetic energy and potential energy of the fluctuations (thermal and/or quantum) about those equilibrium positions. The kinetic energy is altered because the boundaries of the system are altered; however, the effect does not depend on having a solid of finite extent, since the underlying reason for the change in kinetic

energy is that the size and/or shape of the "box" localizing each atom has changed, guaranteeing a kinetic energy change by the uncertainty principle. This dependence upon shape (even if the volume is unchanged) is known to be present in the analogous case of electromagnetic zero-point fluctuations.[3]

The deformation shifts the equilibrium positions of the atoms. The method of calculating the perturbations to the energy or free energy is to find a coordinate transformation which undoes the shift of the equilibrium positions; then, the perturbations can be expressed in terms of known unperturbed averages.

The Hamiltonian of the helium atoms is, in terms of the positions and momenta of the atoms I,

$$H = \sum_I \left[p_I^2 / 2m_I + \sum_{J<I} V(\vec{r}_{IJ}) \right]. \tag{3.1}$$

A strain is applied to the crystal, such that a small mass moves from position X in the crystal to position $\underline{x}$. The components of the displacement are $u_i = \underline{x}_i - X_i$. The new positions are related to the old by $\underline{x}_i = \alpha_{ij} X_j$, where $\alpha_{ij} = \dfrac{\partial \underline{x}_i}{\partial X_j}$ and the inverse transformation $\xi_{ij} = \dfrac{\partial X_i}{\partial \underline{x}_j}$ satisfies $\alpha_{ij}\xi_{jk} = \delta_{ik}$. We use the summation convention for repeated lower case Roman indices.

Since we regard the crystal as a continuum, we can express the deformation in terms of the displacement gradients

$$u_{ij} \equiv \frac{\partial u_i}{\partial X_j} = \alpha_{ij} - \delta_{ij}. \tag{3.2}$$

Examples of deformations in 2 dimensions are pure compression or expansion,

$$\mathbf{u} = \begin{bmatrix} a & 0 \\ 0 & a \end{bmatrix} \tag{3.3a}$$

$$\boldsymbol{\alpha} = \begin{bmatrix} 1+a & 0 \\ 0 & 1+a \end{bmatrix} \tag{3.3b}$$

$$\boldsymbol{\xi} = \begin{bmatrix} \dfrac{1}{1+a} & 0 \\ 0 & \dfrac{1}{1+a} \end{bmatrix} \tag{3.3c}$$

and pure shear

$$\mathbf{u}=\begin{bmatrix} a & 0 \\ 0 & -a \end{bmatrix} \tag{3.4a}$$

$$\boldsymbol{\alpha}=\begin{bmatrix} 1+a & 0 \\ 0 & 1-a \end{bmatrix} \tag{3.4b}$$

$$\boldsymbol{\xi}=\begin{bmatrix} \dfrac{1}{1+a} & 0 \\ 0 & \dfrac{1}{1-a} \end{bmatrix}. \tag{3.4c}$$

In order to find the expectation value of the perturbed Hamiltonian in the original symmetrical ground state (at zero temperature) or the thermal average with respect to the unperturbed density matrix, the coordinates and momenta are rescaled to realign the boundaries with the original. New coordinates $\vec{x} \equiv \boldsymbol{\xi} \cdot \underline{\vec{x}}$ are defined. The momenta rescale also (since $\vec{p} \equiv \frac{\hbar}{i}\vec{\nabla}$) to $\vec{p} = \boldsymbol{\alpha} \cdot \underline{\vec{p}}$. Inserting these into the Hamiltonian gives

$$\begin{aligned} H &= \sum_I \left[\frac{(\vec{p}\cdot\boldsymbol{\xi})_I \cdot (\vec{p}\cdot\boldsymbol{\xi})_I}{2m_I} + \sum_{J<I} V(\vec{r}_{IJ}\cdot\boldsymbol{\alpha}) \right] \\ &= \sum_I \left[\frac{p_{iI}\xi_{ji}p_{kI}\xi_{jk}}{2m_I} + \sum_{J<I} V(r_{iIJ}\alpha_{ij}) \right]. \end{aligned} \tag{3.5}$$

To go further with this description of the system we temporarily concentrate on the potential energy. While it is not necessary, we make the approximation (excellent for helium) that the atoms interact by central forces. This allows the potential to be regarded as a function of r^2 and thus simplifies the expansion about the equilibrium positions. We now drop the uppercase Roman subscripts that labeled the atoms and implicitly assume that unspecified sums are over all lattice positions. Using

$$\underline{r}^2 = \underline{x}_i^2 = x_j \alpha_{ij} x_k \alpha_{ik}, \tag{3.6}$$

this becomes, to second order in the distortion parameters u_{ij},

$$\begin{aligned} V(\underline{r}^2) = V(r^2) + (\alpha_{ij}\alpha_{ik} - \delta_{jk}) x_j x_k \dot{V}(r^2) + \\ \tfrac{1}{2}(\alpha_{ij}\alpha_{ik} - \delta_{jk}) x_j x_k x_l x_m (\alpha_{il}\alpha_{im} - \delta_{lm}) \ddot{V}(r^2) \end{aligned} \tag{3.7}$$

where $\dot{f}$ indicates differentiation of f with respect to r^2. The quantity

$$\eta_{jk} \equiv \tfrac{1}{2}(\alpha_{ij}\alpha_{ik} - \delta_{jk}) = \tfrac{1}{2}(u_{ij} + u_{ji} + u_{ki}u_{kj}) \tag{3.8a}$$

is precisely the strain tensor of classical elasticity theory, measuring the increase in distance between two points when the deformation is applied according to the equation

$$|\Delta x|^2 - |\Delta X|^2 = 2\eta_{ij}\Delta X_i \Delta X_j \tag{3.8b}$$

or

$$x_i^2 = \alpha_{ij}\alpha_{ik}X_i X_k = X_k^2 + 2\eta_{ij}X_i X_j . \tag{3.8c}$$

Thus the potential in terms of strains is

$$V(\underline{r}^2) = V(r^2) + 2\eta_{jk}x_j x_k \dot{V}(r^2) + 2\eta_{jk}\eta_{lm}x_j x_k x_l x_m \ddot{V}(r^2). \tag{3.9a}$$

By inserting the expression for η_{ij} in terms of u_{ij} we can convert this equation to the form

$$V(\underline{r}^2) = V(r^2) + 2u_{jk}x_j x_k \dot{V}(r^2) + 2u_{jk}u_{lm}[x_j x_k x_l x_m \ddot{V}(r^2) + x_k x_m \delta_{jk}\dot{V}(r^2)]. \tag{3.9b}$$

A similar expansion is made of the kinetic energy in the primed momenta, using Cramer's rule to find the elements of ξ in terms of those of α, namely

$$\xi = \begin{bmatrix} \alpha_{22} & -\alpha_{12} \\ -\alpha_{21} & \alpha_{11} \end{bmatrix} / det(\alpha) , \tag{3.10}$$

Since det(α) is the Jacobian of the coordinate transformation, it is also the ratio of volumes in the two coordinate systems.

Thus, the kinetic energy becomes

$$\begin{aligned} &\textstyle\sum \vec{p}^2 / 2m + (\xi_{ji}\xi_{jk} - \delta_{ik}) \sum p_i p_k / 2m \\ &= \textstyle\sum \vec{p}^2 / 2m + ((-1)^{i+k}(2\eta_{ik} + \delta_{ik})(det(\alpha))^{-2} - \delta_{ik}) \sum p_{3-i} p_{3-k} / 2m \end{aligned} \tag{3.11}$$

where $(det(\alpha))^{-2} = 1 - 2\eta_{ll} + 4\eta_{ll}^2 - 4\det(\eta)$ to second order in u_{ij} or η_{ij}. The second equation in (3.11) and the expression for $(det(\alpha))^{-2}$ are derived from expressions in terms of u_{ij} assuming that $u_{21} = u_{12}$, which must be true in the absence of external torques on the crystal.

The Hamiltonian neatly divides into the original unperturbed Hamiltonian (in the new coordinates) plus pieces linear and quadratic in η_{ij}. Denoting the linear parts by H_{11} and the total by H_1, the perturbed ground state energy can

be expressed to second order in η_{ij} as

$$E \approx E_0 + H_1^{00} + \sum_{\text{states } n \neq 0} \frac{H_{11}^{0n} H_{11}^{n0}}{E_0 - E_n} \tag{3.12a}$$

where superscripts indicate matrix elements between unperturbed eigenstates. Similarly, the statistical perturbation expansion and minimum principle for the free energy [1] gives

$$F \leq F_0 + \langle H_1 \rangle_{H_0} + \frac{\beta}{2} \langle H_{11} \rangle_{H_0}^2 - \tfrac{1}{2} \langle \int_0^\beta e^{wH_0} H_{11} e^{-wH_0} H_{11} dw \rangle_{H_0} \tag{3.12b}$$

where the thermal averages are taken with the unperturbed density matrix and $\beta = 1/(k_B T)$. The last term of (3.12b) can be reduced to

$$-\tfrac{1}{2} e^{\beta F_0} \sum_{m \neq n} \frac{e^{-\beta E_m} - e^{-\beta E_n}}{E_n - E_m} |H_{11}^{mn}|^2 - \frac{\beta}{2} \frac{\sum_n |H_{11}^{nn}|^2 e^{-\beta E_n}}{\sum_n e^{-\beta E^n}}. \tag{3.13}$$

The quantum virial theorem can be used to express some of the first-order averages in terms of the initial external stress in the unperturbed state (a uniform pressure, P, in the case of helium). The virial theorem[3,1] states that $-\langle \sum r \partial_r V \rangle + 2 \langle \sum p^2 / 2m \rangle = 2P$ in two dimensions. Since $r \partial_r V(r) = 2r^2 \partial_{r^2} V(r^2)$ the form of the theorem used here is $\sum -r^2 \dot{V}(r^2) + \langle \sum p^2 / 2m \rangle = P$.

The format of the result is

$$E - E_0 \approx \sum \tau_{ij} \eta_{ij} + \tfrac{1}{2} \sum C_{ijkl} \eta_{ij} \eta_{kl} = \sum \tau_{ij} u_{ij} + \tfrac{1}{2} \sum A_{ijkl} u_{ij} u_{kl} \tag{3.14a}$$

where the relation between A_{ijkl} and C_{ijkl},

$$A_{ijkl} = C_{ijkl} + \tau_{jl} \delta_{ik}, \tag{3.14b}$$

is obtained by substituting equation (3.8a) for η in terms of u_{ij}. The coefficient of η_{ij} is the stress applied in the initial state ($-P\delta_{ij}$ in our case) and the term is the work done against that stress in deforming the crystal. The coefficient of $\eta_{ij}\eta_{kl}$ is the elastic constant.

To find the elastic constants, we must take the appropriate averages of in equations (3.12) and compare them with (3.14). The pieces are

$$H_{11}=2((-1)^{i+k}\eta_{ik}-\eta_{ll}\delta_{ik})\sum p_{(3-i)}p_{(3-k)}/2m+2\eta_{jk}\sum x_j x_k \dot{V}(r^2) \qquad (3.15)$$

$$H_1=H_{11}+2\eta_{ij}\eta_{kl}\sum x_i x_j x_k x_l \ddot{V}(r^2)+$$
$$4(-(-1)^{i+k}\eta_{ik}\eta_{ll}+\eta_{ll}^2\delta_{ik}-\delta_{ik}\det(\eta))\sum p_{(3-i)}p_{(3-k)}/2m. \qquad (3.16)$$

Expanding H_{11} in components we find,

$$H_{11}=-4\eta_{21}(\sum p_1 p_2/2m-\sum x_1 x_2 \ddot{V}(r^2))-2\eta_{11}(\sum p_1^2/2m- \qquad (3.17)$$
$$\sum x_1^2 \ddot{V}(r^2))-2\eta_{22}(\sum p_2^2/2m-\sum x_2^2 \ddot{V}(r^2))$$

These coefficients can be evaluated using the symmetry of the lattice. For a triangular lattice, the atoms are centers of symmetry and the ground state has sixfold rotation symmetry and 2 perpendicular reflection lines. Thus, averages over the unperturbed ground state of the form $\langle x^m y^n f(r)\rangle$ and $\langle p_x^m p_y^n g(p)\rangle$ can be related to isotropic averages $\langle r^{m+n} f(r)\rangle$ and $\langle p^{m+n} g(p)\rangle$ for all positive values of m and n with $m+n\leq 6$.

The relevant angular averages are given by

$$\langle x^m y^n f(r)\rangle=\langle p_x^m p_y^n g(p)\rangle=0, \qquad (3.18a)$$

for odd values of m or n,

$$\langle x^2 f(r)\rangle=\langle y^2 f(r)\rangle=\tfrac{1}{2}\langle r^2 f(r)\rangle, \qquad (3.18b)$$

$$\langle x^2 y^2 f(r)\rangle=\tfrac{1}{4}\langle r^2\sin^2(2\vartheta) f(r)\rangle=\frac{1}{8}\langle r^4 f(r)\rangle \qquad (3.18c)$$

$$\langle x^4 f(r)\rangle=\langle y^4 f(r)\rangle=\frac{3}{8}\langle r^4 f(r)\rangle, \qquad (3.18d)$$

and similarly for functions of p. These can be easily checked by considering these quantities for the 6 nearest neighbors of a particular atom.

Equations (3.18) and (3.16), together with the quantum virial theorem, yield the necessary quantum averages.

$$\langle H_{11}\rangle=-P\eta_{ll} \qquad (3.19)$$

$$\langle H_1\rangle=-P\eta_{ll}+2(\eta_{ll}^2-2\det(\eta))\langle\sum p^2/2m\rangle+$$
$$2\eta_{ij}\eta_{kl}(\frac{1}{8}\delta_{ij}\delta_{kl}(1-\delta_{ik})+\frac{3}{8}\delta_{ij}\delta_{kl}\delta_{ik}+(\delta_{ik}\delta_{jl}+\delta_{il}\delta_{jk})(1-\delta_{ij}))\langle\sum r^4 \ddot{V}(r^2)\rangle \qquad (3.20)$$

A slightly more elaborate version of these arguments has been suggested by Feynman to deal with the second order perturbations with H_{11}. It makes use of

the fact that while the eigenstates of the system may not have the full symmetry of the ground state, each excited state is a member of a submanifold of states with the same energy which can be obtained from one another by the symmetry operations (rotations and reflections) of the crystal.

For any such submanifold n with states $|i_n>$, a symmetry operation $\hat{R}$ produces a mixture in the submanifold,

$$\hat{R}\,|i_n>=M_{ij}\,|j_n> \tag{3.21a}$$

while the ground state clearly obeys

$$\hat{R}\,|0>=|0>. \tag{3.21b}$$

The sum over the submanifold of any functions of position and momentum can be shown to be invariant under a symmetry operation of the crystal first by proving that the matrix elements taken between the rotated states sum to the unrotated value (using 3.21a,b and the unitary nature of M), and then the general rule that

$$<\hat{R}i_n\,|\,\hat{Z}\,|\,\hat{R}^{-1}0>=<i_n\,|\,\hat{R}\hat{Z}\hat{R}^{-1}\,|\,0> \tag{3.22}$$

for any unitary or orthogonal $\hat{R}$. Thus,

$$\sum_{n,i}\frac{<0|\hat{R}\hat{Z}_1\hat{R}^{-1}|i_n><i_n|\hat{R}\hat{Z}_2\hat{R}^{-1}|0>}{E_0-E_n}=\sum_{n,i}\frac{<0|\hat{Z}_1|i_n><i_n|\hat{Z}_2|0>}{E_0-E_n}. \tag{3.23}$$

Considering $x\to -x$ or $y\to -y$ reflections, it is clear that for Z_1, Z_2 of the form $x^k y^l f(r)$ or $p_x^m p_y^n g(p)$ that the second order perturbation sum will vanish if $k+m$ or $l+n$ is odd, and that other combinations of powers will behave as those of the ground state averages discussed earlier. For example, defining $Q_{ij}^{n0}\equiv<n\,|\sum x_i x_j\,\dot{V}(r^2)-\sum\frac{p_i p_j}{2m}|0>$ we have the result

$$Q_{11}^{n0}Q_{11}^{n0}=Q_{22}^{n0}Q_{22}^{n0}=3Q_{11}^{n0}Q_{22}^{n0} \tag{3.24}$$

Since

$$\sum_n \frac{H_{11}^{0n}H_{11}^{n0}}{E_0-E_n}=4\sum_n(E_0-E_n)^{-1}\times$$
$$[\eta_{11}^2 Q_{11}^{0n}Q_{11}^{n0}+\eta_{22}^2 Q_{22}^{0n}Q_{22}^{n0}+\eta_{11}\eta_{22}(Q_{11}^{0n}Q_{22}^{n0}+c.c.)+$$
$$4\eta_{12}^2|Q_{12}^{0n}|^2+2\eta_{11}\eta_{12}(Q_{12}^{n0}Q_{11}^{0n}+c.c.)+2\eta_{22}\eta_{12}(Q_{12}^{n0}Q_{22}^{0n}+c.c.)] \quad (3.25)$$

we can evaluate all the terms in equation (3.12a). The last two terms, which mix diagonal and off-diagonal elements of η must vanish in the sum. By comparing the coefficients of η_{ij} and $\eta_{ij}\eta_{kl}$ in equation (3.12a) with equations (3.20) and (3.25) inserted, with those of equation (3.14), we find

$$\tau_{ij}=-P\delta_{ij} \quad (3.26a)$$

and

$$C_{1112}=C_{1222}=0 \quad (3.26b)$$

as expected, but the classical results

$$C_{1111}=C_{2222}=3C_{1122}=3C_{1212} \ \textit{wrong in QM} \quad (3.26c)$$

become

$$C_{1111}=\frac{3}{4}<\sum r^4\ddot{V}(r^2)>+2<K.E.>+\frac{3}{2}Q \quad (3.27a)$$
$$C_{1122}=C_{2211}=\tfrac{1}{4}<\sum r^4\ddot{V}(r^2)>+\tfrac{1}{2}Q \quad (3.27b)$$
$$C_{1212}=C_{2121}=C_{1221}=C_{2112}$$
$$=\tfrac{1}{4}<\sum r^4\ddot{V}(r^2)>+<K.E.>+\tfrac{1}{2}Q \quad (3.27c)$$

where

$$Q\equiv\sum_n \frac{|<n|-\sum p^2/2m+\sum r^2\dot{V}(r^2)|0>|^2}{E_0-E_n} \quad (3.28)$$

where the kinetic energy, $<K.E.>=<\sum p^2/2m>$. Using the conventional definition of the shear and bulk moduli, μ and B, we have

$$C_{1111}=B+\mu \quad (3.29a)$$
$$C_{1122}=B-\mu \quad (3.29b)$$
$$C_{1212}=\mu \quad (3.29c)$$

and

$$B-2\mu=C_{1111}-3C_{1212}=-<K.E.>. \quad (3.30)$$

In classical elasticity theory, only the terms involving the second deriva-

tives of the potential appearing in equation (3.16) appear in the final answers for the elastic constants, and for situations like the helium lattice, where the atoms interact by central forces and are located at centers of symmetry, the equation (3.30) is called a Cauchy relation ($B_{classical}=2\mu_{classical}$). We see that in the quantum mechanical case, the symmetry of the problem is slightly altered by the presence of the zero-point motions.

Table 5.3 shows the elastic properties of the helium films in the solid range for both isotopes. The kinetic energy can in principle be estimated from the difference between B and 2μ (for the periodic substrate, γ calculated in chapter 5 must also be known). Since $B>2\mu$ in the data, the Cauchy relation is violated, because the kinetic energy must be positive. Whether this arises from the presence of γ and the related external torques applied by the substrate will be discussed in a future publication.

2. Sound Waves at Long Wavelength

There is no completely satisfactory dynamical theory of solid helium in either 2 or 3D owing to two effects arising from the large zero-point motion.

1. The zero-point motion causes an expansion of the solid to an equilibrium lattice spacing beyond the inflection point on the attractive side of the He-He pair potential, which results in the potential of an atom in the solid having a hump at the equilibrium position (see figure 3.1). A classical harmonic analysis gives an absolute instability for such a crystal, making a perturbation calculation of the average behavior unfeasible. However, a bound state can be found by calculating the potential experienced by any atom averaged over the zero-point motion of its neighbors.

2. The large scale of the zero-point motion means that atoms would frequently penetrate each other's repulsive cores if their motions were not correlated so

that they stay out of each other's way. The net result is that each atom moves in an effective potential obtained by averaging in a self-consistent way over its own motions and those of its neighbors. Any theoretical approach to this problem must include correlations of the atoms over long distances in collective phonon motions and over short distances owing to the strong zero-point repulsion.

These theoretical approaches [4] are quite complex and produce results with significant inaccuracies. The phenomenological tack taken in this work allows the use of simpler models of the solid with recourse to the experimental data for parameters. In this spirit, there follows a discussion of the long-wavelength properties of phonons in the 2D helium solids and a justification of the greatly simplified approach taken here to obtain those properties.

The results obtained so far in this chapter give the response of the system to an infinitesimal infinite-wavelength distortion of the 2D crystal, to second order in the strains. The elastic coefficients obtained contain averages over the zero-point or thermal plus zero-point motions. The next task is to extend them painlessly to long but not infinite wavelength.

The easiest way to do this is by analogy to standard calculations of classical elastic theory, in which the thermal and zero-point motions are ignored and the response to a sinusoidal force on the boundary, or the normal modes of the system with the distorted equilibrium positions regarded as the dynamical variable, are found.

In our case, we argue that the long-wavelength sound waves of the system have very low frequencies. Time-averaging the atomic motions on scales short compared to the period of the wave investigated, but long compared to the periods of high-frequency zero-point or thermal oscillations, reveals that these time-averaged motions are nearly identical over long distances (look like nearly homogeneous deformations), that the solid locally can be considered to be in

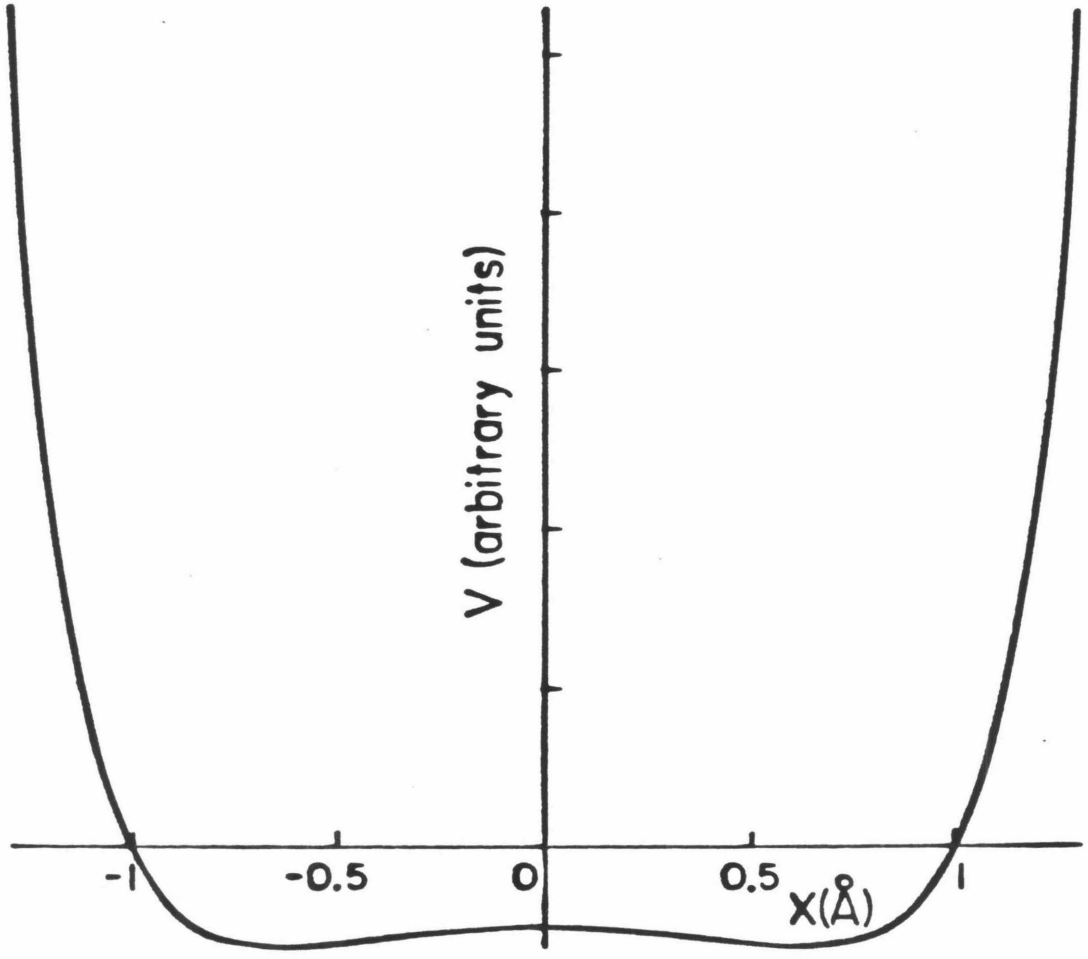

Figure 3.1. The potential near a lattice site on a linear chain of atoms interacting with a Lennard-Jones potential with hard core parameter σ=2.56Å and a lattice spacing of 3.54Å. These are characteristic parameters for helium solids. Correlated zero-point motions smear out the hump at the lattice site.

equilibrium with a distortion given by the slowly-varying time-averaged motion, and that the restoring forces for the waves are given by the infinite wavelength elastic constants obtained earlier, at least within an approximation that becomes increasingly good as the wavelength approaches infinity.

Thus we can, just as in the classical calculation, regard the elastic coefficients (in reality containing averages of the dynamical quantities) as constant and treat the time-averaged distortions as dynamical variables. The improvement here is that the classical calculation uses the values of the potential at the equilibrium positions (which gives imaginary frequencies for helium), while the present calculation uses a quantum or thermal average potential containing some effects of the fluctuations.

Using this procedure it is easy to find the wave speeds, which we expect to be independent of wavelength for long-wavelengths. Because the triangular lattice has the same long-wavelength elastic properties as an isotropic continuum (as we show below), the two sound polarizations are true longitudinal and transverse waves in any direction of propagation.

The Lagrangian density for the displacements averaged over short times can be written $\mathbf{L}=\frac{1}{2}\rho\dot{u}_i^2-\Phi(u_i)$, where Φ is the total potential energy. The equation of motion for the system is thus

$$\rho\ddot{u}_i=\frac{\partial}{\partial X_k}\frac{\partial\Phi}{\partial\partial u_i/\partial X_k}=\frac{\partial}{\partial X_k}\frac{\partial\Phi}{\partial u_{ik}}. \tag{3.31}$$

As expected, no $\partial\mathbf{L}/\partial u_i$ terms appear because only the relative displacements are important. For the potential appearing in these equations, we use the right hand side of (3.14), which is the potential of the slow distortion, and gives

$$\begin{aligned}\rho\ddot{u}_i&=\partial_k[\tau_{ik}+\tfrac{1}{2}A_{pqrs}(u_{pq}\delta_{ri}\delta_{ks}+u_{rs}\delta_{pi}\delta_{qk})]\\&=\tfrac{1}{2}(A_{rsik}u_{rsk}+A_{ikrs}u_{rsk})\equiv\hat{A}_{ikrs}u_{rsk}\end{aligned} \tag{3.32}$$

Putting in plane wave solutions

$$\vec{u}=\vec{u}_0e^{i(\vec{q}\cdot\vec{x}-\omega t)} \tag{3.33}$$

yields

$$-\omega^2\rho u_i = -\hat{A}_{ijkl}\, q_j\, q_l\, u_k \tag{3.34}$$

and inserting values of A_{ijkl} from (3.14b) and (3.29) we find that

$$\rho\omega^2\vec{u} = (\mu - P)q^2\vec{u} + B\vec{q}\,(\vec{q}\cdot\vec{u}) \tag{3.35}$$

which is identical to the equations of motion for a classical isotropic continuum with speeds of sound

$$\rho c_t^2 = \mu - P \tag{3.36a}$$

$$\rho c_l^2 = B + \mu - P \tag{3.36b}$$

These last equations can be derived by decomposing $\vec{u}$ into components $\vec{u}_t$ and $\vec{u}_l$ transverse and parallel to $\vec{q}$. Inserting this decomposition into (3.35), making two new equations by taking scalar and cross products with $\vec{q}$, and noting that $\vec{q}\cdot\vec{u}_t = \vec{q}\times\vec{u}_l = 0$, we find

$$\rho\omega^2(\vec{q}\times\vec{u}_t) = (\mu - P)q^2(\vec{q}\times\vec{u}_t) \tag{3.37a}$$

$$\rho\omega^2(\vec{q}\cdot\vec{u}_l) = (\mu - P)q^2(\vec{q}\cdot\vec{u}_l) + Bq^2(\vec{q}\cdot\vec{u}_l) \tag{3.37b}$$

which give equations (3.36).

3. Sound Speeds on a Periodic Substrate

As we will show in more detail in chapter 4, the presence of a periodic substrate with hexagonal symmetry of the same type as the helium monolayers distorts the monolayers as the atoms try to move into the nearest substrate potential well, interacting elastically with their neighbors as they do so. Because the two lattices are incommensurate, the helium lattice can translate freely on the graphite surface without change in energy (since for every atom that is shifted into a well, another must be emerging somewhere else). The distortions induced by the substrate have the substrate periodicity and are equivalent to the displacements of the helium atoms as would be found in a snapshot of the crystal excited by a standing wave phonon of the same periodicity. The energy of the static density wave (SDW) and the degree of excitation of transverse and longitu-

dinal SDW's depends on the relative angle of orientation of the two lattices, and has a mininum at an angle calculated in chapter 5. Thus, there must be a restoring torque to suppress local deviations from that orientation, and at long-wavelengths, an additional term in the energy of the system and a new elastic constant γ also calculated in chapter 5. The zero degree energy of a distorted system can now be written (cf. equation (3.14)

$$E-E_0-\Delta E(\vartheta_{LOCK})=\sum\tau_{ij}u_{ij}+\tfrac{1}{2}\sum A_{ijkl}u_{ij}u_{kl}+\tfrac{1}{2}\sum\gamma(u_{12}-u_{21})^2 \qquad (3.38)$$

where $u_{12}-u_{21}=\varepsilon_{ij}u_{ij}=2\Delta\vartheta$.

Following through the same derivation of the sound speeds carried out in the previous section, we find the transverse sound speed raised and the longitudinal speed unchanged,

$$\rho c_t^2=B+\mu-P \qquad (3.39a)$$

$$\rho c_t^2=\mu-P+\gamma. \qquad (3.39b)$$

These equations are used extensively in the succeeding chapters.

References

1. R. P. Feynman, *Statistical Mechanics: A Set of Lectures* (W. A. Benjamin, Inc., Reading, Mass., 1972) and private communication..
2. L. D. Landau and E. M. Lifshitz, *Quantum Mechanics – Non-relativistic Theory* (Pergamon Press, New York, 1977) Third Edition.
3. L. D. Landau and E. M. Lifshitz, *Statistical Physics* (Pergamon Press, New York, 1980) Third Edition.
4. N. R. Werthamer, *Am. J. Phys.* **37**, 763(1969).

Chapter 4

Evaluation of the Heat Capacity near Melting in the Dislocation Unbinding Theory and Comparison with Experiments on Helium Monolayers.

1. Introduction

Since the information on helium films on graphite is more nearly complete than that of any other quasi-two-dimensional system, it was hoped that it could be used to definitively test the dislocation unbinding theory of 2-D melting, hereafter called the KTHNY theory.[1,2,3] Of course, even if a crucial comparison could be performed, the theory would not be verified or disproved; at best, its applicability to the particular experimental system could be determined. If the theory were found applicable, it would be surprising since it is formulated in the framework of classical elasticity theory and the helium monolayer solids exhibit strong quantum effects. Nonetheless, the helium system is probably the only one for which the experimental thermodynamic data are sufficiently good that a comparison can even be attempted.

In fact, the theory as set forth in references [1] and [2] is with high probability inapplicable to helium monolayers except possibly qualitatively, because it takes into account no quantum effects. Several important conclusions about it can nonetheless be drawn, and there is some hope of using phenomenological

techniques to extend it to quantum systems, although we have not been able to justify the techniques theoretically.

The following conclusions can be drawn from the work described in the rest of this chapter:

1 It should not be expected that the theory as formulated will apply to 2-D melting of most real systems, since it is actually only valid for materials whose melting temperature greatly exceeds the Debye temperature, that is, completely classical systems, which are rare amongst simple solids. This is not to say that the dislocation unbinding mechanism in inapplicable, but only the classical treatment of it.

2 The theory in principle can be used away from the transition, but it is really a theory only of the dislocation contribution to the various properties and thus will be a close approximation to the behavior of all the degrees of freedom of the system only where the strongly fluctuating variables which dominate the behavior are the dislocation degrees of freedom. This occurs in the region asymptotically close to the transition. Most of the quantitative theoretical predictions have focussed on this asymptotic behavior and some regrettable confusions have arisen from those predictions. One of these is that since the melting transition occurs when a single phonon mode of infinite wavelength softens to zero velocity, the transition is characterized by a essential singularity and all of the thermodynamic functions are smooth at the transition. This is correct; however, it should not be concluded that the dislocations do not cause observable changes in the thermodynamic functions. In fact, they cause the heat capacity to rise spectacularly in a small region near the transition, mirroring, qualitatively at least, the experimental curves, which deviate rather sharply from Debye-law behavior in the same temperature range. Thus, thermodynamic data may

not give useful information about the critical exponents of the phase transition, or precisely pin down the transition temperature, but they provide a lot of information about the influence of dislocations, nonetheless.

3 The theory, although it may correctly describe the phenomena above the transition, is almost impossible to use there given currently known methods of approximating it. This is the result of several factors. First, the renormalization transformation diverges from the fixed point of the Hamiltonian above the transition, and since the recursion relations of that transformation are approximate, they break down and become unphysical not too far away from the transition. The known methods of avoiding the divergence are to integrate the recursion relations to some high temperature at which they are still valid, and then use a high-temperature approximation for the behavior of a 2-D dislocation plasma. Unfortunately, the range of validity of the high-temperature approximation suggested in reference [2] does not overlap with the region of validity of the renormalization group equations. Furthermore, the importance of the dislocations in the degree of disorder of the material diminishes as the temperature rises high enough so that translational order is essentially lost. Then, if the theory is correct, there is still orientational order which is enhanced by the substrate and weakened by another type of topological singularity, the disclination, whose effects are not accounted for in the dislocation Hamiltonian or the renormalization group transformation of it. Finally, one would expect to be able to use the asymptotic critical behavior of the theory over some reasonable temperature range around the transition; however, as we show in chapter 6, that region is very small

$$t \equiv \left| \frac{T - T_m}{T_m} \right| \ll .001. \tag{4.1}$$

This causes several problems, discussed in more detail in chapter 6. First,

the transition temperature as estimated in experiments to date is known only to within a few percent, and the width of the transition region owing to substrate inhomogeneity is probably of the same order as the size of the critical region or larger. Second, the transition temperature observed in any current experiment is almost guaranteed to be much further from the transition temperature for an infinite solid than t=.001, since the theory predicts this region can only be observed in experiments on extremely large spatial and time scales.

2. Overview of the Dislocation Unbinding Theory

We begin the description of the dislocation unbinding theory of 2-D with a conceptual overview. This overview contains some oversimplifications and questionable assumptions which are dissected in detail later in the discussion. The purpose is to provide the reader enough general knowledge to see past the complications brought up later.

The theory treats the solid as a classical elastic continuum normalized to a lattice spacing a_0 with the symmetry of the actual crystal structure (the helium triangular lattice is isotropic, as was shown in chapter 3, if substrate perturbations are ignored). The solid is described by an elastic Hamiltonian, an expansion of the potential energy terminated at the second order. It is regarded as perfectly harmonic, except for the effect of the dislocations. The kinetic energy of the system in classical statistical mechanics always separates out of the partition function and is ignored in this approach, contributing $\frac{1}{2}k_B T$ per atomic momentum coordinate to the internal energy.

The atomic displacements in any configuration of the solid are then regarded as the sum of two contributions, one a static displacement from the symmetric equilibrium positions produced by the strain field of dislocations in the material, and the other the dynamical quantity whose average is zero about

these new positions, produced by thermal phonons in the material. Since the thermal or time average of the phonon displacements is zero, it is claimed that when the total displacement (or its gradient in continuum theory) is squared, the cross term between thermal and dislocation contributions vanishes on the average.

Thus the partition function for the potential energy of the system separates again into independent contributions from thermal phonons and dislocations. For a classical harmonic theory, the potential energy of the smooth phonon displacements contributes $\frac{1}{2}k_B T$ to the internal energy for each atomic coordinate, so does nothing interesting. The alert reader may already notice that somehow the system has acquired additional degrees of freedom, beyond the two momentum and position variables for each atom. This is a weakness of the theory which has not been dealt with well.

It remains to deal with the dislocation contribution (which is computed using renormalization group techniques), after a brief digression on the nature of these singular distortions of the solid.

The topological distortion of a solid called a dislocation has been studied since the 19th century. Dislocations and their role in various aspects of the behavior of solids including plastic flow, work hardening, cracking, heat transfer, etc., are discussed in several treatises.[4,5,6,7,8] While more complicated types exist in three dimensions, a dislocation in two dimensions consists of a configuration of the solid produced by introducing an extra half-line of atoms into the material and allowing it to relax to a configuration of mechanical equilibrium. Figure 4.1a and figure 4.2 show a dislocation in a square and a triangular lattice, respectively. Where the extra half-line of atoms ends, the strains from the perfect lattice are very large (in fact, in continuum theory, they become infinite at the center of the dislocation) and linear elasticity theory should not

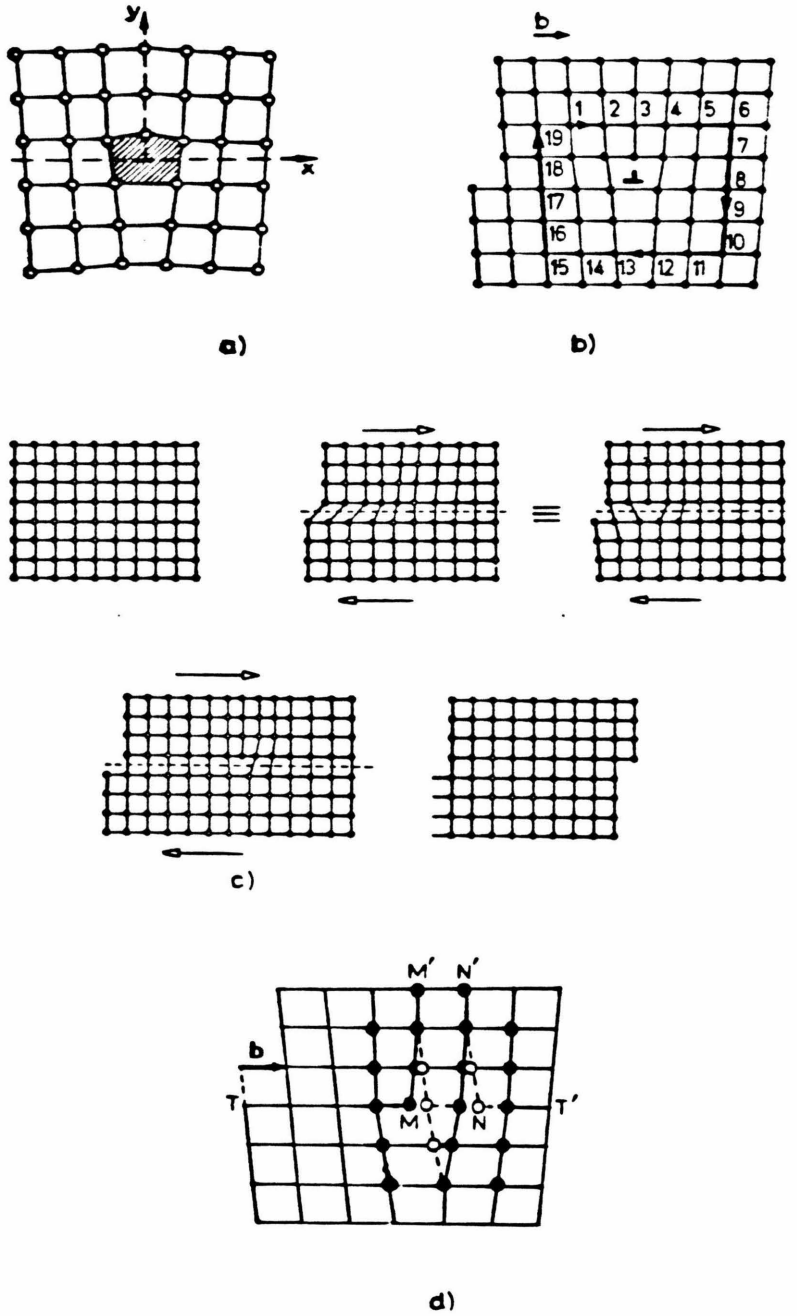

Figure 4.1. (a) A dislocation in a square lattice. (b) A path around such a dislocation fails to close by an amount equal to the Burgers' vector $\vec{b}$. (c) A dislocation moves across the crystal under shear stress. (d) The changes in position of the atoms near the extra half line as the crystal slips are all small compared to the lattice spacing.

predict correctly the energy or stresses in the material. If another half-line of atoms is inserted into the opposite half-plane parallel to the first, but which ends at any other location than the end of the first, as in figure 4.3, the solid is essentially undisturbed at large distances, and has distortions that are significant only on the scale of the distance between the dislocations. Such a configuration is called a dislocation pair or dipole because of its resemblance to a separated pair of electric charges, whose field is significant only at distances characteristic of the scale of the pair, and whose effects nearly cancel at large distances.

The topological characterization of the dislocation is based upon the fact that any closed path in the perfect solid will fail to close if it bounds a region containing a net number of dislocations (a pair of opposite dislocations counts as zero). The paths in figures 4.1 and 4.3 illustrate this principle and would be square paths in the perfect solid. The amount by which the path fails to close is a vector called the Burgers' vector $\vec{b}$ and acts like a vector charge. Its direction depends upon which direction the path is traversed, and the conventional definition is to traverse counterclockwise. The reader can easily verify by drawing paths that circle the individual dislocations in figure 4.3 (rather than the entire pair), that they have opposite Burgers' vectors with length a_0.

The relation between the dislocations and the state of the system (solid or liquid) can be understood from simple Gedanken experiments on the lattices of figures 4.1 and 4.3. If a uniform shear (hold the bottom row of atoms fixed and push the top of the crystal rightwards) is applied to crystal, the extra half-line of atoms is pushed closer to its right neighbor and if the force is increased, the crystal rearranges itself so that the next half-line to the right becomes the "extra" half-line. In effect, the dislocation has hopped one lattice spacing to the left and relieved part of the stress. Of course, if the lines connecting the atoms

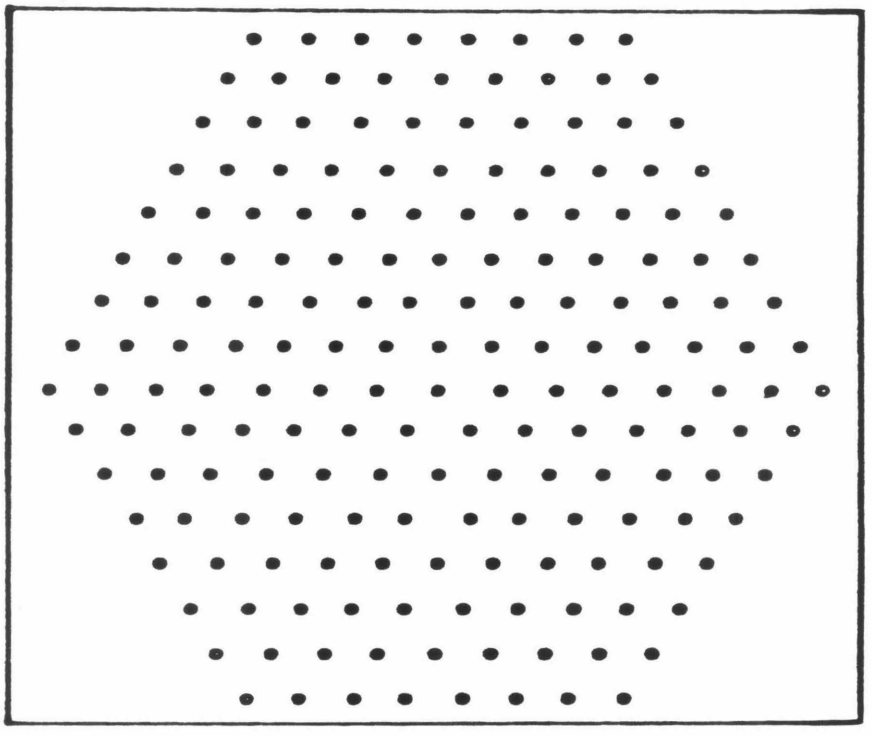

Figure 4.2. The configuration of atoms in a dislocation in a triangular lattice, as computed by Englert and Tompa.[9]

Figure 4.3. A pair of dislocations in a square lattice whose strain fields nearly cancel except in the immediate vicinity of the pair. A path around the pair closes so the net Burgers' vector is zero, while a path that includes only one of the dislocations will have a non-vanishing Burgers' vector.

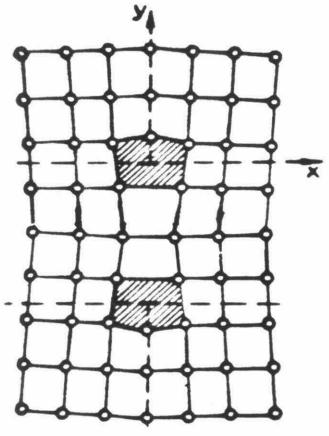

were not drawn in figure 4.1d, the effect would be more obvious, and the reconnection of the lines is only in the mind of the reader. It is also clear that the dislocation will move across the crystal to the edge if the force is continuously applied. When the force is removed, the crystal will not regain its original form, but will have a kink at the edge where the dislocation emerged. This is shown in figure 4.1c. Thus the dislocation is responsible for plastic deformation of the crystal. If there were many free dislocations in the crystal, it could not support shear stresses, and would be a liquid.

If one considers the same Gedanken experiment in the configuration of figure 4.3, it becomes clear that the members of the pair of dislocations are moved in opposite directions, each motion helping to reduce the shear stress. However, the size of the distorted region increases as they separate, and this has a large cost in elastic energy. Another way of saying this is that oppositely charged dislocations attract each other (and if they coincided, would annihilate regenerating the perfect crystal). This prevents the pair from flowing under shear stress. What motion there is is bounded, and can be regarded as the polarization and stretching of the dipole, along the direction of the Burgers vectors.

The dislocation unbinding theory attempts to explain melting in 2-D as a transition from a state in which free dislocations and hence flow under shear are not favored thermodynamically, to one in which they are. The argument can be treated in two stages, the first that led Kosterlitz and Thouless to the theory in the first place, and the second, a refinement that makes the theory a quantitative one.

A single dislocation has a strain field which decays at large distances as $1/r$ and hence, when the energy of the distortion is computed by integrating the stress ($\propto$ strain) times the strain over the crystal

$$E=\tfrac{1}{2}\int_A d^2\vec{r}\,u_{ij}\,\sigma_{ij}=\tfrac{1}{2}\int_A d^2\vec{r}\,u_{ij}\,\tilde{C}_{ijkl}\,u_{kl} \tag{4.2}$$

(where u is the displacement gradient, $\tilde{C}$ the elastic tensor and A the area of the crystal) it is $\pi K(ln(R/a_0)+C)+angular\ part$ where R measures the size of the crystal, and K is some combination of elastic constants. It is thus infinite in an infinite system. In computing the integral, a suitable cutoff must be imposed nearby the dislocation where the elastic theory breaks down. This region, of size on the order of a_0, is characterized by its own contribution, πKC, to the energy of the system and is called the dislocation core.

The free energy of the dislocation is

$$F=E-TS \tag{4.3}$$

and the entropy, S depends only upon the number of configurations containing a dislocation. In fact, it is given by

$$S=k_B\ln(A/a_0^2)=2k_B\ln(R/a_0). \tag{4.4}$$

This is also clearly infinite for an infinite 2-D solid.

However, if K varies slowly with temperature, it must be true that there is some temperature at which the sign of F becomes negative (its magnitude is always infinite in this crude picture, except at the transition), and this must be an estimate of the transition temperature. Below this temperature, the free energy of the dislocation is $+\infty$, so the probability of creating a dislocation thermally is nil. Above it, the free energy is $-\infty$ so the crystal will fill up with dislocations and lose all resistance to shear. In this crude model, the transition temperature is given by

$$T_m(crude)=\pi K/2k_B. \tag{4.5}$$

Kosterlitz and Thouless indicated a method for refining this calculation of the transition temperature, by taking into account the effects of thermally-excited dislocation pairs, and Nelson and Halperin [2] (hereinafter referred to as NH), and Young [3] developed a renormalization group technique for performing

that refinement.

The pairs, since their size is finite, have only a finite area of significantly distorted material, hence a finite energy, which turns out to be roughly $2\pi K(\ln(r/a)+C)$ for each pair, where r is the separation of the charges in the pair. Thus they are present and thermally excited at all temperatures to some degree. Of course, the assignment of dislocations to one pair or another is somewhat arbitrary (not completely) but as long as the net dislocation charge in the solid is zero, the energy must be finite. Each dislocation interacts with all the others.

The detailed behavior of the dislocation system is thus extremely complicated, even though the dislocations are assumed to be fixed on the sites of the lattice dual to the atomic mesh. The interaction energy only appears in the thermal average to favor one possible configuration over another, rather than actually causing the dislocations to move. However, it is not extremely difficult to work out the qualitative nature of the interaction between pairs, by analogy with charges. If we fix the positions of the dislocations in a large pair, and consider some smaller pair, the energy will be lowest if the Burgers' vectors of opposite sign on the two pairs are close together, which favors some orientations over others, depending upon the location of the pairs. Similarly, fixing the small pair produces favorable orientations for the large one.

In general, the presence of a small pair implies that the interaction between the members of the large pair is partially screened, so the attractive force is weakened. This effect will be treated using linear response theory in the same way it applies to charges in a dielectric.

Thus, we can explain the phase transition in the following way: At low temperature, there is a small population of thermally-excited pairs, almost all of small size. As the crystal is heated, more of these pairs are created. As the gas

of pairs becomes less dilute, interactions become important, and smaller pairs screen the larger ones, making the effective force (and effective K) between the elements of a large pair weaker. This increases the likelihood of creating larger pairs, and as the temperature increases, the process runs away. When a single dislocation pair separates to infinite distance, the elements will flow under even an infinitesimal shear force, so the system has become a liquid, which behaves like large patches of solid with free dislocations.

Another way of describing this process is to say that the K at long wavelength (which is roughly proportional to the shear modulus), is weakened by the presence of polarizable dislocation pairs, and in the infinite wavelength limit, drops to zero at the transition. Once free dislocations appear in the system, the screening becomes complete at shorter and shorter distances, the resistance to transverse shear goes to zero at shorter and shorter wavelengths.

This means that the effective elastic constants, governing the propagation of transverse phonons are weakened. The mechanism of this effect is clear -- a transverse phonon produces a shear stress that it approximately uniform on the scale of one half-wavelength, and that shear polarizes pairs smaller than a wavelength or so in size. This response of the pair implies the displacements of atoms from the shear are greater than it would be in the undistorted material, which means that the effective elastic resistance is smaller.

It is important to mention the criteria which determine the degree of order above and below the transition, but we will leave the details of the proofs to references 2 and 3. In the solid phase even at very low temperatures, it is well known that Bragg peaks in scattering experiments are not δ–functions as they are in bulk, but have a form characteristic of algebraic (that is, power law) decay of positional correlations at large distance, owing to diverging amplitudes of thermal fluctuations at long wavelengths. This is called quasi long-range

order, since the short-range order of the liquid state is characterized by exponentially decaying correlation functions. At the same time, there is long-range order in the correlations between the angles between atomic bonds at long distances. When the dislocations unbind, the positional correlations become short-range and exponentially decaying, while the angular correlations become algebraic, producing a liquid-crystal like order.

This overview of the theory will conclude with a description of the renormalization group treatment that makes the coupled-dislocation problem manageable.

The renormalization group technique [10] is an attempt to solve a complicated dynamical or statistical problem with many interacting degrees of freedom by an iterative method, in which the system is viewed at progressively larger and larger scales. Objects smaller than the current scale are grouped into composites which, if the grouping is done properly, behave like the smaller objects with different interaction coupling constants. What is done is to find a model of the problem which can be rescaled, in the following sense. (We restrict the discussion to rescaling in position-space for conceptual reasons only; the procedures all have analogues in momentum space.) The interacting degrees of freedom in some small patch of the system are averaged over to produce an effective single degree of freedom for the patch which interacts with the neighboring patches by a perhaps different law than the original microscopic degrees of freedom. If the model and the averaging region are chosen properly, the partition sum can be cast into the form of an overall factor which represents the contribution of the degrees of freedom that have been integrated out, times a partition sum identical in form to the original one but with fewer degrees of freedom and altered couplings between them (altered only in numerical value). Finding the transformation for a particular problem is the part of the program

which requires cleverness.

Now the transformation is iterated, and at each iteration, the problem is rescaled to the original lattice size. We have described the iteration as a discrete procedure, but the scale can also be changed continuously in many problems, including the one of interest here, so the change of the couplings with scale can be represented as differential equations (called renormalization group recursion relations). A trajectory of the differential equations in the space of all possible couplings (the phase space of the differential equations) represents the evolution of the equations as the scale is changed, and also is the locus of related physical problems with different sets of couplings. What this means is that, for example, a complicated interacting problem can be transformed (by moving along a trajectory) to another problem in which one or more of the couplings are weak or vanishing, and which can be solved exactly or by some approximation. The result can then be rescaled to the original problem.

This is exactly the technique that is used in the dislocation problem. Let us assume starting conditions in the solid, with a given set of bare elastic constants (those determined at 0 K where no dislocations are present). At finite temperature the presence of many interacting pairs makes the dislocation free energy essentially impossible to find directly. What is done is to notice that the parameters that determine how many and what size dislocation pairs are excited are the values of K and C. These are the couplings. If we look at all pairs smaller than some initial size, we can ignore the details of their interaction, since it affects only a small portion of the solid, except insofar as they screen larger pairs, and make the effective elastic constants on larger scales smaller. Thus if we blur our view of the solid to scales bigger than the initial size, any patch of the solid of that size is regarded as containing only the net number of dislocations enclosed in a Burgers' circuit around it. The core size and the lattice size

is raised to the size of the patch. The core energy is increased to reflect the larger area (to account for all the possible microscopic cores inside), and the coupling between the dislocation (if any) in the patch and any other patch is governed by the effective elastic constants on that scale. Then we pretend that the new patch size is actually the old patch size and rescale all the distances accordingly.

Of course, as the core energy increases at fixed temperature, fewer pairs are excited, so in every iteration, we transform the problem into a closer approach to the dilute neutral weakly-interacting gas of dislocations. Since at finite temperature, the probability of finding a pair of a given size is proportional to a Boltzmann factor of the energy, and hence proportional to r^{-K}, as we iterate the RG transformation, there are fewer and fewer pairs to blur away, so the screening effect vanishes, the effective K becomes constant, and the core energy approaches infinity.

The highest temperature for which renormalization procedure removes all the pairs from the problem is the melting temperature. Above that temperature, the dislocations have weakened the crystal enough that the members of a pair can separate to infinite distance, i.e., ionize. Thus at that scale, there is no longer resistance to shear (effective shear modulus is zero). At the same time, the effective core energy has also decreased to zero, so free dislocations tend to fill the crystal, the density increasing rapidly above the transition. When a shear is applied to the crystal, pairs are pulled apart to infinity and additional ones created until the stress is relieved.

The essence of the particular RG transformation used in this problem is that at any stage, the computational work of finding the new couplings is done by solving a simple statistical physics problem. Instead of having to treat a multitude of interacting dislocations, the partition function that is summed is that

for a single pair with size in the range from a to $a+da$. If the microscopic core energy of the system is large enough, at any stage of the iterative procedure, the dislocation gas is dilute enough so another pair of the same size is not likely to be near enough to the pair of interest to create difficulties. At each stage of the iteration, the elements of the pair of interest are actually the net dislocation charges in the renormalized cores interacting by the effective K.

In the next section, the overview presented here will be filled in somewhat and the various approximations used in the theory will be discussed.

3. The Dislocation Unbinding Theory

In this section, an attempt is made to discuss the dislocation unbinding theory of 2-D melting with emphasis on using it to compute the heat capacity predicted for the dislocations. The presentation roughly follows references 2 and 3, but rather than repeat details covered there, we try to amplify and comment upon the procedures and assumptions used.

First, the elastic Hamiltonian used in references 2 and 3 for the monolayer must be corrected (in the case of helium) for finite initial pressure without which the solid will not form. This was discussed in chapter 3. Thus the correct equation for the elastic potential energy in the harmonic approximation in the presence of finite applied pressure is

$$H=\int d\mathbf{r}^2(-\varphi u_{ii}+\tfrac{1}{2}A_{ijkl}u_{ij}u_{kl}) \tag{4.6}$$

where u_{ij} is the gradient of the i^{th} component of the displacement in the j^{th} direction, φ is the 2-D pressure. The modified elastic constants are given as in chapter 3 by

$$A_{ijkl}=C_{ijkl}-\varphi\delta_{jl}\delta_{ik} \tag{4.7}$$

with

$$C_{ijkl}=\mu(\delta_{ik}\delta_{jl}+\delta_{il}\delta_{jk}-\delta_{ij}\delta_{kl})+B\delta_{ij}\delta_{kl}+\gamma\varepsilon_{ij}\varepsilon_{kl}$$
$$=\mu(\delta_{ik}\delta_{jl}+\delta_{il}\delta_{jk})+\lambda\delta_{ij}\delta_{kl}+\gamma\varepsilon_{ij}\varepsilon_{kl} \qquad (4.8)$$

where the notation is as in chapter 3 and ε is the second rank totally antisymmetric tensor. As pointed out in chapter 3, the second order term in u_{ij} can be mapped onto the zero-pressure Hamiltonian by replacing μ by $\mu-\varphi$ in the latter result. The term linear in u_{ij} is irrelevant to thermal averages over either phonon or dislocation strains, since it averages to zero.

The dislocation energy must also be corrected for the effect of pressure, since the formation of the dislocation requires work against the pressure forces. It turns out that the energy of the dislocation given by equation (4.17) is modified in exactly the same way as the elastic Hamiltonian, namely, by the replacement $\mu\rightarrow\mu-\varphi$. This can be proved in the following way.

Wallace[11] demonstrates that a finite strain η_{ij} relative to a configuration with zero strain with initial stress τ^0_{ij} applied, produces a stress

$$\tau_{ij}=\tau^0_{ij}+B_{ijkl}\eta_{kl}+O(\eta^2) \qquad (4.9)$$

where

$$B_{ijkl}=\tfrac{1}{2}(\tau^0_{il}\delta_{jk}+\tau^0_{jl}\delta_{ik}+\tau^0_{jk}\delta_{il}+\tau^0_{ik}\delta_{jl}-2\tau^0_{ij}\delta_{kl})+C_{ijkl}. \qquad (4.10)$$

For the case where τ^0_{ij} is a pressure, this reduces to

$$B_{ijkl}=-\varphi(\delta_{il}\delta_{jk}+\delta_{ik}\delta_{jl}-\delta_{ij}\delta_{kl})+C_{ijkl}$$
$$=(\mu-\varphi)(\delta_{ik}\delta_{jl}+\delta_{il}\delta_{jk})+(\lambda+\varphi)\delta_{ij}\delta_{kl}+\gamma\varepsilon_{ij}\varepsilon_{kl} \qquad (4.11)$$

where we have used equation (4.8). Thus the stress in a configuration with a single dislocation and initial pressure is to leading order in the strains

$$\tau_{ij}=-\varphi\delta_{ij}+[(\mu-\varphi)(\delta_{ik}\delta_{jl}+\delta_{il}\delta_{jk})+(\lambda+\varphi)\delta_{ij}\delta_{kl}+\gamma\varepsilon_{ij}\varepsilon_{kl}]u_{kl} \qquad (4.12)$$

while a dislocation in an unstressed medium produces a stress

$$\tilde{\tau}_{ij}=[\tilde{\mu}(\delta_{ik}\delta_{jl}+\delta_{il}\delta_{jk})+\tilde{\lambda}\delta_{ij}\delta_{kl}+\tilde{\gamma}\varepsilon_{ij}\varepsilon_{kl}]\tilde{u}_{kl}. \qquad (4.13)$$

The equations of mechanical equilibrium are

$$\frac{\partial\tau_{ij}}{\partial x_j}=0 \qquad (4.14)$$

with boundary condition (that stress be continuous at the edge of the crystal)

$$\tau_{ij}^{\text{surface}} = \begin{cases} 0 & \text{free surface} \\ -\varphi\delta_{ij} & \text{hydrostatic pressure applied} \end{cases} \tag{4.15}$$

Thus, if we define

$$\tau_{ij} \equiv -\varphi\delta_{ij} + \bar{\tau}_{ij} \tag{4.16}$$

the boundary value problem for $\bar{\tau}_{ij}$ is identical to that for $\tilde{\tau}_{ij}$ as long as we replace $\tilde{\mu}$ by $\mu-\varphi$ and $\tilde{\lambda}$ by $\lambda+\varphi$.

Thus the energy of a dislocation is gotten from the standard solution of this boundary value problem as in references [2] and [3] with the above replacements. It is (in the notation of Young)

$$E_{dis} = \pi K^{\tau}(\ln(R/a_0 + C) \tag{4.17}$$

where the integral of the term in equation (4.6) linear in the strains over the crystal vanishes by symmetry because using Hooke's law it can be transformed into an integral over the stresses, which in polar coordinates are

$$\tau_{rr} = \tau_{\vartheta\vartheta} \propto \sin(\vartheta)/r \tag{4.18a}$$

$$\tau_{r\vartheta} \propto -\cos(\vartheta)/r \tag{4.18b}$$

This $1/r$ dependence of the stress and strain fields of the dislocation is guaranteed by the condition that any closed path around the dislocation fail to close by an amount equal to the Burgers vector,

$$\oint du_i = \oint u_{ij}\, dx_j = b_i \tag{4.19}$$

since this implies that paths with the same shape scaled up or down in size must produce the same result. Thus we can guess that the leading order behavior of the dislocation energy, the stress times the strain integrated over the crystal (excluding the core region) will be proportional to $\ln(R)$ and by a multipole-type expansion we can see that the energy of a pair will be proportional to $\ln(r)$ where R is the crystal size and r the pair separation. The full Hamiltonian in Young's notation is

$$-H_D/k_BT=2\pi\sum_{i<j}\left\{K_0^{\parallel}\vec{b}^i\cdot\vec{b}^j\ln(r^{ij}/a^0)-K_0^{\beta}\left[(\vec{b}^i\cdot\vec{r}^{ij})(\vec{b}^j\cdot\vec{r}^{ij})/(r^{ij})^2-\tfrac{1}{2}\vec{b}^i\cdot\vec{b}^j\right]\right\}+\ln y_0\sum_i(b^i)^2 \quad (4.20)$$

where $\vec{r}^{ij}=\vec{r}^i-\vec{r}^j$ the positions of dislocations at sites i and j, $\ln y_0$ is related to the core energy and acts like a fugacity for the dislocations, and the configurations of $\{\vec{b}^i\}$ are restricted to cases of total neutrality, $\sum_i\vec{b}^i=0$. The parameters $K_0^{\parallel}$ and K_0^{β} depend on the bare elastic constants (measured in the absence of dislocations at 0K),

$$K_0^{\parallel}=\frac{1}{2\pi^2}\frac{a_0^2}{k_BT}\left[\frac{\mu_0B_0}{\mu_0+B_0}+\frac{\mu_0\gamma_0}{\mu_0+\gamma_0}\right] \quad (4.21a)$$

$$K_0^{\beta}=\frac{1}{2\pi^2}\frac{a_0^2}{k_BT}\left[\frac{\mu_0B_0}{\mu_0+B_0}-\frac{\mu_0\gamma_0}{\mu_0+\gamma_0}\right] \quad (4.21b)$$

and are equal when the substrate is smooth and $\gamma_0=0$. Equation (4.21b) corrects a typographical error in reference 3.

Examination of the fugacity term in equation (4.20) reveals that since the energy is proportional to the square of the charge, charges greater than one unit are of low probability because they are unstable to the formation of several unit charges.

Since references 2 and 3 present detailed (and different) versions of the methods used to obtain the renormalization group recursion relations, for tutorial reasons we briefly sketch two methods for obtaining them for simplified problems and then describe more fully the approach of Young that leads most directly to the RG relation for the free energy, which we need to compute the heat capacity. This latter description is intended to outline the process for the reader without reproducing the evaluation of integrals and other mathematical details needed in intermediate stages.

Dielectric theory can be used to obtain the recursion relations for the simplified dislocation Hamiltonian with no angular interactions and the Burgers'

vectors treated as scalars. This Hamiltonian is equivalent to that for vortices in a 2-D superfluid and was first solved by Kosterlitz.[12] The potential of two charges in two dimensions which satisfies Poisson's equation is $-2q_1q_2\ln(r_{12}/a_0)$, so we can map the dislocation problem onto the Coulomb gas with the correspondence $\pi K_0=q^2/k_BT$. Two opposite charges at large separation r are screened by smaller dipoles, so the force $qE=2\pi K_0/r$ is reduced. Treating the smaller dipoles as a continuous medium, the reduced field E can be written in terms of the displacement field D from the two test charges of our large pair in the absence of the smaller dipoles divided by the dielectric constant of the medium $\varepsilon=1+4\pi\chi$ where χ is the susceptibility. The reduction in force increases with separation, so the relevant dielectric function is scale-dependent. This can also be subsumed into an effective scale-dependent $K(r)=K_0/\varepsilon(r)$. The susceptibility of all the dipoles with size smaller than r, $\chi(r)$ is given by

$$\chi(r)=\int_{a_0}^{r}\rho(r',\vartheta)\alpha(r')r'dr'd\vartheta \tag{4.22}$$

where $\alpha(r')$ measures the polarizability, $\frac{1}{2}\pi K_0r'^2$, of a single dipole of separation r' and $rho(r',\vartheta)$ is the density of pairs of separation r' making an angle ϑ to some arbitrary axis. This thermal density is evaluated with the partition function determined by the simplified dislocation Hamiltonian, with the interaction between the pairs modified from K_0 to $K(r')$ by the screening of even smaller pairs. The density is thus given by

$$rho(r',\vartheta)=(y_0/a_0^2)(r'/a_0)^{-2\pi V(r')} \tag{4.23}$$

to leading order in y_0, where V is the potential energy integrated from the force

$$V(r)\ln(r/a_0)\equiv K_0\int_{\ln a_0}^{\ln r}\frac{d\ln r'}{\varepsilon(r')}. \tag{4.24}$$

The self-consistent equation for $K(r)$ derived from this (letting $l=\ln(r/a_0)$) is

$$K^{-1}(l)=K_0^{-1}+4\pi^3y_0^2\int_0^l\exp\left[4l'-2\pi\int_0^{l'}K(l'')dl''\right] \tag{4.25}$$

which can be simplified by defining a scale-dependent fugacity

$$y(l)=y_0\exp\left[2l'-\pi\int_0^{l'}K(l'')dl''\right] \tag{4.26}$$

which can be used to turn equation (4.25) into the coupled differential equations of the renormalization transformation

$$\frac{dK^{-1}}{dl}=4\pi^3y^2 \tag{4.27a}$$

$$\frac{dy}{dl}=(2-\pi K)y. \tag{4.27b}$$

This same method (with some complications) can be used to treat the dislocation problem for the smooth substrate and triangular adsorbate including the angular part of the dislocation Hamiltonian and the vector nature of the "charges". The two main complications are in the angular averages, which lead to Bessel functions, and the possibility of two Burgers' vectors which are not opposite being paired with a third one opposite to the vector sum of the first two, i.e. "dipoles" with one element being a composite of two elementary Burgers vectors at 120° (the charge of such a composite is still one unit).

Nelson and Halperin approach the recursion relations by finding the perturbing effect of a single dislocation pair on the reduced elastic tensor, where reduced means that elastic constants are multiplied by a_0^2/k_BT. The inverse of that tensor is written in terms of a correlation function

$$\bar{C}^{-1}_{R,ijkl}=<U_{ij}\,U_{kl}>/Aa_0^2 \tag{4.28}$$

of a quantity U that is essentially the total strain in the crystal and is given by

$$U_{ij}=-\tfrac{1}{2}\int_P(u_in_j+u_jn_i)dl \tag{4.29}$$

where the integration is taken around the boundary of the crystal, P, with unit normal $\vec{n}$. The displacements and therefore U have contributions from the phonons and singular parts from the dislocations. Since the displacement u is discontinuous for a complete path around a dislocation, branch cuts are drawn between each dislocation and the origin and contribute the value of the

discontinuity of $\vec{u}$ $(=\vec{b})$, to the equivalent area integral derived by Green's theorem from equation (4.29),

$$U_{ij}^{sing}=\int d^2r u_{ij}^{sing}(\vec{r})+\sum_{\vec{R}}{}'\tfrac{1}{2}a_0[b_i(\vec{R})\varepsilon_{jk}R_k+b_j(\vec{R})\varepsilon_{ik}R_k] \tag{4.30}$$

In fact, the first term vanishes by symmetry (if the boundary stress is continuous), so the only contribution from the dislocations is that of the cuts. There are three kinds of pairs (for the three possible directions of Burgers' vectors on a triangular lattice) and each contributes to the correlation function with weight dependent upon the probability of it being excited, which in turn depends on the separation of its elements and the angle the Burgers' vector makes to the vector joining those elements. The contribution to the elastic constant from a single pair is thus

$$\bar{C}_{R,ijkl}^{-1}=\bar{C}_{ijkl}^{-1}+\tfrac{1}{4}y^2\sum_{p=1}^{3}(e_{p,i}\varepsilon_{js}+e_{p,j}\varepsilon_{is})(e_{p,k}\varepsilon_{jt}+e_{p,l}\varepsilon_{kt}) \tag{4.31}$$
$$\times\int_{|\vec{R}|>a}\frac{d^2RR_sR_t}{a^4}Q_p\left[\frac{R}{a}\right]^{-\pi K}+O(y^3)$$

where $\vec{e}_p$ are the unit vectors along which Burgers' vectors can point, Q_p are corresponding angular factors, and the first term on the right side of equation (4.31) is the bare inverse elastic tensor (arising from the smooth parts of U)

$$\bar{C}_{ijkl}^{-1}=\frac{1}{4\bar{\mu}}(\delta_{ik}\delta_{jl}+\delta_{il}\delta_{jk}-\delta_{ij}\delta_{kl})+\frac{1}{4\bar{B}}\delta_{ij}\delta_{kl}+\frac{1}{4\bar{\gamma}}\varepsilon_{ij}\varepsilon_{kl} \tag{4.32}$$

and the overbar indicates a reduced elastic constant.

This perturbation to the components of the reduced inverse elastic tensor begins to behave badly near the transition, suffering an infrared divergence in the integral when the temperature changes such that $\pi K_0 \to 2$. Nonetheless, by using RG methods, it is possible to use the perturbation approach without incorporating higher order terms directly. The renormalization group relations for the variation of these components of the inverse elastic tensor are then derived by breaking the integral into two parts

$$\int_a^{\infty} \frac{dR}{a} \rightarrow \left(\int_a^{ae^{\delta}} + \int_{ae^{\delta}}^{\infty}\right) \frac{dR}{a} \tag{4.33}$$

for small δ. The small R portion is absorbed into redefinitions of $\bar{\mu}$, $\bar{B}$ and K. Then the large R parts can be rescaled to range from a to ∞, creating extra factors absorbed into redefined values of y. The same considerations of composite Burgers' vectors pairing must be accounted for.

Finally, having prepared for the most complicated of the calculations, we recount Young's approach to the full dislocation problem with K_0 not necessarily equal to K_0^{ϑ}, that is, the problem of melting on a periodic substrate.

The partition function for the vector "charges" can be written as a sum over all possible configurations, parametrized by the number n_α of dislocations of each 6 kinds (along $\pm\vec{e}_p$),

$$Z = \sum_{\{n_\alpha\}} \prod_{\alpha=1}^{6} \left[\frac{1}{n_\alpha!}\right] \int \prod_{i=1}^{N} d^2\mathbf{r}^i \left[\frac{y}{a_0^2}\right]^N e^{H(\{n\})}, \tag{4.34}$$

where N is the total number of dislocations and H is the dislocation Hamiltonian (divided by $-k_B T$) without the term containing y_0 and with a fixed set of n_α. The dislocations are not allowed to get within one core spacing (a_0) of each other. The reduced Hamiltonian is put into the form

$$H(\{n\}) = 2\pi \sum_{i<j} b_p^i \varepsilon_{pq} b_r^j \varepsilon_{rs} M_{qs}(\vec{r}^{ij}) \tag{4.35}$$

where

$$M_{pq}(\vec{r}) = K^T \delta_{pq} G(r) + K^{\vartheta}(r_p r_q / r^2 - \tfrac{1}{2}\delta_{pq}) \tag{4.36}$$

and $G(r) = \ln(r/a_0)$ is the Green's function for a point charge in 2-D. We now consider a dipole (i,j) with separation between a_0 and $a_0(1+\delta l)$ for some small δl. The part of the Hamiltonian pertaining to this pair consists of the interaction of its elements, producing a contribution to the partition function

$$\exp(H_{ij}^0) = \exp(\pi K^{\vartheta} \cos 2\vartheta), \tag{4.37}$$

and the interaction of each element with all the other dislocations,

$$\overline{H}_{ij}=2\pi b_p^i \varepsilon_{pq} \sum_k [M_{qr}(\vec{r}^i-\vec{r}^k)-M_{qr}(\vec{r}^j-\vec{r}^k)]b_s^k \varepsilon_{sr}. \tag{4.38}$$

(This looks asymmetrical and is missing $\vec{b}^j$ because that vector is equal and opposite to $\vec{b}_i$.) The plan is to integrate over $\vec{r}^i$ and $\vec{r}^j$ to remove those degrees of freedom from the partition function. The integral of $\vec{r}^i$ is over the annulus of width δl and radius a_0 around $\vec{r}_j$, which is correct as long as the pairs are dilute enough that we can neglect the possibility of another pair coming within a_0 of the one in question. Then $\vec{r}_j$ is integrated over the entire crystal, except in disks of size a_0 around each of the other dislocations.

The result of this integration, after complex and tedious manipulations, is proportional to δl and can be broken into 3 terms, two of which resemble the terms of equation (4.36). These terms must therefore be the changes to the couplings K^τ and K^ϑ. The remaining term is the contribution to the free energy of all configurations containing one pair at this separation. That is, if we denote the annulus by δ_j and the disk by D_j, the integration can be written in the form

$$3\int_{D_j} d^2r_j \int_{\delta_j} d^2r_i\, e^{H_{ij}+H_{ij}^0}$$

$$=\frac{a_0^4 \delta F}{y^2}+\frac{2\pi a_0^4}{y^2}\sum_{k<l}\left[\delta K^\tau \delta_{pq} G(r^{kl})-\delta K^\vartheta\left[\frac{r_p^{kl}r_q^{kl}}{(r^{kl})^2}-\frac{\delta_{pq}}{2}\right]\right]b_p^k b_q^l \tag{4.39}$$

with each of δF, δK^τ, δK^ϑ proportional to δl. The manipulations to produce this form are messy but the results can be summarized by the differential equations

$$A^{-1}\frac{dF}{dl}=6\pi I_0(\pi K^\vartheta)y^2/a_0^2 \tag{4.40}$$

$$\frac{dK^\tau}{dl}=-6\pi^3 y^2\left\{[(K^\tau)^2+(K^\vartheta)^2]I_0(\pi K^\vartheta)-K^\tau K^\vartheta I_1(\pi K^\vartheta)\right\} \tag{4.41a}$$

$$\frac{dK^\vartheta}{dl}=-6\pi^3 y^2\left\{2K^\tau K^\vartheta I_0(\pi K^\vartheta)-\tfrac{1}{2}[(K^\tau)^2+(K^\vartheta)^2]I_1(\pi K^\vartheta)\right\} \tag{4.41b}$$

where A is the area of the system. It is important to note that equation (4.40) is *not* the recursion relation for the free energy of the system because it still contains a_0. In Young's paper, this factor is missing from equation (4.40). We have described the first iteration of the renormalization group, in which pairs of size

a_0 are integrated out; in general, the current core size $a_0 e^l$ should be used in equation (4.40).

It is possible to put equations (4.41) into a slightly simpler form by making the change of variables

$$K_L = \tfrac{1}{2}(K^r - K^\vartheta), \quad K_T = \tfrac{1}{2}(K_r + K^\vartheta) \tag{4.42}$$

which has the physical meaning of the transverse and longitudinal couplings in the sense that the Fourier transform of the dislocation Hamiltonian of equation (4.20) can be shown to decompose with transverse interaction governed by K_T and longitudinal interaction governed by K_L. The smooth subtrate is thus characterized by a purely transverse interaction between dislocations. The recursion relations for these couplings are given by

$$\frac{dK_L^{-1}}{dl} = 12\pi^3 y^2 [I_0(\pi K^\vartheta) + \tfrac{1}{2} I_1(\pi K^\vartheta)] \tag{4.43a}$$

$$\frac{dK_T^{-1}}{dl} = 12\pi^3 y^2 [I_0(\pi K^\vartheta) - \tfrac{1}{2} I_1(\pi K^\vartheta)]. \tag{4.43b}$$

The renormalization procedure is completed by the following manipulations: Rearrange the summation over $\{n_\alpha\}$ to account for the pair that is gone from the explicit partition sum, taking into account the three possible charge directions for a pair, and then reexponentiate the terms proportional to δl in equation (4.39), changing the couplings to $K^r + \delta K^r$ and $K^\vartheta + \delta K^\vartheta$. The hard core distance has been expanded, so we must replace all occurences of a_0 in the partition sum by $a'_0 = a_0(1+\delta l)$. Each of the terms y/a_0^2 becomes to leading order, $y(1+2\delta l)/a'^2_0$ and the term in the exponential involving $G(r)$ is rewritten in terms of a'_0 producing a term $e^{-\pi K^r \delta l} \approx 1 - \pi K^r \delta l$ to leading order.. We cannot integrate charges at distance a_0 which are not opposite, but must treat them as "composite" if they sum to another unit vector. After the rescaling operation, any charge can either be an original charge or a composite one. The effect of this is added to the above contributions to the renormalization of y to produce

$$\frac{dy}{dl}=(2-\pi K^{\tau})y+2\pi I_0(\pi K^{\vartheta})y^2. \tag{4.44}$$

The rescaling of a_0 in the free energy term is cumulative, so after enough iterations of the procedure that the scale has changed from a_0 to $a_0 e^l$, the correct recursion relation for the free energy must be written

$$A^{-1}\frac{dF}{dl}=\frac{6\pi y^2 e^{-2l} I_0(\pi K^{\vartheta})}{a_0^2}. \tag{4.45}$$

Equations (4.41) or equations (4.43), equation (4.44) and equation (4.45) form a complete set of recursion relations for the full dislocation problem.

Combining these results with the Nelson-Halperin approach, it is possible to derive recursion relations for the elastic constants themselves. These are

$$\frac{d\bar{\mu}^{-1}}{dl}=3\pi y^2 I_0(\pi K^{\vartheta}) \tag{4.46a}$$

$$\frac{d\bar{B}^{-1}}{dl}=3\pi y^2[I_0(\pi K^{\vartheta})-I_1(\pi K^{\vartheta})] \tag{4.46b}$$

$$\frac{d\bar{\gamma}^{-1}}{dl}=3\pi y^2[I_0(\pi K^{\vartheta})+I_1(\pi K^{\vartheta})]. \tag{4.46c}$$

We will discuss these recursion relations in detail shortly.

We next discuss the structure and solution of the recursion relations. The controlling equation is equation (4.44). In the equation for y, if the initial value of y is small enough that the first term dominates and $K_0^{\tau}>2/\pi$, then y will decrease and be driven to zero. Thus in equations (4.41), the couplings K will increase more and more slowly as $y\to 0$, and eventually stop changing significantly with y and l. On the other hand, if the sign of the first term is positive, y is guaranteed to increase (this corresponds to increasing the concentration of dislocations as one rescales until the approximation of dilute pairs no longer applies). In the intermediate region, if the initial value of y is large enough, even though the first term may be negative initially, if K^{τ} ever becomes smaller than $2/\pi$ while y is nonzero, y will increase and diverge. Visualizing this behavior in (y, K^{τ}, K^{ϑ}) space, we find a critical (in the sense of differential equation phase plane theory) surface $y=0$ which is stable for $K^{\tau}>2/\pi$ and unstable

in the opposite case, that is, a small perturbation away from the surface grows, or a trajectory that comes arbitrarily close to the surface in the unstable region turns away from it and recedes to infinity. This surface is a fixed surface of the renormalization group transformation (every point of it is a critical point). The stability of the fixed surface changes along the line $K^T = 2/\pi$.

By specializing to the case $K^T = K^6$ we can learn a bit more. Now $y = 0$ is a fixed line. A single curve terminating at the edge of the stable region ($y = 0$, $K = 2/\pi$) separates the trajectories that hit the fixed surface from those that diverge away. This curve, called the separatrix, is found by starting at the terminating point and integrating the ratio of equation (4.43b) to equation (4.44) in the direction of decreasing K^{-1}. Figure 4.4 displays the phase plane of these differential equations along with the separatrix and several other trajectories.

Clearly the melting transition occurs when the fully renormalized K is exactly $2/\pi$, since that is the point at which the behavior changes from renormalization towards a more and more dilute gas of dipoles to one in which there is a nonzero concentration of dislocations on infinite scales. It is easy to show that the couplings K^T and K^6 at any scale have the same form as equations (4.21) with the elastic constants replaced by the partially renormalized elastic constants at that scale. Thus, the phase transition temperature is given by

$$T_m = \frac{1}{4\pi} \frac{a_0^2}{k_B} \left[\frac{\mu_R B_R}{\mu_R + B_R} + \frac{\mu_R \gamma_R}{\mu_R + \gamma_R} \right] \tag{4.47}$$

where the renormalized elastic constants are determined from equations (4.46).

In order to complete our understanding of this system we must deduce the initial conditions. At any temperature, they are determined by the bare elastic constants and the core parameter C such that

$$y_0 = e^{(-\pi C K_0 / k_B T)} \tag{4.48}$$

which is shown for "typical " values of C by the dashed curves in figure 4.4 When

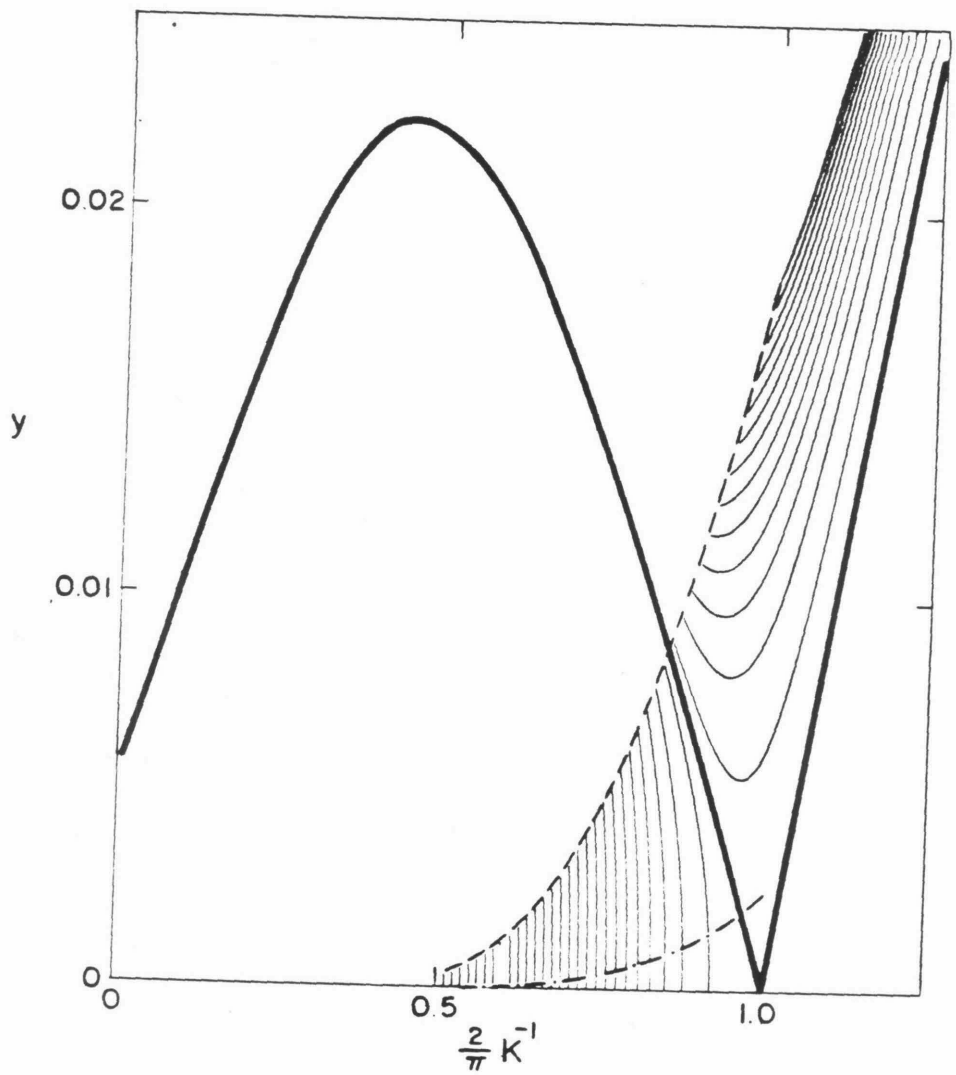

Figure 4.4. Phase plane of renormalization group recursion relations in the notation of reference 3. The heavy lines comprise the separatrix the dashed curve is the line of starting points for core parameter C=2 and the dot-dashed curve is the line of starting points for C=3. The solid region is the region below the left hump of the separatrix, where the RG trajectories intersect the K^{-1} axis.

the temperature and core parameter are such that K_0^T, y_0 lies on the separatrix, the renormalization must proceed along that trajectory to the critical value of K_R^T, so the separatrix represents the phase boundary of the system. Below the separatrix in figure 4.4, the system is solid, above, it is not. In fact, if the core parameter C is not a function of density or temperature, the intersection of the separatrix with the curve of initial conditions (known in the trade as the line of starting points) represents the entire melting curve of the system. (The reader should recall that K_0 contains a_0 and is thus a function of the density of the system.)

For the case $y_0=0$, the calculation of the heat capacity is straightforward, and for non-zero y_0 it is only manageably more complicated, so we next proceed to the description and analysis of the heat capacity computation.

4. Comparison of Experimental Data on Helium Monolayers with the Dislocation Unbinding Theory

In this section, comparisons are attempted between the predictions of the dislocation unbinding theory and observed thermodynamic data, particularly the heat capacity, of helium monolayers. It was hoped that even though a crucial parameter characterizing the energy of the dislocation core was unknown, some range of core energies would produce consistency with the experimental data, in a sense to be discussed below, but it turned out that this does not seem to be the case. The heat capacity data were summarized in chapter 2, and we will discuss various aspects of it in sequence.

First, we point out that the theory as formulated by NH and Young cannot possibly predict melting temperatures as high as the observed heat capacity peak temperatures. This can be established by the following argument: The melting temperature is a function only of the renormalized elastic constants, which can only be determined in terms of the measured or calculated bare

elastic constants if the core energy is known. However, an upper bound on the melting temperature can be found by replacing the renormalized elastic constants in equation (4.47) with the bare ones. At the melting temperature predicted by the theory, the value of K from the bare elastic constants (determined by the intersection of the line of starting points with the separatrix) is greater than the renormalized value $2/\pi$, as can be seen in figure 4.4. Thus the temperature determined by setting the bare K to $2/\pi$, which can be called the "unrenormalized" melting temperature, is greater than the renormalization group prediction of the melting temperature. Furthermore, the melting temperature predicted by the theory is actually an absolute stability criterion for the solid -- melting could occur at a lower temperature if some other mechanism preempted the dislocation unbinding, but if the solid exists at T_m, it must be unstable to the formation of free dislocations. Thus, it is guaranteed (at least for classical solids) that the "unrenormalized" melting temperature estimated from the bare elastic constants is outside the solid region of the phase diagram of the substance. Since the heat capacity peaks plotted in figures 4.5a and 4.5b are significantly above these "unrenormalized" melting temperatures, they cannot mark the melting transition.

Precise predictions of the true melting temperature from the theory cannot be made because the initial conditions for the renormalization procedure cannot be specified without the value of C, the core parameter. This core parameter is essentially a non-physical concept, since it is to some extent arbitrary (but not completely). Essentially it is a means of cutting off the integral of the total elastic energy of a dislocation at some small distance from the dislocation, such that the integral is carried out over the region over which linear elasticity theory correctly describes the strains, and the excess energy in the central region is subsumed into the core parameter. The core parameter is *not*, as

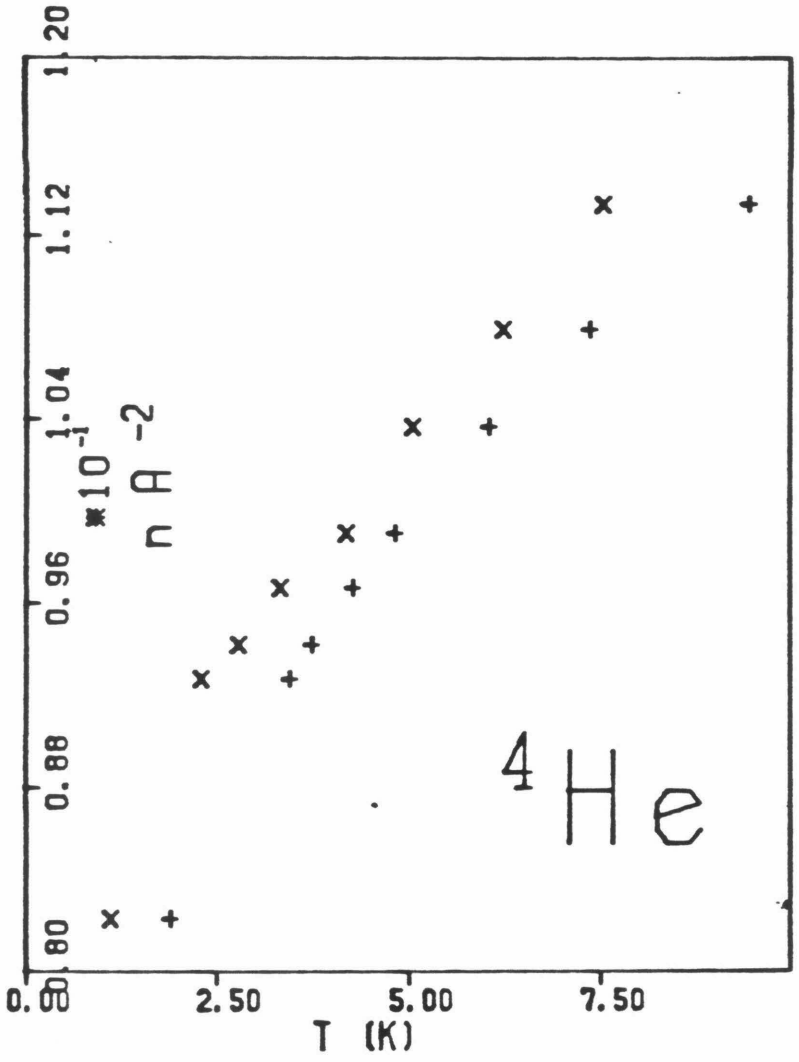

Figure 4.5a. Heat capacity peak temperature(+), "unrenormalized " melting temperature(x) for several coverages for ^{4}He.

Figure 4.5b. Heat capacity peak temperature(+), "unrenormalized" melting temperature(x) for several coverages of ^{3}He.

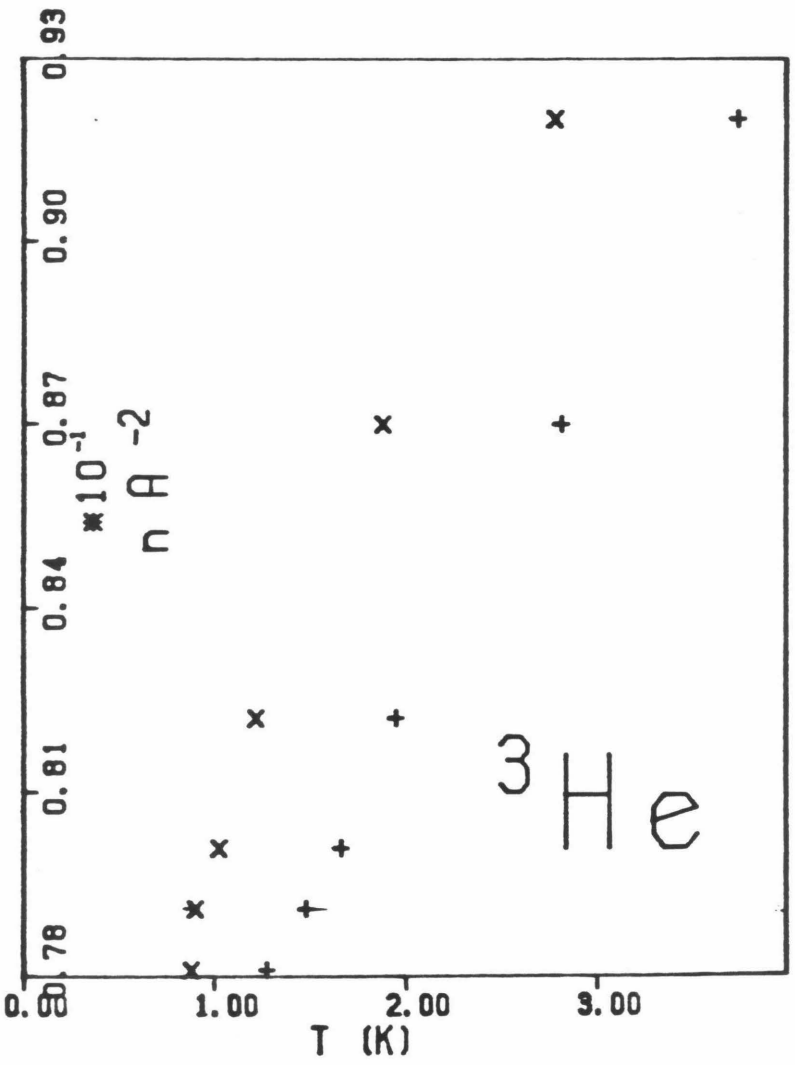

it is sometimes described, simply an indication of the size of the cutoff. The core parameter is only known for certain simple systems. One such case is the classical Lennard-Jones solid, for which it has been evaluated by Englert and Tompa[9] by an iterative relaxation method applied to a collection of 184 atoms forming a triangular lattice bound by nearest neighbor forces only and containing a single dislocation. They did not evaluate the core parameter explicitly, but found the strain energy of the dislocation in terms of the Lennard-Jones parameters to be 8.65ε, where the Lennard-Jones potential is $V(r)=4\varepsilon((\frac{\sigma}{r})^{12}-(\frac{\sigma}{r})^{6})$ and the equilibrium spacing of the classical (zero-pressure) solid is $2^{1/6}\sigma$, if only nearest neighbor forces are included. Using the methods of chapter 3 to evaluate the elastic constants of this classical solid

$$\mu_{class}=\tfrac{1}{2}B_{class}=\frac{54}{\sqrt{3}}\frac{\varepsilon}{a_0^2} \tag{4.49}$$

(it is also easy to show that the second-nearest neighbor forces increase these by less than 9%), we can compare the energy computed by Englert and Tompa with the equation for the energy of a dislocation (assuming a smooth substrate)

$$E_{dis}=\frac{a_0^2}{2\pi}\frac{\mu B}{\mu+B}(\ln(R/a_0)+C) \tag{4.50}$$

where R is related simply (by $\pi R^2=NV_{cell}$) to the size of the sample treated by Englert and Tompa. This comparison yields C of .65, which is smaller than the value 1.5 usually suggested in standard dislocation theory treatises, and far smaller than numbers that produce reasonable heat capacities for helium monolayers.

No one has yet made a similar calculation for a quantum system, nor has anyone even predicted in which direction the quantum corrections will go. Since the equation (4.48) for the line of starting points contains C in the exponent, a factor of 4-6 in the core parameter makes a very substantial difference in the concentration of dislocation pairs, especially at low temperature. The larger the

core energy, the closer the line of starting points is to the fixed surface $y=0$ and the more dilute the gas of dislocation pairs. Thus, the larger the core parameter, the smaller the degree to which the elastic constants are renormalized, and the closer the predicted T_m to the "unrenormalized" estimate. Figure 4.4 shows the relationship of the line of starting points to the core parameter, for the case where the substrate is smooth.

In this case, the procedure for calculating the heat capacity is relatively simple. The bare elastic constants μ and B are obtained from the experimental data for a particular coverage as explained in chapter 2, and we choose a value of the core parameter. The intersection of the line of starting points determined by this information with the separatrix is found numerically to determine the melting temperature corresponding to this core energy. For the purposes of extending the calculation of the heat capacity above this melting temperature, we also arbitrarily choose a crystal size, the use of which will be explained below. Then, at each of a sequence of temperatures between 0K and the heat capacity peak temperature the renormalization group equations for K_T^{-1}, y, and F are numerically integrated, beginning at the appropriate point on the line of starting points for each temperature. Second differences with respect to temperature of the values of $F_R(T)$ give the heat capacity

$$C_{dis}(T)=-T\frac{\partial^2 F}{\partial T^2} \quad . \tag{4.51}$$

According to the theory, this dislocation contribution to the heat capacity should be added to the heat capacity of the bare phonons, which we take to obey a Debye model, for comparison with the experimental heat capacity.

We require that the heat capacity calculated here must be less than the experimental heat capacity if it is to be considered consistent with the data. In general, the Debye model gives the correct behavior at very low temperatures, but at moderate temperatures, the van Hove singularities which must occur in

the phonon density of states (where $d\omega/dk=0$) usually raise the heat capacity *above* that predicted by the Debye model, because it is guaranteed that there be at least one maximum in the dispersion curve at lower k than the first minimum. Figure 4.6 shows the heat capacity predicted for the phonon spectrum displayed in figure 5.8 of chapter 5, in comparison with the pure Debye heat capacity corresponding to the zero-degree speeds of sound, as an example of this effect. Anharmonicity of the solid, which is completely ignored here except for the part produced by the dislocations, can either increase or more usually, decrease the departures from the Debye law, [11] so the requirement that the dislocation heat capacity be less than the measured heat capacity is not strictly correct. However, the actual deviations in the experimental heat capacity from Debye-law behavior occur in a narrow range of temperature right near where, for some values of the core parameter, the dislocation heat capacity is predicted to become large, while anharmonicity usually causes more gradual effects, and also usually is only important at higher temperatures.

In the case of a periodic substrate, the separatrix becomes a surface in $(K^{\tau}, K^{\sigma}, y)$ space which reaches the fixed surface $y=0$ along the line $K^{\tau}=2/\pi$.

For this case, the computation of the heat capacity is slightly more complicated. Given the bare elastic constants, including γ_0 as obtained in chapter 5, the determination of the melting temperature is somewhat trickier than in the smooth substrate case. A brute-force method was chosen: a likely point on the line of starting points was chosen and the RG equations were integrated until they either reached $y=0$ or passed through a minimum. A binary search method was used to find the place on the line of starting points for which the resultant trajectory passed through $K^{\tau}=2/pi$, $y=0$, within some tolerance. The temperature at that initial point is the melting temperature. The rest of the computation of the heat capacity proceeds as before, except that the full set of

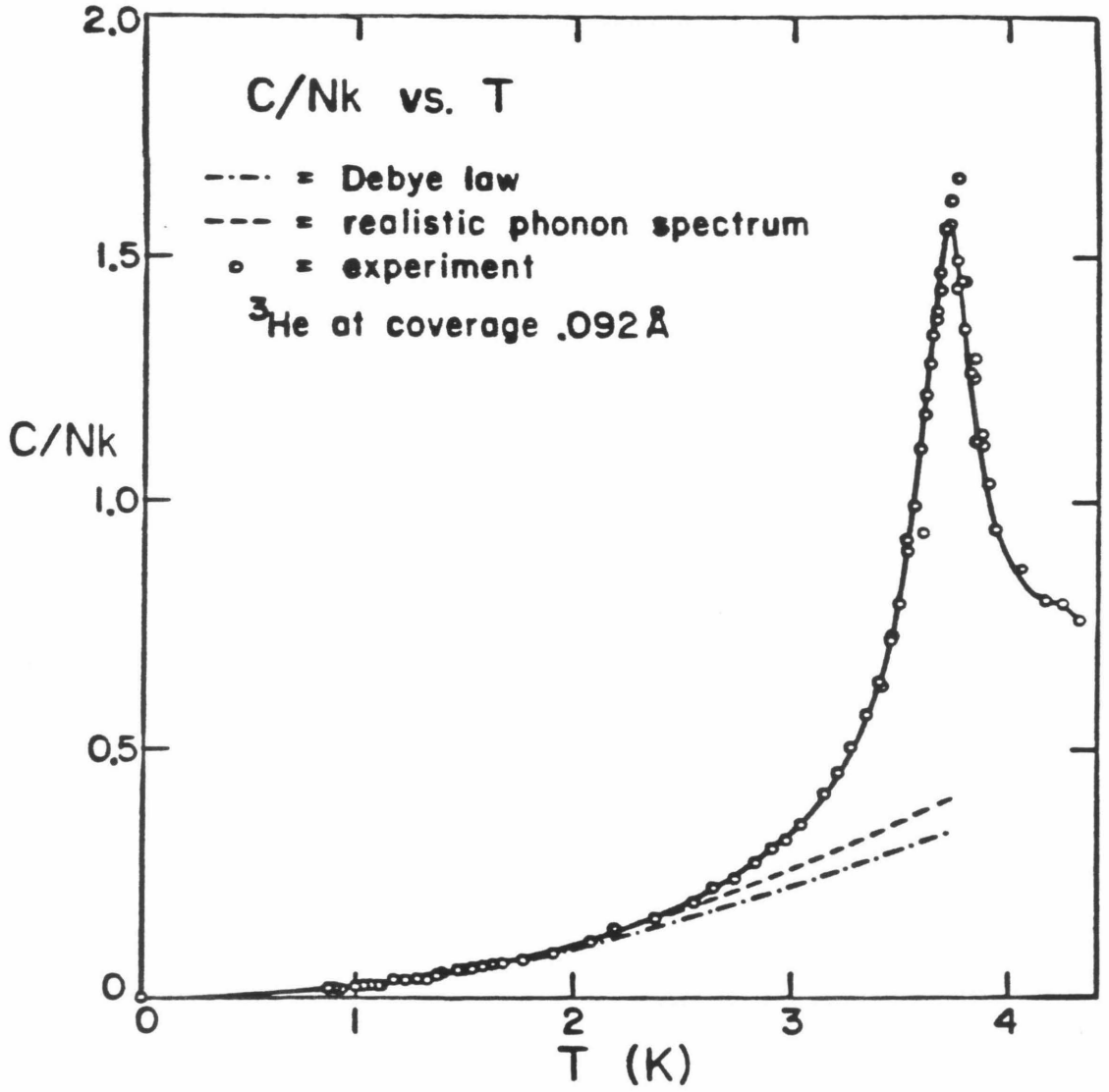

Figure 4.6. The heat capacity for a realistic phonon spectrum (upper curve on the spectrum of figure 5.8) compared with the Debye law (lower curve) and experimental points for this coverage.

recursion relations, equations (4.41), (4.44), (4.45) must be used.

Before presenting the results of these calculations we will try to unify them with some alternate methods of computing the heat capacity and refinements to the various methods that allow some estimates of the heat capacity above the transition temperature.

To get any results at all above the transition temperature, we use a finite size crystal. The theory states that the screening between elements of a pair is only complete when they are infinitely far apart right at the transition, and then the screening length becomes smaller as the temperature rises. Thus a patch of finite size (in the infinite medium, so boundary conditions and image dislocation fields cause no trouble) remains solid until some temperature higher than that marking the onset of flow under infinite wavelength shear. If we calculate the heat capacity of the dislocations in this finite patch assuming it is neutral (by renormalizing only out to a scale-length equal to the patch size) and similarly calculate the bare phonon heat capacity of the patch by including wavelengths smaller than the patch size, we should have underestimated the total heat capacity/atom. Until the screening length becomes equivalent to our patch size, the RG equations will be well-behaved and can be used as before. When the temperature reaches a value that lowers the screening length to the patch size, we stop trying to calculate further. This is in practice determined by a more ad-hoc criterion of stopping the integration at any temperature for which the renormalization group equations start becoming inaccurate ($y>0.1$) before we reach the scale equivalent to the patch size.

While carrying out the renormalization group integrations, it is possible to use the results in an equivalent calculation that is more easily modified to incorporate quantum effects, although we have only managed to do that in a physically motivated, but *ad hoc* fashion.

At the outset, instead of separating the displacement field into phonon and dislocation parts, we can use linear response theory on the entire elastic Hamiltonian to understand the behavior under arbitrary applied stress. This leads to a relationship between the temperature-dependent, effective elastic constants and a correlation function of the strains, which in turn can be used to predict the thermodynamic and dynamic behavior of the system in terms of only the renormalized and bare elastic constants. Now the results of our RG integration can be used numerically to evaluate the equations generated. Since the problem has now been characterized in terms of effective phonons, it is easier to see how to approach the real quantum mechanical problem, and we will display an interpolation formula for the heat capacity in terms of bare and renormalized elastic constants which has the correct high and low-temperature limits, but essentially no other physical justification.

Linear response theory [13, 14] is a formal method for analyzing the dynamical response of a system to an small external perturbation. To first order in the perturbation, the shift in the thermal average of any quantum-mechanical operator $\hat{A}$ is given by

$$\delta<\hat{A}(t)>=\frac{i}{\hbar}\int_{-\infty}^{t}dt'<[\hat{H}^{ext}(t'),\hat{A}(t)]>. \tag{4.52}$$

In particular, if $\hat{H}^{ext}$ takes the form $\sum_i \int d\vec{r}\hat{A}_i(\vec{r},t)\sigma_i^{ext}$ where σ is a generalized force coupling to the operators $\hat{A}_i$ then the linear reponse of one particular operator is given by

$$\delta<\hat{A}_i(\vec{r},t)>=-\frac{i}{\hbar}\int_{-\infty}^{t}dt'\int d\vec{r}'<[\hat{A}_i(\vec{r},t),\hat{A}_j(\vec{r}\ ',\ t')]>\sigma_j^{ext}(\vec{r}',t'). \tag{4.53}$$

Thus, the response of any operator is proportional in this approximation to the applied force, and proportional to the space and time correlation function of itself with other dynamical quantities. By Fourier transforming equation (4.53) in time and space, we can obtain a similar relationship between the operators

and the force as functions of frequency and wavevector, and if the system is translationally invariant in space and time and the force is local, that relationship decouples responses at different frequencies and wave numbers.

For the simple case of a single dynamical operator, the response depends on the autocorrelation function, and in the long-wavelength, low frequency limit corresponds to the static response. For example, in the case of a magnetic system in a weak external field, the change in the local magnetization is proportional to the magnetization autocorrelation function. But the temperature-dependent static susceptibility is defined to determine exactly that response, $\delta M = \chi \delta h$, so the correlation function is related to a susceptibility.

In our problem, the analogue of the magnetization is a strain component, and the force is an applied stress. The Hamiltonian is the full elastic Hamiltonian, of equation (4.6), making no attempt to decompose it into phonon and dislocation contributions. Once again, the long-wavelength, low-frequency limit tells us how to interpret the correlation functions that occur -- they must obey Hooke's law, $\sigma_{ij} = C_{ijkl} u_{kl}$, so the correlation function $\langle u_{ij} u_{kl} \rangle$ is proportional to the inverse elastic tensor, C^{-1}_{ijkl} which plays the role of a temperature-dependent susceptibility. Clearly, at finite wavelength and frequency, (or a finite distance and time) the generalized susceptibility represents the compliance of the system to disturbances of this scale and time dependence. Since the thermal average in the correlation function is over strains produced both by phonons and dislocations, the susceptibility clearly must represent the renormalized scale- and frequency- dependent elastic constants, and in fact the correlation function is sometimes used as an alternative definition of the elastic constants.

The internal energy of the system, whose temperature derivative is the heat capacity, is given by the correlation function evaluated at equal times and at the same space position, i.e., ignoring pressure terms and the kinetic energy,

$$E(T)=\tfrac{1}{2}\int d^2r\, C^0_{ijkl}\langle u_{ij}(\vec{r})u_{kl}(\vec{r})\rangle. \tag{4.54}$$

Fourier transforming this equation and putting in the elastic tensor for the 2-D isotropic continuum (shown in chapter 3 to be equivalent to the triangular lattice) we find (using dimensionless wavevectors)

$$E(T)=\tfrac{1}{2}\int \frac{d^2q}{4\pi^2} D^0_{ij}\langle u_i(\vec{q})u_j(-\vec{q})\rangle, \tag{4.55}$$

where the bare dynamical matrix is a function of the bare elastic tensor,

$$D^0_{ij}(q)=\mu_0 q^2\left[\delta_{ij}-\frac{q_i q_j}{q^2}\right]+2B_0 q_i q_j, \tag{4.56}$$

and thus is determined by the properties at $T=0$ where there are no dislocations. Using linear response theory, the correlation function at finite (nonzero) wavevector (below the transition temperature) for a classical isotropic elastic solid can be written as15

$$k_B T\left[\frac{1}{\mu_R(q,T)}\left[\delta_{ij}-\frac{q_i q_j}{q^2}\right]+\frac{1}{\mu_R(q,T)+B_R(q,T)}\frac{q_i q_j}{q^2}\right]=q^2\langle u_i(\vec{q},t)u_j(-\vec{q},t)\rangle \tag{4.57}$$

which, combined with equation (4.56) and equation (4.55), gives for the classical internal energy,[16]

$$E(T)=\tfrac{1}{2}k_B T\int \frac{d^2q}{4\pi^2}\left[\frac{\mu_0}{\mu_R(q,T)}+\frac{B_0+\mu_0}{B_R(q,T)+\mu_R(q,T)}\right]. \tag{4.58}$$

At this point, we still do not know how to calculate the renormalized elastic constants (or equivalently, the correlation function) directly, since they are the result of statistical averages over the full Hamiltonian. However, our approach is wholly equivalent (so long as we consider a classical system) to the renormalization group approach, so we can use the results of those calculations of the renormalized elastic constants, if we can make a correspondence between $\mu_R(l)$ and $\mu_R(q)$. The obvious such correspondence is $q=\pi/a_0 e^l$, which can only be in error by a factor of order unity.

Thus, the temperature derivative of equation (4.58) is entirely equivalent to the heat capacity calculation described above in which the dislocation contribution is added to that of the bare phonons. It certainly has the correct qualitative behavior. If there were no dislocations, the renormalized elastic constants would be the same as the bare ones, and the heat capacity would simply be k_B, or exactly what one gets from the equipartition theorem applied to the potential energy of a classical system of oscillators. Since the renormalized elastic constants are always smaller than the bare ones (the dislocations always weaken the restoring forces), we always get an excess contribution above the bare phonon contribution, exactly what one would expect from the calculation in which the phonons and dislocations are decoupled.

To try to improve this calculation for a quantum system, we must assess the places where we have not taken quantum mechanics into account. The most obvious place is in the treatment of the bare phonons, since we have not noticed that they are quantized, will not be fully excited at low temperature, and thus will have a heat capacity that falls to zero as the temperature decreases, and is proportional to T^2 at low enough temperature.

If this were the only area in which quantum mechanical effects have been neglected, correcting the oversight would be trivial -- the dislocation contribution to the heat capacity as calculated from the RG equations would remain the same, while the bare phonon heat capacity could be replaced by a quantum mechanical model, of complexity ranging from a simple Debye law to a fully self-consistent phonon calculation based only on the interatomic potential. (It would not be extremely useful to employ this latter model, because we have neglected all anharmonic terms which lead to further couplings between the dislocations and phonons.)

Unfortunately, even though dislocation pairs are relatively high-energy

excitations of the system, and owing to the non-zero core energy are not expected to be significantly excited or contribute importantly to the heat capacity of the system at low temperatures, it is not correct to treat them classically. Essentially, the quantum properties of the dislocations arise from the fact that they are not actually fixed to positions on the lattice, but are free to move slightly in response to local stresses. The part of the motion which moves dislocations around in the lattice is presumably accounted for in the configuration integrals in the partition function, which favor arrangements of the dislocations on the lattice which minimize their energy. The motions on smaller scales, including quantum jitter, are not taken into account.

Motion along the Burgers vector, called glide, is easy and occurs under sustained shear, as discussed in section 4.2. It is essentially this motion which we understand physically to produce the weakening of the effective elastic constants at large scales, the polarization and stretching of dislocation pairs in a shear force. (Motion perpendicular to the Burgers vector, called climb, is very difficult, because it requires that the extra half-line of atoms be either lengthened or shortened, which can only be done by nucleation of vacancies or interstitials in the crystal.) When the disturbing shear is on a scale large compared to the size of a particular pair then polarizing motion takes place. When, on the other hand, it occurs at a wavelength small compared to the size of the pair, the shear is, on the average, opposite at the two members of the pair and hence they move in the same direction, producing no net effect. Thus there is a crossover in the effect of applied shear on a particular pair which occurs when the variation of the shear is over wavelengths comparable to the size of the pair. For wavelengths above the crossover, the pair's response is to increase the amplitude of the local displacements, and thus mimic a weakening of the elastic response at that wavelength. There are also variations in the response depend-

ing upon the timescale of the applied shear, resembling retardation effects in the interaction of light with bound charges.

Thus the evaluation of the quantum mechanical correlation function is more complicated than what has been done above, and we have not carried it out. Instead, we have approximated that correlation function, which depends on both wavevector and an integral over all frequencies, by the result of the static (but scale-dependent) calculation of the interaction of dislocation pairs.

There is a more or less empirical way to include some of the quantum mechanical effects of dislocations, by finding a simple, unjustified interpolation formula which agrees with equation (4.58) and reduces to the correct 0 Kelvin result.

We assume that the bare phonons are described by a Debye-like model with angular frequencies given by $\omega_{T,L}^0(q)=c_{T,L}^0 q$ for transverse and longitudinal modes, with the sound speeds c given by equations (3.39) in terms of the bare elastic constants. We notice that we can reproduce the classical result (4.58) if we write

$$E(T)=\sum_{q,p}\hbar\omega_p^0(q)\frac{\omega_p^0(q)}{\omega_p^R(q)}\bar{n}_p^R(q) \tag{4.59}$$

where $\bar{n}$ is the usual Bose occupation number at inverse temperature $\beta=1/k_B T$ for the renormalized frequency ω_p^R,

$$\bar{n}^R(q)=[e^{\beta\hbar\omega_p^R(q)}-1]^{-1} \tag{4.60}$$

since in the limit of high temperature (small β), $\bar{n}$ reduces to $k_B T/\hbar\omega_p^R(q)$ and since the elastic constants, bare or renormalized, are proportional to ω^2. The zero-degree limit is also reproduced by equation (4.59), since at low temperature, the renormalized frequencies approach the bare ones and equation (4.59) just becomes the usual mode sum for phonons (ignoring the zero-point energy which does not contribute to the heat capacity).

One can attempt to concoct justifications for equation (4.59) on the grounds that it mimics a system of phonons whose frequencies are unchanged but whose occupation numbers are altered by the presence of dislocations, but it is less pretentious to treat it as an interpolation formula like the Debye law itself.

We now compare the experimental data on the excess heat capacity of helium films above the Debye law result, with the results of the calculations based upon equation (4.59) with the Debye law subtracted out, and with the dislocation contribution to the heat capacity as calculated from the RG equations (recall that this is also an estimate of that excess, since we ignore the bare phonons). Since in general, quantum mechanical heat capacities tend to zero faster than classical ones as the temperature decreases, we expect the result of equation (4.59) to be less than the pure RG result, and the expectation is confirmed.

Figures 4.7 thru 4.10 show these heat capacities for ^{3}He (^{4}He is similar) for several coverages with core parameter C chosen roughly to optimize the fit of the classical dislocation heat capacity to the experimental data. Figures 4.11 thru 4.14 shows roughly optimal results for the interpolation formula at several coverages. The largest temperature on the curves is the heat capacity peak temperature, and the dislocation unbinding temperature for the particular core parameter is indicated to be substantially below the peak temperature. In general, the steep rise of the calculated heat capacity occurs at higher temperature, the larger the core parameter. The results of the interpolation formula for several different values of the core parameter are plotted in figure 4.15.

As mentioned above, the calculations are carried above the dislocation unbinding temperature by treating a finite-size patch of solid. The crystal patch size is taken to be the mean platelet size of 140Å (or about 40 lattice spacings.) as determined recently (for krypton-plated graphite) from modelling of experi-

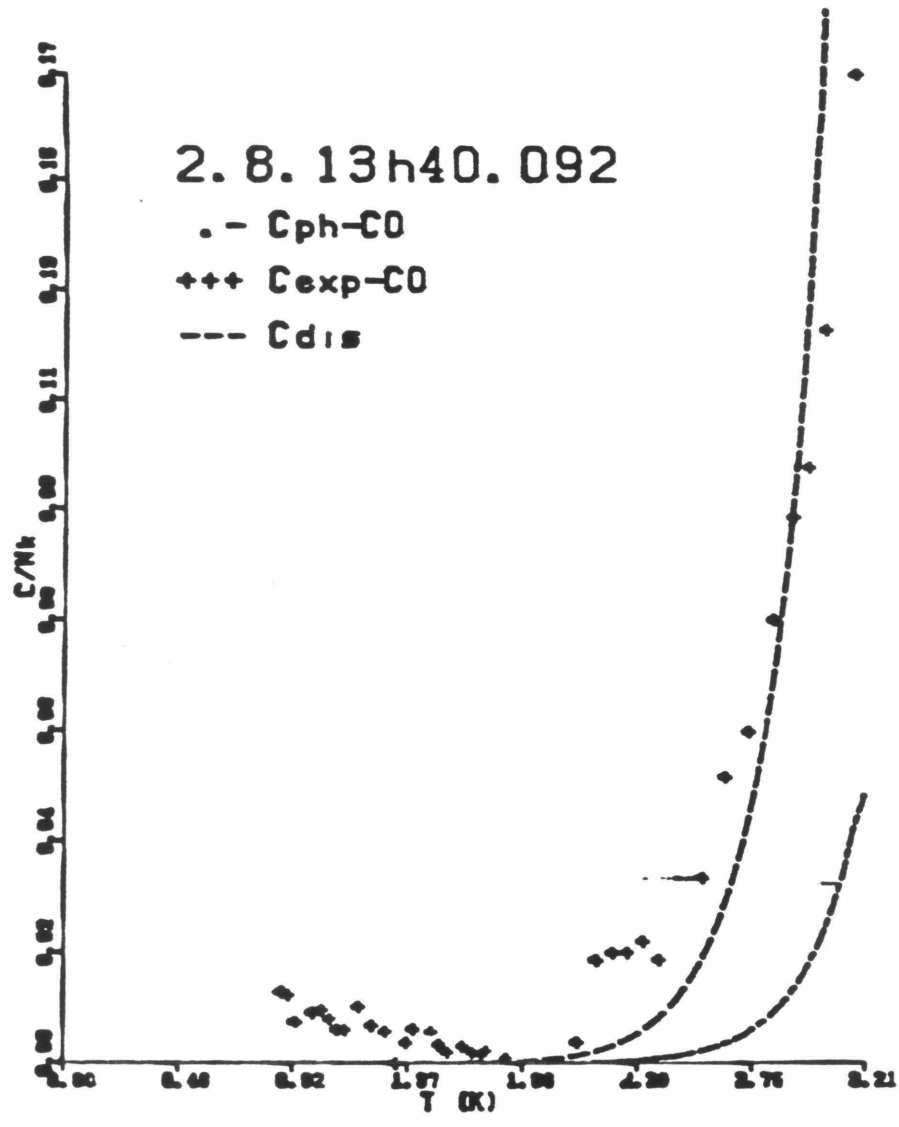

Figure 4.7 Heat capacity from experimental data, from RG equations (C-dis), and from *ad hoc* interpolation formula, all measured as excess above Debye law, for ^{3}He at coverage .092 Å^{-2}, core 2.8, gamma .13 and lattice size 40 spacings.

Figure 4.8 Heat capacity from experimental data, from RG equations (C-dis), and from *ad hoc* interpolation formula, all measured as excess above Debye law, for ^{3}He at coverage .087 Å^{-2}, core 3.3, gamma .114 and lattice size 40 spacings.

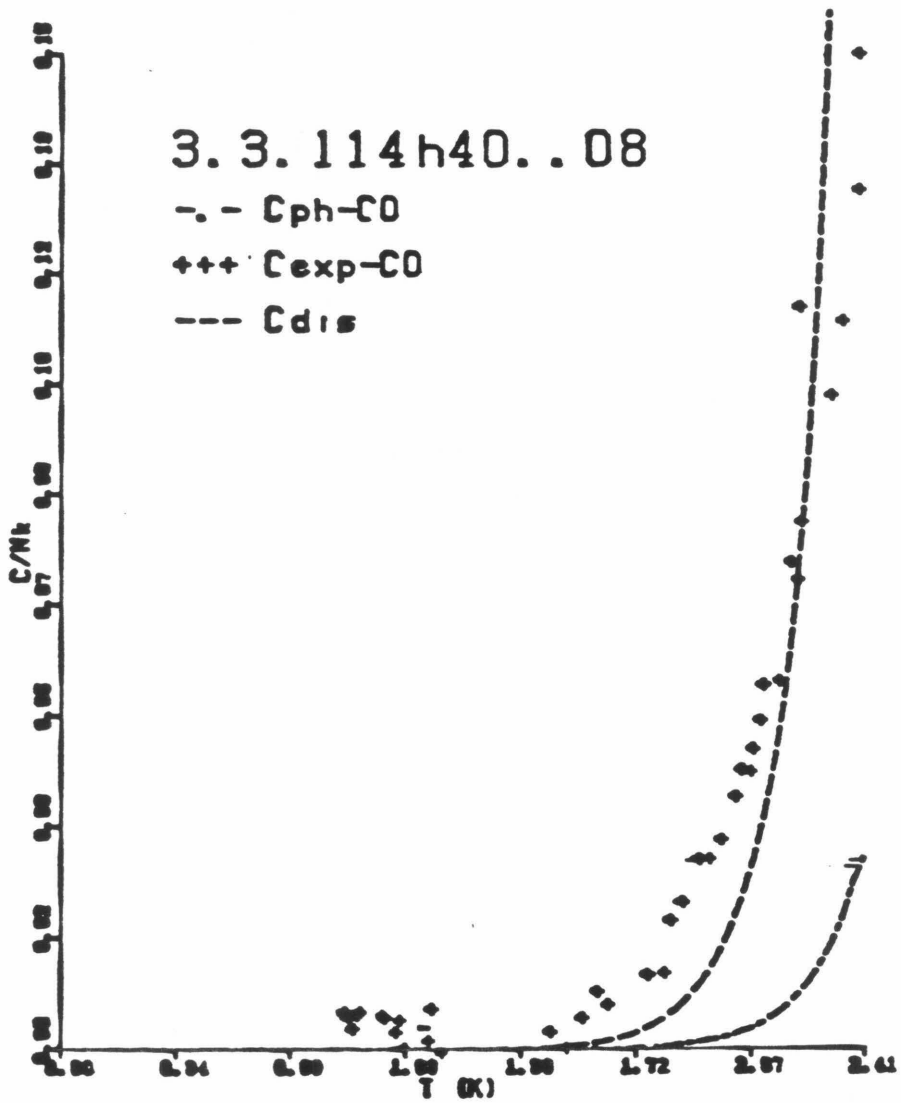

Figure 4.9 Heat capacity from experimental data, from RG equations (C-dis), and from *ad hoc* interpolation formula, all measured as excess above Debye law, for ^{3}He at coverage .0822 Å^{-2}, core 3.8, gamma .0982 and lattice size 40 spacings.

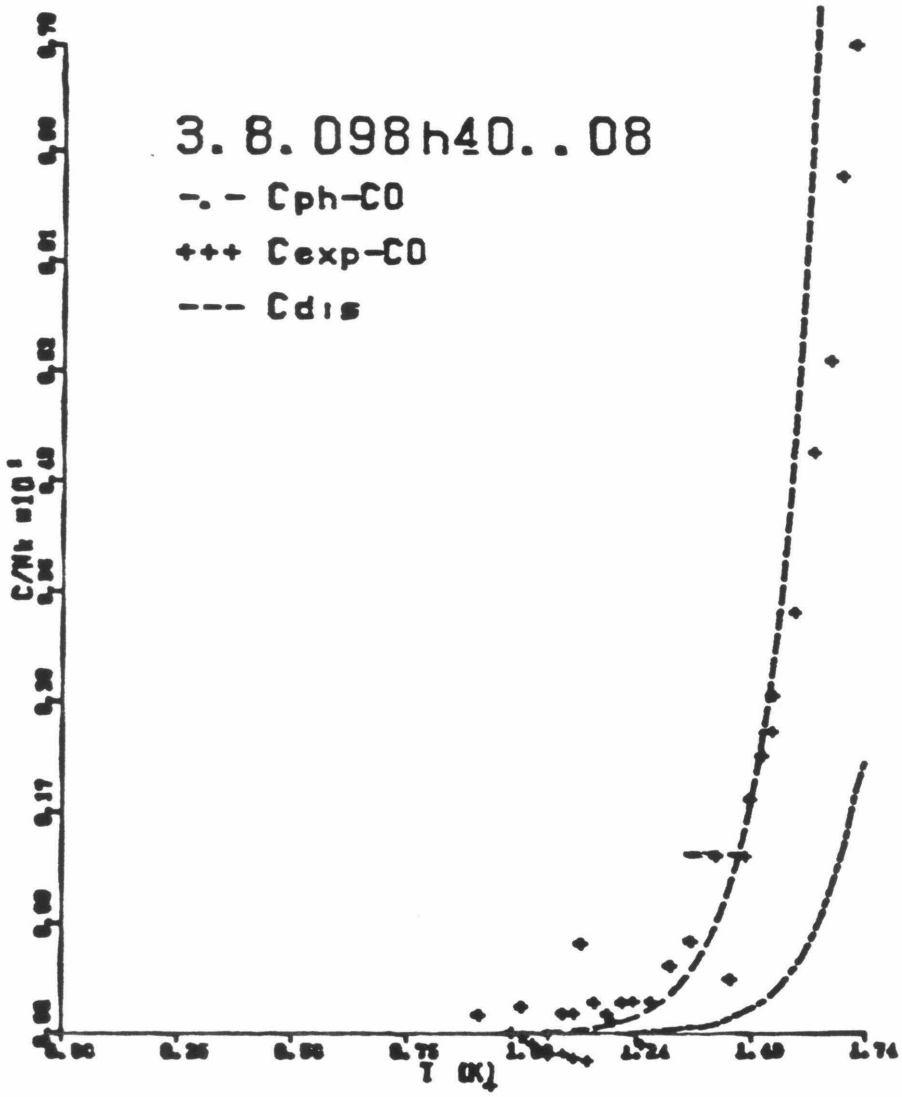

Figure 4.10 Heat capacity from experimental data, from RG equations (C-dis), and from *ad hoc* interpolation formula, all measured as excess above Debye law, for ^{3}He at coverage .0801 Å^{-2}, core 4.2, gamma .11 and lattice size 40 spacings.

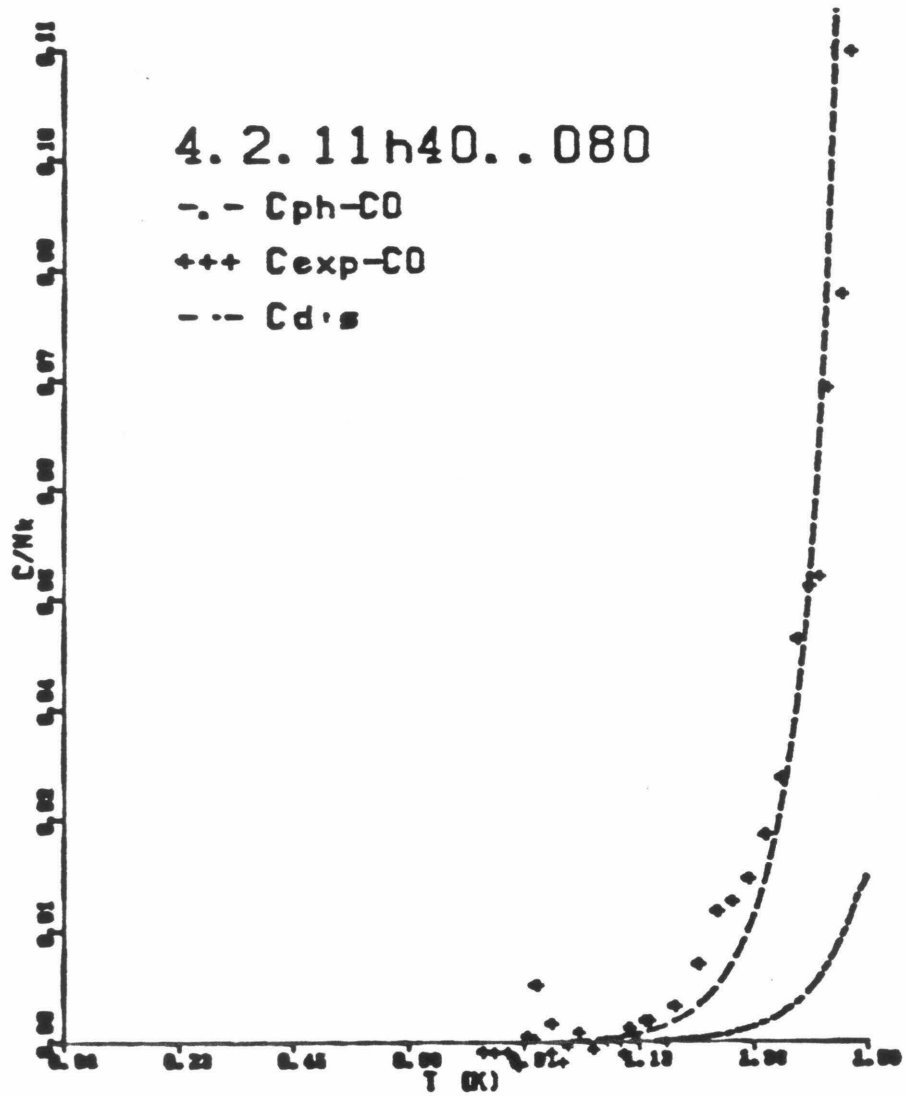

Figure 4.11 Heat capacity from experimental data, from RG equations (C-dis), and from *ad hoc* interpolation formula, all measured as excess above Debye law, for ^{3}He at coverage .092 Å^{-2}, core 2.3, gamma .13 and lattice size 40 spacings. The predicted dislocation unbinding temperature is 2.458 K.

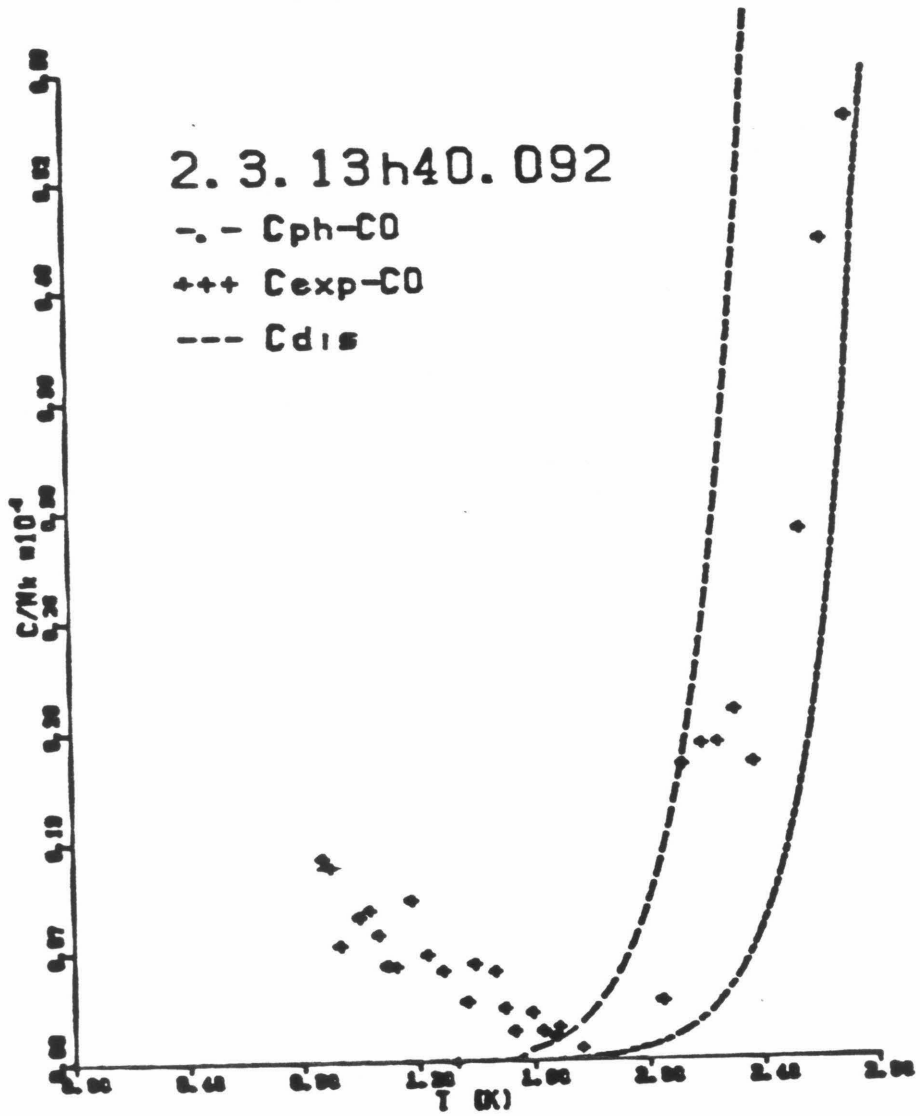

Figure 4.12 Heat capacity from experimental data, from RG equations (C-dis), and from *ad hoc* interpolation formula, all measured as excess above Debye law, for ^{3}He at coverage .087 Å^{-2}, core 2.7, gamma .11 and lattice size 40 spacings. The predicted dislocation unbinding temperature is 1.757 K.

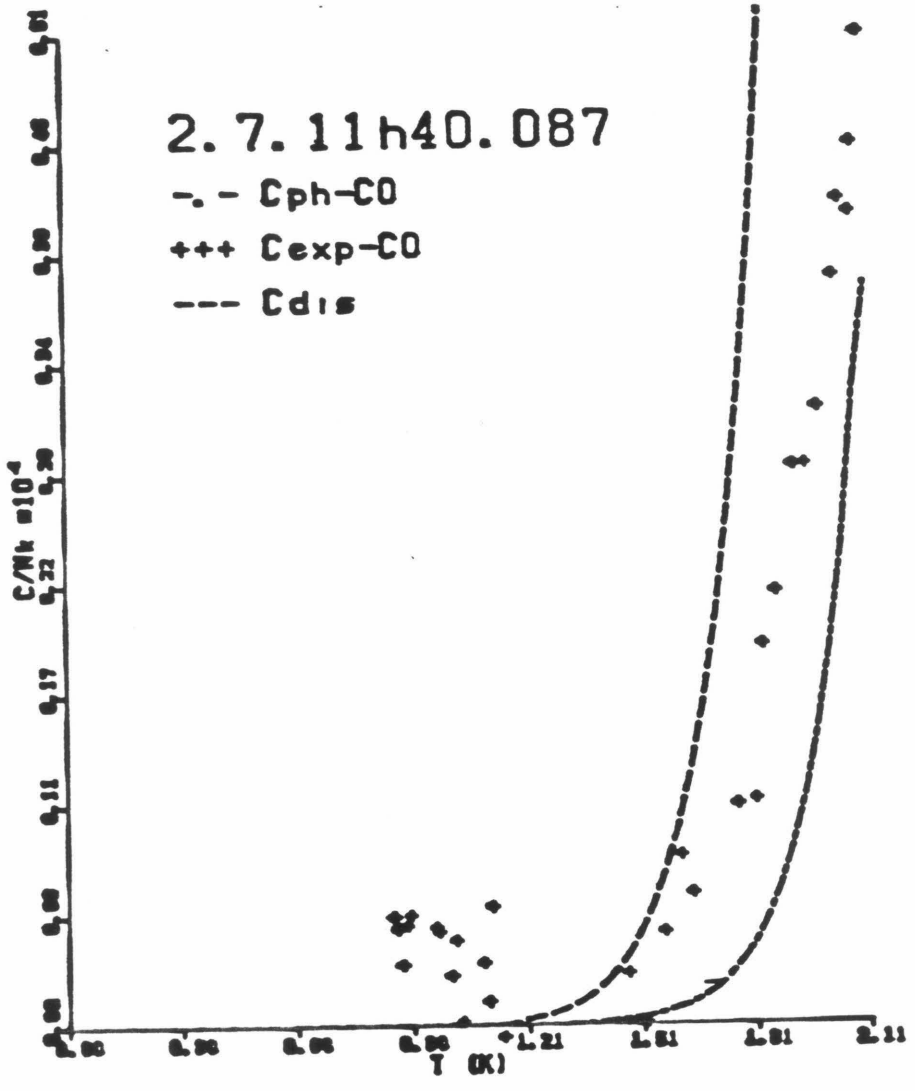

Figure 4.13 Heat capacity from experimental data, from RG equations (C-dis), and from *ad hoc* interpolation formula, all measured as excess above Debye law, for ^{3}He at coverage .0822 Å^{-2}, core 3.4, gamma .0982 and lattice size 40 spacings. The predicted dislocation unbinding temperature is 1.205 K.

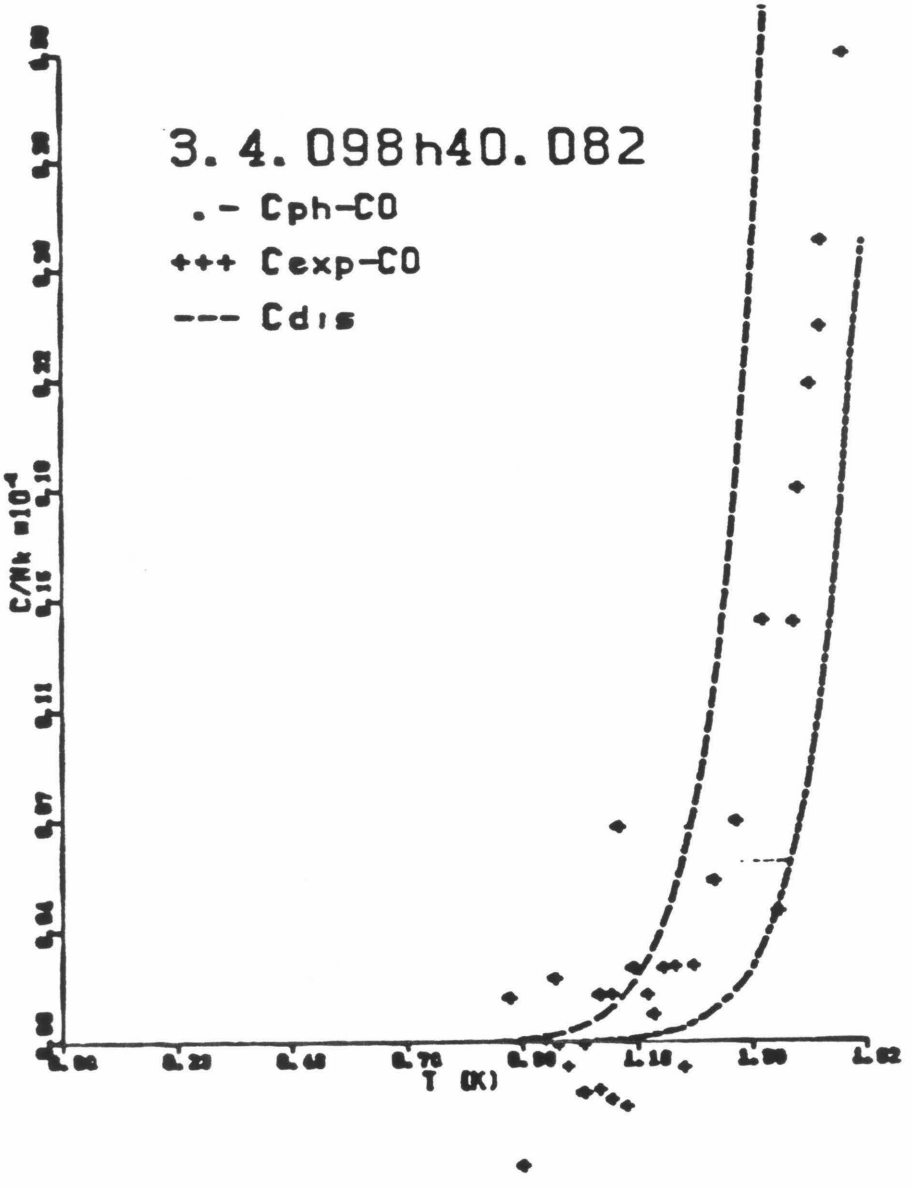

Figure 4.14 Heat capacity from experimental data, from RG equations (C-dis), and from *ad hoc* interpolation formula, all measured as excess above Debye law, for ^{3}He at coverage .0801 Å^{-2}, core 3.7, gamma .11 and lattice size 40 spacings. The predicted dislocation unbinding temperature is 1.037 K.

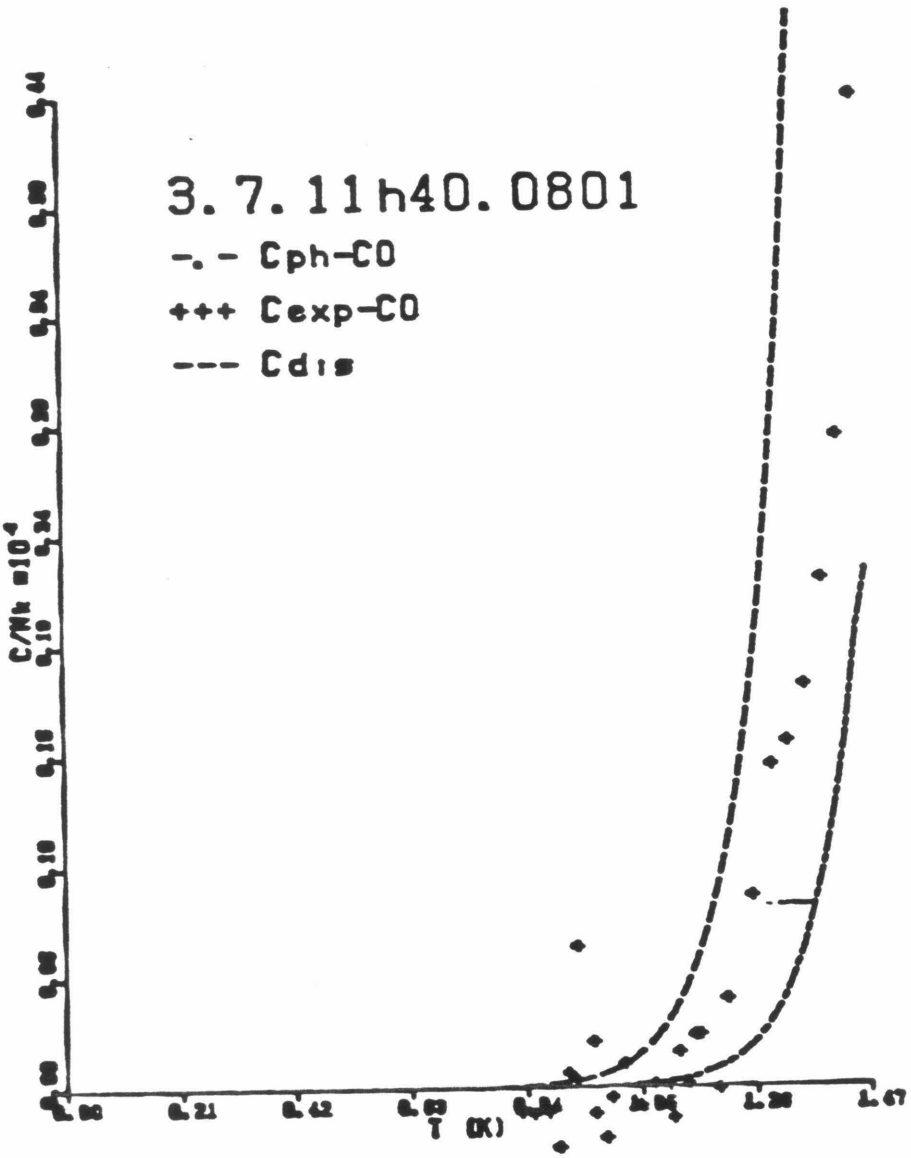

Figure 4.15. Experimental points vs. curves of interpolation formula for the heat capacity of ^{3}He at coverage $n = .092 Å^{-2}$, for values of the core parameter 2.3, 2.4 2.6 2.8, reading from left to right.

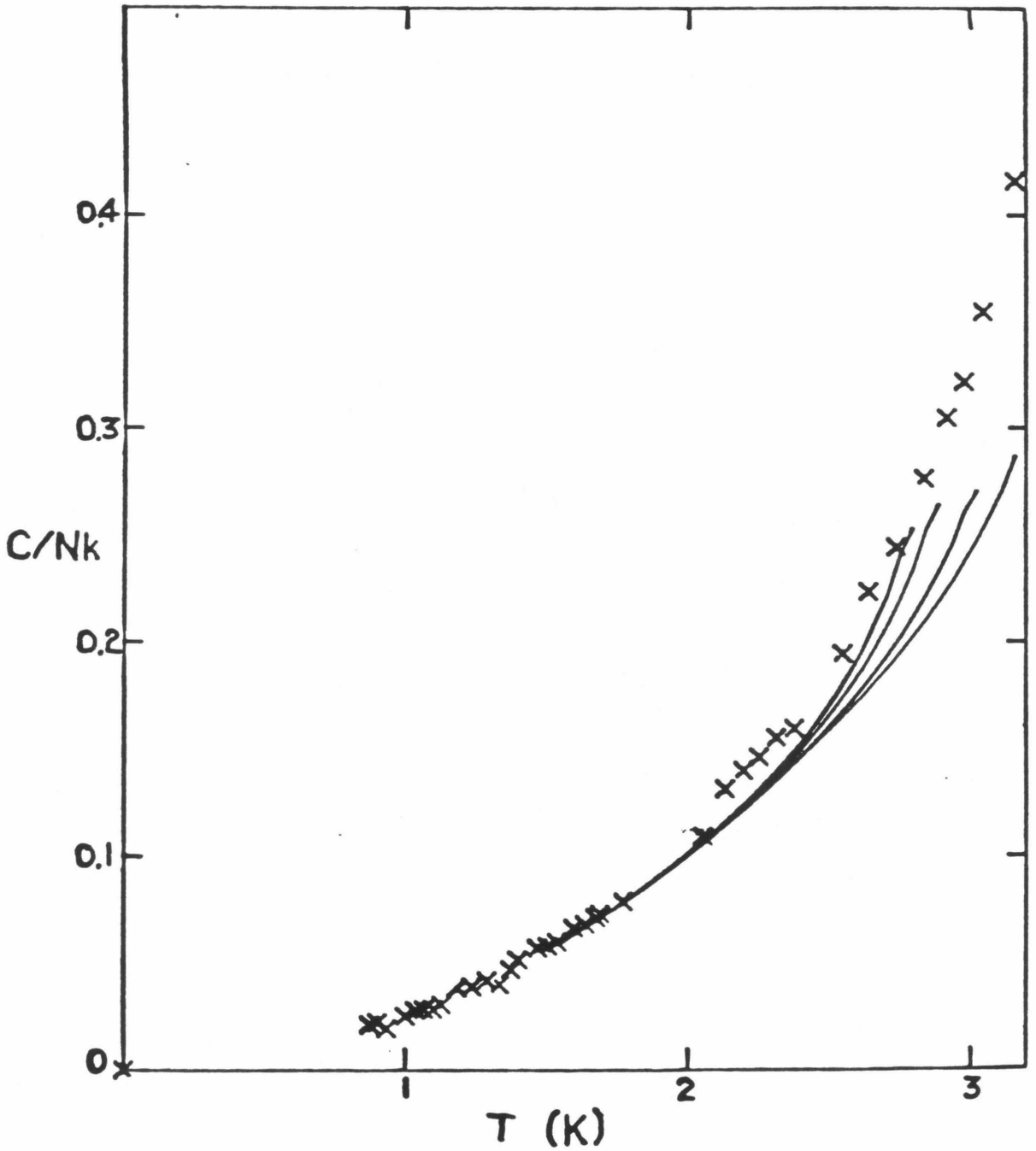

mental heat capacity near the registry transition by Callaway and Schick using RG methods.[17,18] Since the same work yields a standard deviation of the platelet size distribution of 106Å, we might expect to see considerable smearing of the heat capacity from different platelets. Figure 4.16 shows the calculated results for several platelet sizes, taken by cutting off the RG integrals at the appropriate scale and taking an appropriate lower limit of mode sums involved in the Debye law and the phonon interpolation formula. These results are surprising -- that near the transition temperature, the size of the crystal in computing the heat capacity does not matter until the size gets smaller than 40 lattice spacings. These are relatively crude estimates of the size effects, since they do not take into account any boundary effects; nonetheless, the scale of the variation in the heat capacity as function of platelet size is probably correct in order of magnitude, at least. Notice also, that the calculated heat capacity rises less steeply and at a higher temperature, the smaller the platelet size.

It is very difficult to draw definite conclusions about these results. It is probably fair to say that the theory does not account for the experimental heat capacity, but do the differences arise from experimental problems (platelet size variation and substrate inhomogeneity) or from some defect of the theory? If the latter, is the defect so fundamental as to invalidate the dislocation unbinding mechanism in this system, or is there some approximation (for example, assuming the system to be a classical elastic continuum) which is overextended for this system, but only causes the theory to lose quantitative predictive power in this case, while retaining validity as a qualitative description of the melting?

Unfortunately, even these vaguer questions are not precisely answerable either. Certainly, the heat capacity produced by the theory can be made, by suitable choice of core parameter, to resemble the data in that it rises steeply in a narrow range of temperatures near the melting transition. The rise must of

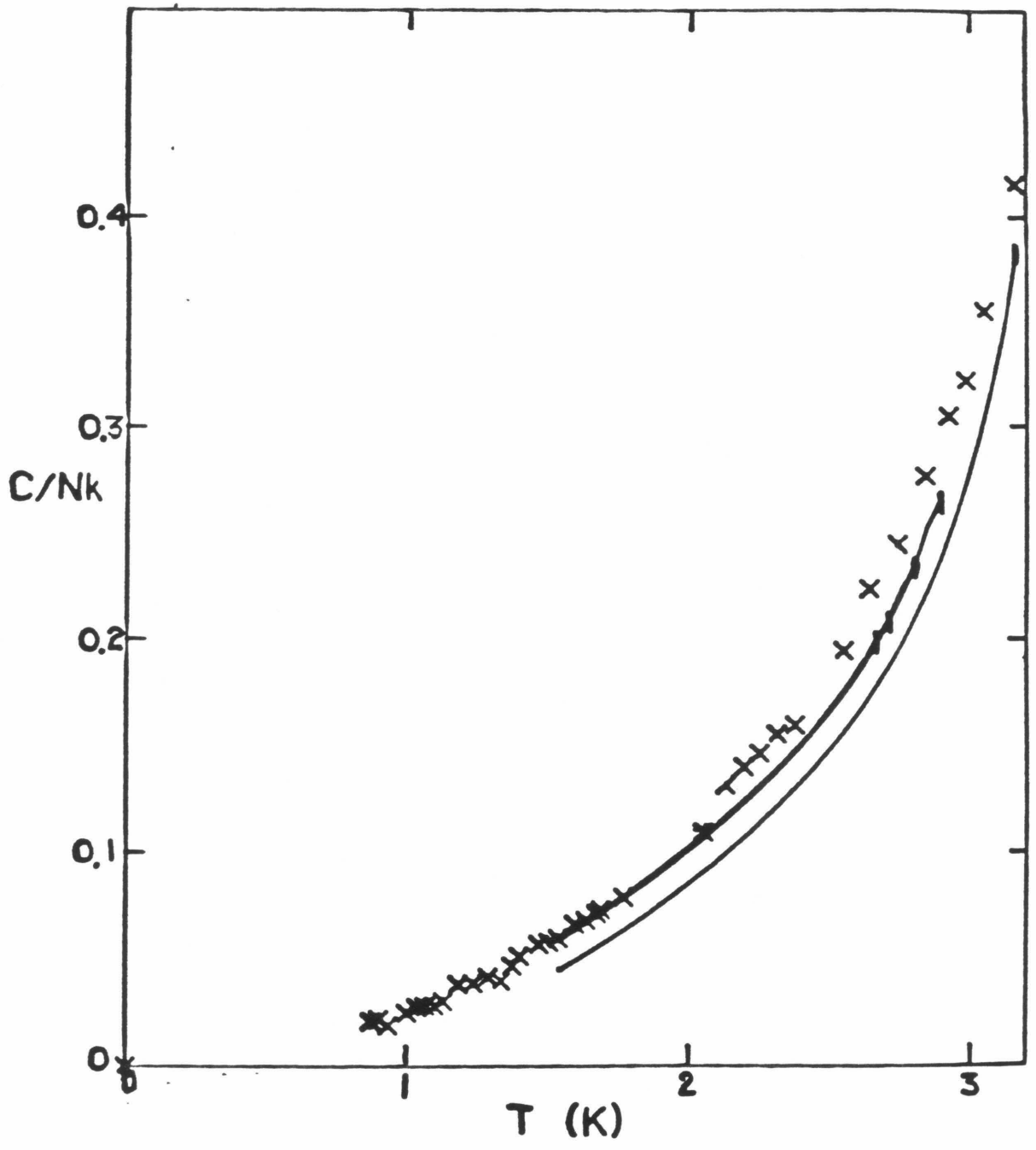

Figure 4.16. Heat capacity vs. T at fixed coverage ($.092 Å^{-2}$) γ=.13 and core parameter 2.4 for ^{3}He for several values of size. The lower curve is for a platelet size of 10 lattice spacings, the upper curve is actually 4 curves essentially unresolved whose endpoints correspond to the effective melting temperature for patch sizes (from right to left, 40, 100, 300, 1000 lattice spacings.

course reverse somewhere, since even if there is no other mechanism, once the dislocation density approaches the atomic density, no more can be created, so the temperature will rise faster for a constant heat input.

However, the calculations always rise much faster than the data above the transition and they are designed to underestimate the heat capacity. By making the core parameter big enough, the exponential rise of the calculations can be pushed to higher and higher temperatures until the calculated heat capacity does not exceed the experimental heat capacity at any temperature at which this method still works, but then the shape of the calculated curve is vastly different from the experimental one. The fact that the core energies are 4-6 times bigger than the classical Lennard-Jones value and 2-4 times bigger than other calculated values is mysterious, but no one knows what the core energy in a quantum solid should be. It is also disturbing that in changing the coverage by about 10%, the optimum core parameter changes by about 25%, but this could be a feature of the rapidly-changing role of correlated zero-point motions in the quantum solid as a function of density.

The experimental difficulties are also only partially characterized. The effect of the periodic substrate can be small or large depending critically on the distance between the substrate and the solid layer (see chapter 5), and our calculation has been carried out using values of the twist elastic constant γ determined in chapter 5 by the distance value at the center of the experimental error bars. We have only crude estimates of the effect of the platelet distribution neglecting the very important effects of boundaries, including image strain fields, and pinning behavior.

How might the true dynamic phonon-dislocation coupling be introduced into the problem?

We recall that the strains or displacements of the atoms can be

decomposed into two components, one arising from the singular dislocation strain fields and the other from the phonon strains. If dislocations are allowed to move in the crystal, this is equivalent to saying that the atomic momenta can also be decomposed into contributions from the oscillatory motion and the motion of the dislocations. We do not know if the decomposition is unique, but on physical grounds guess that it might well be. Now the kinetic energy does not just make a trivial contribution to the internal energy of $\frac{1}{2}k_B T$ per momentum coordinate, but just as for the displacements, there is an extra contribution from the dislocation motion. The problem is actually extremely complicated, since the dislocations are essentially only free to jitter slightly about their sites on the lattice unless the stresses become large enough so they can hop from site to site as explained in section 2. Also there are complications that motions perpendicular to the Burgers vector can only occur in large energy fluctuations, since vacancies and interstitials must be created or absorbed. Thus the elements of a pair do not in general spontaneously annihilate each other, but persist for long periods without having to orbit each other the way the charges in positronium do. It is not likely that quantitative statistical mechanics calculations involving interactions between thermal phonons and dislocations in a real crystal will be available in the near future, and presumably we will have to rely on the calculations which have been performed on dislocations in continua.[19,20] We have not, despite some effort, made significant progress toward elucidating this aspect of dislocation motion in melting.

We close this chapter with a speculation on the possible cause of the heat capacity peak. One tentative explanation of the peak as a saturation effect of filling up the crystal with dislocations has been mentioned above. Another possibility is suggested by NH. They point out that even after the dislocations unbind, the material still has some quasi-long-range order in orientation of the bonds

between atoms, that correlation functions of these orientations decay algebraically with distance above the melting transition, which implies a liquid-crystal order. If the substrate is smooth, at high enough temperature there must be a transition to a true liquid, for which angular correlations decay exponentially. If the substrate is periodic and has the same symmetry as the adsorbate, it imposes long-range orientational order to infinite temperature, so there need be no second transition, although the order gets weaker and weaker as the temperature increases. However, we have shown in chapter 5 that substrate locks the adsorbate at an angle of about ±20° (depending on coverage) from alignment of symmetry axes. Thus there are two equivalent orientations that are favored (and a small continuous variation of energy between them), so the possibility exists for an Ising-like transition between a system of large domains with one or the other preferred orientation (ferrooriented), to one in which the orientation of individual bonds or small groups of bonds was randomly either of the preferred ones (paraoriented). This transition would produce a heat capacity peak, but probably only a small one. We do not know how to estimate this effect, and in any case, it would be superimposed on the dislocation behavior. Some dynamical experiments on ^{3}He using neutron scattering,[21] and nuclear magnetic resonance[22] have claimed to detect anomalies near the heat capacity peak temperatures but the interpretation of these experiments is far from clear.

Nelson and Halperin predict that the mechanism of the breakup or weakening of orientational order is another topological one, namely the unbinding of pairs of disclinations. A disclination in a triangular lattice is a rotational distortion of very high energy made by adding to or removing from the crystal a single atom, producing one 5- or 7-fold coordinated atom somewhere, and then letting the crystal relax. This is not the same as a vacancy or interstitial, which can be regarded as dislocation pairs whose elements are separated by two lattice spac-

ings. In fact, looking at the configuration of a single dislocation in a triangular lattice, one sees at the center one 5-fold and one 7-fold coordinated atom, so a single dislocation is a disclination dipole. NH predict that at some temperature these dipoles will unbind (unless some other mechanism preempts the transition, or in the case of the periodic substrate, suppresses it) by a similar mechanism to dislocation unbinding, and destroy the liquid-crystal order. They map the problem onto the scalar Coulomb gas problem solved by Kosterlitz for vortices in a 2-D superfluid, and carry through the results from there. It is this transition that is suppressed by the periodic substrate, and this one which could in principle be superseded by an Ising-like transition. Considerably more experimental and theoretical work is needed to determine whether the heat capacity peak is sharp enough (after inhomogeneities have been deconvolved) to be a phase transition and to determine the mechanism for it.

Acknowledgments

The author thanks S. Koonin, L. Yaffe and S. Wolfram for productive discussions and D. Nelson for illuminating correspondence. Some of the work reported here was assisted by the SMP program for computer algebra.

References

1. J. M. Kosterlitz and D. J. Thouless, *J. Phys.* **C6**, 1181(1973).
2. D. R. Nelson and B. I. Halperin, *Phys. Rev.* **B19**, 2457(1979).
3. A. P. Young, *Phys. Rev.* **B19**, 1855(1979).
4. J. Friedel, *Dislocations* (Pergamon Press, Oxford, 1964).
5. F. R. N. Nabarro, *Theory of Dislocations* (Clarendon, Oxford, 1967).
6. , *Dislocations in Solids* (North-Holland , New York, 1979) a recent 5-volume set of review papers..

7. L. D. Landau and E. M. Lifshitz, *Theory of Elasticity* (Pergamon Press, New York, 1970) 2nd. ed..

8. I. Kovács and I. Zsoldos, *Dislocations and Plastic Deformation* (Pergamon Press, New York, 1973).

9. A. Englert and H. Tompa, *J. Phys. Chem. Solids* **21**, 306(1961).

10. S. K. Ma, *Modern Theory of Critical Phenomena* (W. A. Benjamin, Inc., Reading, MA., 1976) and references cited there..

11. D. C. Wallace, *Thermodynamics of Crystals* (McGraw-Hill, New York, 1972).

12. J. M. Kosterlitz, *J. Phys.* **C7**, 1046(1974).

13. D. Forster, *Hydrodynamic Fluctuations, Broken Symmetry, and Correlation Functions* (W. A. Benjamin, Inc., Reading, Mass., 1975).

14. A. L. Fetter and J. D. Walecka, *Quantum Mechanics of Many-Particle Systems* (McGraw-Hill , New York, 1971).

15. D. J. Bergmann and B. I. Halperin, *Phys. Rev.* **B13**, 2145(1976).

16. D. R. Nelson, private communication.

17. D. Callaway and M. Schick, *Phys. Rev.* **B23**, 3494(1981).

18. D. Callaway and M. Schick, in *Ordering in Two Dimensions*, ed. S. Sinha, (North-Holland, New York, 1980).

19. J. Kiusalaas and T. Mura, *Phil. Mag.* **9**, 1(1963).

20. A. N. Stroh, *Phys. Rev.* **128**, 55(1962).

21. H. J. Lauter, H. Wiechert, and R. Feile, in *Ordering in Two Dimensions*, ed. S. Sinha, (North-Holland, New York, 1980).

22. A. Widom, J. R. Owers-Bradley, and M. G. Richards, *Phys. Rev. Lett.* **43**, 1340(1979).

Chapter 5 Orientational Ordering in Incommensurate Solid Helium Monolayers on Graphite

Note

Most of the contents of this chapter is an amplification of a published paper,[1] so there is an unavoidable overlap with material discussed in other parts of this thesis.

1. Introduction

Certain adsorbates, such as helium, neon and argon, are known to form incommensurate solid phases when adsorbed at appropriate temperatures and densities on graphite substrates. Novaco and McTague[2,3] predicted that although such adsorbate lattices could translate freely over the substrate without change in free energy, in equilibrium there would be preferred orientations with respect to the substrate. They estimated the angle for argon and the other heavy rare gas elements assuming them to be classical harmonic solids. Novaco[4] revised the theory of this effect to account for quantum behavior and obtained the small quantum corrections to the argon alignment angle.

In this chapter, we present similar predictions for the quantum systems ^{3}He and ^{4}He. It is found that the helium lattice prefers to be misaligned by about 17-25° (depending upon coverage) from the corresponding crystal axis in the substrate. We also present calculations of an elastic constant γ, which measures the restoring force against departures from that alignment.

Aside from their intrinsic interest, the results presented here are important because they may govern the qualitative nature of the melting transition in these monolayer solids. Nelson and Halperin[5] have presented a detailed theory of the melting of the two-dimensional (2D) solid by means of dislocation unbinding, in which γ plays a crucial role. According to the theory, if the substrate were smooth (i.e. $\gamma = 0$), melting would proceed in two steps, from solid into a liquid-crystal-like "hexatic" phase, then into a fluid. By contrast, on a periodic substrate, the second transition is not expected, because the substrate imposes long range orientational order at all temperatures if the adsorbate and substrate have the same symmetry. However, it may be replaced by a qualitatively different kind of transition with an Ising-like character, with two degenerate misalignment angles providing the two states of the Ising system. [6] In chapter 4 of this thesis we analyze the melting of He monolayers, making use of the results presented here.

The misalignment of axes between the film and substrate results from distortions (static density waves or SDW) in the adsorbate as adsorbate atoms seek more favorable positions in the periodic potential wells of the substrate. These changes of position are resisted by the elastic interaction of adsorbate atoms, and a new equilibrium configuration balancing the competing effects is achieved.

For quantum adsorbates, like helium, the size of the distortions produced by the substrate is greatly reduced owing to zero-point motion. Since each adsorbate atom samples in its motion large regions of varying substrate potential, even if there were no interactions between adatoms, an adatom moving from the least to most favorable spot on the substrate would gain an energy less than the difference in potential at those spots. By treating the phonons of the adsorbate self-consistently, it is possible to take account of this effect.[4]

Thus, the calculation requires detailed knowledge of the corrugations of the

substrate potential, and the phonon spectrum of the adsorbate (in order that the balance of substrate force and elastic response can be found). The corrections from zero-point motion also depend on the adsorbate phonon spectrum. We derive this spectrum from an effective potential determined by the experimental values of the elastic constants of the He monolayer films. The substrate potential has become known through recent advances which have made the He-graphite interaction one of the best understood phenomena in surface physics,[7] and we make extensive use of those results.

The calculation leads to curves of energy versus orientation angle for the system at 0K. An example at a typical density is shown in figure 5.1 The minimum in the curve gives the preferred orientation and the curvature around the minimum (divided by 4) yields γ. In the following sections, we describe in detail how the calculation is performed, pointing out the ways in which the extensive experimental data on helium on graphite make it possible to obtain reliable results using simpler, more phenomenological approaches than were needed for argon, and we describe and discuss the results.

In section 2 we discuss the nature of incommensurate and commensurate phases, the physical origin of orientational ordering, and an outline of Novaco's theory of the effect. The next two sections describe the ingredients of our phenomenological calculation of the orientational ordering. In section 3 we present our description of the elastic properties of the adsorbate. In section 4 the helium-graphite potential is discussed. In section 5 we describe an iterative computation of the static density wave distortions and energy using the elements of sections III and IV. In section 6 we present and discuss the results.

2. Origin of Orientational Ordering

The peculiar orientational ordering studied in this chapter only occurs for an incommensurate 2-D solid. The strict definition of incommensurability, that

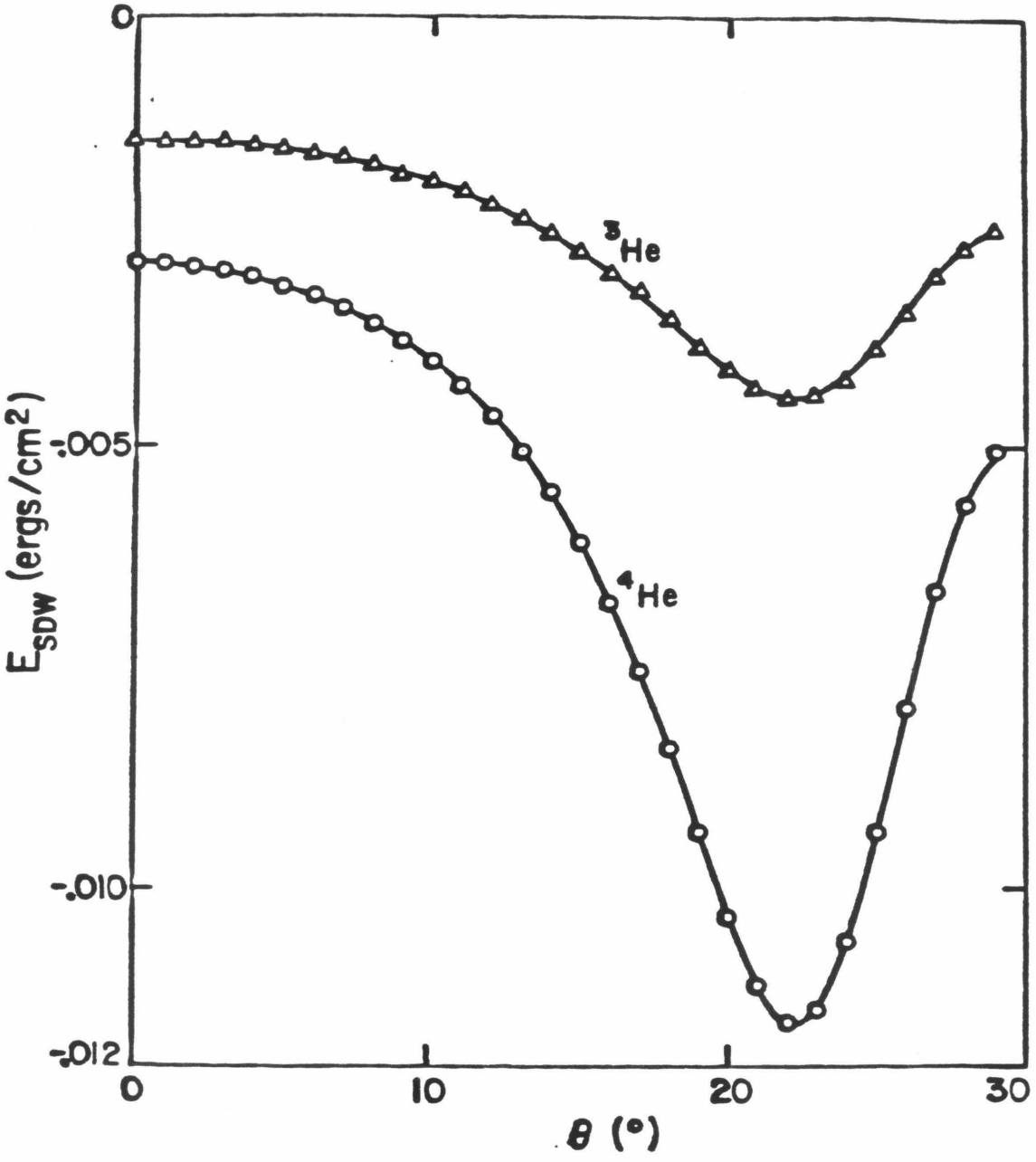

Figure 5.1 Static density wave energy versus relative angle of ^{3}He and ^{4}He adsorbed on graphite at a density of .092 Å^{-2}. The calculation is done using equations 12 and 13 assuming the distance of the adsorbate from the substrate to be 2.85 Å for ^{4}He and 2.89 Å for ^{3}He.

the ratio of unit cell areas of adsorbate and substrate be an irrational number, cannot be satisfied by every film in the continuous range of densities covered in this study, yet, as we will now argue, all the films can be expected to behave like incommensurate solids, except above the melting temperature and at extremely low temperatures. The strict definition is, in any case, a sort of red herring, since any irrational number is arbitrarily close to some rational number. It might be wondered why registry is not observed at or arbitrarily near any physical density. The solution of these questions can be understood by considering the energetics and thermodynamics of the transition to registry from a density close to a registered density. The details of the commensurate-incommensurate transition are quite complicated and just beginning to be understood, but the central arguments are clear.

While any film density is arbitrarily close to a rational multiple of the substrate density (in this discussion only, density refers to ratio of unit cell areas of substrate to adsorbate), the forces tending to produce registry at that rational multiple are quite weak, except in special cases. When the density is not a ratio of small whole numbers, only a small percentage of the adsorbed atoms actually lock in substrate wells, and many of the others are in unfavorable positions, as can be seen from the two 1-D examples of atoms registered at 2/3 and 3/5 density shown in figure 5.2.

It is clear that as long as the potential is purely sinusoidal, the average energy is independent of the relative position of the two lattices, except for exact submultiples $1/n$ of the substrate density. This is only true if the adsorbate lattice is rigid, since from figure 5.2 it is clear that if the unfavorably located atoms shift their positions downward into the wells, thus changing the lattice constant of the adsorbate, the potential energy of the system is lower than in the configuration shown, even when the increased repulsion between

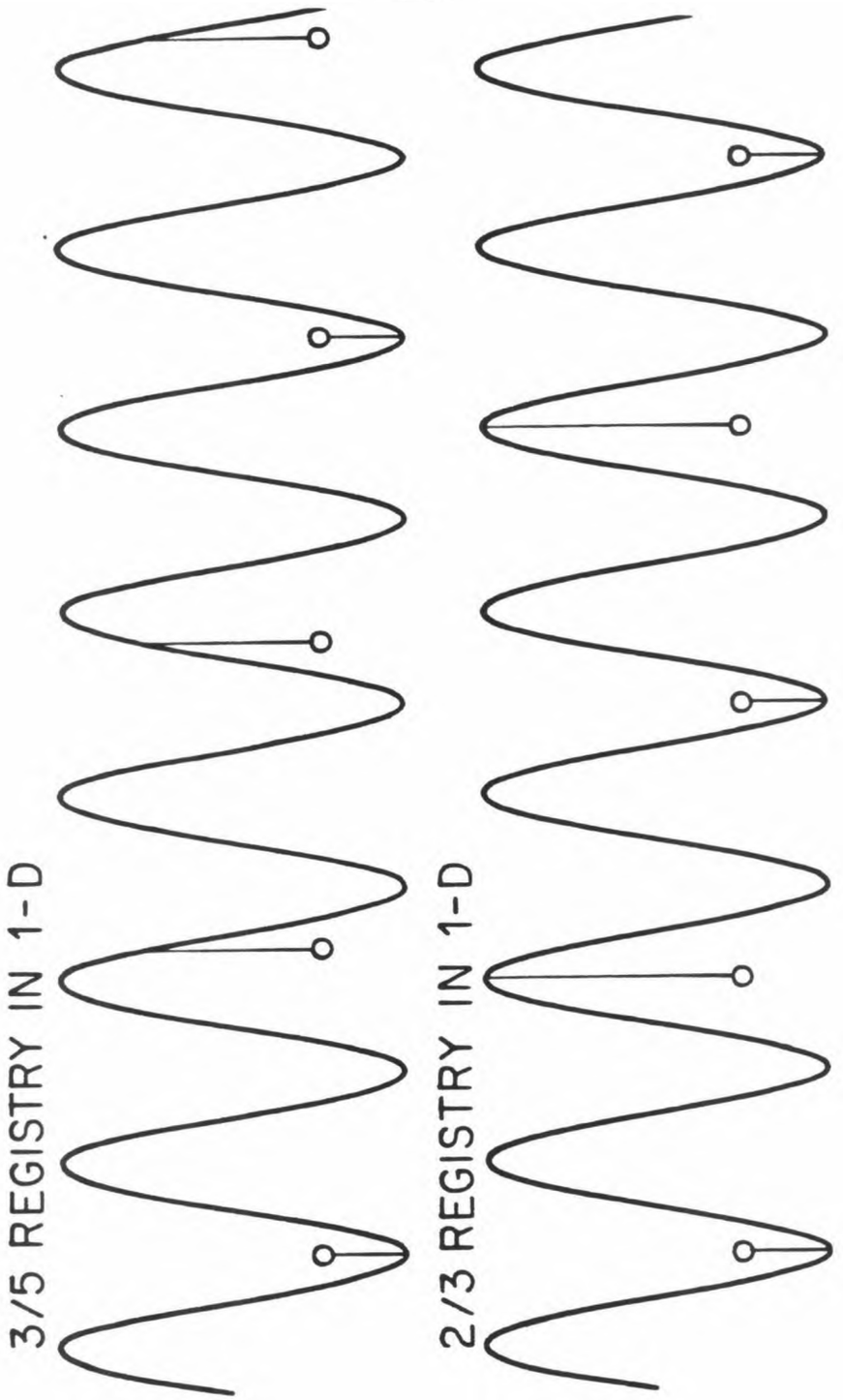

Figure 5.2. Schematic picture of a rigid chain of atoms in registry at 2/3 density (top) and 3/5 density (bottom) in a one-dimensional sinusoidal potential.

adsorbate atoms is taken into account. There must be a point of stable force balance. Similar distortions of the lattice occur when the material is not registered but is at a commensurate density. The difference in energy between the registered and "floating" states is determined by the energy gain of the locked atoms (the ones whose positions at the bottom of substrate wells) are not changed in the distortion, and clearly decreases as the ratio of the number of those atoms to the total number decreases, i.e., as the density ratio becomes the ratio of larger and larger integers.

Any marginal improvement depends on the amplitude of the m-th Fourier component of the substrate potential (for a density m/n). That is, the first Fourier components of the substrate potential that have minima at the positions of the atoms marked in figure 5.2 are the second and third, respectively. For the graphite substrate of interest here, table 5.2 shows that the substrate Fourier components decrease extremely rapidly with wavevector. It must also be pointed out that the distortions produced by the different Fourier components of the potential will often counteract each other partially, and the net effect depends upon the particular density ratio and the relative amplitudes of those components.

A film with a truly incommensurate density, say $1/\sqrt{2}$, can be pulled into registry by one of several mechanisms:

1. The coexistence of two registered phases, one at higher and one at lower density, or the coexistence of a commensurate and incommensurate phase.

2. The breakup of the surface into domains of registered phase with various possible kinds of boundary. The registered phase usually can take several different positions on the crystal -- i.e., several different superlattices are possible. As an example of this, shown in figure 5.3, consider the 1/3 registry on graphite -- one adatom for each 3 graphite hexagons -- which has three possible superlattices.

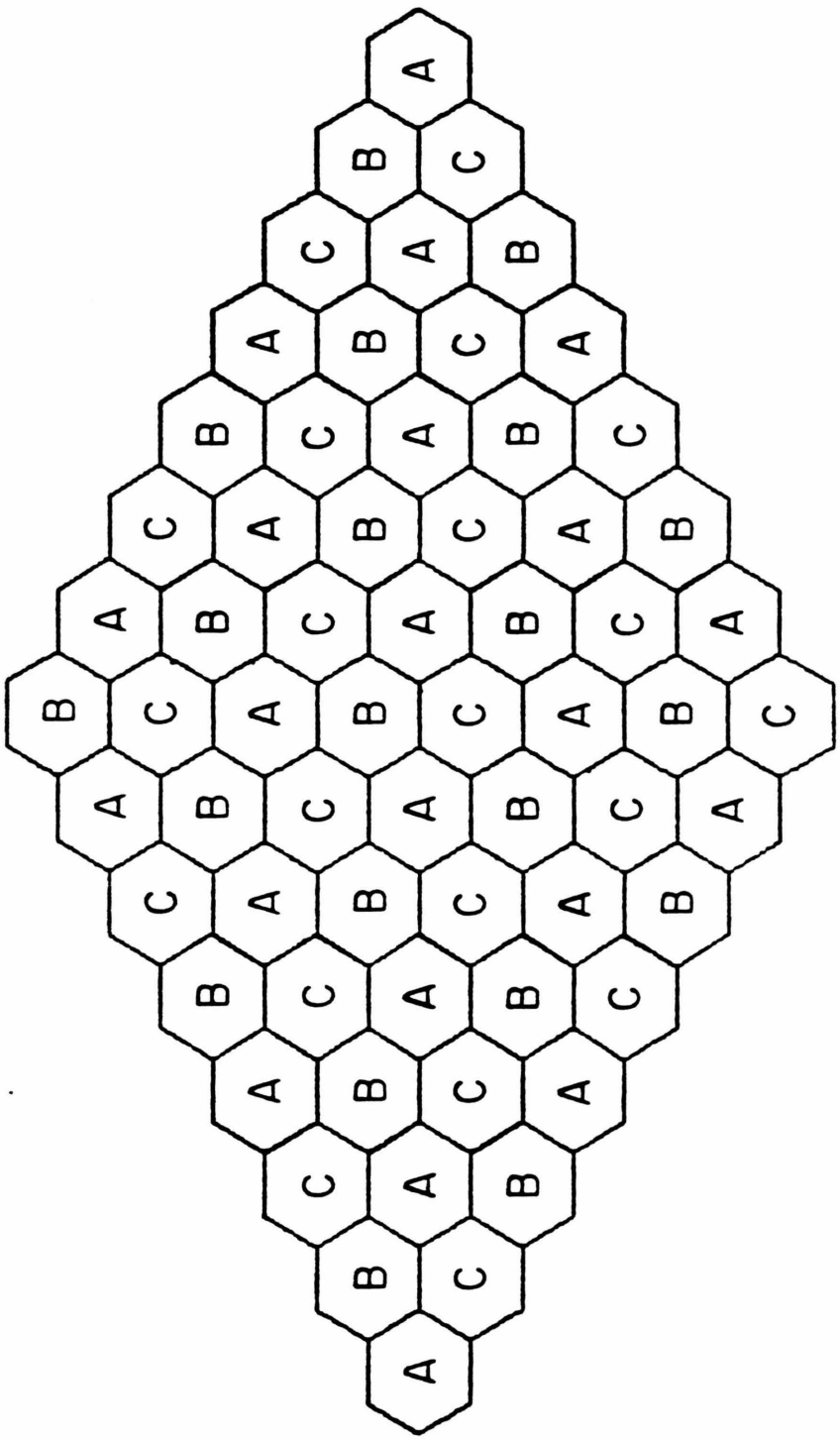

Figure 5.3. Schematic picture of basal plane surface of graphite (with one carbon atom at each hexagon vertex) and three possible superlattices for a registered phase at density 1/3.

Regions of the crystal where one superlattice is occupied can be abutted with regions of occupation of one of the others, with some kind of unregistered boundary of higher or lower density between them. Domain structures observed include stripes, hexagonal domains, and irregular honeycomb structures all of whose walls are parallel to one of the six symmetry directions but have irregular lengths.[8] The domain walls can be regarded as collections of defects, patches of incommensurate phase or in several other ways.

The phase boundaries clearly must have higher free energy than the uniform incommensurate material, so the transition to the registered state will only occur if there is a significant lowering of the free energy of the registered portions of the film, i.e. if the appropriate Fourier components of the substrate potential are large enough. Also, the difference between the registry density and the initial density is important, since the smaller that difference, the smaller the irregular regions of the surface (the shorter the length of domain wall or phase boundary) needed to fit all the atoms onto the substrate. Thus, for a $1/\sqrt{2}$ film, we would expect that a 100/141 registry would be more likely than a 10/14 registry because the former is closer to actual density; yet, we would expect neither to be very likely because neither the 100th or the 5th harmonic (10/14 = 5/7) of the fundamental substrate corrugation should have large amplitude.

Steric considerations and the strength of the adsorbate-adsorbate interaction are also important. Helium, for instance, cannot form a monolayer on graphite at $1/\sqrt{2}$ density because some atoms are squeezed off the surface into the second layer. Also, the 2-D case is more complicated than the 1-D case since the substrate symmetry is important. It is readily apparent from figure 5.3 that 1/3 is a highly favorable registry on graphite, while it is impossible to produce a uniform triangular lattice at density 1/2 for which every atom is in a substrate well.

Despite the weakness of the registering forces on the adsorbed atoms at all but a few very special densities, every commensurate component of the potential produces an infinite energy gain if the adsorbate atoms lock into substrate wells. Thus every harmonic of the potential will register a narrow band of densities at $T=0$, and there will be no incommensurate solid. What happens at finite temperature?

The relevant quantities at finite temperature are the free energies of the registered and unregistered phases which depend on both the energy and entropy. Ignoring the thermal motions, the energy of the registered phase is independent of temperature, as is the entropy (given by the number of possible superlattices times the number of atoms, i.e. also infinite). The free energy can thus be written for the registered phase (that is the locked adsorbate)

$$F_{REG}=-N\delta V-Nk_B T\ln l \qquad (5.1)$$

where N is the number of atoms in the adsorbate, δV the energy difference between the registered and floating potential energy, per atom, k_B Boltzmann's constant and l the number of superlattices. The contribution of each Fourier component of the potential to δV is proportional to nV_n/m, where numerator of the density ratio is m, For the unregistered phase (that is, the same adsorbate in arbitrary position with respect to the symmetry point of the substrate, but possibly still locked at a preferred angle), the average energy is zero but the entropy is much larger (and not easy to calculate).

We can roughly estimate the transition temperature for a particular registered density (ignoring the effects of nearby registries) by equating the potential energy gain of the registered state (per atom) with $k_B T$. Presumably at this point, the thermal entropy of the floating state will dominate the potential energy gain of the registered state. This is an overestimate, since we have ignored the effects of nearby registries (each of which tends to disrupt the

other).

For the particular case of helium on graphite, there is only one corrugation wave vector of importance, the lowest (and its 5 counterparts at multiples of 60°). At the lower densities, the helium film forms a gas in preference to a solid. The 1/3 ordering does occur, and is used as a coverage calibration for comparing data from different laboratories. The ordered phase occurs for a narrow band of densities around 1/3, separate from the denser helium solids discussed in this thesis.

Nelson and Halperin[5] have argued that as the temperature approaches zero, every Fourier component of the substrate potential, no matter how weak, is able to lock the adsorbate in a tiny range of density into registry, and as the temperature decreases, the phase diagram becomes filled with an increasingly complex proliferation of registered and incommensurate phases, but with some kind of registered phase for every density at zero temperature. (Their arguments are made for classical systems, and it is not completely understood what role the strong quantum effects in the helium solids play in this discussion, except that the zero-point motion should reduce the effective strength of any potential corrugation that tries to register the film.)

Our calculation of the orientational ordering at zero Kelvin ignores this registry, for the following reasons. The only necessity for performing the calculation at 0 K is that the sound speeds must be deduced from the Debye temperature, which is a 0 K extrapolation of the low temperature data. However, we do not expect the elastic constants to change significantly at low temperature, nor do we expect to see significant thermal effects on the orientational ordering at extremely low temperature. Thus, we expect our calculation to be accurate at (still low) temperatures above which the registry is destroyed if it is produced by high order substrate potential corrugations, even though we have neglected

the registry energy at lower temperatures.

The sets of reciprocal lattice vectors (hk) are given by $\vec{G}_{hk}=h\vec{G}_{10}+k\vec{G}_{01}$ with $|G_{hk}|^2=(h^2+k^2-hk)G_{01}^2$ for a triangular substrate, and similarly for the adsorbate. Thus, registry is produced for unit cell areas in the ratio $\frac{h^2+k^2-hk}{l^2+m^2-ml}$ and the ones with small (hk) will be the strongest. As we shall show, the strength of the substrate Fourier components in this range is less than .04 of the strength of the fundamental corrugation which is the only one that contributes to the orientational ordering. Furthermore, the zero point motion renormalizes these components to lower values, and the result is that the minimum length corrugation with which the films can be exactly in registry has a renormalized strength 7×10^{-4} times smaller than the primitive substrate corrugation, which produces the 1/3 registered phase that becomes a gas above 3K.

We point out that the physical arguments made here do not agree with the arguments of Nelson and Halperin, whose criterion for the transition between a registered and unregistered solid at the same density is independent of the strength of the substrate potential in the weak-coupling limit.

If the material is not registered, the main effect of the substrate potential is not to tend to lock the film to a particular position with respect to some symmetry point of the substrate, moving each atom an equal amount. Rather, it is to distort the helium lattice in an inhomogeneous way, pulling each atom some distance into the nearest graphite potential well. The size of the distortion is governed by the strength of the elastic forces of the helium crystal which get larger as the atoms are pulled together or pushed apart.

Once again, a classical 1-D model helps to elucidate the nature of the distortion, as in figure 5.4. The atoms are displaced slightly from their undistorted positions, moving just far enough to reach mechanical equilibrium with the elas-

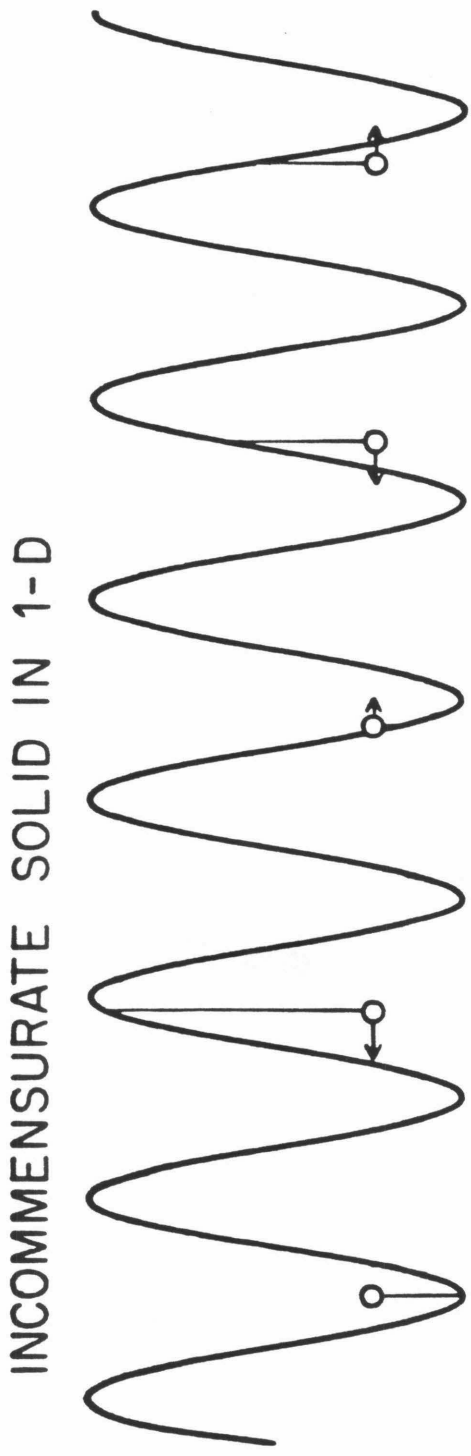

Figure 5.4. Distortions in a one-dimensional linear chain in an incommensurate sinusoidal potential. Atoms are pulled toward the bottom of the nearest well.

tic He-He forces. The substrate potential variation from this particular corrugation component is $V_G e^{-iQx}$ so the force moving the atom is $+iGV_G e^{-iQx}$. If we imagine the atoms to be connected by harmonic springs, the elastic response of the distortion for atom n is $-K(2u_n - u_{n+1} - u_{n-1})$. It is clear that since the forces and responses must be periodic with wave vector $\vec{G}$, the displacements are exactly those that would be produced by a standing wave phonon of the same wave vector at some instant, and the elastic energy is just the phonon potential energy at that instant. Since the corrugation occurs at a wave vector shorter than the He-He spacing, such a phonon is equivalent to (i.e., as far as the He atoms can tell, indistinguishable from) one in the first Brillouin zone of the He -- in figure 5.4, the longer wavelength mode labelled $\vec{q}$, with $\vec{q} = \vec{G} - \vec{\tau}$ and $\vec{\tau}$ a reciprocal lattice vector of the He. The energy change for this distortion is given by

$$E_G(classical\ 1\text{-}D) = -\sum_x (iGV_G u_G - m\omega_q^2 u_G^2/2) \qquad (5.2)$$

where u_G is determined by minimizing this energy with respect to it, or, equivalently, by balancing the forces, and is thus,

$$u_G(classical\ 1\text{-}D) = -i\sum_x GV_G/(m\omega_q^2). \qquad (5.3)$$

The two terms in equation (5.2) are, respectively, the potential energy gained by moving deeper into substrate wells, and that lost by exciting some amplitude of the "static phonon" $\vec{q}$.

The 2-D case is similar but for this important effect: the "static phonon" wave vector $\vec{q}$ has a length and orientation which depends upon the angle between $\vec{G}$ and $\vec{\tau}$ (see figure 5.5). A distortion along $\vec{G}$ can be analyzed into components transverse and parallel to $\vec{q}$, giving the amplitudes of the static transverse and longitudinal phonons excited. (Strictly speaking, the components must be along the polarizations of the $\vec{q}$ phonons even if they are not precisely transverse and longitudinal.)

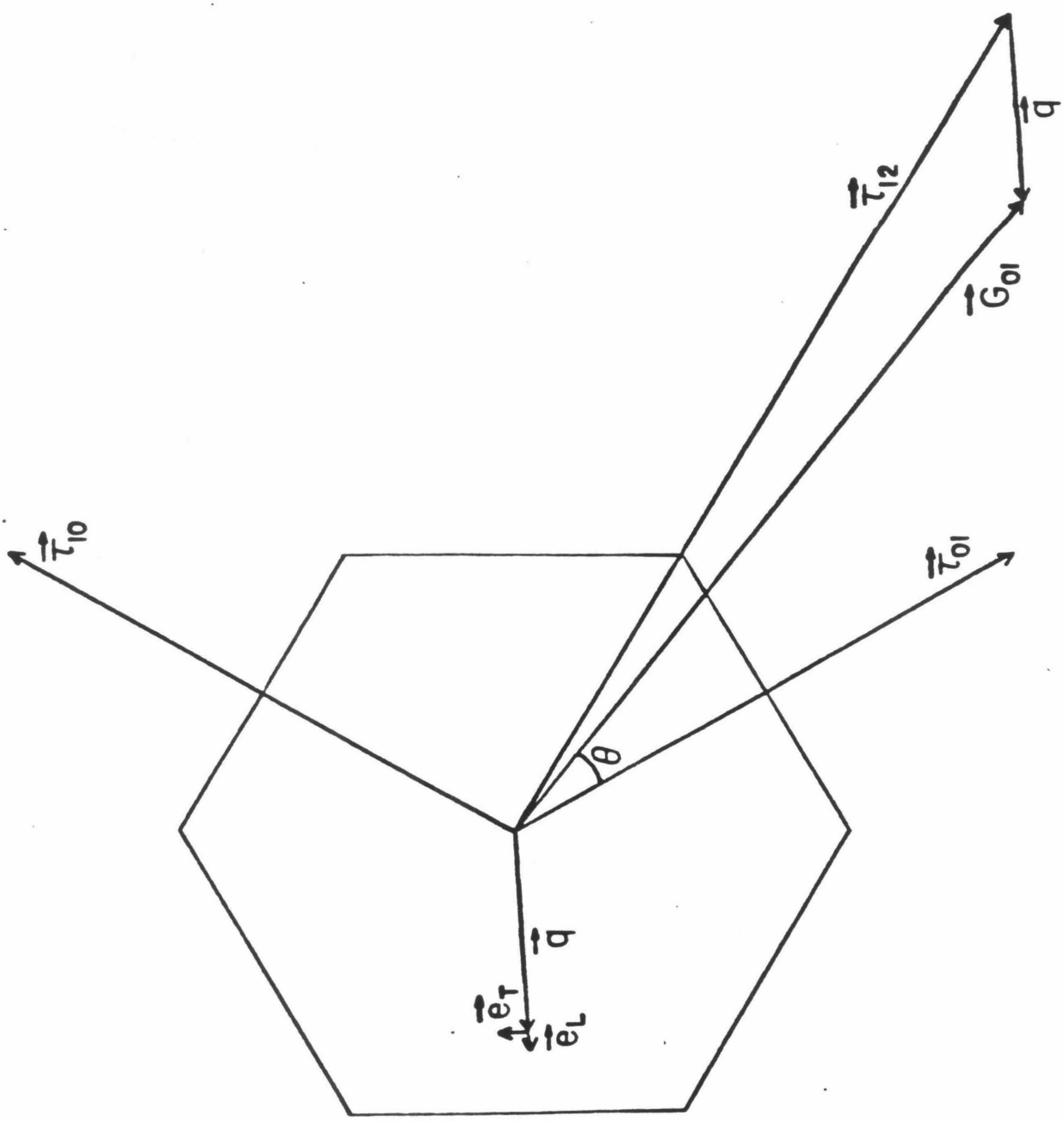
$\vec{\tau}_{12}$
$\vec{q}$
$\vec{G}_{01}$
$\vec{\tau}_{10}$
$\vec{\tau}_{01}$
θ
$\vec{q}$
$\vec{e}_T$
$\vec{e}_L$

Figure 5.5.

Figure 5.5. The geometrical determinants of orientational ordering are shown for the same conditions as in figure 1. The Brillouin zone of the adsorbate, the reciprocal lattice basis vectors $\vec{\tau}_{01}$ and $\vec{\tau}_{10}$ are drawn to scale relative to the substrate primitive reciprocal lattice vector $\vec{G}_{01}$. The adsorbate reciprocal lattice vector $\vec{\tau}_{12}$ is the nearest in magnitude and direction to $\vec{G}_{01}$ for these experimental conditions and when subtracted from $\vec{G}_{01}$ produces the vector q, which is the vector in the first Brillouin zone of the adsorbate which has the same phonon eigenfrequencies and polarizations e_L and e_T as $\vec{G}_{01}$. The angle ϑ is the orientation ordering angle, the angle of the minimum in energy of figure 1. Note that neither $\vec{e}_L \cdot \vec{G}_{01}$ nor $\vec{e}_T \cdot \vec{G}_{01}$ vanishes, so both transverse and longitudinal distortions occur at this angle. Since the Fourier component of the substrate potential with wave vector $\vec{G}_{01}$ produces the only significant contribution to the distortion energy, this figure shows the influence of the geometry almost completely. If $\vec{G}_{01}$ were aligned with $\vec{\tau}_{12}$, the denominator of equation 13 (and hence the distortion energy from longitudinal displacements) would be reduced, but then $\vec{e}_T \cdot \vec{G}_{01}$ would vanish, and there would be no contributions from transverse distortions. The energy minimum occurs at a maximum of $\frac{(\vec{e}_T \cdot \vec{G}_{01})^2}{w_T^2} + \frac{(\vec{e}_L \cdot \vec{G}_{01})^2}{w_L^2}$.

The energy gain depends upon how much of the distorting force is transverse to $\vec{q}$ -- a mostly transverse force is less strongly resisted; thus the distortion is large before mechanical equilibrium is reached, and the energy gain larger. Examination of figure 5.5 makes it clear that the amount of transverse force increases as the angle between $\vec{G}$ and $\vec{\tau}$ is increased; however, at the same time the length of $\vec{q}$ increases, and, except near the zone boundary, this means that the energy of the $\vec{q}$ phonons increase also, so the energy gain and distortion tends to be reduced by this second effect.

Thus, the preferred orientation angle is determined by the balance of two competing effects -- one tending to increase the angle to excite a larger amplitude of the weaker phonon polarization, the other tending to decrease the angle to reduce the energy of the phonons excited, and hence the resistance to strain. As long as the transverse phonons have considerably lower energy than the longitudinal ones, the locking angle will be away from any symmetry direction in the crystal by a finite amount.

From these considerations, the 2-D analogs of equations (5.2) and (5.3) can be readily written down:

$$E_{\vec{G}}(classical\ 2\text{-}D)=\sum_{x}\ (-i\vec{u}_{\vec{G}}\cdot\vec{G}V_{\vec{G}}-\sum_{poll}m\omega_{\vec{q}l}^{2}u_{\vec{G}}^{2}/2) \tag{5.4}$$

$$\vec{u}_{\vec{G}}=-i\sum_{x}\sum_{l}\frac{\vec{e}_{\vec{q}l}\cdot\vec{G}V_{G}\vec{e}_{\vec{q}l}}{m\ \ \omega_{\vec{q}l}^{2}} \tag{5.5}$$

This analysis makes transparent the details of the SDW theory of Novaco, as long as we carefully carry over our arguments to the case of a quantum mechanical adsorbate. The only missing piece is the role played by the zero-point energy.

The major effect of the zero-point motion is to reduce the strength of the distorting potential. Since the distortion is proportional to the strength of the potential, it is reduced by the same factor, and the energy (quadratic in the dis-

tortion) is reduced by the square of that factor. The atoms move over a substantial fraction of the unit cell, so that the advantage of an atom sitting at the bottom of a substrate potential well over one at an unfavorable position is much less than the difference in potential between the two sites, since the first atom spends a substantial fraction of its time in places where the potential is less favorable, and the latter atom spends time in better positions than its average position. This smearing produces a Gaussian renormalization of each substrate Fourier component of the form $e^{-\vec{G}\cdot\mathbf{W}\cdot\vec{G}}$. This smearing factor contains the tensor W which resembles the mean square vibration amplitude of any atom

$$W^{\alpha\beta} = \tfrac{1}{2}\langle \delta u^{\alpha} \delta u^{\beta} \rangle = \frac{1}{2N}\sum_{k,l} e_l^{\alpha}(\vec{k}) e_l^{\beta}(\vec{k}) \frac{\hbar}{m\omega_l(\vec{k})}[n_l(\vec{k})+\tfrac{1}{2}]. \qquad (5.6)$$

where the $\vec{e}_l$ and ω are polarizations and frequencies of the phonons of the undistorted lattice and $n_l(\vec{k})$ is the usual Bose factor (and is zero at 0K where this calculation is done). The summation is over the entire adsorbate Brillouin zone and over all three modes. N is the number of atoms in the adsorbate. Strictly speaking, the phonon frequencies and polarizations used in equation (5.6) should be those of the distorted lattice, but, as Novaco has shown, when the zero-point amplitude is large and the distortion amplitude is small, (which we verify *a posteriori*), the phonon spectrum of the undistorted adsorbate can be used. This is convenient because the undistorted lattice is highly symmetric, and is isotropic at long wavelengths. Since large zero point motion reduces the distortion amplitude, unless the substrate potential has very strong periodic components, the approximation of the spectrum of the distorted lattice by the undistorted one is excellent for quantum systems like He.

Suffice it to say that this effect reduces the size of the distorting potential seen by any atom by a factor of order 8 (and the distortion by the same proportion) from the classical value, and hence the SDW energy and γ by a factor of order 60. There are other, more subtle effects, e.g. a change in the phonon

energies and polarizations when the adsorbate is distorted, but in part owing to the large quantum fluctuations, the distortions are small enough that this effect can be neglected.

3. Theory of Static Density Waves and Orientational Ordering

In this outline of Novaco's theory of static density waves in 2-D incommensurate solids,[4] an attempt is made to convey the essentials of the derivation of the results just reached by physical reasoning.

The approach is to minimize the free energy of the system of film plus film-substrate interactions (the substrate is assumed to be too stiff to be affected by the presence of the film) by a variational calculation in which the variation parameters are the Fourier components of the distortions and the frequencies and polarizations of the phonons of the distorted lattice. The results are the equilibrium values of those quantities. Since the relevant thermal averages are taken over the equilibrium distribution (which depends on the unknown parameters), the results appear as self-consistent equations for those parameters.

Fortunately, in the case of helium on graphite, for which the zero-point and thermal oscillations are large and the distortions small, it is not necessary to solve the self-consistent equations. Instead, the phonon frequencies and polarizations of the undistorted lattice can be used (although they also satisfy self-consistent equations) and the distortions computed as a linear response to the perturbing substrate corrugations, just as has just been done for the classical case. In fact, the only difference between the classical and quantum film in this approximation is that the He-He and He-graphite couplings are both renormalized by the motion of the He atoms, and for the latter, the renormalization of the corrugation at wave vector $\vec{G}$ is through a corresponding Debye-Waller (or smearing) factor $e^{-\vec{G}\cdot\mathbf{W}\cdot\vec{G}}$ discussed earlier, where $\mathbf{W}=\frac{1}{2}\langle\delta u^{\alpha}\delta u^{\beta}\rangle$ is a tensor measuring the mean square displacements of the atoms. The Hamiltonian of the

monolayer is

$$\hat{H}=\frac{1}{2m}\sum_J \hat{p}^2+\hat{\Phi}+\hat{U}$$

where $\hat{\Phi}$ is the He-He potential and $\hat{U}$ the He-graphite potential. Letting R_J^α be components of the undistorted equilibrium position of atom J, $\hat{u}_J^\alpha$ be components of its displacement, we can write

$$\hat{\Phi}=\tfrac{1}{2}\sum_{IJ}\xi_{IJ}\sum_{\text{all }\vec{q}} V_{\vec{q}}\, e^{i\vec{q}\cdot(\vec{R}_I-\vec{R}_J)} e^{iq^\alpha(\hat{u}_I^\alpha-\hat{u}_J^\alpha)}$$

$$\hat{U}=\sum_J\sum_{\vec{G}} U_{\vec{G}}\, e^{(-i\vec{G}\cdot\vec{R}_J)} e^{(-iG^\alpha\hat{u}_J^\alpha)}$$

where $V_{\vec{q}}$ is the Fourier transform of the He-He potential, $U_{\vec{G}}$ the Fourier component of the substrate potential corrugation of wave vector $\vec{G}$. The sum marked *all* $\vec{q}$ means a sum over all q-space rather than over the first Brillouin zone of the undistorted adsorbate.

Phonon creation and annihilation operators can be introduced in the usual way, but the thermal averages of single creation and annihilation operators do not vanish, because the distortion is non-zero. A canonical transformation is made to a representation using new creation and annihilation operators which have the average value (the distortion) subtracted out. If those average values of the original operators are denoted by $\sqrt{N}\,\zeta_{\vec{q}l}=\langle\hat{a}_{\vec{q}l}\rangle$, the Fourier components of the distortion can be written

$$\vec{u}_{\vec{q}}=\sum_l \vec{\varepsilon}_l(\vec{q})\sqrt{\hbar/m\,\omega_l(\vec{q})}\,(\zeta_{\vec{q}l}+\zeta^*_{-\vec{q}l})$$

Since these distortions are standing waves we expect the amplitudes to be real, so the corresponding velocity average $\propto(\ \zeta^*_{\vec{q}l}-\zeta_{-\vec{q}l})$ must vanish in equilibrium and Novaco demonstrates this. In this equation, $\vec{\varepsilon}_l(\vec{q})$ is the polarization vector and $\omega_l(\vec{q})$ the frequency of the phonon of wave vector $\vec{q}$, mode index l. These parameters, along with $\vec{u}_{\vec{q}}$ are to be found.

The free energy is now given by $F=\langle\hat{H}\rangle-TS$, where the average is calcu-

lated by taking diagonal matrix elements in the new phonon basis and the new phonon modes are treated as non-interacting.

The details of the actual variational calculation are tedious and described sufficiently well in Novaco's paper to avoid repeating them here. The variations of F with respect to $n_l(\vec{q})$ produce the usual boson thermal occupation

$$n_l(\vec{q}) = \frac{1}{e^{\beta\hbar\tilde{\omega}_l(\vec{q})}-1}$$

where $\hbar\tilde{\omega}_l(\vec{q}) \equiv \frac{\delta<\hat{H}>}{\delta n_l(\vec{q})}$ and turns out to be equal to $\omega_l(\vec{q})$ when F is varied with respect to $\omega_l(\vec{q})$, as expected. The frequencies and polarizations of the phonons turn out to be given the eigenvalues and eigenvectors of the usual dynamical matrix formed by Fourier transforming the entire potential (He-He plus He-graphite), also as expected. Finally, the variations with respect to $\vec{u}_{\vec{q}}$ are carried out, and since only the potential energy terms depend upon it, the self-consistent equations are

$$\omega_l^2(\vec{q}) = \vec{\varepsilon}_l(\vec{q}) \cdot D(\vec{q}) \cdot \vec{\varepsilon}_l(\vec{q})$$
$$D(\vec{q}) \cdot \vec{\varepsilon}_l(\vec{q}) = \omega_l^2(\vec{q}) \vec{\varepsilon}_l(\vec{q})$$
$$\frac{\delta<\hat{U}>+\delta<\hat{\Phi}>}{\delta u_q^\gamma} = 0$$

with

$$\frac{\delta<\hat{\Phi}>}{\delta u_{\vec{p}}^\gamma} = \frac{i}{2}\sum_{IJ}\xi_{IJ}\sum_{\alpha\beta\vec{q}} V_q q^\gamma e^{i\vec{q}\cdot(\vec{R}_I-\vec{R}_J)} e^{iq^\alpha(\hat{u}_I^\beta-\hat{u}_J^\beta)} e^{(-\frac{1}{2}\vec{q}\cdot\Gamma_{IJ}\cdot\vec{q})} e^{i\vec{q}\cdot(\vec{R}_I-\vec{R}_J)}$$

$$\frac{\delta<\hat{U}>}{\delta u_q^\gamma} = i\sum_J\sum_{\vec{G}} G^\gamma U_{\vec{G}} e^{(i\vec{G}\cdot\vec{R})} e^{(i\vec{G}\cdot<\vec{u}_J>)} e^{(-\vec{G}\cdot W\cdot\vec{G})} e^{(i\vec{q}\cdot\vec{R})}$$

where

$$\Gamma_{IJ}^{\gamma\beta} = 2(<\delta\hat{u}_I^\gamma\delta\hat{u}_I^\beta - \delta\hat{u}_I^\gamma\delta\hat{u}_J^\beta>) = \frac{1}{2N}\sum_{\vec{q},l}\varepsilon_l^\gamma(\vec{q})\varepsilon_l^\beta(\vec{q})\frac{\hbar}{m\omega_l(\vec{q})}[n_l(\vec{q})+\tfrac{1}{2}][1-e^{i\vec{q}\cdot(\vec{R}_I-\vec{R}_J)}].$$

The dynamical matrix $D(\vec{q})$ is the sum of terms arising from the substrate and adatom potentials,

$$D = D_1 + D_2$$

with

$$D_1^{\alpha\beta} = \frac{1}{N}\sum_J \frac{1}{m}\sum_{\vec{G}} -G^\alpha G^\beta U_{\vec{G}} e^{-\vec{G}\cdot W\cdot\vec{G}} e^{i\vec{G}\cdot\langle\vec{u}_J\rangle} e^{(i\vec{G}\cdot\vec{R}_J)}$$

and

$$D_2^{\alpha\beta}(\vec{p}) = \frac{1}{Nm}\sum_{IJ}\xi_{IJ}\sum_{\vec{q}} -q^\alpha q^\beta V_q e^{i\vec{q}\cdot(\vec{R}_I-\vec{R}_J)} e^{iq^\alpha(\hat{u}_I^\beta-\hat{u}_J^\beta)} e^{(-\frac{1}{2}\vec{q}\cdot\Gamma_{IJ}\cdot\vec{q})} e^{i\vec{p}\cdot(\vec{R}_I-\vec{R}_J)}.$$

The equations for the variation of $\langle\hat{\Phi}\rangle$ and $\langle\hat{U}\rangle$ now are approximated (because they are quite complicated) by assuming the distortions to be small, expanding $e^{i\vec{G}\cdot\langle\vec{u}_J\rangle}$ in powers of u, keeping only terms linear in u. In terms of the dynamical matrix in the absence of strains,

$$D_0^{\alpha\beta}(\vec{p}) = \frac{1}{Nm}\sum_{IJ}\xi_{IJ}\sum_{\vec{q}} -q^\alpha q^\beta V_q e^{i\vec{q}\cdot(\vec{R}_I-\vec{R}_J)} e^{(-\frac{1}{2}\vec{q}\cdot\Gamma_{IJ}\cdot\vec{q})}(1-\cos[\vec{q}\cdot(\vec{R}_I-\vec{R}_J)]) \quad (5.7)$$

the approximate forms of the potential variations are

$$\frac{\delta\langle\hat{\Phi}\rangle}{\delta u_{\vec{p}}^\gamma} = NmD_0^{\gamma\beta}(\vec{p})u_{-\vec{q}}^\beta$$

where the term independent of u is zero, and

$$\frac{\delta\langle\hat{U}\rangle}{\delta u_{\vec{q}}^\gamma} = \sum_{\vec{G}} G^\gamma U_{\vec{G}} e^{(-\vec{G}\cdot W\cdot\vec{G})}\delta_{\vec{p},\vec{G}+\vec{q}}$$

where only the term independent of u is retained. In terms of the eigenvalues $\omega_l(\vec{q})$ and eigenvectors $\vec{e}_l(\vec{q})$ of D_0 the variation of $\langle\hat{\Phi}\rangle$ can be rewritten

$$\frac{\delta\langle\hat{\Phi}\rangle}{\delta u_{\vec{p}}^\gamma} = Nm\sum_l e_l^\gamma(\vec{q})\vec{e}_l(\vec{q})\cdot\vec{u}_{-\vec{q}}.$$

The two sum of the potential variations is set equal to 0 producing the solution

$$\langle\vec{u}_J\rangle = i\sum_{\vec{G}} u_{\vec{G}}\sin(\vec{G}\cdot\vec{R})$$

with $\vec{u}_{\vec{G}}$ given by

$$u_{\vec{G}}^\beta = -i\sum_l \frac{e_l^\alpha(\vec{G})U_{\vec{G}}(z)exp(-G^\mu G^\nu W^{\mu\nu})}{m\omega_l^2(\vec{G})}\vec{e}_l(\vec{G})\cdot\vec{G}.$$

To evaluate the strain energy of the distortions, the term $e^{i\vec{p}\cdot(\vec{R}_I-\vec{R}_J)}$ in $\langle\hat{\Phi}\rangle$ is expanded to second order in u and in $\langle\hat{U}\quad\rangle$ is expanded to first order in u, both terms contributing to the energy to second order in $U_{\vec{G}}$, producing the result

$$E_{SDW}(\vartheta) = -\tfrac{1}{2}i\sum_{\vec{G}} U_{\vec{G}}(z)\exp(-G^{\mu}G^{\nu}W^{\mu\nu})G^{\beta}u_{\vec{G}}^{\beta}.$$

plus an additional termnon-zero only for commensurate systems

$$E_{REG}=N\sum_{\vec{G}}\sum_{\vec{\tau}}\delta_{\vec{G},\vec{\tau}}U_{\vec{G}}e^{(-\vec{G}\cdot\vec{r}\cdot\vec{G})}$$

and another term independent of u which gives the usual potential energy associated with the thermal and zero-point phonon motion.

When the substrate-adsorbate potential is purely sinusoidal with wavevector $\vec{G}$ (and its symmetric equivalents), and the wavevector $\vec{q}$ in the first Brillouin zone equivalent to it (see figure 5.5) is sufficiently small in magnitude, the orientational ordering can be discussed in a more illuminating fashion and all the results can be derived analytically. In this case, the sum in equation (5.10) reduces to a single term, the strength of the sinusoidal component of the substrate potential and the smearing factor arising from zero-point motion do not influence the angular dependence, and the phonons appearing in the denominator of eq. (5.13) can be approximated by isotropic sound waves with velocities c_L and c_T.

The substitution of eq. (5.13) in eq. (5.10) under these conditions gives

$$E_{SDW} \propto \frac{-1}{(1+\chi^2-2\chi\cos\vartheta)^2}\left[\frac{(1-\chi\cos\vartheta)^2}{\psi}+(\chi\sin\vartheta)^2\right] \qquad (5.8)$$

where ϑ is the angle between $\vec{G}$ and $\vec{\tau}$ and χ is the ratio of the magnitudes of $\vec{G}$ and $\vec{\tau}$. This ratio varies with coverage as the adsorbate lattice spacing changes and possibly with orientation angle since as the two lattices are rotated with respect to one another, the particular $\vec{\tau}$ needed to reduce $\vec{G}$ to the first Brillouin zone may shift. In eq. (5.8), ψ is $(\frac{c_L^2}{c_T^2})$.

It is clear that for all ϑ for which this particular $\vec{\tau}$ is the closest to $\vec{G}$, all of the angular dependence, including the value of angle producing a minimum in E_{SDW}, is a function only of χ and the ratio of the speeds of sound. Differentiating

eq. (5.8) with respect to ϑ gives an equation for the angle of the minimum energy in terms of these parameters.

$$\cos(\vartheta) = \frac{1+(2\psi-1)\chi^2}{(\psi-1)\chi^3+(\psi+1)\chi} \qquad (5.9)$$

Figure 5.6 shows plots of this angle vs. χ^2 (χ^2 is inversely proportional to the density as long as $\vec{\tau}$ remains the closest adsorbate reciprocal lattice vector to $\vec{G}$) for several values of sound-speed ratio. Note that ϑ in figure 5.5 is measured with respect to $\vec{\tau}_{21}$, the nearest adsorbate reciprocal lattice vector to $\vec{G}$, and this τ is at an angle of 30° to an angle which would bring the two lattices into absolute alignment, so an angle of 5° in figure 5.6, for example, corresponds to one of 25° in figure 5.7. The only known cases of registered helium solids on graphite occur when $\vec{G}_{01}=\vec{\tau}_{21}$ or for ϑ=0 in figure 3 and 4 and for ϑ=30° and coverage of .06366Å^{-2} in the notation of figure 5.7.

The physical content of equations (5.8) and (5.9) can be summarized by the following observations. For a given value of χ, the preferred angle increases as the shear force weakens (ψ increases) but the dependence is weak for most values of χ. For a fixed value of ψ, the angle approaches zero as the lattices approach a particular registry for which χ=1. (There is an additional piece in the energy when the two lattices are commensurate, but it is ignored here.)

The incommensurate helium monolayer solids occur only in density ranges in which the most important Fourier component of the substrate potential, U_{01} (where the subscripts are the Miller indices), is quite different from the nearest $\vec{\tau}$, so the very sharp minima developing as registry is approached are not observed. Even though some other reciprocal lattice vector of the substrate may be close to some reciprocal lattice vector of the adsorbate (i.e. the lattices are nearly in partial registry) the Fourier components of the potential fall off rapidly as the Miller indices increase, and the exponent in the smearing factor is proportional to the square of G, so the effects of these accidental approaches to

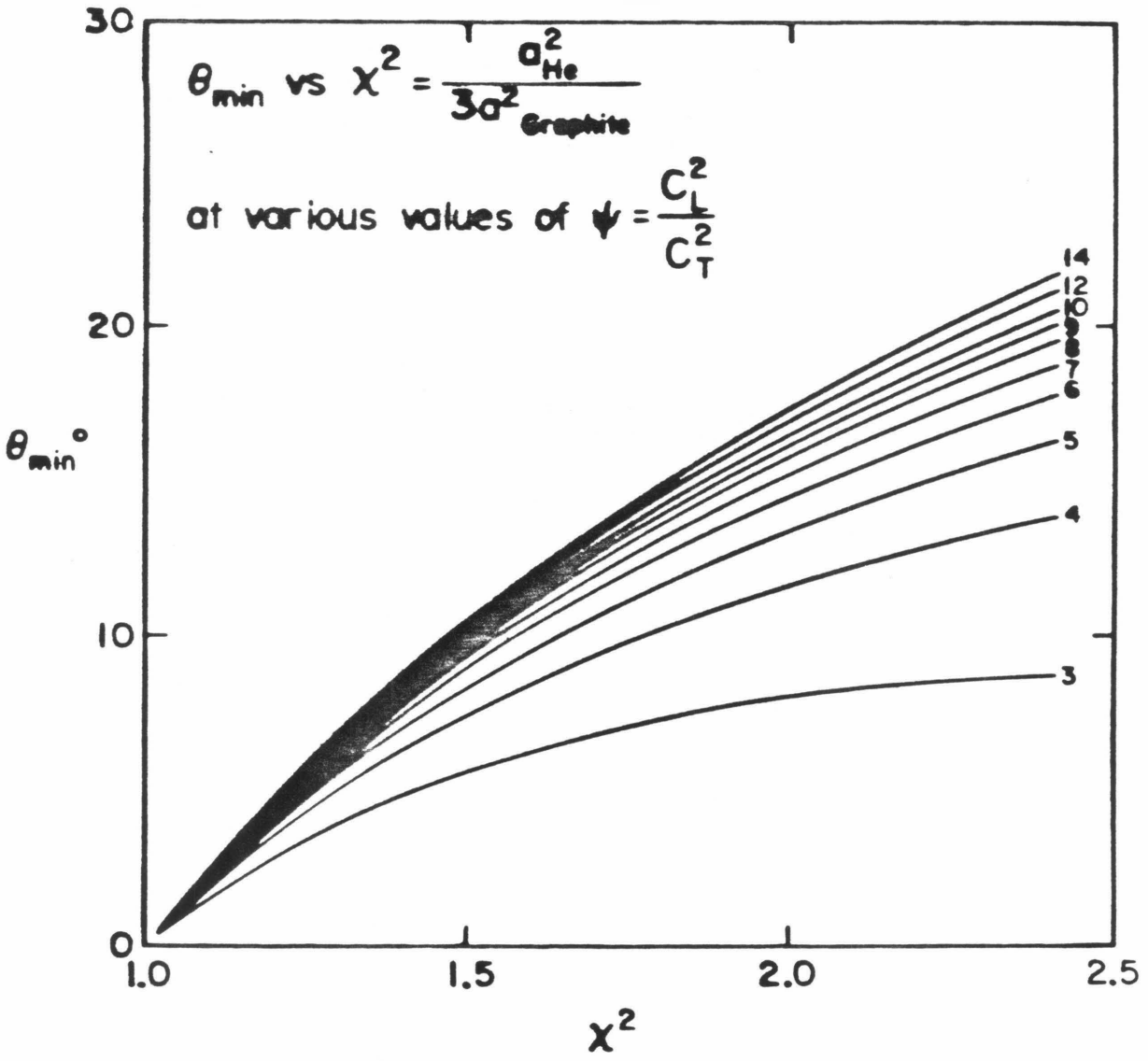

Figure 5.6. Locking angle vs. χ^2 for various values of ψ.

registry are negligible. (The term neglected in these calculations which is nonzero only at exact registry contributes an energy linear instead of quadratic in U_G and in the smearing factor, but is still insignificant except when the unit cell areas of the two lattices are exactly in the ratio of very small whole numbers.)

1. Elastic Properties of the Helium Monolayer

Any theoretical approach to the elastic behavior of helium solids is complicated by the strong quantum effects present. The monolayer solids behave similarly to bulk material in that the harmonic analysis of the solids at the equilibrium spacing produces imaginary frequencies, which become real when the extremely large zero-point motion (which averages the potential over large areas of the unit cell) is taken into account. Furthermore, strong correlations between the atoms in the solid cannot be ignored, for if they were not present, the large amplitude of zero-point motion would frequently carry atoms deep into the repulsive cores of their neighbors. A considerable theoretical machinery known as self-consistent phonon theory[9] has been developed for treating this difficult problem, and has produced useful, but not extremely accurate results. For the bulk solids, this is true despite the accurate knowledge of the He-He potential. In the monolayer, the free space He-He interaction is modified by the dielectric properties of the graphite substrate, and while these modifications have recently been calculated[10] it was decided that a full-blown self-consistent phonon calculation for the monolayer solids would probably be less accurate overall than a phenomenological approach. Since an effective potential arises from a self-consistent calculation in any case, we use an effective He-He potential for the undistorted lattice whose parameters are determined by experimentally derived speeds of sound.

The potential was proposed by Novaco.[11] The essential idea of the approximate spectrum is that since the monolayer solidifies only under 2-D pressure, the elastic properties are predominantly influenced by the repulsive part of the potential. The effective potential is thus taken to be a purely exponential repulsion, $v(r)$, whose first and second derivatives, evaluated at the equilibrium lattice spacing for a nearest-neighbor Born-von Karman calculation are

$$v' = -\frac{v''}{B}(n_0\frac{\sqrt{3}}{2})^{-\frac{1}{2}} \tag{5.10a}$$

$$v'' = M\omega_0^2 e^{B(1-1/\sqrt{n/n_0})} \tag{5.10b}$$

where n is the areal density, n_0 a convenient reference density and B and ω_0^2 are the parameters to be determined from the sound speeds by the equations

$$B = \frac{\sqrt{n/n_0}(3(\frac{c_L^2}{c_T^2}) - 1)}{(\frac{c_L^2}{c_T^2})-3} \tag{5.11a}$$

$$\omega_0^2 = \frac{4}{\sqrt{3}}nc_L^2\frac{e^{-B(1-1/\sqrt{n/n_0})}}{3-\frac{\sqrt{n/n_0}}{B}} \tag{5.11b}$$

Table 5.1 displays the values of the spectral parameters at several densities of both helium isotopes.

The crudeness of this model of the film is compensated by the determination of its parameters entirely by experimental elastic data. By using the experimental data to determine the parameters of the model potential, we effectively do a self-consistent phonon calculation. We also assume that for each 2-D wave vector there are 3 modes, one each transversely and longitudinally polarized in the plane of the adsorbate (at long wavelength) and a third transverse optical mode polarized normal to the substrate at long wavelength, with energy determined by the difference of the lowest excited state of the substrate-He potential and the ground state,[12] 6.24 meV for ^{3}He and 5.70 mev for ^{4}He.

It can be shown[5] that when the substrate and adsorbate attain their

optimum orientation the energy of small deviations (in the plane) from equilibrium can be written

$$H = \tfrac{1}{2} \sum_{atoms} (2\mu u_{ij}^2 + \lambda(u_{ij}\delta_{ij})^2 + \gamma(\partial_j u_i - \partial_i u_j)^2) \qquad (5.12)$$

where μ and λ are the 2-D Lamé constants, u_{ij} are symmetrized displacement gradients, $u_{ij} = \frac{1}{2}(\partial_j u_i + \partial_i u_j)$ in the plane of the adsorbate (Roman *indices signify* 2-D components) and γ is the elastic constant restoring local twists of the adsorbate relative to the substrate. Actually, the initial pressure without which the monolayer solid will not form adds a correction to this equation. If the elastic constants are defined in the conventional way, that is, as the second derivatives of the free energy with respect to strain evaluated at the equilibrium configuration, then the 2-D pressure, φ, can be properly included by replacing λ by $\lambda + \varphi$ and μ by $\mu - \varphi$ in equation (5.12) and adding a term $\sum_{atoms} -\varphi\delta_{ij}u_{ij}$.[13,14]

The sound speeds for waves in the distorted medium are given by[14]

$$\rho c_T^2 = \mu - \varphi + 2\gamma \qquad (5.13a)$$

$$\rho c_L^2 = 2\mu - \varphi + \lambda \qquad (5.13b)$$

for transverse(T) and longitudinal(L) sound, respectively. ρ is the mass per unit area of adsorbate.

The sound speeds are obtained from experimental measurements of heat capacity and chemical potential of the monolayer solids, which yield the Debye temperature Θ_D, the compressibility κ and the spreading pressure φ. For thermodynamic data needed to generate the elastic properties of ^{4}He monolayers see Elgin and Goodstein,[15] and Bretz, *et al.*[16] Data on ^{3}He are contained in Hering, *et al.* [17] and unpublished work of Elgin, Greif and Goodstein. The summary of the elastic theory of helium monolayers is contained in reference (14). Since

$$\Theta_D^2 = \left(\frac{2\pi\hbar}{k_B}\right)^2 \frac{2\rho}{\pi}\left[\frac{1}{c_L^2} + \frac{1}{c_T^2}\right] \qquad (5.14)$$

and

$$\frac{1}{\kappa} = 2\gamma + \rho(c_L^2 - c_T^2) \tag{5.15}$$

the experimental data together with an assumed value of γ allow equations (5.14) and (5.15) to be solved for the sound speeds, which then determine the Lamé constants along with B and ω_0^2. Our procedure is to iteratively refine these parameters and γ simultaneously until a consistent set is found. This is done by guessing a value of γ (usually zero), solving equations (5.14) and (5.15) for the sound speeds, proceeding with the rest of the calculation as described below to obtain a new value of γ, which is then used to generate a new solution of equations (5.14) and (5.15). The procedure eventually converges to a value of γ which does not change from iteration to iteration.

To make use of the elastic properties of the He monolayer, we calculate (for a phonon of wavevector $\vec{q}$) the dynamical matrix, which has eigenvalues equal to the square of the angular frequencies of the 3 phonon modes and normalized eigenvectors along the direction of polarization of these modes. The phonon energies and polarizations are used below to find the size of the distortions and their energies. The dynamical matrix for our model is[11] (using Greek indices for 3-D vector components)

$$D^{\alpha\beta}(\vec{q}) = \omega_p^2 \delta^{\alpha\beta}\delta^{\alpha z} + \frac{1}{M}\sum_{j=1}^{6} \Phi^{\alpha\beta}(R_j)(1 - \cos(\vec{q}\cdot\vec{R}_j)) \tag{5.16}$$

with ω_p representing the vibration frequency of the optical mode at long wavelength. The force constants Φ are given by

$$\Phi^{\alpha\beta}(\vec{R}_j) = v''(\vec{R}_j)\left[\partial_\alpha\eta\,\partial_\beta\eta - \frac{(n_0\frac{\sqrt{3}}{2})^{-\frac{1}{3}}}{B}\partial_\alpha\partial_\beta\eta\right] \tag{5.17}$$

where $\eta^2 = x^2+y^2+z^2$. The dynamical matrix of equation (5.16) is used as an approximation to the undistorted D_0 of equation (5.7). A typical phonon spectrum in the symmetry directions of the adsorbate crystal is shown in figure 5.8.

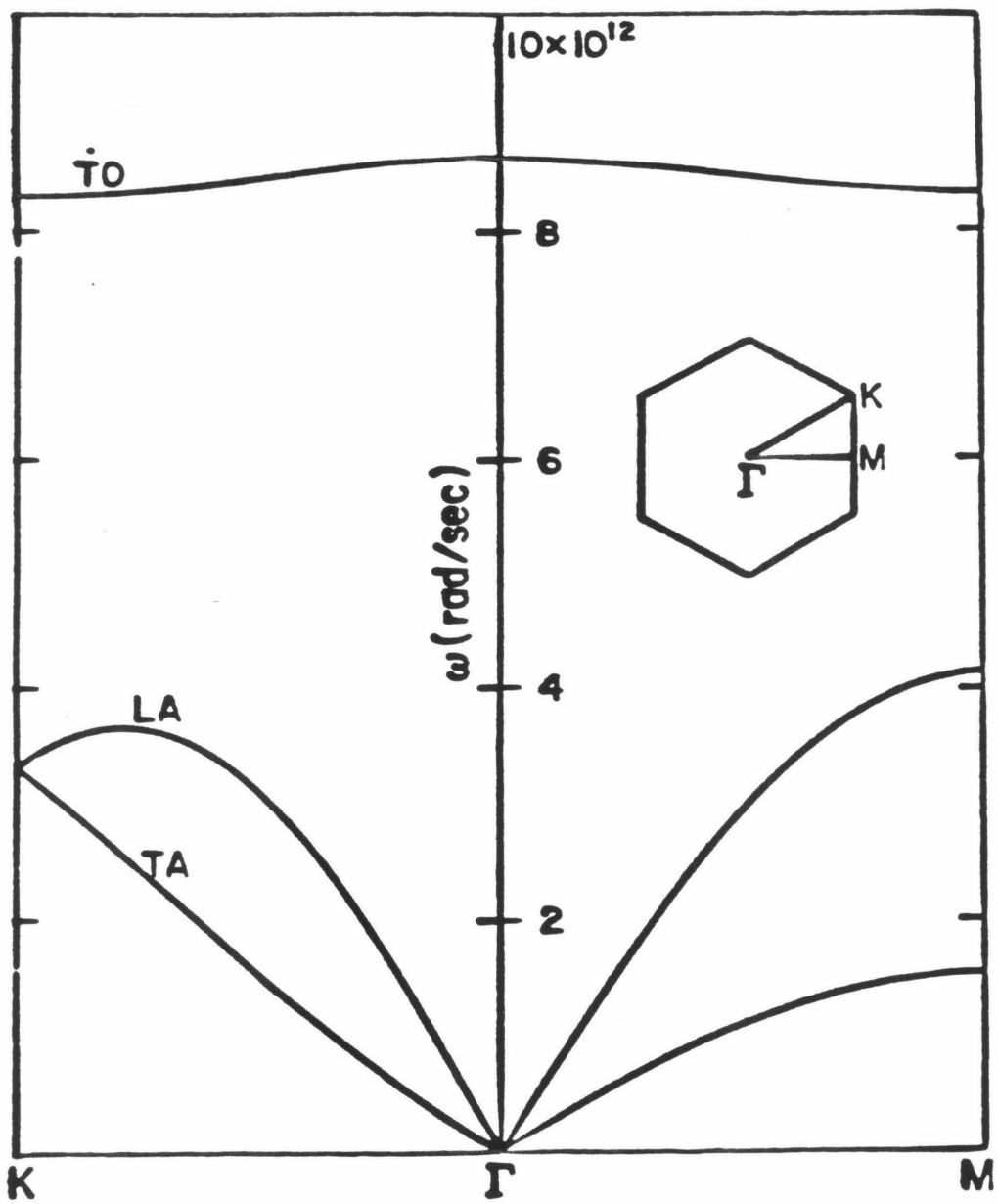

Figure 5.8. Phonon spectrum (angular frequency vs. wave vector) in the symmetry directions of ^{4}He adsorbed on graphite at coverage of .092 $Å^{-2}$ calculated according to the model of section 2. The three modes in order of increasing energy are transverse acoustic, polarized parallel to the substrate, longitudinal acoustic, and transverse optical polarized normal to the substrate. The inset shows the Brillouin zone and the symmetry directions.

2. The Helium-Graphite Potential

Atomic scattering experiments[18,19] have been used[12] to produce the most accurately-known of any substrate-adsorbate potential for the system of helium on graphite. The results include detailed knowledge of the Fourier components of the potential. Other calculations involving this potential have produced remarkable agreement with experiment.[7] One important result of the study of the He-graphite potential is that it cannot be analyzed as a sum of isotropic He-C pair potentials, but must include contributions from the anisotropic electron distribution in the graphite layers, thus enhancing the corrugations of the potential and the degree of orientational ordering.

The substrate-adatom potential is written as

$$U(z) = U_0(z) + \sum_{\vec{G}} U_{\vec{G}}(z) e^{-i\vec{G}\cdot\vec{r}} \tag{5.18}$$

where z is the height above the substrate, $\vec{r}$ is a vector in the plane of the substrate, and the sum is over the reciprocal lattice vectors of the substrate $\vec{G}$. The leading term is

$$U_0(z) = \frac{4\pi\varepsilon\sigma^6}{ad^4}\left[\frac{2}{5}\left(\frac{\sigma}{d}\right)^6\zeta(10, z/d) - \zeta(4, z/d)\right] \tag{5.19}$$

and the Fourier components are given by

$$U_{\vec{G}}(z) = \frac{\pi\varepsilon\sigma^6\beta_{\vec{G}}}{a}\left(\frac{G}{z}\right)^2 \times \tag{5.20}$$

$$\left\{\left(\frac{\sigma^2 G}{z}\right)^3 \frac{1}{480}\left[K_5 + \alpha_R\left(K_5 - \frac{Gz}{10}K_6\right)\right] - \left[K_2 + \alpha_A\left(K_2 - \frac{Gz}{4}K_3\right)\right]\right\}.$$

Here ζ is the generalized Riemann zeta function, K_i are modified Bessel functions of argument Gz, α_R and α_A are parameters characterizing the anisotropy, ε and σ are effective 2-D Lennard-Jones parameters fitted from the experimental bound state energies and matrix elements between bound states to excellent accuracy. The rest of the parameters characterize the graphite crystal and are identical to those tabulated in reference (12).

Theory and experiment also provide limits on the distance of the helium monolayer from the substrate. A WKB calculation in the laterally-averaged substrate potential gives 3.00 Å for ^{4}He and 3.04 Å for ^{3}He, while numerical integration of the Schrodinger equation for the laterally-averaged potential predicts 2.92 Å for ^{4}He,[12] and a more careful accounting of the anisotropy predicts 2.89 Å.[20] Preliminary experimental neutron scattering results[21] give 2.85 Å for this distance. We use the experimental values in our calculations, but the results are tested for dependence upon this parameter, as we shall see below.

3. Determination of Orientational Ordering

We now calculate, for a particular alignment angle, the energy per adatom of the static density waves produced by the triangular graphite lattice on the triangular helium monolayer. Repeating for convenience the results of section 2, the energy as a function of misalignment angle ϑ, is given by[4]

$$E_{SDW}(\vartheta) = -\tfrac{1}{2}i\sum_{\vec{G}} U_{\vec{G}}(z)\exp(-G^\mu G^\nu W^{\mu\nu})G^\beta u_{\vec{G}}^\beta. \tag{5.21}$$

Here $u_{\vec{G}}^\beta$ are components of the distortions of the adatom equilibrium positions caused by a particular density wave at wavevector $\vec{G}$. (If the two solids are commensurate, an additional vector is needed to describe the displacement of the origin (a center of symmetry of the adsorbate) from a center of symmetry of the substrate. For infinite incommensurate lattices, however, it is always possible to locate the origin at a place in the adsorbate where the two centers of symmetry coincide, and thus this additional vector cannot appear in the final answer and has been set to zero. See references 1 and 3.) They are given by

$$u_{\vec{G}}^\beta = -i\sum_l \frac{e_l^\alpha(\vec{G})U_{\vec{G}}(z)\exp(-G^\mu G^\nu W^{\mu\nu})}{m\omega_l^2(\vec{G})}\vec{e}_l(\vec{G})\cdot\vec{G}. \tag{5.22}$$

Here m is the helium atomic mass. ω is the angular frequency of the phonon of the undistorted lattice at the wavevector $\vec{G}$ in the extended zone scheme for the adsorbate, and the $\vec{e}_l$ are polarization vectors for these phonons with mode

indexed by l.

Figure 5.5 shows the adsorbate Brillouin zone, a representative $\vec{G}$ of the substrate, and the importance of the geometry of the two lattices in determining E_{SDW}. In the diagram, $\vec{\tau}_{ij}$ are reciprocal lattice vectors of the adsorbate, and the angle between the two lattices in reciprocal space is denoted by ϑ. To determine the phonon energies and polarizations appearing in equation (5.22), we find the unique $\vec{\tau}$ which reduces $\vec{G}$ to the first Brillouin zone of the adsorbate. The equivalent first-zone wave vector is $\vec{q}=\vec{G}-\vec{\tau}$. It has the same eigenfrequencies and polarizations $\vec{e}$ as $\vec{G}$. Thus, a phonon transverse to $\vec{q}$ will not be transverse to $\vec{G}$ and $\vec{e}\cdot\vec{G}$ will be non-zero. The substrate corrugation $U_{\vec{G}}$ thus produces distortions with sizes determined by the phonons corresponding to $\vec{q}$. The angle-dependent factors in equation (5.22) arise from the reduction of $\vec{G}$ to the first Brillouin zone, and thus appear in the phonon frequency and the scalar product of $\vec{e}$ and $\vec{G}$.

Our calculation proceeds by the iterative scheme alluded to in section III. We guess a value of γ, usually zero. With this choice, the speeds of sound can be determined from the experimental parameters.

The sound speeds determine the parameters of the phonon spectrum needed (see section II) to evaluate equations (5.21) and (5.22) at any angle. The minimum energy (5.21) is located crudely by testing at 1° intervals through the possible 30° range of distinct alignment angles, and then found to arbitrary numerical accuracy by an iterative parabolic fit. The curvature of this minimum is a new prediction of 4γ. A new guess is made partway between the old and new values of γ and the whole process iterates until the new and old values are the same. Convergence occurs for all experimental coverages of both isotopes of He for which incommensurate solids are known to occur.

Each time the angle is changed, the eigenvalues and eigenvectors of the phonon spectrum at wavevector $\vec{G}$ must be found for each Fourier component of the substrate potential considered (and for a representative set of wave vectors for the sum in equation 14). The distortions and their energy are computed for 21 distinct Fourier components of the potential (each has sixfold symmetry), although only 3 of those make appreciable contributions, and to a good approximation, only the lowest $\vec{G}$ is necessary. Table 5.2 presents values of the substrate potential Fourier components for reciprocal lattice vectors ordered by their Miller indices, and typical values of the smearing factors for those components.

For the highly symmetric helium solids (at least before they are distorted by the substrate), it is easily shown that the only non-zero components of W are the diagonal ones, and $W^{xx} = W^{yy}$. Since the z-component of $\vec{G}$ is zero, the tensor contraction $\vec{G}\cdot\overleftrightarrow{W}\cdot\vec{G}$ reduces to $W^{xx}G^2$, so the dependence of the smearing factor on the reciprocal lattice vector is easily found to be

$$S_{kl} = S_{01}^{(k^2+l^2-kl)} \tag{5.23}$$

where S_{kl} is the exponential smearing factor for $\vec{G}_{kl} = k\vec{G}_{10} + l\vec{G}_{01}$. Thus as the length of $\vec{G}$ increases, the smearing factor decreases very rapidly, and hence the contribution from the larger reciprocal lattice vectors to the orientational ordering is depressed.

In fact, we find in retrospect that the contribution of U_{01} to the SDW energy is an excellent approximation to the full result. For this case (see reference 2), the preferred orientation angle is independent of the magnitude of $U_{\vec{G}}$ (although the energy and γ are not) and depends only on the adsorbate density and ratio of speeds of sound, through their influence on the shape of the model phonon spectrum.

4. Discussion of Results

The results of the calculation are summarized in table 5.3, which presents the elastic properties of films at several different coverages of ^{3}He and ^{4}He. Figure 5.9 displays the value of orientation angle vs. coverage. (The angles for argon and neon layers are respectively, 26.5° and 12°.)[2] Figure 5.7 is a graph of γ vs. coverage for each helium isotope.

It is expected that the orientational ordering should be weaker in ^{3}He than in ^{4}He, as the results confirm, for two reasons. First, the ^{3}He is at a larger distance from the substrate, which implies a weaker coupling. Second, the zero-point motion for ^{3}He is substantially larger than that of ^{4}He, as is evidenced by the smearing factors in table 5.2.

All the above results are calculated assuming the adsorbate is localized 2.85 Å above the substrate for ^{4}He and 2.89 Å above for ^{3}He. The ^{4}He value agrees with the experimental results and the ^{3}He value is chosen to produce the same ratio of distances as the WKB calculation in the laterally averaged potential. In table 5.4, we compare the results with those computed at a particular coverage at the theoretically predicted distances discussed above, and at the limits of precision of experimental measurement. From table 5.4, it becomes clear that the estimated error in the experimentally determined ^{4}He-substrate distance of ±.05Å is too large to give a precise value of γ.

The reason for this is shown in figure 5.10, which is a schematic picture of the anisotropy of the substrate potential (based on reference 10), measured above the center of a graphite hexagon (position S) and above a carbon atom (position A). The major component of the corrugation amplitude $U_{01}(z)$ is proportional to the vertical distance between the curves at a particular value of z. The corrugation decreases to a negligible value for $z \geq 3.2$Å, where γ would be zero, but moving toward the potential minimum it increases roughly linearly as

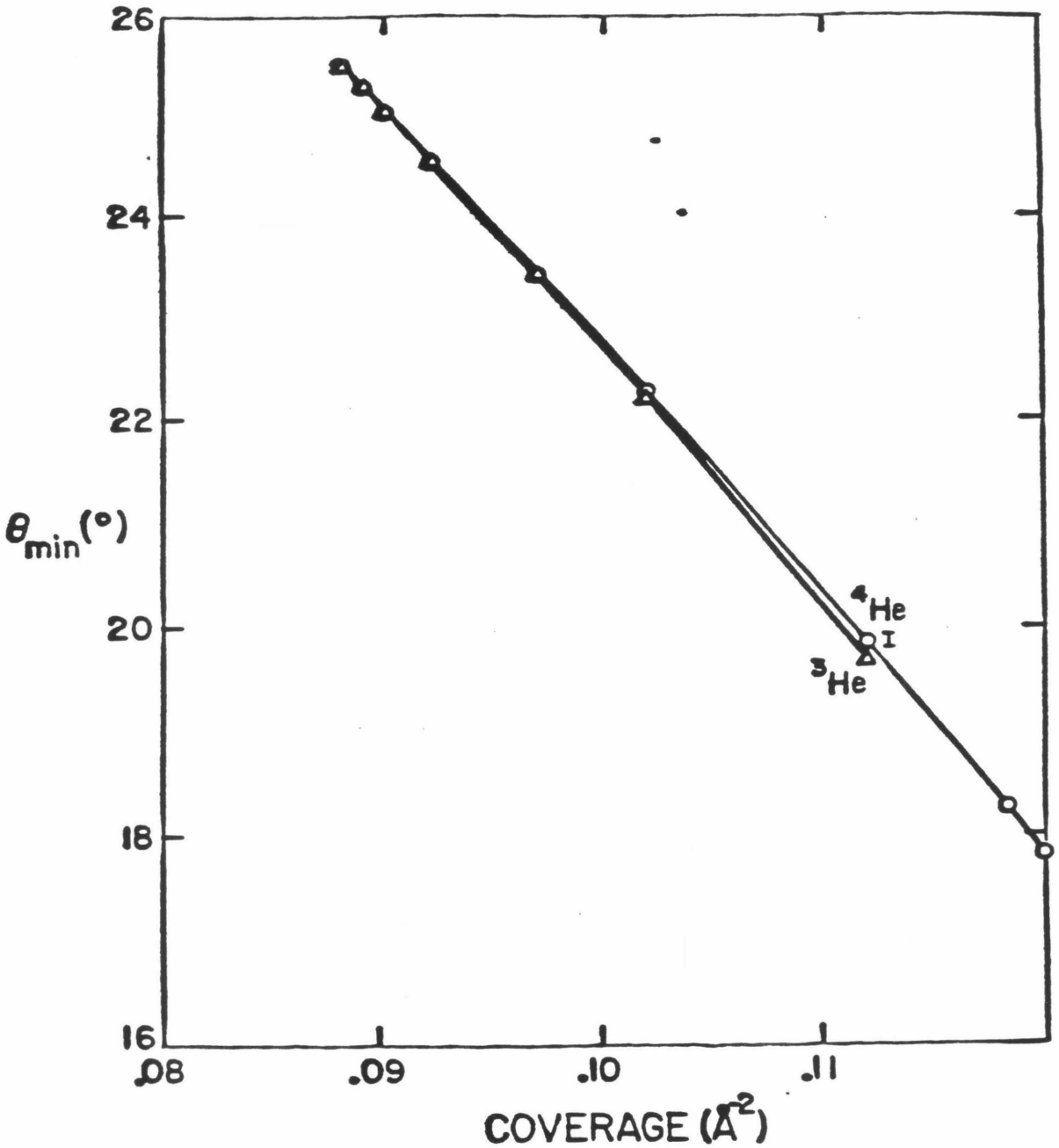

Figure 5.9 Angle of preferred orientation versus coverage for ^{4}He and ^{3}He on graphite, assuming the adsorbate-substrate distances of figure 1. Since only one Fourier component contributes significantly to the distortion energy, the angle is determined primarily by the ratio of substrate to adsorbate lattice spacing, and secondarily by the ratio of adsorbate speeds of sound as explained in reference 2.

Figure 5.7 Coverage dependence of γ, the elastic constant measuring resistance to relative twist of the adsorbate and substrate about the preferred orientation angle, calculated for the adsorbate-substrate distances of figure 1.

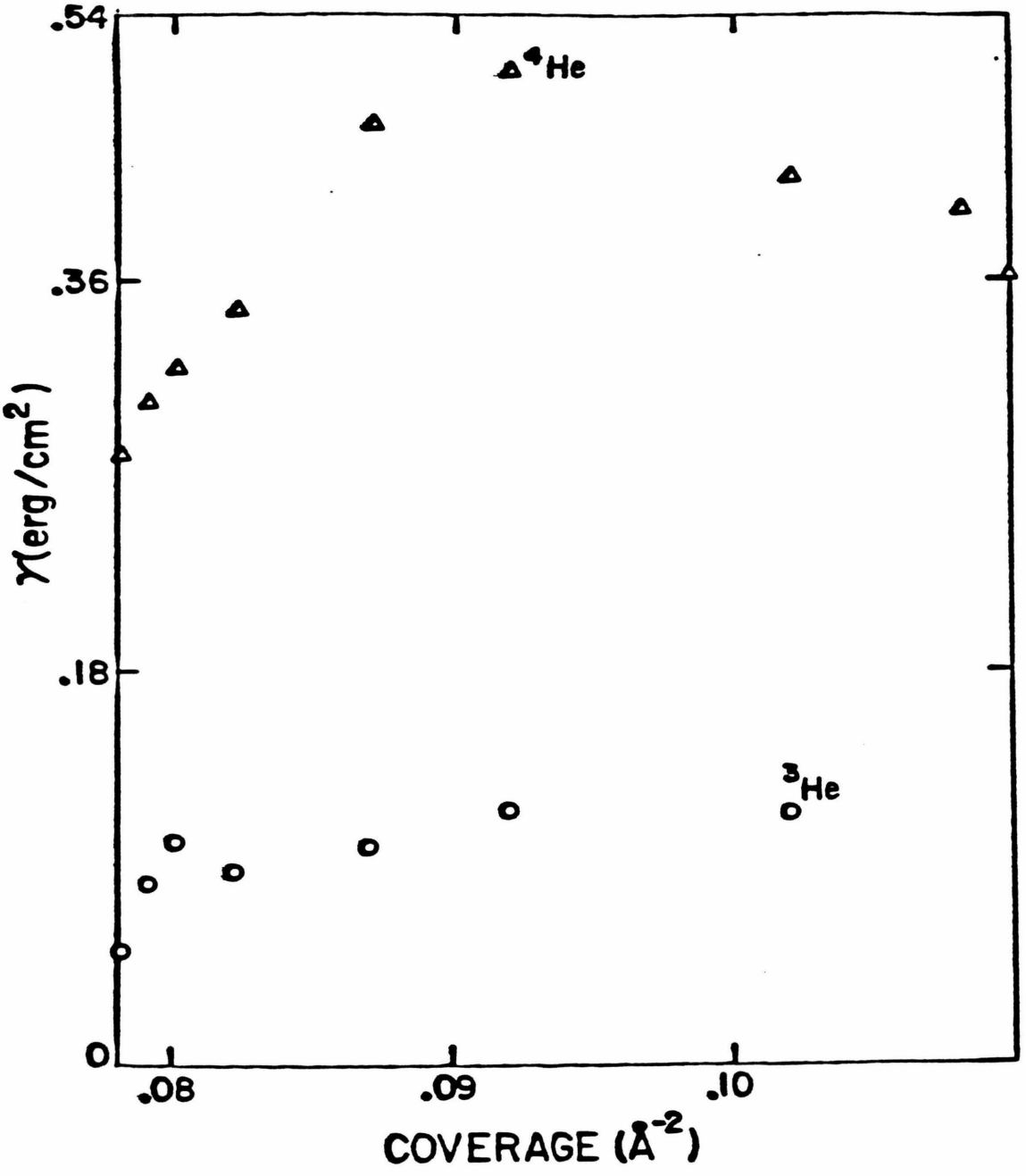

Figure 5.10. He-graphite potential deduced from the He-graphite scattering data in reference 10, as measured above the center of a graphite hexagon (S) and above a carbon atom (A), as shown in the inset. The vertical difference between the curves is 9 times the most important Fourier component of the corrugation of the potential, U_{01}. The size of the corrugation becomes negligible when the helium atoms are more than about 3.2 Å from the substrate, and increases rapidly at shorter distances.

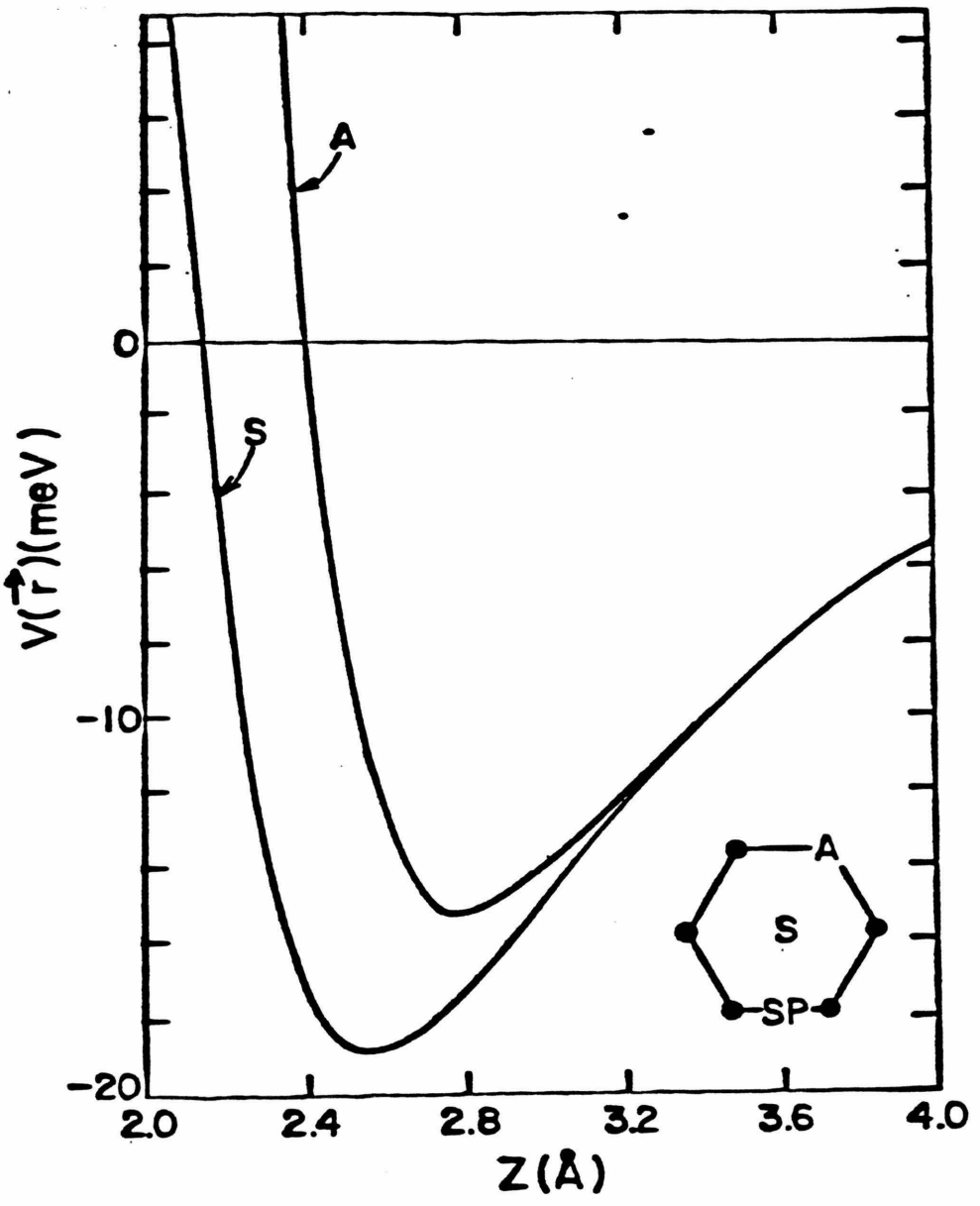

z *decreases*. Since the strain energy and γ vary quadratically with U_{01}, which is, as we have seen, the principal contributor to E_{SDW}, we expect γ to increase quadratically with decreasing z with a zero near 3.2 Å as shown in figure 5.11. As long as only one corrugation wavelength is important, the angle is nearly independent of z, and the slight shifts in the orientation angle arise from the weak dependence of ϑ_{min} on the ratio of the undistorted sound speeds. (The experimental measurements yield the actual sound speeds, so for a given set of experimental sound speeds, the derived undistorted sound speeds will depend upon z). Clearly this uncertainty in the distance between substrate and adsorbate dominates all others in the calculation of γ. Fortunately, values of γ as a function of z may be estimated from those in Table 5.4 using the observations that γ is very nearly proportional to $U_{01}^2(z)$. (If a more precise measurement of the average z becomes possible and the current result was reportedly difficult to obtain, a possible further improvement in the calculation would be to compute an average value of $U_{\vec{G}}$ taking into account the excursions of the adsorbate atoms perpendicular to the substrate. This will increase the values of $\gamma(z)$ reported in table 5.4, owing to the quadratic dependence discussed above. The root-mean-square spread of the atoms has been estimated in Cole, Frankl and Goodstein to be .25 Å.)

Besides the uncertainty in distance of the adsorbate from the boundary, there are other approximations in our calculation whose effects are smaller. The linear response approximation (assuming the distortions to be small and using the phonon spectrum of the undistorted lattice) produces errors of order $(\frac{u_{\vec{G}}}{a})^2$ where a is the lattice spacing. For the helium solids this quantity is small, as can be seen by comparing u_{01} in table 5.3 to the lattice spacing of about 3.6Å. In fact, the distortions are small compared with the zero-point amplitude which is measured by the square root of the trace of W displayed in

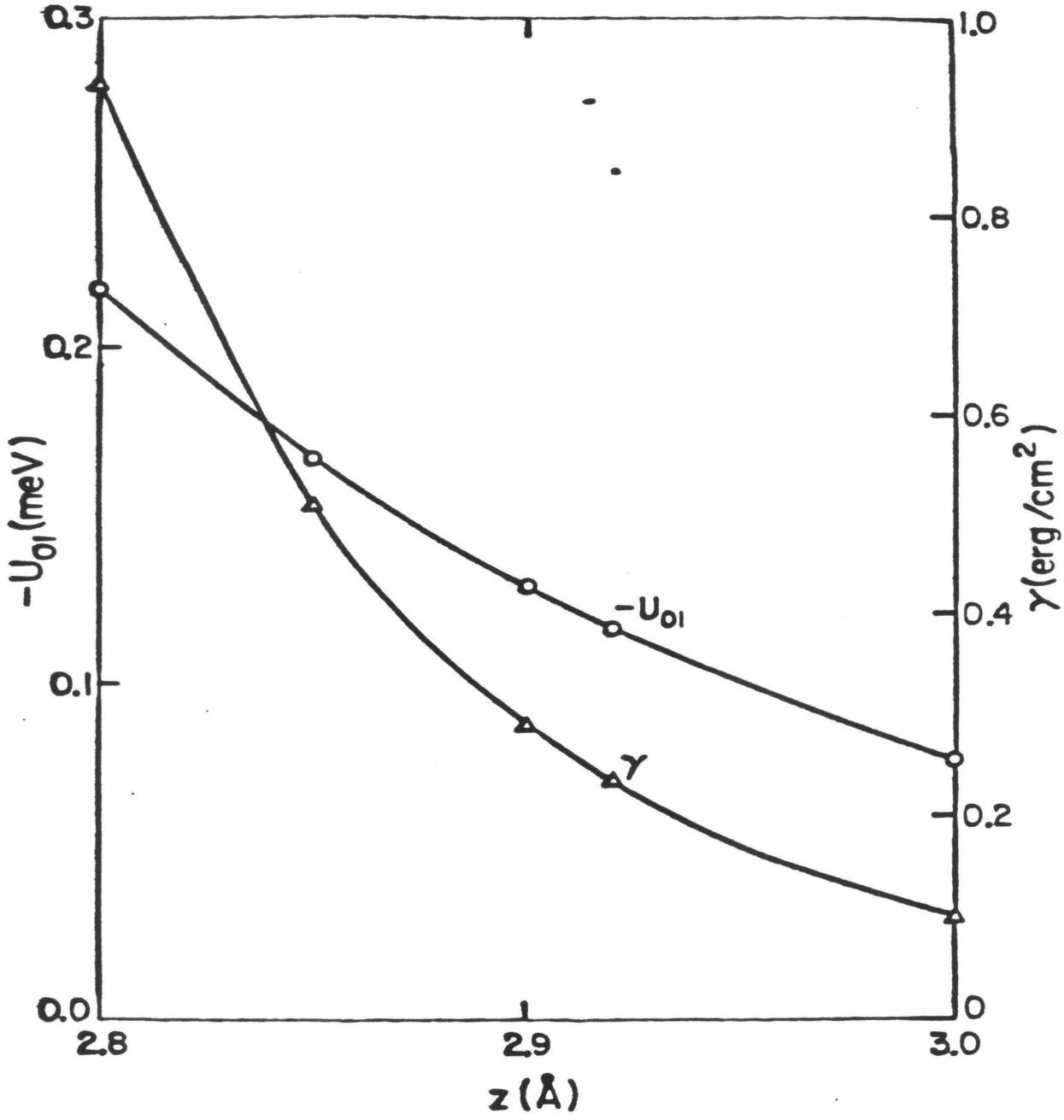

Figure 5.11. The amplitude of the principal corrugation Fourier component of the substrate potential, U_{01}, and γ, the elastic constant governing restoration of twist of substrate relative to adsorbate about the angle of preferred orientation, are displayed as functions of z, the height of the adsorbate above the substrate. Equation (5.22) predicts that γ should be quadratic in U_{01} in cases such as this one in which no other components of the substrate potential corrugation are important. This figure, along with table 5.4, illustrate the rapid variation of γ with z.

table 5.2. We expect the errors from these two sources to be of the order of 10 percent or less in γ and negligibly small in the orientation angle, which is more strongly influenced by geometry than anything else.

It is more difficult to estimate the errors due to our model of the phonon spectrum. These affect two separate aspects of the distortion energy, the value of w in the denominator of eq. (5.22), and the smearing tensor W. Neither has a significant effect on the orientation angle since the errors in the phonon spectrum occur primarily at short wavelength, while the angle is usually fixed by the geometry and by the long-wavelength behavior in turn determined by experimental results. For the same reason, the first effect produces only small errors in the values of E_{SDW} and γ. The second effect appears in the smearing factor which is the primary determinant of the size of γ and E_{SDW}. (For argon, the exponential factor in eq. (5.21) is about 0.8, while for helium, it ranges from a maximum of about .15 to 10^{-27} for the Fourier components considered. In fact, calculations done by the method of reference 1, essentially identical to the present one but leaving out the effect of zero-point motion produce very large distortions and unphysical values of γ and E_{SDW} even far from registry.)

For completeness, we mention several other implicit approximations producing very small errors in the results. For one, the film may not be a plane parallel to the substrate, but rather a slightly buckled plane. This should be a small effect because the corrugation of the substrate-He potential is small compared with the overall attraction. Essentially, one might expect that the overall distortions of the helium lattice could be slightly increased in the plane if they were accompanied by a correlated set of distortions perpendicular to the plane which slightly reduced interatomic repulsions. This effect must be small since the strength and steepness of the surface-averaged potential as a function of z is large compared to either the corrugations or the helium-helium potential.

We have decoupled the motion perpendicular to the substrate from the in-plane motion, and that decoupling is probably somewhat inadequate. We have reduced the problem of calculating all the phonon modes of the distorted system to the problem of calculating the shift of the low frequency modes (i.e. of γ) which is surely an oversimplification. We have also ignored the perturbations of the substrate by the adsorbate on the grounds that the substrate is much stiffer than the adsorbate.

We believe that if the precision of the adsorbate-substrate distance were improved, the accuracy of this calculation would be limited by that of the experimentally determined elastic constants on which it is based.

The helium monolayer solids occur in a region of the coverage-temperature plane bounded by sharp heat capacity peaks which seem to occur at substantially higher temperatures[22] than Kosterlitz-Thouless [23] dislocation unbinding temperatures predicted by renormalization group theories.[5,24] It is easy to speculate that these peaks are the signatures of a possibly Ising-like transition marking the end of angular order.[6] The present calculation may provide an energy scale for an estimation of the temperature of this phase transition.

5. Possible Experimental Measurements of Orientational Ordering

Orientational ordering has been observed in other noble gas films on graphite using low energy electron diffraction (LEED), [25] but there is as yet no definite confirmation of the effect in helium.

No measurements of γ have ever been made, for any system, nor have any obviously feasible experimental methods been proposed for making the measurement. Since the calculated value of γ depends so strongly on the mean height above the surface, which is known to about 3%, a measurement of γ is less a check of the present computation than a confirmation or refinement, which

depends on the quality of that computation, of the measurement by neutron scattering of the mean height $\bar{z}$ of the film above the substrate.

A study is now underway to determine the feasibility of making neutron scattering measurements to measure at least the orientation angle of helium films on graphite. As part of that study, we present the current knowledge of the expected elastic neutron scattering structure factor for such a film.

At least two effects should be present in the neutron scattering. The first of these is a reproducible angle between the adsorbate reflections and substrate reflections, which varies with density as predicted earlier in this chapter. The graphite reflections are a large background signal, easily detectable, so it should be possible to see the locking angle whenever helium reflections are visible at all, unless the experiment must be done on unoriented substrate or the neutrons are not sufficiently collimated or monochromatic.

A preferred orientation could also be produced by various kinds of dirt effects -- pinning of the helium film at the edges of small patches of smooth substrate, impurities in or on the graphite. To distinguish the effects, the results for the angle should be independent of the particular substrate sample used and there should also be some way of measuring the SDW distortion of the helium lattice from perfectly triangular. This distortion should produce a decrease in intensity of each helium Bragg peak (which will probably be undetectable without an undistorted reference) and satellite peaks substantially displaced from the primary peaks in reciprocal space.

The general formula for the neutron scattering dynamic structure factor (the Fourier transform of the density-density correlation function of the system) can be written

$$S(\vec{q},\omega)=\frac{1}{N}\sum_{\vec{R}\vec{R}'} e^{-i\vec{q}\cdot(\vec{R}-\vec{R}')}\int \frac{dt}{2\pi} e^{i\omega t} \langle \exp(i\vec{q}\cdot\vec{u}(\vec{R}'))\exp(-i\vec{q}\cdot\vec{u}(\vec{R},t))\rangle \quad (5.24)$$

where $\vec{q}$ and ω are wave vector and frequency, N the number of atoms in the crystal, and R , $\vec{R}'$ the positions of atoms. If the average distortion is extracted from the thermal average by decomposing $\vec{u}$ into $\langle\vec{u}(\vec{R})\rangle+\delta\vec{u}(\vec{R},t)$ where the average value (the distortion) is computed from the SDW theory, then

$$S(\vec{q},\omega)=\frac{1}{N}\sum_{\vec{R}\vec{R}'} e^{-i\vec{q}\cdot(\vec{R}-\vec{R}')}e^{-i\vec{q}\cdot\langle\vec{u}(\vec{R})\rangle}e^{+i\vec{q}\cdot\langle\vec{u}(\vec{R}')\rangle}\times \tag{5.25}$$

$$\int\frac{dt}{2\pi}e^{i\omega t}\langle\exp(i\vec{q}\cdot\delta\vec{u}(\vec{R}'))\exp(-i\vec{q}\cdot\delta\vec{u}(\vec{R},t))\rangle$$

The distortion $\langle\vec{u}(\vec{R})\rangle=\sum_{\vec{G}}\vec{u}_{\vec{G}}\sin(\vec{G}\cdot\vec{R})$, where the static density wave amplitude $\vec{u}_{\vec{G}}$ produced by the substrate corrugation at wave vector $\vec{G}$ has been calculated earlier in the chapter. The static part of the structure factor (gotten, e.g., by expanding the exponentials in the thermal averages in the integral of equation (5.13.6), taking the zero-order term and performing the time integral) is proportional to

$$S(\vec{q})\propto e^{-2\vec{q}\cdot\vec{W}\cdot\vec{q}}\prod_{\vec{G}\vec{G}'}\sum_{\vec{R}\vec{R}'} e^{-i\vec{q}\cdot(\vec{R}-\vec{R}')}e^{-i\vec{q}\cdot\vec{u}_{\vec{G}}\sin(\vec{G}\cdot\vec{R})}e^{+i\vec{q}\cdot\vec{u}_{\vec{G}}\sin(\vec{G}'\cdot\vec{R}')} \tag{5.26}$$

where $\vec{G}$ are *substrate* reciprocal lattice vectors.

Finding this static structure factor involves sums over the lattice of the form $\sum_{\vec{R}}e^{-i\vec{q}\cdot(\vec{R}+\vec{B}\sin\vec{G}\cdot\vec{R})}$ which will always lead to Bessel functions. McTague and Novaco[3] have calculated these sums for situations in which the neutron momentum transfer vector $\vec{q}$ is in the plane of the adsorbate. They find

$$S(\vec{q})\propto e^{-2\vec{q}\cdot\vec{W}\cdot\vec{q}}\left[\prod_{\vec{G}}J_0(\vec{q}\cdot\vec{u}_{\vec{G}})\Delta(\vec{q})+\right.$$

$$\left.2\sum_{\vec{G}'}\Big(\prod_{\vec{G}\neq\vec{G}'}J_0(\vec{q}\cdot\vec{u}_{\vec{G}})\Big)J_1(\vec{q}\cdot\vec{u}_{\vec{G}'})\Delta(\vec{q}+\vec{G}')+\cdots\right] \tag{5.27}$$

where $\Delta(\vec{q})\equiv\sum_{\vec{\tau}}\delta_{\vec{q},\vec{\tau}}$ and $\{\vec{\tau}\}$ are *adsorbate* reciprocal lattice vectors. As noted above, the first term represents the reduced primary reflections, and the second term gives the satellite peaks, which occur for $\vec{q}$ at a substantial distance into the Brillouin zone (see figure 5.5). Since the sums over $\vec{G}$ can be

truncated after including just the six equivalent lowest wave vectors, without significant loss of accuracy, many details of the neutron experiments can be predicted using our earlier results for $\vec{u}_{\vec{G}}$.

It will be difficult, and is probably impossible with current technology, to observe this effect,[26] because the neutron scattering cross section for He is so low and there is so much background from diffuse scattering from graphite as well as various crystallographic reflections from the graphite. In the absence of neutron beams of high enough intensity and monochromaticity to attempt to observe the angle between helium and graphite primary reflections on a single crystal substrate (where the amount of adsorbed material is much less than on polycrystalline substrates with large surface area), it is the only possible way of observing orientational ordering with neutrons scattering.

Acknowledgments

The authors thank R. P. Feynman, M. W. Cole, and A. D. Novaco for fruitful discussions, and J. G. Dash and O. E. Vilches for unpublished data.

References

1. J. M. Greif and D. L. Goodstein, *J. Low Temp. Phys.* **44**, (3/4)(1981).
2. A. D. Novaco and J. P. McTague, *Phys. Rev. Lett.* **38**, 1286(1977).
3. J. P. McTague and A. D. Novaco, *Phys. Rev.* **B19**, 5299(1979).
4. A. D. Novaco, *Phys. Rev.* **B19**, 6493(1979).
5. D. R. Nelson and B. I. Halperin, *Phys. Rev.* **B19**, 2457(1979).
6. B. I. Halperin, in *Ordering in Two Dimensions*, ed. S. Sinha, (North-Holland, New York, 1980).
7. M. W. Cole, D. R. Frankl, and D. L. Goodstein, *Rev. Mod. Phys.* **53**, (2)(April 1981).
8. M. Nielsen, J. Als-Nielsen, and J. P. McTague, in *Ordering in Two Dimensions*, ed. S. Sinha, (North-Holland, New York, 1980).
9. C. Varma and N. R. Werthamer, in *The Physics of Liquid and Solid Helium*, ed. K. H. Benneman and J. B. Ketterson, (J. Wiley & Sons, Inc., New York, 1976) present a good review.
10. G. Vidali and M. W. Cole, *Phys. Rev.* **B22**, 4661(1980).
11. A. D. Novaco, in *Monolayer and Submonolayer Films*, ed. J. G. Daunt and E. Lerner, (Plenum , New York, 1973).
12. W. E. Carlos and M. W. Cole, *Surf. Sci.* **91**, 339(1980).
13. D. C. Wallace, *Thermodynamics of Crystals* (McGraw-Hill, New York, 1972).
14. J. M. Greif and D. L. Goodstein, to be published.
15. R. L. Elgin and D. L. Goodstein, *Phys. Rev.* **A9**, 2657(1974).
16. M. Bretz, J. G. Dash, D. C. Hickernell, E. O. McLean, and O. E. Vilches, *Phys. Rev.* **A8**, 1589(1973).

17. S. V. Hering, S. W. van Sciver, and O. E. Vilches, *J. Low Temp. Phys.* **25**, 793(1976).

18. G. Boato, P. Cantini, C. Guidi, R. Tatarek, and G. P. Felcher , *Phys. Rev.* **B20**, 3957(1979).

19. G. Derry, D. Wesner, W. E. Carlos, and D. R. Frankl, *Surf. Sci.* **87**, 629(1979).

20. M. W. Cole and F. Toigo, *Phys. Rev.* **B23**, 3914(1981).

21. K. Carneiro, L. Passell, W. Thomlinson, and H. Taub, to be published

22. J. M. Greif, A. F. Silva-Moreira, and D. L. Goodstein, in *Ordering in Two Dimensions*, ed. S. Sinha, (North-Holland, New York, 1980).

23. J. M. Kosterlitz and D. J. Thouless, *J. Phys.* **C6**, 1181(1973).

24. A. P. Young, *Phys. Rev.* **B19**, 1855(1979).

25. C. G. Shaw, S. C. Fain, Jr., and M. D. Chinn, *Phys. Rev. Lett.* **41**, 955(1978).

26. L. Passell, private communication.

Table 5.1			
n	$w_0^2 \times 10^{-24}$	B	v''
$Å^{-2}$	$(rad/sec)^2$		erg/cm^2
	^3He		
.0781	2.78	4.409	6.400
.0791	3.10	3.779	8.214
.0801	3.48	3.787	9.471
.0822	3.65	4.297	9.740
.0870	4.79	5.450	12.87
.0920	6.30	6.410	18.48
.1021	9.05	8.569	35.51
	^4He		
.0781	2.10	3.577	7.38
.0791	2.21	3.620	7.974
.0801	2.35	3.681	8.616
.0822	2.66	3.820	10.11
.0870	3.46	4.130	14.34
.0920	4.46	4.536	20.28
.1021	6.81	5.456	38.70
.1083	8.32	6.042	55.71
.1100	8.73	6.222	61.36

Table 5.1

Parameters of the phonon spectrum at several values of coverage for both helium isotopes. All the parameters are defined in the text. The calculation assumes an adsorbate-substrate distance of 2.85 Å for ^4He and 2.89 Å for ^3He.

Table 5.2

Miller indices		$U_{\vec{G}}$ (meV)	Smearing factor	
			^{4}He	^{3}He
0	1	-1.665×10^{-1}	1.356×10^{-1}	1.146×10^{-1}
0	2	-6.438×10^{-4}	3.381×10^{-4}	1.725×10^{-4}
1	2	6.616×10^{-3}	2.493×10^{-3}	1.505×10^{-3}
0	3	1.775×10^{-6}	1.550×10^{-8}	3.409×10^{-9}
1	3	-9.794×10^{-6}	8.430×10^{-7}	2.596×10^{-7}
2	3	-9.794×10^{-6}	8.430×10^{-7}	2.596×10^{-7}
0	4	-7.737×10^{-10}	1.307×10^{-14}	8.850×10^{-16}
1	4	-1.296×10^{-8}	5.241×10^{-12}	5.880×10^{-13}
2	4	7.040×10^{-8}	3.865×10^{-11}	5.131×10^{-12}
3	4	-1.296×10^{-8}	5.241×10^{-12}	5.880×10^{-13}
0	5	-5.143×10^{-13}	2.025×10^{-22}	3.017×10^{-24}
1	5	2.238×10^{-11}	5.990×10^{-19}	1.749×10^{-20}
2	5	-5.744×10^{-11}	3.258×10^{-17}	1.332×10^{-18}
3	5	-5.744×10^{-11}	3.258×10^{-17}	1.332×10^{-18}
4	5	2.238×10^{-11}	5.990×10^{-19}	1.749×10^{-20}
0	6	5.708×10^{-16}	5.772×10^{-32}	1.351×10^{-34}
1	6	-7.424×10^{-15}	1.259×10^{-27}	6.835×10^{-30}
2	6	-5.875×10^{-14}	5.050×10^{-25}	4.541×10^{-27}
3	6	2.393×10^{-13}	3.724×10^{-24}	3.963×10^{-26}
4	6	-5.875×10^{-14}	5.050×10^{-25}	4.541×10^{-27}
5	6	-7.424×10^{-15}	1.259×10^{-27}	6.835×10^{-30}

Table 5.2

Amplitude of corrugations of the substrate-adatom potential for the wavevectors equalling the lowest 21 substrate reciprocal lattice vectors in a 60° sector of momentum space, along with representative smearing factors $e^{-\vec{G}\cdot\overleftrightarrow{\sigma}\cdot\vec{G}}$ calculated with an adsorbate-substrate separation of 2.85 Å for ^{4}He and 2.89 Å for ^{3}He. See equations (5.20) and (5.23).

Table 5.3

n	$1/\kappa$	Θ_D	φ	μ	c_L	c_T	c_{TU}	$\vartheta_{\min}$	γ	$E_{\min}$	δu_{rms}	u_{01}
						^{3}He						
.0781	6.61	17.60	1.911	3.078	446.	177.	172.	25.53	.0578	-.0732	.959	.050
.0791	8.73	17.90	2.006	3.147	499.	176.	169.	25.29	.0926	-.0962	.937	.055
.0801	10.07	19.20	2.115	3.418	532.	187.	180.	25.06	.1137	-.1296	.904	.057
.0822	10.15	21.10	2.383	4.031	535.	206.	200.	24.53	.0982	-.1531	.873	.050
.0870	12.99	26.90	3.000	5.820	602.	259.	254.	23.41	.1114	-.2744	.785	.043
.0920	18.31	33.70	3.887	8.434	704.	318.	314.	22.24	.1292	-.4392	.706	.038
.1021	34.25	49.40	6.475	16.62	931.	448.	445.	19.70	.1281	-.7497	.587	.029
						^{4}He						
.0781	7.911	15.41	1.788	2.704	412.	153.	132.	25.53	.3100	-.2947	.910	.115
.0791	8.539	16.11	1.892	2.896	426.	159.	138.	25.31	.3385	-.3355	.891	.111
.0801	9.207	16.83	2.004	3.116	440.	166.	144.	25.07	.3558	-.3847	.871	.108
.0822	10.75	18.43	2.261	3.640	471.	179.	158.	24.55	.3861	-.5013	.831	.101
.0870	15.12	22.48	2.988	5.149	546.	213.	193.	23.44	.4817	-.8022	.751	.087
.0920	21.13	27.33	3.882	7.413	630.	253.	236.	22.28	.5107	-1.151	.678	.073
.1021	39.49	39.36	7.051	14.85	835.	348.	339.	19.86	.4538	-1.758	.562	.052
.1083	56.25	48.38	9.843	21.97	975.	418.	410.	18.29	.4373	-2.036	.508	.043
.1100	61.76	51.09	10.76	24.40	1015.	438.	432.	17.84	.4027	-2.102	.494	.041

Table 5.3

Elastic properties of ^{3}He and ^{4}He films on graphite assuming the adsorbate-substrate distance to be 2.85 Å for ^{4}He and 2.89 Å for ^{3}He. The coverage n is in $Å^{-2}$. The elastic constants $1/\kappa$, μ, γ, and the 2-D pressure φ are all measured in ergs/cm^2, and the SDW energy at the preferred orientation is in units of 10^{-2}erg/cm^2. The Debye temperature Θ_D is in Kelvins. The speeds of sound

c_L, c_T, and c_{Ty} (the latter being the derived transverse speed for the undistorted lattice) are tabulated in m/sec. The rms zero-point amplitude δu and the major contribution to the distortion u_{01} are given in Å. The orientation angle is in ° relative to a crystal axis of the substrate exactly aligned with one of the adsorbate. (Registry occurs at an angle of 30 °.)

Table 5.4					
z	U_{01}	u_{01}	$E_{min} \times 10^2$	γ	ϑ_{min}
Å	meV	Å	erg/cm^2		°
2.80	-.2166	.099	-1.855	.9321	22.31
2.85	-.1665	.073	-1.151	.5107	22.27
2.90	-.1284	.055	-.6987	.2925	22.27
2.92	-.1158	.049	-.5713	.2357	22.26
3.00	-.0769	.032	-.2550	.1017	22.26

Table 5.4

Orientational ordering as a function of the height of the ^4He adsorbate (at a coverage of .092 $Å^{-2}$) above the substrate, z. The preferred angle of orientation hardly varies but the size of surface potential corrugations, and the distortions and static density waves they induce are strong functions of z.

Chapter 6

The Critical Region in the Dislocation Unbinding Theory

1. Analysis of Asymptotic Behavior

The KTHNY theory of 2-D melting has been used mostly to predict the behavior of systems in the immediate vicinity of the transition, where strongly fluctuating variables determine that behavior. Although in principle the theory should be a complete description of the contribution of topological defects at all temperatures, when it is used away from the immediate neighborhood of the transition, various complications ensue.

One of these is that other effects may become important, for example, other kinds of anharmonicity in the solid, or diffusion in the liquid crystal phase above the melting temperature. Another complication is that the main tools of the theory, the renormalization group (RG) equations, rapidly become essentially unusable above the transition.

Since the critical properties of the the transition are among the easiest to calculate from the theory, the question naturally arises as to whether those properties are experimentally accessible, that is, whether they apply over a sufficient range of temperatures to be observable, given the current experimental and theoretical uncertainty in the transition temperature itself.

Below the transition, for a given set of initial conditions and core parameter C, the dislocation contribution to any thermodynamic property can be calculated by using the the RG equations. These can be integrated over all scales, and, since they always converge to the fixed point $y(\infty)=0$, $dK^{-1}/dy(\infty)=0$ are numerically well-behaved.

Above the transition, the RG trajectories diverge to $y(\infty)=\infty$. This indicates that they have broken down, since $y=e^{-E_c/k_BT}$ and the core energy should never be negative. The breakdown occurs because the gas of dislocations is not dilute much above T_m. Thus, truncating the expansions in powers of y at the second order is invalid in this region, and produces unphysical results. The only way to use the RG equations above the transition is to integrate from the bare melted state, with mixtures of bound and free dislocations, to higher temperature and larger but finite scale, where the renormalized problem of mostly free dislocations can be treated with some other approximation appropriate to high-temperature "plasmas". This procedure has been carried out successfully by Solla and Riedel[1] for the scalar Coulomb gas model of vortices in a 2-D superfluid, but has not been used for the dislocations in a solid, partly because at temperatures substantially above that of the transition, disclinations would be expected to dominate the thermodynamic behavior and they are not incorporated into the dislocation Hamiltonian.

Thus, it is important to determine the width of the transition region, over which the properties can be determined with reasonable accuracy by the asymptotic critical relations.

We now present a new analysis of the behavior in the transition region, which produces the same critical exponents as NH [2] and Young[3] but corrects some errors in their treatment, and also leads to criteria for the width of the critical region. Some of this work was carried out in collaboration with A.F.

Silva-Moreira.

In particular, we examine the behavior of the correlation length ξ_+ approaching the melting temperature from above. This correlation length is proportional to the mean distance between free dislocations, so the density of free dislocations varies as the inverse square of the correlation length, $n_f \sim \xi_+^{-2}$. The technique used makes use of the well-known behavior of the correlation length under the RG transformation,

$$\xi_+(0)=e^l \xi_+(l). \tag{6.1}$$

This result is essentially a bit of dimensional analysis which is equivalent to saying that when the system is examined on scale e^l times bigger, the correlation length is e^l times smaller than the physical correlation length. We determine the correlation length in the critical region by integrating the RG equations to some value of the scale l^* far from the transition such that the correlation length is small and slowly varying as a function of l. When the scale-dependent correlation length reaches the order of one lattice spacing (at the current scale), then further iterations of the renormalization transformation will not change it. Then, $\xi_+ \approx e^{l^*} \times constant$ and l^* is a parameter which depends on the closeness of the starting point to the transition and determines at what scale we have gotten far enough from the transition that the correlation length (viewed on that scale) is slowly varying. Thus, l^* depends upon the reduced temperature t. We will show that $l^* \sim |t|^{-\bar{\nu}}$ where $\bar{\nu}=.3693...$ The scaling law for the correlation length is thus $\xi_+ \sim e^{\chi/|t|^{\bar{\nu}}}$ where χ is a non-universal constant.

Near the critical point, $K^{-1}=1/16\pi$, $y=0$, the separatrix bounding the solid and hexatic liquid crystal phases can be regarded as a pair of straight lines with slopes

$$m_\pm = \frac{B \pm \sqrt{B^2+24A^2}}{12\pi A} = \begin{cases} 0.0341 \\ -0.0212 \end{cases} \tag{6.2a}$$

$$A=e^2(2I_0(2)-I_1(2))=21.937 \tag{6.2b}$$

$$B=eI_0(2)=6.195 \tag{6.2c}$$

where I_n are imaginary Bessel functions. The analysis that follows is restricted to core parameters large enough so the initial conditions for the integration are in the region near the critical point where the separatrices can be regarded as straight lines. For smaller values of the core parameter, the same behavior occurs, but over an even narrower range of reduced temperature.

By changing variables to (x,y) with $K^{-1}(l)=\frac{1}{16\pi}(1+x(l))$, the smooth-substrate RG equations of NH can be written

$$\frac{dx}{dl}=12\pi^2Ay^2 \tag{6.3a}$$

$$\frac{dy}{dl}=2xy+2\pi By^2. \tag{6.3b}$$

Defining the deviation from the incoming and outgoing separatrices

$$D(l)\equiv y(l)-m_-x(l) \tag{6.4a}$$

$$E(l)\equiv y(l)-m_+x(l) \tag{6.4b}$$

equation (6.3b) can be written as

$$\frac{dD}{dl}=-2xD+12\pi A^2m_+D^2 \tag{6.5a}$$

near the incoming separatrix and

$$\frac{dE}{dl}=-2xE+12\pi A^2m_-E^2 \tag{6.5b}$$

near the outgoing separatrix. Either of the equations is valid anywhere equation (6.3b) is, but each is useful only near the appropriate separatrix.

A typical RG trajectory above the transition is shown in figure 6.1. It hugs first the left and then the right separatrix. The intersection of the line of starting points

$$y_0=e^{\frac{-CK_0}{8\pi k_BT}} \tag{6.6}$$

with the trajectory gives the initial conditions (x_0,D_0) or (x_0,y_0). (In equation (6.6), $K_0=\frac{4a_0^2\mu_0B_0}{\mu_0+B_0}$ where μ_0 and B_0 are the bare shear and bulk moduli and a_0

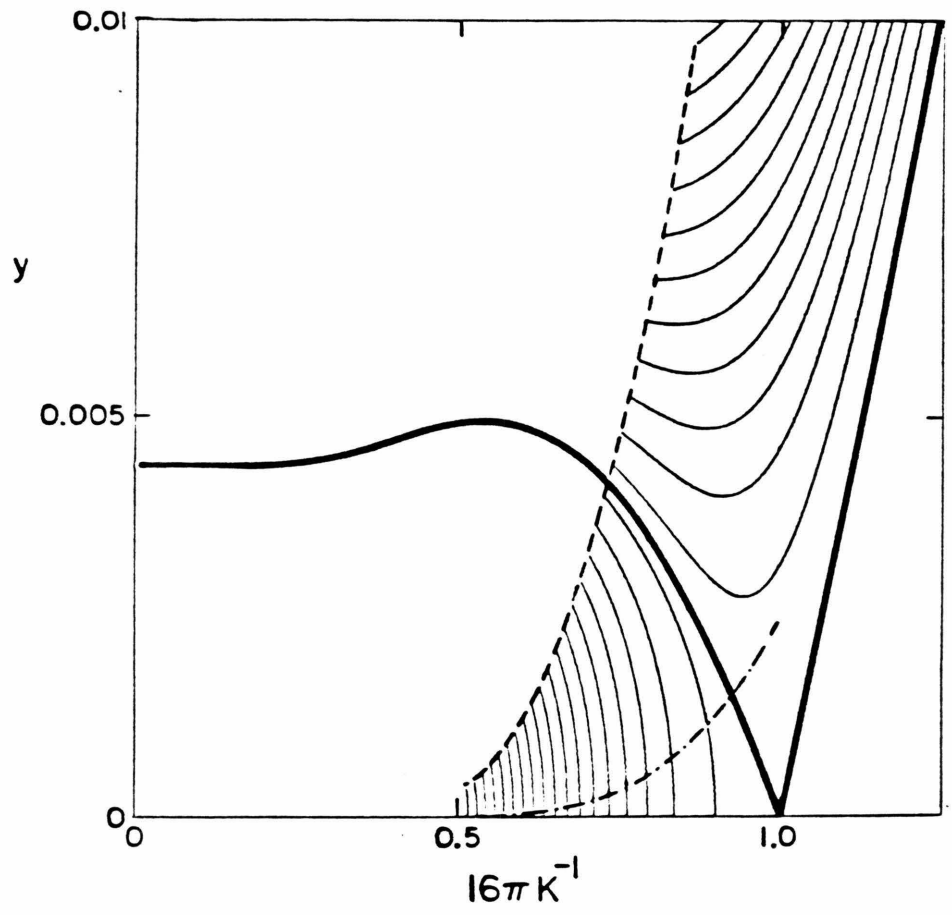

Figure 6.1. Phase plane of the RG equations for a smooth substrate of Nelson and Halperin. Heavy lines represent the separatrices, the dashed line is a line of starting points for C=2, and the dot-dashed line shows initial conditions for C=3. The remaining curves are RG trajectories. The region below the left separatrix contains all possible solid states.

is the lattice spacing. The endpoint (x_1,E_1) is determined by the criterion for cutting off the RG integral when the correlations are roughly constant. There are several such criteria which we have shown numerically [4] to be essentially identical, e.g. $x=0.1$ or $y=0.01$. The trajectory passes through a minimum where $\frac{dy}{dl}=0$ in equation (6.3b), namely when

$$y=-\frac{1}{\pi B}x \tag{6.7a}$$

or equivalently, when

$$D^*=-(\frac{1}{\pi B}+m_-)x^* \tag{6.7b}$$

or

$$E^*=-(\frac{1}{\pi B}+m_+)x^*. \tag{6.7c}$$

In integrating the RG equations, equation (6.5a) is used from the starting point to the minimum, and then equation (6.5b) out to the cutoff point. By expanding the line of starting points around the value where it intersects the incoming separatrix, it becomes clear that $D_0 \propto |t|$ where t is reduced temperature, $(T-T_m)/T_m$.

The equations (6.3a,3b) do not depend on l explicitly, so we may consider their quotient

$$\frac{dx}{dy}=\frac{6\pi^2 Ay}{x+\pi By}, \tag{6.8}$$

which, upon substitution of $y=vx$ can be shown to have the solution

$$(y-v_+x)^\alpha(y-v_-x)^\beta=\kappa \tag{6.9}$$

with $v_\pm=m_\pm$, $\beta=6\pi^2 Am_-^2/(1+6\pi^2 Am_-^2)=\bar{\nu}$ and $\alpha=1-\beta$. Clearly the starting point and endpoint must lie on the trajectory, so

$$\kappa=(y_0-v_+x_0)^\alpha(y_0-v_-x_0)^\beta \tag{6.10a}$$

$$\kappa=(y_1-v_+x_1)^\alpha(y_1-v_-x_1)^\beta \tag{6.10b}$$

or in terms of D and E

$$\kappa = D_0^{\beta}(D_0 + (v_- - v_+)x_0)^{\alpha} \tag{6.11a}$$

$$\kappa = E_1^{\alpha}(E_1 + (v_- - v_+)x_1)^{\beta}. \tag{6.11b}$$

When D_0 is sufficiently small and x_1 sufficiently large that

$$D_0 \ll |v_- - v_+||x_0| \tag{6.12a}$$

$$E_1 \ll |v_+ - v_-|x_1 \tag{6.12b}$$

a relationship can be established between starting points and endpoints,

$$E_1 \approx D_0^{\beta/\alpha} \frac{(v_- - v_+)x_0}{[(v_- - v_+)x_1]^{\beta/\alpha}}. \tag{6.13}$$

Rewriting the trajectory in terms of D and E,

$$\kappa = D^{\beta}[D + (v_- - v_+)x]^{\alpha} \tag{6.14a}$$

$$\kappa = E^{\alpha}[E + (v_- - v_+)x]^{\beta}. \tag{6.14b}$$

and solving each one for x we find

$$x = \frac{\kappa^{1/\alpha}}{(v_- - v_+)D^{\beta/\alpha}} - \frac{D}{(v_- - v_+)} \equiv \frac{\Gamma}{D^{\beta/\alpha}} - \frac{D}{(v_- - v_+)} \tag{6.15a}$$

$$x = \frac{\kappa^{1/\beta}}{(v_+ - v_-)E^{\alpha/\beta}} - \frac{E}{(v_+ - v_-)} \equiv \frac{\tilde{\Gamma}}{E^{\alpha/\beta}} - \frac{E}{(v_+ - v_-)} \tag{6.15b}$$

where the constants Γ and $\tilde{\Gamma}$ contain all the dependence on initial or final conditions. When the approximations of equation (6.12) are valid,

$$\Gamma \approx D_0^{\beta/\alpha} x_0 \tag{6.16a}$$

$$\tilde{\Gamma} \approx E_1^{\alpha/\beta} x_1. \tag{6.16b}$$

Inserting equations (6.15) into equations (6.5) we find

$$\frac{dD}{dl} = -2\Gamma D^{1-\beta/\alpha} + GD^2 \tag{6.17a}$$

$$\frac{dE}{dl} = -2\tilde{\Gamma} E^{1-\alpha/\beta} + HE^2 \tag{6.17b}$$

where

$$G \equiv 12\pi^2 A m_+ + \frac{2}{(v_- - v_+)} \tag{6.18a}$$

$$H \equiv 12\pi^2 A m_- + \frac{2}{(v_+ - v_-)}. \tag{6.18b}$$

Now the integral of the renormalization group trajectory is the sum of two quadratures with no closed form solution, i.e.

$$l^* = l_1^* + l_2^* \tag{6.19}$$

where

$$l_1^* = \int_{D_0}^{D^*} \frac{dD}{-2\Gamma D^{1-\beta/\alpha} + GD^2} \tag{6.20a}$$

$$-l_2^* = \int_{E_1}^{E^*} \frac{dE}{-2\tilde{\Gamma} E^{1-\alpha/\beta} + HE^2}. \tag{6.20b}$$

How does l^* depend on $|t|$?

It is tempting to discard the second term in the denominator of each integral on the grounds that for small D and E, the first term dominates. For small D_0 and E_1, D and E are small near the endpoints, but, as we now show, become larger near the minimum (D^* and E^*), where, in fact, both terms in the denominator of each integral are of similar size.

Inserting equations (6.15) into equations (6.7) we find solutions

$$D^* = R\Gamma^{\alpha} \sim D_0^{\beta} \tag{6.21a}$$

$$E^* = S\tilde{\Gamma}^{\beta} \sim E_1^{\alpha} \tag{6.21b}$$

with R and S constants independent of D_0 and E_1. Comparing equation (6.21a) and equation (6.21b) we find that

$$D_0^{\beta} \sim E_1^{\alpha}. \tag{6.22}$$

Rearranging the denominators of equation (6.20) we find at the minimum,

$$\Gamma^2 \alpha(-2R^{1-\beta/\alpha} + GR^2) \tag{6.23a}$$

$$\tilde{\Gamma}^2 \beta(-2S^{1-\alpha/\beta} + HS^2) \tag{6.23b}$$

so the dependence upon starting point factors out. The universal constants in equation (6.23a), for example, are nearly the same

$$\frac{R^{1-\beta/\alpha}}{R^2} = 50.567\ ,\ G = 76.08 \tag{6.24}$$

so the integrals for l^* must be evaluated without truncating the denominator.

This is done by rescaling the equations to remove the dependence on D_0 from the integrand. Let $P \equiv D/D_0^s$ and determine s such that all the dependence upon D_0 factors out of the integral in equation (6.20a). Not surprisingly, $s = \beta$. Similarly, the substitution $Q \equiv E/E^{\alpha}$ produces the following set of integrals

$$l_1^* = D_0^{-\beta} \int_{P_0}^{P^*} \frac{dP}{-2x_0 P^{1-\beta/\alpha} + GP^2} \tag{6.25a}$$

$$-l_2^* = E_1^{-\alpha} \int_{Q_0}^{Q^*} \frac{dQ}{-2x_1 Q^{1-\alpha/\beta} + HQ^2} \tag{6.25b}$$

where equation (6.12) has been used to simplify Γ and $\tilde{\Gamma}$. Now differentiate the integrals with respect to D_0 and E_1, respectively, to find

$$\frac{dl_1^*}{dD_0} = \frac{-\beta l_1^*}{D_0} - D_0^{-\beta} \frac{\alpha D_0^{-\beta}}{-2x_0 P_0^{1-\beta/\alpha} + GP_0^2} \tag{6.26a}$$

$$\frac{-dl_1^*}{dE_1} = \frac{-\alpha l_2^*}{E_1} - E_1^{-\alpha} \frac{\beta E_1^{-\alpha}}{-2x_1 Q_1^{1-\alpha/\beta} + HQ_1^2}. \tag{6.26b}$$

Since

$$P_0 = D_0 / D_0^{\beta} = D_0^{\alpha} \tag{6.27a}$$

and similarly,

$$Q_1 = E_1^{\beta}. \tag{6.27b}$$

The second term in each of the differential equations (6.26) above arises from differentiating the lower limit of the integrals in equations (6.25). The upper limit makes no contribution, because by choice of P and Q and equations (6.21), P^* and Q^* are independent of D_0 and E_1, respectively.

Inserting equations (6.27) into equations (6.26), the differential equations can be solved by the usual use of integrating factors, yielding,

$$l_1^* = D_0^{-\beta} \int_{\Delta}^{D_0} \frac{\alpha d\Delta}{\Delta^{\alpha}(-2x_0 + G\Delta)} \tag{6.28a}$$

$$-l_2^* = E_1^{-\alpha} \int_{\varepsilon}^{E_1} \frac{\beta d\varepsilon}{\varepsilon^{\beta}(-2x_1 + H\varepsilon)}. \tag{6.28b}$$

The second term in the denominators of equation (6.28) can now be discarded, for suitably small values of D_0 and E_1, and the integrals yield

$$l_1^* \approx \frac{\alpha}{-2x_0\beta} + MD_0^{-\beta} \tag{6.29a}$$

$$l_2^* \approx \frac{\beta}{2x_1\alpha} + NE_1^{-\alpha} \tag{6.29b}$$

where M and N are constants. Since $E_1 \sim D_0^{\beta/\alpha}$, we have

$$l^* = l_1^* + l_2^* \sim D_0^{-\beta} \sim |t|^{-\beta} \tag{6.30}$$

which agrees with the result from NH.

The present calculation improves that of NH because their analysis of the behavior of l^* worked by means of an incorrect approximation. They integrated from the initial point toward the minimum, and stopped when D became significant (before the minimum), then arbitrarily jumped across the minimum and added a piece gained from integrating along the outgoing separatrix. We have shown numerically that nearly all the contribution to l^* comes near the minimum, but since that part also $\sim |t|^{-\beta}$, NH accidentally got the correct dependence, although the constants of proportionality were wrong.

The only approximations in the treatment above are those of equations (6.12) and the truncation of the denominator of equations (6.25). (These latter could be removed by performing a Taylor series expansion to any desired accuracy, but we are only concerned with the leading order behavior.) The approximations produce bounds on the validity of the scaling law, and hence give an indication of the width of the critical region.

From equation (6.12) we find

$$D_0 \ll |.0564 x_0| \tag{6.31a}$$

$$E_1 \ll |.0564 x_1| \quad or \quad D_0 \ll |.0564 x_1|^{(1-\beta)/\beta} \tag{6.31b}$$

and from the integrals,

$$GD_0 \ll 2x_0 \implies D_0 \ll .0341 x_0 \tag{6.31c}$$

$$HE_1 \ll 2x_1 \implies D_0 \ll (.0223 x_1)^{(1-\beta)/\beta}. \tag{6.31d}$$

Clearly, the controlling approximations are equations (6.31c) and (6.31d). Since $(1-\beta)/\beta = 1.71$, we can rewrite equation (6.31d) as

$$D_0 \ll .0015 x_1^{1.71}. \tag{6.31e}$$

Choosing $x_1 = 0.1$ (supposedly far enough from the transition that ξ_+ is roughly constant) and $x_0 = -.01$, the controlling approximation is equation (6.31e),

$$D_0 \ll 2.9\times10^{-5}. \tag{6.32}$$

It remains only to find the proportionality between D_0 and $|t|$, from the equation of the line of starting points. Expanding equation (6.6) around the intersection with the separatrix we obtain

$$y_0 \approx y_s\left(1+\frac{CK_0}{8\pi k_B T_s}t\right) \tag{6.33a}$$

$$x_0 \approx x_s+\frac{K_0}{16\pi k_B T_s}t \tag{6.33b}$$

where the subscript s refers to values at the intersection of the line of starting points with the separatrix,

$$y_s = m_- x_s. \tag{6.33c}$$

Thus,

$$D_0 = y_0 - m_- x_0 = Q_s t\left(y_s - \frac{m_-}{2C}\right) \tag{6.34}$$

where $Q_s = CK_0/8\pi k_B T_s$. At the intersection of the separatrix with the line $y=0$, the value of Q_s is $2C$, and since K_0 varies by less than 30% over the region where the separatrix is approximately linear, we take $Q_s \approx 6$, for $C \approx 3$, and $y_s \sim .001$, $m_- = -.021$, we have $D_0 \approx .03t$. Since $x_s \approx -.05$ from equation (6.33c), we have $x_0 \approx -.05+t$. Thus for typical values of the core parameter C, for values of

$$t \ll .001 \tag{6.35}$$

the inequality (6.32) is satisfied. This inequality is actually general, being satisfied over the entire region where the separatrix is nearly linear, since for larger C, the last term of equation (6.34) is dominated by $m_-/2C$, so D_0 approaches $m_- t$. For smaller values of C, even more restrictive criteria hold because an RG trajectory through any point on the line of starting points for $C=3$ intersects lines of starting points for smaller C closer to the separatrix. Thus the width of the transition region is characterized by equation (6.35).

2. Numerical Tests

The predictions of the analysis of the previous section were tested by numerical integrations of the RG equations. The numerical results for the core parameter C=2 are shown in table 6.1, where the choice of l^* was made in several ways to ensure that the cutoff procedure did not influence the results. An unresolved numerical precision problem caused the results to be unreliable for l^*>500.

Table 6.1

t	Criterion		
	$16\pi\bar{K}^{-1}=1.1$	$y=0.1$	y diverges
10^{-6}	469.0	473.5	474.0
10^{-5}	195.0	199.0	200.0
10^{-4}	78.0	82.4	83.0
10^{-3}	29.0	33.0	34.0

Figure 6.2 displays a sensitive test of the critical exponent $\bar{\nu}$. It plots $l^* t^{\bar{\nu}}$ vs. log$t$ normalized to a convenient value for C=2 and C=3. Except for the slightly inaccurate results at very small values of t, the points are nearly constant over several orders of magnitude in t, beginning to deviate from the horizontal line near $t \sim 10^{-3}$.

3. Conclusions

There have been no measurements of this level of accuracy that can be interpreted as indicators of a 2-D melting transition, so any confirmation of the scaling law for the correlation length, or any other critical behavior predicted by the theory must be left to some future generation of experiments, which must begin by finding extremely accurate values of the transition temperature and then look at a narrow range of reduced temperature on either side.

T_m is the lowest temperature at which y and $\bar{K}^{-1}$ diverge as $l \to \infty$, and thus cannot be determined exactly in any experiment sensitive to the behavior of the system on finite scales. Dynamical experiments thus do not determine the

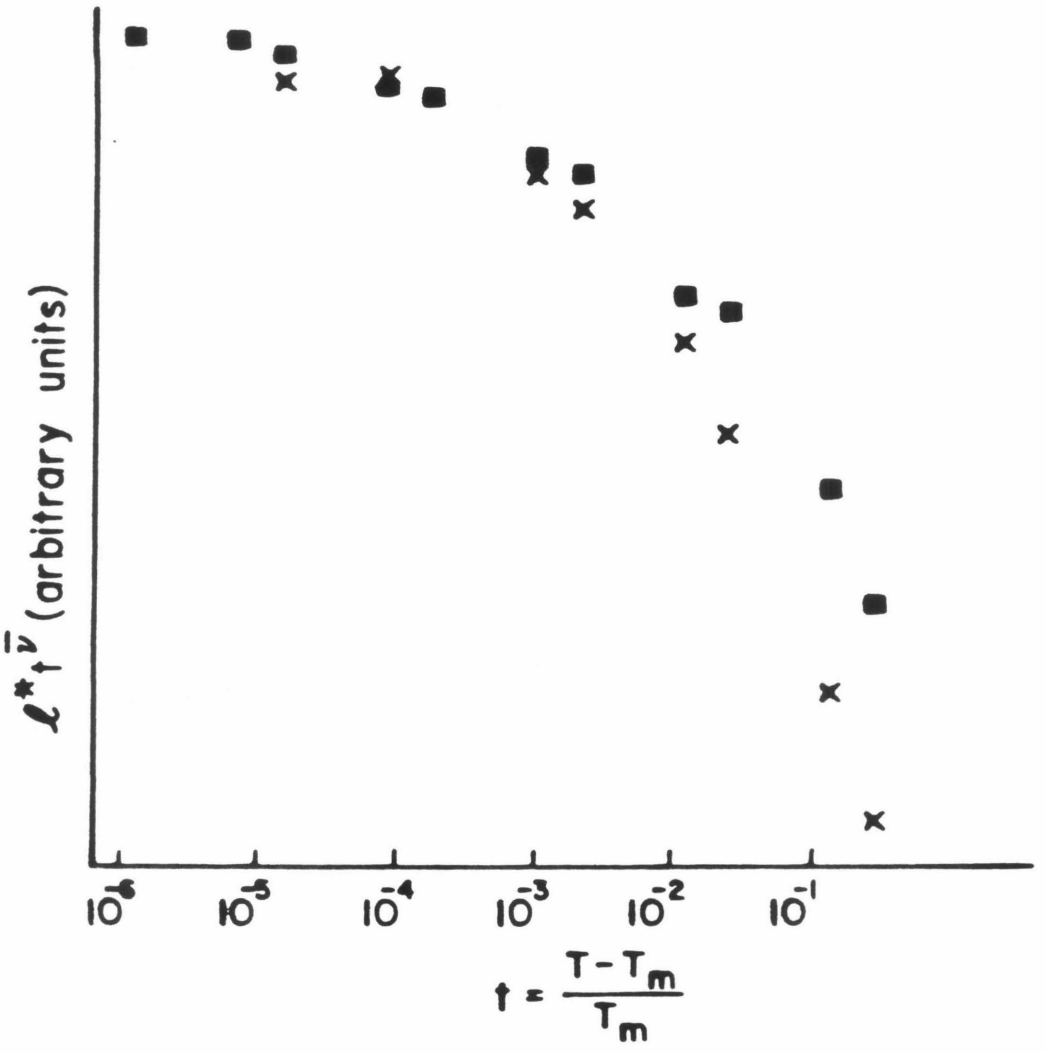

Figure 6.2. $l^* t^{\bar{\nu}}$ *vs.* log$t$ for C=2 (x) and C=3 (•) from numerical integration of RG equations.

exact transition temperature since they probe finite wavevectors.

Using the data of table 6.1 we can estimate the difficulty. The asymptotic *critical* behavior is observable if $t<\sim 10^{-3}$ which means a correlation length larger than $e^{30}\approx 10^{13}$ lattice spacings. On smaller length scales, the medium remains solid up to a higher temperature. Typical experiments are performed on lattices of order 10^2-10^7 lattice spacings. Thus, in practical cases, the experiments cannot probe the prediction of the exponent $\bar{\nu}$.

Even for very large samples, the nature of the experiment must be carefully considered. A neutron scattering experiment, for example, could detect critical behavior in the necessary range of reduced temperature only for momentum transfers smaller than about 10^{-13} in units of the reciprocal lattice spacing. The related requirement on frequencies implies that such experiments must be done on very long time scales.

Since many experiments are done on very small samples (i.e. Grafoil, which has homogeneous patches of order 100–2000Å), we have plotted in figure 6.3 the apparent melting temperature as a function of sample size using parameters (elastic constants) applicable to ^{3}He with an assumed core energy parameter $C=2.8$. A more realistic treatment of the problem of a finite substrate would have to take into account conditions at the sample boundary and other complications; however, figure 6.3 does correctly describe the temperature at which the correlation length does become of the order of the size of a corresponding patch in an infinite solid. It was deduced from numerical integration of the RG equations.

While the theory may yield other testable predictions, the asymptotic critical behavior seems beyond the range of current experiments.

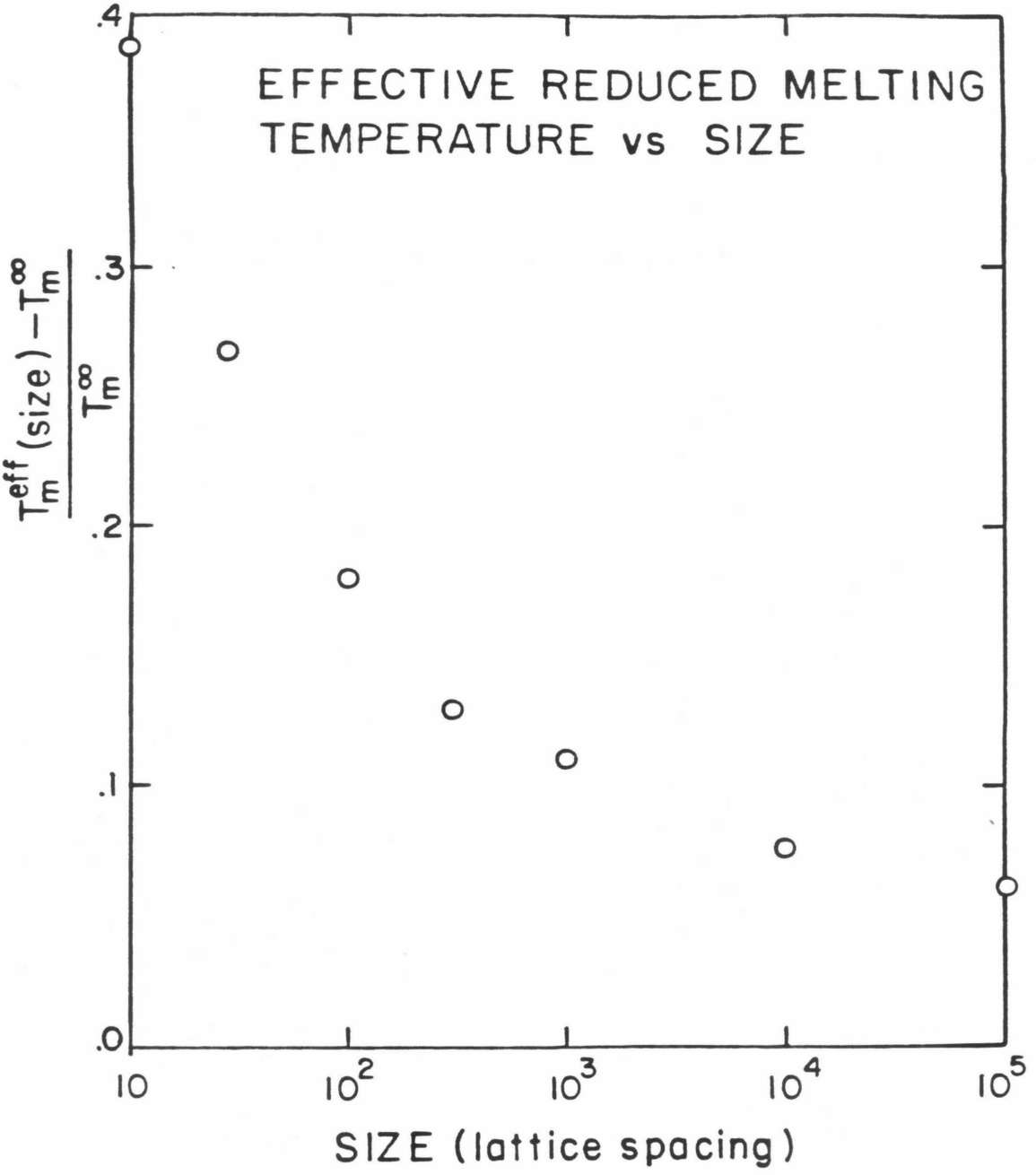

Figure 6.3. Apparent reduced melting temperature (relative to that for an infinite medium) for a patch of given size (in the infinite medium).

References

1. S. Solla and E. Riedel, preprint.

2. D. R. Nelson and B. I. Halperin, *Phys. Rev.* B19, 2457(1979).

3. A. P. Young, *Phys. Rev.* B19, 1855(1979).

4. J.M. Greif, D. L. Goodstein, and A.F. Silva-Moreira, to be published.

Appendix: Generation of Thermodynamic Tables for ^{3}He

This appendix presents tables of the thermodynamic functions for ^{3}He films on Grafoil for submonolayers over the range 0-19K and for 2 layer films above 2.4K, and describes how these tables were produced from three separate experimental sources.

The "Raw" Data

The so-called raw data are from three sources. From Caltech there is the mixture of heat capacity and vapor pressure measurements made by Robert Elgin at Caltech over the temperature range 2.4-19.5K and from .003 to 2 layers. From the University of Washington there are two sets of data. One is heat capacity measurements by Bretz, *et al.* [1] These were taken at coverages between roughly .1 and .7 layers and temperatures between 0.037 and 4.2K. The data of Hering,[2] and Hering, van Sciver and Vilches [3] comprise 3 runs of heat capacities between .04 and .15 layers and .05-1.5K and much denser data between .6-1.0 layers and .05-4.2K.

The Caltech and Washington data are rather different in character. The Caltech data are a systematic grid in the coverage-temperature plane at 57 coverages and 24 temperatures. All the measured Caltech heat capacities are averages over the 10% temperature intervals used in the tables. The vapor pressure was measured whenever it was observable, that is at high temperatures and coverages. The data was reduced by the experimenter to produce the high temperature part of the tables displayed here, according to methods described in

detail in Elgin and Goodstein.[4] The heat capacities were all corrected for the effect of desorption into the bulk gas in equilibrium with the film.

The technique used by Elgin, of averaging over 10% temperature intervals, is not useful for elucidating features of sharp heat capacity peaks, but essentially provides the glue that allows the rest of the data to be connected by thermodynamic relationships and makes possible a survey of the entire phase diagram. The functions which should be most accurately deduced from these data alone are functions integrated up from the data, for example, the entropy from the heat capacity. The coarseness of the data grid in the coverage vs. temperature (n-T) plane means that reduction methods should treat the data as histograms, each bin representing, e.g. the average heat capacity over the temperature interval spanned. The vapor pressure, however, is quite accurate at the temperature and coverage where it was measured, and does not repesent an average over any changes in thermodynamic variables.

The Washington data are generally more intensive in "interesting" regions and sparse elsewhere. Heat capacities were measured over small intervals (as small as 1mK) near peaks and at many points on peaks. There are runs at several coverages near the ordering transition in the Bretz data which cover only a narrow temperature range like 2.5-3.5K.

The raw data discussed in Bretz, *et al.* were provided in the form of a table of heat capacities at various temperatures and coverages for both ^{3}He and ^{4}He, and it was necessary to use the table rather critically to weed out typographical errors.

The heat capacity data from Hering, *et al.*, were easier to verify, since the necessary heater input and thermometer readings were included, except in the case of the three low-coverage runs, which were read from unpublished graphs.

None of the Washington heat capacity data is corrected for desorption.

Preparing the Thermodynamic Tables

Several attempts were made to prepare self-consistent tables of the thermodynamic functions. The difficulties were mostly in dealing with scatter and highly variable density of data from Washington.

The goal of the procedure was to extend the tables of Elgin downward in temperature,continuing his regular grid of 10% intervals at the coverages he used. Thus the basic procedure required interpolating each Washington run (at fixed coverage) to produce heat capacities at the "magic" grid temperatures, and then interpolating between coverages at these temperatures to produce results at the grid coverages, that is,a bivariate interpolation of a non-standard sort.

First, a brief review of the method used by Elgin on the high-temperature data will be presented. By equating film and vapor chemical potentials,and using the ideal gas law (with virial corrections when necessary) the measured vapor pressures determined the chemical potential of the film where vapor pressures could be measured.

An extremely difficult problem for these measurements in certain ranges of pressure is that of determining the pressure in a cold chamber, e.g., at 4K, with a gauge at room temperature when a long thin tube connects the warm and cold regions. The pressure is different in the warm and cold regions, basically owing to the different effusion rates of warm and cold gas through the tube, but complicated by details of the inner surface of the tube, the temperature gradient along it, and other effects. The gauge must be calibrated for the particular tube, gas, temperature and pressure range by empirical methods. This effect is called thermal transpiration.

The coverage was determined by keeping track of the total 3He in the system and the amount in the gas (again using the corrected pressures). Where chemical potentials existed at nearby temperatures, a Maxwell relation converted $\left.\frac{\partial \mu}{\partial T}\right]_n$ to $-\left.\frac{\partial S}{\partial n}\right]_T$. This could be integrated from zero coverage (where the entropy is zero) to produce entropy values at high temperature where the vapor pressures were measured. The heat capacity and vapor pressure data overlapped at each coverage,so starting from known entropy values, the heat capacity could be integrated downward to extend the entropy to lower temperatures. Comparing entropies at different coverages, the Maxwell relation above could be used to extend the chemical potential and pressure data downward in temperature as well.

In extending these tables further downward in temperature using the data from Washington,the procedure was the same,with a few exceptions. Because his data were corrected for desorption and very smooth,Elgin could reliably take derivatives simply by subtracting neighboring values and dividing by the interval (or using next-nearest-neighboring values and assigning the derivative to the point in between) and integrate by treating his data as histograms.

By contrast,the Washington data is irregular and has lots of scatter. This is not to say it is less accurate (since it is based on much smaller heat inputs than Elgin used) but rather that it attempts finer resolution. Desorption corrections are only necessary when the pressure of the gas is high (how high depends on the dead volume of the system — the corrections are to account for changes in the surface coverage owing to thermal promotion of atoms into the gas) and in practice, turned out to be unimportant below 3K or so. This left some overlap of heat capacities,but not as much as would be desired for consistency checking. Even at lower coverages where desorption was unimportant even above 3K, the Washington calorimeter was reported to have uncorrected temperature drifts

above 3K making some of that data unreliable.

In any case, the scatter in the data made it impossible to differentiate it directly. It was thought that since the entropy was to be derived from the heat capacity by integration, the scatter would be filtered,but even this turned out to produce $\left.\frac{\partial S}{\partial n}\right]_T$ values of wildly oscillating signs,etc. It was necessary to smooth the data, and their variable density made this difficult. The scatter was worst on the sides of sharp peaks, where small errors in measuring the temperature cause sharp oscillations in the curves drawn through the data points. Various techniques of fitting were tried – low order polynomial fits (up to 20th degree), and similar techniques using orthogonal polynomials, truncated Fourier series fits, and fits using spline functions. All of these methods had similar difficulties -- wherever the fitting functions were not constrained by many data points, i.e. at the ends of the interval or where the data were sparse, they would diverge or bend far from the rest of the data, seriously affecting the quality of the fit for considerable distances into the dense data. All but the spline fits failed to follow peaks correctly.

What finally worked was a method known as B-splines on an irregular mesh, which are explained at the end of this section. It is not necessary to know how they work,since plots of the data points and the smoothed curves fitting them clearly show that the procedure introduces nothing pathological, except rounding of the peaks (at the very top). See figure (A.1) The curves are essentially the same as would be drawn by eye and French curve, except they have characteristic mathematical properties because they are best fits in a certain sense.

The B-splines that were used to smooth the heat capacities and other thermodynamic functions are easily integrated and differentiated. The Elgin data were analyzed to find starting values of the entropy that weren't too near any

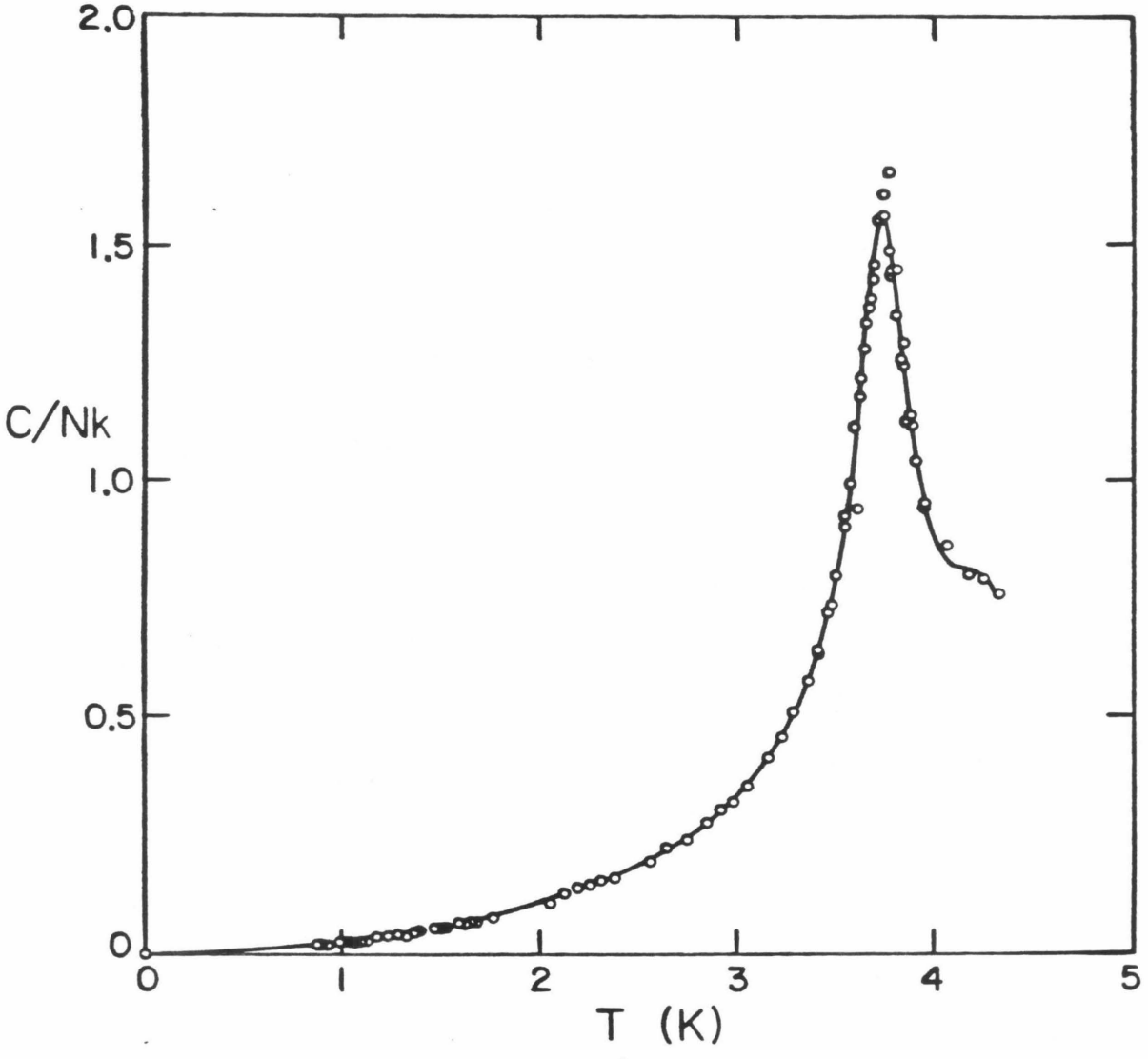

Figure A.1 – Experimental heat capacity run for ^{3}He and the B-spline approximation to it, with knots chosen at every fourth data point.

phase transitions (to avoid problems matching to the histogram type results). From these starting values, the integrated C/T values were subtracted to extend the entropies to the lowest temperatures for which heat capacities existed at each coverage,including at all the "magic" temperatures in the range. This table of entropies was interpolated to the grid points between coverages. The entropies were then smoothed and differentiated with B-splines to generate new values of chemical potential from the Elgin starting values at 2.4119K. The temperature integrations of $\left.\frac{\partial \mu}{\partial T}\right)_n$ were both upward and downward, the upward ones being designed to check the consistency of the reduction by comparing with Elgin's derived chemical potentials. They are not completely consistent but the differences are small. They probably arise from two effects. One is that these chemical potentials are derived from the unreliable high-temperature heat capacities from Washington, uncorrected for desorption, which should have significant effects on $\left.\frac{\partial S}{\partial n}\right)_T$ at least at high coverage. The other is that nearly all the Elgin chemical potentials below 4.2K are derived from his histogram procedure, rather than from direct measurement of vapor pressures at these temperatures, and the B-spline procedure should be more accurate with dense,scattered data. In all cases checked so far, the change in chemical potential computed between 2.4 and 4.2K is larger than the change computed by Elgin.

In the course of generating the entropy tables, it was found necessary to fill out the heat capacity tables in certain regions to prevent the fitting functions from misbehaving in nearby regions where data exist. This "fake" data were inserted in the following places:

1. In the 3 Hering runs at very low coverage, the upper temperature limit was 1.5K. Entropies and heat capacities between 2.4 and 4.2K were interpolated between nearby Elgin coverages and although there was no overlap of the data from Caltech and Washington here, the integrations were carried out anyway (using a very large first step). The results at very low coverage and temperature cannot be taken very seriously.
2. Several of the runs in the solid region extended only down to about 1K. To prevent messing up the edges of nearby regions where the data extended to much lower temperature,these runs were extrapolated toward zero temperature using a T^2 law with Debye temperatures from Hering's analysis of her own data.
3. Several runs near the registry density which contained only points near the peak were ignored during the preparation of the general tables.

Nature of B-splines[5,6,7]

Consider a real interval [a,b] and a set of values c0,c1,...cn in that interval.The points a,c0,c1,...,b are a set of knots on the interval. On this set of knots we can construct functions with following properties:

1. On each sub-interval between two knots,the function is a cubic polynomial.
2. Each of the cubic polynomials joins onto its neighbors smoothly, matching function values, first and second derivatives at the knots.

The set of all such functions on a particular set of knots forms a function space. If we have a function defined at any set of points on the interval [a,b], there is a unique member of the function space which is a best fit (in the least squares sense) to the arbitrary function, that is, out of all the members of this function space, it comes closest to the arbitrary function.

It turns out that there is a way to choose a basis for the function space

(with some trickery at the ends of the interval [a,b]) with the property that on any sub-interval, only four of the basis functions are nonzero (the total number of basis functions is n+4, where n is number of subintervals). All the functions in the space are linear combinations of basis functions, so the least squares fit can be represented as a linear regression to find the coefficients of the linear combination, and since only four functions are defined on any subinterval,the matrix equation is banded and easy to solve and store,even if there are many knots and data points. The problem is always well-posed if a decent choice of the knots is made. A good rule of thumb is to make sure that every sub-interval has at least one data point in it — if it doesn't, the polynomial may go crazy in that subinterval. For that reason,standard spline smoothing (which spaces the knots at regular intervals), fails. Each of these functions which is a smooth joining of cubic polynomials is by definition a spline function and the space is the space of B-splines on a given set of knots.

The way the scattered heat capacity data were treated was to place the knots at every k-th data point (typically, k=4).

Notice that this fitting procedure is different from the procedure of spline interpolation (also used in this data reduction project). The fitting procedure finds the spline curve that comes closest to a set of data points given a perhaps unrelated set of knots, while the interpolation procedure fixes one knot at each data point, constructs the unique spline function that passes through all the data points, and uses it to interpolate between the data points.

Thermodynamic tables for ^{3}He

The table of the thermodynamic functions for ^{3}He films follow. The columns are identified and their units set forth below.

The first line of each page contains the coverage, first in units of $Å^{-2}$ and

then as a fraction of the 1/3 registry. The columnar data are, from left to right

1. Temperature in Kelvins
2. Chemical potential in Kelvins
3. Natural log of the 3-D gas pressure in torr
4. Entropy per atom in Boltzmanns
5. Bulk modulus in $ergs / cm^2$
6. Landau potential density in $ergs / cm^2$ (same as 2-D pressure)
7. Helmholtz free energy density in $ergs / cm^2$
8. Internal energy density in $ergs / cm^2$

References

1. M. Bretz, J. G. Dash, D. C. Hickernell, E. O. McLean, and O. E. Vilches, *Phys. Rev.* **A8**, 1589(1973).

2. S.V.'Hering, Ph.D. thesis, University of Washington, Seattle, WA, 1975.

3. S. V. Hering, S. W. van Sciver, and O. E. Vilches, *J. Low Temp. Phys.* **25**, 793(1976).

4. R. L. Elgin and D. L. Goodstein, *Phys. Rev.* **A9**, 2657(1974).

5. C. L. Lawson and R. A. Hanson , *Solving Least Squares Problems* (Prentice-Hall , Englewood Cliffs, N.J., 1974).

6. C. de Boor, *J. Approx. Theory* **6**, 50(1972).

7. C. de Boor, *J. Approx. Theory* **1**, 219(1968).

Table of Thermodynamic Functions of ^{3}He on graphite.

n= .3859e-03 ang**-2 or n/nc= .6062e-02

T	u	Ln(P3D)	S/Nk	B	-P2d=W	F	E
2.4119	-263.65	-1.018e+02	1.3820	4.770e-02	-.0230	-.1247	-.1234
2.6421	-263.60	-9.202e+01	1.4323	4.750e-02	-.0229	-.1246	-.1231
2.8943	-263.54	-8.308e+01	1.4574	4.720e-02	-.0227	-.1244	-.1228
3.1707	-263.48	-7.490e+01	1.4825	4.690e-02	-.0226	-.1242	-.1224
3.4735	-263.41	-6.740e+01	1.5077	4.650e-02	-.0224	-.1240	-.1220
3.8051	-263.34	-6.055e+01	1.5579	4.610e-02	-.0222	-.1238	-.1215
4.1686	-263.26	-5.427e+01	1.5831	4.560e-02	-.0220	-.1235	-.1210
4.5667	-263.17	-4.851e+01	1.6333	4.510e-02	-.0217	-.1232	-.1204
5.0029	-263.08	-4.324e+01	1.6836	4.450e-02	-.0214	-.1229	-.1197
5.4808	-262.98	-3.841e+01	1.7590	4.380e-02	-.0210	-.1225	-.1188
6.0045	-262.89	-3.398e+01	1.8092	4.300e-02	-.0206	-.1221	-.1179
6.5784	-262.83	-2.993e+01	1.9600	4.200e-02	-.0201	-.1216	-.1166
7.2072	-262.83	-2.621e+01	2.0354	4.090e-02	-.0195	-.1210	-.1153
7.8958	-262.93	-2.282e+01	2.1861	3.940e-02	-.0188	-.1203	-.1136
8.6503	-263.16	-1.971e+01	2.4123	3.770e-02	-.0179	-.1195	-.1114
9.4770	-263.60	-1.688e+01	2.7138	3.570e-02	-.0169	-.1186	-.1087
10.3830	-264.38	-1.430e+01	2.9148	3.350e-02	-.0158	-.1178	-.1061

n= .6119e-03 ang**-2 or n/nc= .9612e-02

T	u	Ln(P3D)	S/Nk	B	-P2d=W	F	E
2.4119	-223.60	-8.519e+01	.9508	7.790e-02	-.0505	-.1873	-.1859
2.6421	-223.77	-7.695e+01	.9667	7.740e-02	-.0502	-.1871	-.1856
2.8943	-223.95	-6.940e+01	.9667	7.700e-02	-.0499	-.1869	-.1852
3.1707	-224.16	-6.249e+01	.9825	7.640e-02	-.0496	-.1867	-.1848
3.4735	-224.40	-5.617e+01	.9984	7.580e-02	-.0492	-.1865	-.1844
3.8051	-224.67	-5.039e+01	1.0142	7.520e-02	-.0487	-.1862	-.1839
4.1686	-224.99	-4.509e+01	1.0301	7.440e-02	-.0482	-.1859	-.1833
4.5667	-225.37	-4.024e+01	1.0459	7.340e-02	-.0476	-.1856	-.1826
5.0029	-225.82	-3.579e+01	1.0935	7.230e-02	-.0470	-.1852	-.1818
5.4808	-226.36	-3.173e+01	1.1410	7.090e-02	-.0462	-.1847	-.1809
6.0045	-227.04	-2.801e+01	1.2202	6.920e-02	-.0452	-.1841	-.1797
6.5784	-227.90	-2.462e+01	1.3312	6.710e-02	-.0441	-.1835	-.1782
7.2072	-229.01	-2.152e+01	1.4579	6.470e-02	-.0427	-.1828	-.1764
7.8958	-230.44	-1.870e+01	1.5847	6.180e-02	-.0410	-.1820	-.1744
8.6503	-232.25	-1.614e+01	1.7432	5.840e-02	-.0390	-.1811	-.1719
9.4770	-234.50	-1.381e+01	1.9967	5.440e-02	-.0367	-.1802	-.1687
10.3830	-237.32	-1.169e+01	2.3137	5.010e-02	-.0342	-.1794	-.1647

n= .9697e-03 ang**-2 or n/nc= .1523e-01

T	u	Ln(P3D)	S/Nk	B	-P2d=W	F	E
2.4119	-186.84	-6.995e+01	.9700	7.780e-02	-.0883	-.2695	-.2673
2.6421	-187.17	-6.310e+01	1.0000	7.760e-02	-.0879	-.2694	-.2668
2.8943	-187.55	-5.683e+01	1.0300	7.730e-02	-.0874	-.2693	-.2664
3.1707	-187.99	-5.109e+01	1.0500	7.690e-02	-.0868	-.2691	-.2659
3.4735	-188.50	-4.584e+01	1.0900	7.640e-02	-.0862	-.2689	-.2653
3.8051	-189.10	-4.104e+01	1.1300	7.570e-02	-.0854	-.2688	-.2646
4.1686	-189.82	-3.665e+01	1.1800	7.470e-02	-.0845	-.2685	-.2638
4.5667	-190.68	-3.264e+01	1.2400	7.350e-02	-.0834	-.2683	-.2628
5.0029	-191.73	-2.898e+01	1.3200	7.200e-02	-.0821	-.2680	-.2616
5.4808	-193.01	-2.565e+01	1.4200	7.010e-02	-.0805	-.2677	-.2601
6.0045	-194.59	-2.261e+01	1.5500	6.790e-02	-.0786	-.2673	-.2583
6.5784	-196.52	-1.985e+01	1.7400	6.540e-02	-.0764	-.2670	-.2559
7.2072	-198.86	-1.734e+01	1.9700	6.270e-02	-.0738	-.2666	-.2528
7.8958	-201.68	-1.506e+01	2.2200	5.990e-02	-.0707	-.2663	-.2493
8.6503	-205.05	-1.299e+01	2.4900	5.700e-02	-.0671	-.2660	-.2451
9.4770	-209.05	-1.112e+01	2.8200	5.410e-02	-.0631	-.2658	-.2399
10.3830	-213.75	-9.419e+00	3.1700	5.140e-02	-.0587	-.2660	-.2341

n= .1537e-02 ang**-2 or n/nc= .2414e-01

T	u	Ln(P3D)	S/Nk	B	-P2d=W	F	E
2.4119	-167.80	-6.206e+01	1.2239	6.350e-02	-.1218	-.3797	-.3751
2.6421	-168.21	-5.592e+01	1.2681	6.300e-02	-.1212	-.3797	-.3746
2.8943	-168.69	-5.031e+01	1.3186	6.230e-02	-.1205	-.3797	-.3739
3.1707	-169.26	-4.518e+01	1.3754	6.140e-02	-.1196	-.3798	-.3731
3.4735	-169.96	-4.050e+01	1.4448	6.030e-02	-.1186	-.3799	-.3721
3.8051	-170.80	-3.623e+01	1.5331	5.900e-02	-.1174	-.3799	-.3710
4.1686	-171.83	-3.233e+01	1.6466	5.750e-02	-.1159	-.3800	-.3695
4.5667	-173.07	-2.878e+01	1.7854	5.580e-02	-.1142	-.3802	-.3677
5.0029	-174.56	-2.555e+01	1.9621	5.410e-02	-.1121	-.3804	-.3653
5.4808	-176.35	-2.261e+01	2.1640	5.230e-02	-.1097	-.3807	-.3625
6.0045	-178.47	-1.992e+01	2.4037	5.070e-02	-.1068	-.3812	-.3590
6.5784	-180.97	-1.748e+01	2.6624	4.940e-02	-.1036	-.3818	-.3548
7.2072	-183.88	-1.526e+01	2.9274	4.820e-02	-.1000	-.3826	-.3502
7.8958	-187.23	-1.323e+01	3.2113	4.750e-02	-.0959	-.3837	-.3448
8.6503	-191.08	-1.138e+01	3.4952	4.710e-02	-.0915	-.3852	-.3387
9.4770	-195.46	-9.685e+00	3.8232	4.730e-02	-.0867	-.3872	-.3315
10.3830	-200.43	-8.135e+00	4.1324	4.800e-02	-.0817	-.3898	-.3238

n= .2436e-02 ang**-2 or n/nc= .3827e-01

T	u	Ln(P3D)	S/Nk	B	-P2d=W	F	E
2.4119	-156.02	-5.717e+01	1.4012	7.780e-02	-.1510	-.5311	-.5228
2.6421	-156.61	-5.153e+01	1.4927	7.560e-02	-.1499	-.5314	-.5218
2.8943	-157.32	-4.638e+01	1.6042	7.350e-02	-.1486	-.5319	-.5205
3.1707	-158.15	-4.168e+01	1.7356	7.130e-02	-.1471	-.5324	-.5190
3.4735	-159.14	-3.738e+01	1.8868	6.900e-02	-.1454	-.5330	-.5171
3.8051	-160.29	-3.347e+01	2.0620	6.670e-02	-.1434	-.5338	-.5147
4.1686	-161.64	-2.989e+01	2.2531	6.460e-02	-.1411	-.5348	-.5119
4.5667	-163.20	-2.662e+01	2.4600	6.270e-02	-.1385	-.5360	-.5087
5.0029	-164.99	-2.364e+01	2.6830	6.110e-02	-.1357	-.5376	-.5049
5.4808	-167.05	-2.091e+01	2.9099	5.990e-02	-.1325	-.5395	-.5006
6.0045	-169.39	-1.841e+01	3.1467	5.890e-02	-.1292	-.5418	-.4958
6.5784	-172.04	-1.613e+01	3.4035	5.850e-02	-.1256	-.5447	-.4902
7.2072	-175.04	-1.403e+01	3.6463	5.840e-02	-.1219	-.5482	-.4842
7.8958	-178.41	-1.211e+01	3.8891	5.850e-02	-.1179	-.5525	-.4777
8.6503	-182.19	-1.035e+01	4.1200	5.960e-02	-.1138	-.5576	-.4708
9.4770	-186.42	-8.732e+00	4.3708	6.080e-02	-.1096	-.5637	-.4628
10.3830	-191.15	-7.243e+00	4.6096	6.230e-02	-.1055	-.5711	-.4545

n= .3660e-02 ang**-2 or n/nc= .6063e-01

T	u	Ln(P3D)	S/Nk	B	-P2d=W	F	E
2.4119	-147.61	-5.368e+01	1.9745	6.440e-02	-.1674	-.7571	-.7388
2.6421	-148.43	-4.843e+01	2.1228	6.310e-02	-.1654	-.7563	-.7366
2.8943	-149.37	-4.363e+01	2.2735	6.200e-02	-.1631	-.7597	-.7343
3.1707	-150.42	-3.924e+01	2.4343	6.120e-02	-.1607	-.7613	-.7315
3.4735	-151.61	-3.522e+01	2.6026	6.050e-02	-.1781	-.7633	-.7284
3.8051	-152.95	-3.154e+01	2.7759	6.020e-02	-.1753	-.7657	-.7249
4.1686	-154.46	-2.817e+01	2.9518	6.030e-02	-.1724	-.7686	-.7211
4.5667	-156.14	-2.508e+01	3.1326	6.070e-02	-.1693	-.7720	-.7168
5.0029	-158.02	-2.224e+01	3.3160	6.140e-02	-.1661	-.7761	-.7120
5.4808	-160.12	-1.964e+01	3.5019	6.260e-02	-.1629	-.7809	-.7068
6.0045	-162.46	-1.726e+01	3.6929	6.410e-02	-.1595	-.7866	-.7010
6.5784	-165.07	-1.507e+01	3.8863	6.600e-02	-.1562	-.7933	-.6947
7.2072	-167.98	-1.305e+01	4.0747	6.830e-02	-.1528	-.8012	-.6878
7.8958	-171.21	-1.120e+01	4.2606	7.110e-02	-.1494	-.8103	-.6804
8.6503	-174.82	-9.498e+00	4.4440	7.430e-02	-.1460	-.8208	-.6724
9.4770	-178.83	-7.931e+00	4.6349	7.790e-02	-.1427	-.8330	-.6634
10.3830	-183.30	-6.485e+00	4.8208	8.200e-02	-.1395	-.8471	-.6539

n= .6119e-02 ang**-2 or n/nc= .9612e-01

T	u	Ln(P3D)	S/Nk	B	-P2d=W	F	E
.0753	-124.17	-1.650e+03	1.3502	5.560e-02	-.2225	-.9823	-.9816
.0825	-124.20	-1.506e+03	1.3708	5.580e-02	-.2225	-.9825	-.9818
.0904	-124.23	-1.375e+03	1.3692	5.600e-02	-.2226	-.9828	-.9820
.0990	-124.27	-1.256e+03	1.3835	5.610e-02	-.2227	-.9831	-.9823
.1085	-124.31	-1.146e+03	1.3961	5.630e-02	-.2228	-.9834	-.9825
.1188	-124.35	-1.047e+03	1.4009	5.660e-02	-.2229	-.9838	-.9828
.1302	-124.40	-9.553e+02	1.3993	5.670e-02	-.2230	-.9842	-.9831
.1426	-124.46	-8.723e+02	1.4167	5.690e-02	-.2231	-.9847	-.9834
.1562	-124.53	-7.965e+02	1.4247	5.720e-02	-.2232	-.9851	-.9838
.1712	-124.60	-7.269e+02	1.4421	5.740e-02	-.2233	-.9857	-.9842
.1875	-124.68	-6.638e+02	1.4405	5.770e-02	-.2234	-.9863	-.9846
.2054	-124.76	-6.061e+02	1.4500	5.790e-02	-.2235	-.9869	-.9851
.2250	-124.86	-5.534e+02	1.4595	5.810e-02	-.2236	-.9876	-.9856
.2465	-124.98	-5.052e+02	1.4659	5.830e-02	-.2237	-.9884	-.9862
.2701	-125.10	-4.611e+02	1.4770	5.860e-02	-.2238	-.9893	-.9868
.2959	-125.24	-4.210e+02	1.4833	5.880e-02	-.2239	-.9902	-.9875
.3242	-125.40	-3.843e+02	1.4896	5.900e-02	-.2239	-.9913	-.9883
.3551	-125.57	-3.509e+02	1.5261	5.920e-02	-.2240	-.9924	-.9891
.3890	-125.77	-3.204e+02	1.5419	5.940e-02	-.2241	-.9937	-.9900
.4262	-126.00	-2.924e+02	1.5483	5.950e-02	-.2241	-.9951	-.9910
.4669	-126.25	-2.670e+02	1.5768	5.960e-02	-.2241	-.9966	-.9921
.5115	-126.53	-2.437e+02	1.5974	5.970e-02	-.2240	-.9983	-.9933
.5604	-126.85	-2.225e+02	1.6370	5.970e-02	-.2240	-1.0002	-.9946
.6139	-127.21	-2.031e+02	1.6671	5.970e-02	-.2240	-1.0024	-.9961
.6725	-127.62	-1.854e+02	1.7321	5.970e-02	-.2239	-1.0048	-.9976
.7367	-128.09	-1.693e+02	1.7733	5.950e-02	-.2237	-1.0075	-.9995
.8071	-128.62	-1.546e+02	1.8002	5.920e-02	-.2234	-1.0105	-1.0016
.8842	-129.23	-1.411e+02	1.8446	5.870e-02	-.2231	-1.0138	-1.0038
.9687	-129.90	-1.289e+02	1.8826	5.820e-02	-.2227	-1.0175	-1.0064
1.0612	-130.66	-1.177e+02	1.9143	5.760e-02	-.2222	-1.0217	-1.0093
1.1625	-131.52	-1.074e+02	1.9761	5.670e-02	-.2216	-1.0263	-1.0123

1.2736	-132.48	-9.810e+01	2.0411	5.570e-02	-.2209	-1.0316	-1.0157
1.3952	-133.58	-8.959e+01	2.1108	5.460e-02	-.2202	-1.0375	-1.0195
1.5285	-134.83	-8.183e+01	2.1568	5.310e-02	-.2192	-1.0442	-1.0240
1.6745	-136.24	-7.475e+01	2.2170	5.130e-02	-.2180	-1.0516	-1.0289
1.8344	-137.84	-6.831e+01	2.2551	4.890e-02	-.2165	-1.0599	-1.0346
2.0097	-139.66	-6.243e+01	2.3533	4.580e-02	-.2145	-1.0691	-1.0402
2.2016	-141.73	-5.708e+01	2.4468	4.260e-02	-.2125	-1.0797	-1.0467
2.4119	-144.08	-5.222e+01	2.6687	3.900e-02	-.2102	-1.0918	-1.0524
2.6421	-144.89	-4.709e+01	2.7859	4.100e-02	-.2082	-1.0948	-1.0487
2.8943	-145.79	-4.240e+01	2.9048	4.330e-02	-.2062	-1.0983	-1.0468
3.1707	-146.80	-3.810e+01	3.0268	4.590e-02	-.2041	-1.1024	-1.0436
3.4735	-147.92	-3.415e+01	3.1520	4.880e-02	-.2020	-1.1071	-1.0401
3.8051	-149.17	-3.054e+01	3.2819	5.190e-02	-.1998	-1.1126	-1.0362
4.1686	-150.55	-2.723e+01	3.4135	5.550e-02	-.1977	-1.1190	-1.0319
4.5667	-152.10	-2.419e+01	3.5498	5.930e-02	-.1956	-1.1263	-1.0271
5.0029	-153.81	-2.140e+01	3.6876	6.370e-02	-.1936	-1.1348	-1.0219
5.4808	-155.72	-1.884e+01	3.8255	6.840e-02	-.1917	-1.1445	-1.0162
6.0045	-157.83	-1.649e+01	3.9665	7.360e-02	-.1899	-1.1557	-1.0099
6.5784	-160.19	-1.432e+01	4.1139	7.930e-02	-.1883	-1.1685	-1.0029
7.2072	-162.81	-1.234e+01	4.2581	8.550e-02	-.1868	-1.1831	-.9953
7.8958	-165.73	-1.051e+01	4.4008	9.240e-02	-.1856	-1.1997	-.9871
8.6503	-168.98	-8.823e+00	4.5402	1.000e-01	-.1847	-1.2187	-.9783
9.4770	-172.60	-7.273e+00	4.6860	1.083e-01	-.1841	-1.2402	-.9685
10.3830	-176.64	-5.845e+00	4.8318	1.172e-01	-.1840	-1.2648	-.9579

n= .9697e-02 ang**-2 or n/nc= .1523

T	u	Ln(P3D)	S/Nk	B	-P2d=W	F	E
.0753	-121.72	-1.618e+03	1.1720	7.020e-02	-.2501	-1.4304	-1.4295
.0825	-121.74	-1.477e+03	1.1850	7.040e-02	-.2503	-1.4308	-1.4298
.0904	-121.76	-1.348e+03	1.1880	7.070e-02	-.2505	-1.4312	-1.4301
.0990	-121.79	-1.231e+03	1.2160	7.110e-02	-.2507	-1.4316	-1.4305
.1085	-121.82	-1.123e+03	1.2280	7.140e-02	-.2509	-1.4321	-1.4308
.1188	-121.85	-1.026e+03	1.2510	7.180e-02	-.2511	-1.4327	-1.4312
.1302	-121.89	-9.359e+02	1.2600	7.210e-02	-.2513	-1.4333	-1.4317
.1426	-121.93	-8.546e+02	1.2860	7.260e-02	-.2516	-1.4339	-1.4322
.1562	-121.98	-7.803e+02	1.2990	7.300e-02	-.2518	-1.4347	-1.4327
.1712	-122.04	-7.119e+02	1.3120	7.340e-02	-.2521	-1.4355	-1.4333
.1875	-122.10	-6.501e+02	1.3380	7.390e-02	-.2523	-1.4364	-1.4340
.2054	-122.18	-5.935e+02	1.3570	7.440e-02	-.2526	-1.4374	-1.4347
.2250	-122.26	-5.418e+02	1.3760	7.490e-02	-.2529	-1.4385	-1.4355
.2465	-122.36	-4.946e+02	1.3910	7.540e-02	-.2531	-1.4397	-1.4363
.2701	-122.47	-4.514e+02	1.4060	7.600e-02	-.2534	-1.4410	-1.4373
.2959	-122.60	-4.120e+02	1.4290	7.650e-02	-.2537	-1.4425	-1.4384
.3242	-122.74	-3.761e+02	1.4460	7.710e-02	-.2539	-1.4441	-1.4395
.3551	-122.90	-3.434e+02	1.4960	7.760e-02	-.2541	-1.4459	-1.4407
.3890	-123.08	-3.135e+02	1.5250	7.820e-02	-.2543	-1.4479	-1.4421
.4262	-123.29	-2.861e+02	1.5430	7.880e-02	-.2545	-1.4501	-1.4437
.4669	-123.53	-2.612e+02	1.5840	7.930e-02	-.2546	-1.4525	-1.4454
.5115	-123.81	-2.384e+02	1.6070	7.990e-02	-.2547	-1.4553	-1.4473
.5604	-124.11	-2.176e+02	1.6550	8.050e-02	-.2548	-1.4583	-1.4493
.6139	-124.46	-1.986e+02	1.6900	8.110e-02	-.2549	-1.4617	-1.4517
.6725	-124.86	-1.813e+02	1.7780	8.180e-02	-.2549	-1.4656	-1.4540
.7367	-125.32	-1.656e+02	1.8290	8.240e-02	-.2548	-1.4700	-1.4569
.8071	-125.85	-1.511e+02	1.8790	8.290e-02	-.2545	-1.4749	-1.4602
.8842	-126.46	-1.380e+02	1.9320	8.330e-02	-.2540	-1.4803	-1.4638
.9687	-127.14	-1.260e+02	1.9610	8.380e-02	-.2536	-1.4864	-1.4680
1.0612	-127.90	-1.151e+02	2.0170	8.420e-02	-.2530	-1.4933	-1.4725
1.1625	-128.79	-1.051e+02	2.0870	8.440e-02	-.2521	-1.5009	-1.4774

1.2736	-129.77	-9.597e+01	2.1420	8.460e-02	-.2511	-1.5095	-1.4831
1.3952	-130.89	-8.767e+01	2.2300	8.490e-02	-.2501	-1.5194	-1.4892
1.5285	-132.19	-8.010e+01	2.2990	8.470e-02	-.2486	-1.5304	-1.4963
1.6745	-133.64	-7.320e+01	2.3520	8.460e-02	-.2468	-1.5427	-1.5046
1.8344	-135.32	-6.693e+01	2.4470	8.390e-02	-.2444	-1.5566	-1.5130
2.0097	-137.24	-6.123e+01	2.5230	8.280e-02	-.2413	-1.5721	-1.5229
2.2016	-139.40	-5.603e+01	2.6350	8.190e-02	-.2380	-1.5898	-1.5335
2.4119	-141.86	-5.130e+01	2.8870	8.090e-02	-.2344	-1.6100	-1.5425
2.6421	-142.54	-4.620e+01	2.9850	8.460e-02	-.2339	-1.6161	-1.5386
2.8943	-143.30	-4.154e+01	3.0820	8.550e-02	-.2335	-1.6230	-1.5355
3.1707	-144.15	-3.726e+01	3.1820	9.290e-02	-.2331	-1.6309	-1.5331
3.4735	-145.10	-3.334e+01	3.2820	9.750e-02	-.2329	-1.6399	-1.5294
3.8051	-146.16	-2.975e+01	3.3850	1.025e-01	-.2328	-1.6501	-1.5252
4.1686	-147.35	-2.646e+01	3.4890	1.078e-01	-.2328	-1.6616	-1.5206
4.5667	-148.67	-2.344e+01	3.5950	1.136e-01	-.2331	-1.6748	-1.5156
5.0029	-150.15	-2.067e+01	3.7020	1.200e-01	-.2336	-1.6896	-1.5100
5.4808	-151.80	-1.813e+01	3.8110	1.269e-01	-.2345	-1.7064	-1.5039
6.0045	-153.63	-1.579e+01	3.9230	1.343e-01	-.2357	-1.7255	-1.4970
6.5784	-155.68	-1.364e+01	4.0379	1.425e-01	-.2373	-1.7470	-1.4894
7.2072	-157.97	-1.166e+01	4.1529	1.514e-01	-.2395	-1.7713	-1.4811
7.8958	-160.52	-9.847e+00	4.2669	1.609e-01	-.2422	-1.7988	-1.4721
8.6503	-163.37	-8.175e+00	4.3809	1.714e-01	-.2455	-1.8297	-1.4622
9.4770	-166.56	-6.636e+00	4.5039	1.828e-01	-.2495	-1.8646	-1.4507
10.3830	-170.12	-5.217e+00	4.6269	1.954e-01	-.2544	-1.9041	-1.4382

*n= .1455e-01 ang**-2 or n/nc= .2286*

T	u	Ln(P3D)	S/Nk	B	-P2d=W	F	E
2.0097	-135.59	-6.040e+01	2.5818	7.600e-03	-.2647	-2.2375	-2.1620
2.2016	-137.50	-5.517e+01	2.7098	3.850e-02	-.2664	-2.2670	-2.1802
2.4119	-139.67	-5.039e+01	2.8084	7.350e-02	-.2684	-2.3007	-2.2021
2.6421	-140.24	-4.533e+01	2.8971	7.980e-02	-.2699	-2.3103	-2.1989
2.8943	-140.87	-4.070e+01	2.9857	8.670e-02	-.2715	-2.3212	-2.1955
3.1707	-141.59	-3.645e+01	3.0743	9.430e-02	-.2734	-2.3335	-2.1917
3.4735	-142.39	-3.255e+01	3.1636	1.025e-01	-.2756	-2.3474	-2.1875
3.8051	-143.29	-2.900e+01	3.2536	1.115e-01	-.2782	-2.3631	-2.1830
4.1686	-144.31	-2.573e+01	3.3443	1.213e-01	-.2811	-2.3808	-2.1780
4.5667	-145.44	-2.274e+01	3.4356	1.318e-01	-.2845	-2.4007	-2.1725
5.0029	-146.72	-1.998e+01	3.5289	1.433e-01	-.2885	-2.4232	-2.1663
5.4808	-148.14	-1.746e+01	3.6228	1.558e-01	-.2930	-2.4485	-2.1596
6.0045	-149.74	-1.514e+01	3.7195	1.694e-01	-.2983	-2.4770	-2.1520
6.5784	-151.53	-1.301e+01	3.8174	1.840e-01	-.3043	-2.5091	-2.1437
7.2072	-153.53	-1.105e+01	3.9167	2.000e-01	-.3112	-2.5451	-2.1344
7.8958	-155.78	-9.246e+00	4.0167	2.175e-01	-.3191	-2.5856	-2.1242
8.6503	-158.29	-7.587e+00	4.1180	2.364e-01	-.3280	-2.6312	-2.1129
9.4770	-161.11	-6.060e+00	4.2253	2.574e-01	-.3383	-2.6824	-2.0998
10.3830	-164.26	-4.653e+00	4.3339	2.804e-01	-.3501	-2.7401	-2.0854

n= .1939e-01 ang**-2 or n/nc= .3046

T	u	Ln(P3D)	S/Nk	B	-P2d=W	F	E
2.4119	-138.97	-5.010e+01	2.6505	3.960e-02	-.2853	-2.9800	-2.8560
2.6421	-139.43	-4.503e+01	2.7340	5.090e-02	-.2892	-2.9928	-2.8527
2.8943	-139.95	-4.038e+01	2.8180	6.330e-02	-.2935	-3.0072	-2.8491
3.1707	-140.54	-3.612e+01	2.9026	7.680e-02	-.2984	-3.0235	-2.8451
3.4735	-141.21	-3.222e+01	2.9871	9.180e-02	-.3038	-3.0419	-2.8407
3.8051	-141.96	-2.865e+01	3.0716	1.080e-01	-.3099	-3.0626	-2.8359
4.1686	-142.82	-2.537e+01	3.1556	1.256e-01	-.3166	-3.0858	-2.8308
4.5667	-143.78	-2.237e+01	3.2411	1.448e-01	-.3242	-3.1120	-2.8250
5.0029	-144.86	-1.961e+01	3.3276	1.658e-01	-.3326	-3.1414	-2.8186
5.4808	-146.07	-1.708e+01	3.4147	1.886e-01	-.3421	-3.1745	-2.8116
6.0045	-147.45	-1.476e+01	3.5037	2.133e-01	-.3527	-3.2116	-2.8037
6.5784	-148.99	-1.262e+01	3.5952	2.403e-01	-.3645	-3.2534	-2.7948
7.2072	-150.73	-1.066e+01	3.6877	2.695e-01	-.3777	-3.3002	-2.7849
7.8958	-152.68	-8.853e+00	3.7807	3.012e-01	-.3924	-3.3528	-2.7740
8.6503	-154.87	-7.193e+00	3.8753	3.356e-01	-.4088	-3.4118	-2.7618
9.4770	-157.35	-5.663e+00	3.9748	3.724e-01	-.4271	-3.4780	-2.7476
10.3830	-160.13	-4.254e+00	4.0768	4.120e-01	-.4475	-3.5524	-2.7317

n= .2424e-01 ang**-2 or n/nc= .3808

T	u	Ln(P3D)	S/Nk	B	-P2d=W	F	E
2.2016	-137.55	-5.519e+01	2.3958	7.100e-03	-.2645	-3.5988	-3.4710
2.4119	-138.61	-4.995e+01	2.4662	7.670e-02	-.2957	-3.6556	-3.5113
2.6421	-138.97	-4.485e+01	2.5502	9.110e-02	-.3025	-3.6712	-3.5079
2.8943	-139.38	-4.018e+01	2.6318	1.070e-01	-.3101	-3.6888	-3.5041
3.1707	-139.86	-3.591e+01	2.7134	1.246e-01	-.3185	-3.7086	-3.5000
3.4735	-140.39	-3.199e+01	2.7951	1.438e-01	-.3278	-3.7309	-3.4956
3.8051	-141.01	-2.840e+01	2.8763	1.652e-01	-.3381	-3.7561	-3.4908
4.1686	-141.70	-2.511e+01	2.9583	1.883e-01	-.3495	-3.7843	-3.4854
4.5667	-142.49	-2.209e+01	3.0407	2.136e-01	-.3620	-3.8161	-3.4795
5.0029	-143.39	-1.932e+01	3.1239	2.413e-01	-.3760	-3.8518	-3.4730
5.4808	-144.41	-1.678e+01	3.2079	2.712e-01	-.3915	-3.8919	-3.4657
6.0045	-145.56	-1.444e+01	3.2939	3.042e-01	-.4085	-3.9370	-3.4575
6.5784	-146.87	-1.230e+01	3.3815	3.398e-01	-.4274	-3.9875	-3.4483
7.2072	-148.35	-1.033e+01	3.4703	3.786e-01	-.4483	-4.0443	-3.4380
7.8958	-150.02	-8.517e+00	3.5599	4.210e-01	-.4714	-4.1079	-3.4266
8.6503	-151.91	-6.851e+00	3.6519	4.669e-01	-.4969	-4.1793	-3.4135
9.4770	-154.06	-5.317e+00	3.7483	5.168e-01	-.5250	-4.2594	-3.3983
10.3830	-156.49	-3.904e+00	3.8467	5.713e-01	-.5561	-4.3495	-3.3813

n= .2909e-01 ang**-2 or n/nc= .4570

T	u	Ln(P3D)	S/Nk	B	-P2d=W	F	E
1.5265	-135.07	-8.199e+01	1.8950	6.500e-03	-.1528	-4.0821	-3.9979
1.6745	-135.52	-7.433e+01	1.9447	5.040e-02	-.1786	-4.1210	-4.0263
1.8344	-136.01	-6.731e+01	2.0164	9.730e-02	-.2085	-4.1652	-4.0576
2.0097	-136.53	-6.087e+01	2.0537	1.442e-01	-.2434	-4.2151	-4.0950
2.2016	-137.16	-5.501e+01	2.1734	1.946e-01	-.2815	-4.2715	-4.1323
2.4119	-137.89	-4.965e+01	2.2770	2.483e-01	-.3242	-4.3354	-4.1756
2.6421	-138.18	-4.455e+01	2.3567	2.629e-01	-.3336	-4.3532	-4.1721
2.8943	-138.51	-3.988e+01	2.4361	2.791e-01	-.3441	-4.3734	-4.1653
3.1707	-138.89	-3.560e+01	2.5154	2.970e-01	-.3557	-4.3961	-4.1641
3.4735	-139.33	-3.168e+01	2.5947	3.171e-01	-.3686	-4.4218	-4.1596
3.8051	-139.84	-2.809e+01	2.6741	3.386e-01	-.3828	-4.4506	-4.1546
4.1686	-140.41	-2.480e+01	2.7541	3.627e-01	-.3985	-4.4832	-4.1492
4.5667	-141.07	-2.178e+01	2.8344	3.889e-01	-.4158	-4.5197	-4.1432
5.0029	-141.83	-1.901e+01	2.9161	4.174e-01	-.4349	-4.5608	-4.1364
5.4808	-142.70	-1.647e+01	2.9981	4.481e-01	-.4559	-4.6069	-4.1289
6.0045	-143.68	-1.413e+01	3.0817	4.816e-01	-.4791	-4.6587	-4.1204
6.5784	-144.80	-1.198e+01	3.1677	5.180e-01	-.5046	-4.7169	-4.1107
7.2072	-146.09	-1.001e+01	3.2547	5.572e-01	-.5326	-4.7822	-4.0998
7.8958	-147.54	-8.203e+00	3.3431	5.996e-01	-.5634	-4.8554	-4.0875
8.6503	-149.20	-6.537e+00	3.4337	6.464e-01	-.5974	-4.9376	-4.0736
9.4770	-151.09	-5.003e+00	3.5291	6.975e-01	-.6347	-5.0299	-4.0570
10.3830	-153.24	-3.591e+00	3.6271	7.534e-01	-.6758	-5.1336	-4.0380

n= .3394e-01 ang**-2 or n/nc= .5331

T	u	Ln(P3D)	S/Nk	B	-P2d=W	F	E
.9667	-133.75	-1.328e+02	1.3888	5.700e-03	-.0473	-4.5868	-4.5412
1.0612	-133.89	-1.207e+02	1.4474	2.560e-02	-.0651	-4.6092	-4.5571
1.1625	-134.04	-1.096e+02	1.5314	4.910e-02	-.0855	-4.6349	-4.5745
1.2736	-134.24	-9.948e+01	1.5651	7.680e-02	-.1080	-4.6640	-4.5963
1.3952	-134.46	-9.023e+01	1.6611	1.092e-01	-.1333	-4.6970	-4.6184
1.5285	-134.72	-8.176e+01	1.7125	1.470e-01	-.1626	-4.7351	-4.6463
1.6745	-135.02	-7.403e+01	1.7634	1.882e-01	-.1952	-4.7778	-4.6776
1.8344	-135.36	-6.695e+01	1.8177	2.273e-01	-.2321	-4.8262	-4.7130
2.0097	-135.74	-6.048e+01	1.8579	2.562e-01	-.2733	-4.8804	-4.7536
2.2016	-136.22	-5.458e+01	1.9714	2.876e-01	-.3183	-4.9417	-4.7944
2.4119	-136.81	-4.920e+01	2.1105	3.170e-01	-.3681	-5.0113	-4.8385
2.6421	-137.04	-4.412e+01	2.1879	3.372e-01	-.3802	-5.0312	-4.8550
2.8943	-137.30	-3.947e+01	2.2654	3.588e-01	-.3936	-5.0537	-4.8312
3.1707	-137.62	-3.520e+01	2.3428	3.826e-01	-.4084	-5.0791	-4.8270
3.4735	-137.98	-3.129e+01	2.4205	4.088e-01	-.4248	-5.1078	-4.8224
3.8051	-138.40	-2.771e+01	2.4985	4.377e-01	-.4428	-5.1400	-4.8173
4.1656	-138.88	-2.443e+01	2.5768	4.688e-01	-.4627	-5.1763	-4.8118
4.5667	-139.44	-2.142e+01	2.6562	5.036e-01	-.4846	-5.2172	-4.8055
5.0029	-140.08	-1.866e+01	2.7368	5.419e-01	-.5088	-5.2632	-4.7985
5.4808	-140.82	-1.612e+01	2.8179	5.837e-01	-.5353	-5.3149	-4.7907
6.0045	-141.68	-1.380e+01	2.9008	6.294e-01	-.5644	-5.3729	-4.7818
6.5784	-142.66	-1.166e+01	2.9859	6.795e-01	-.5964	-5.4382	-4.7715
7.2072	-143.76	-9.695e+00	3.0719	7.351e-01	-.6316	-5.5115	-4.7601
7.8958	-145.07	-7.890e+00	3.1585	7.955e-01	-.6701	-5.5937	-4.7473
8.6503	-146.54	-6.229e+00	3.2485	8.621e-01	-.7126	-5.6861	-4.7324
9.4770	-148.22	-4.701e+00	3.3419	9.357e-01	-.7593	-5.7899	-4.7150
10.3830	-150.14	-3.293e+00	3.4382	1.020e+00	-.8111	-5.9069	-4.6953

n= .3879e-01 ang**-2 or n/nc= .6093

T	u	Ln(P3D)	S/Nk	B	-P2d=W	F	E
.0753	-131.93	-1.753e+03	.5082	7.545e-01	.0262	-5.0915	-5.0900
.0825	-131.95	-1.600e+03	.5307	7.503e-01	.0263	-5.0921	-5.0904
.0904	-131.97	-1.461e+03	.5540	7.455e-01	.0264	-5.0926	-5.0907
.0990	-131.99	-1.334e+03	.5810	7.410e-01	.0264	-5.0934	-5.0911
.1085	-132.01	-1.217e+03	.5980	7.362e-01	.0264	-5.0942	-5.0917
.1188	-132.03	-1.111e+03	.6277	7.310e-01	.0264	-5.0952	-5.0923
.1302	-132.06	-1.014e+03	.6465	7.260e-01	.0262	-5.0963	-5.0930
.1426	-132.08	-9.258e+02	.6745	7.209e-01	.0260	-5.0976	-5.0938
.1562	-132.11	-8.451e+02	.6980	7.156e-01	.0256	-5.0991	-5.0949
.1712	-132.14	-7.710e+02	.7180	7.103e-01	.0250	-5.1008	-5.0960
.1875	-132.18	-7.038e+02	.7417	7.048e-01	.0244	-5.1028	-5.0974
.2054	-132.21	-6.423e+02	.7637	6.996e-01	.0235	-5.1050	-5.0990
.2250	-132.25	-5.862e+02	.7857	6.938e-01	.0223	-5.1076	-5.1008
.2465	-132.29	-5.349e+02	.8062	6.886e-01	.0209	-5.1106	-5.1029
.2701	-132.33	-4.879e+02	.8242	6.830e-01	.0192	-5.1140	-5.1053
.2959	-132.38	-4.451e+02	.8474	6.779e-01	.0172	-5.1178	-5.1081
.3242	-132.43	-4.060e+02	.8672	6.728e-01	.0147	-5.1221	-5.1112
.3551	-132.48	-3.703e+02	.9017	6.679e-01	.0117	-5.1270	-5.1146
.3890	-132.53	-3.377e+02	.9262	6.631e-01	.0080	-5.1327	-5.1188
.4262	-132.58	-3.079e+02	.9399	6.588e-01	.0036	-5.1392	-5.1236
.4669	-132.63	-2.807e+02	.9722	6.543e-01	-.0016	-5.1464	-5.1288
.5115	-132.69	-2.558e+02	1.0004	6.517e-01	-.0078	-5.1548	-5.1349
.5604	-132.75	-2.330e+02	1.0324	6.508e-01	-.0149	-5.1642	-5.1418
.6139	-132.81	-2.122e+02	1.0672	6.512e-01	-.0232	-5.1750	-5.1496
.6725	-132.88	-1.933e+02	1.0969	6.505e-01	-.0329	-5.1873	-5.1586
.7367	-132.94	-1.759e+02	1.1339	6.487e-01	-.0444	-5.2012	-5.1688
.8071	-133.01	-1.600e+02	1.1619	6.458e-01	-.0576	-5.2171	-5.1807
.8842	-133.08	-1.455e+02	1.2054	6.412e-01	-.0727	-5.2350	-5.1936
.9687	-133.16	-1.322e+02	1.2537	6.416e-01	-.0900	-5.2554	-5.2083
1.0612	-133.26	-1.201e+02	1.3059	6.438e-01	-.1093	-5.2786	-5.2248
1.1625	-133.37	-1.090e+02	1.3844	6.481e-01	-.1316	-5.3053	-5.2428

1.2736	-133.51	-9.891e+01	1.4182	6.557e-01	-.1566	-5.3356	-5.2655
1.3952	-133.67	-8.966e+01	1.5047	6.669e-01	-.1849	-5.3701	-5.2887
1.5285	-133.85	-8.119e+01	1.5509	6.779e-01	-.2175	-5.4098	-5.3178
1.6745	-134.07	-7.346e+01	1.6016	6.872e-01	-.2536	-5.4543	-5.3502
1.8344	-134.35	-6.641e+01	1.6536	6.750e-01	-.2924	-5.5040	-5.3863
2.0097	-134.74	-5.998e+01	1.6999	6.231e-01	-.3323	-5.5587	-5.4262
2.2016	-135.22	-5.413e+01	1.8086	5.614e-01	-.3755	-5.6208	-5.4664
2.4119	-135.84	-4.880e+01	1.9501	4.802e-01	-.4220	-5.6911	-5.5087
2.6421	-136.01	-4.373e+01	2.0251	4.984e-01	-.4365	-5.7124	-5.5048
2.8943	-136.22	-3.909e+01	2.1006	5.217e-01	-.4528	-5.7365	-5.5007
3.1707	-136.46	-3.483e+01	2.1764	5.490e-01	-.4708	-5.7640	-5.4963
3.4735	-136.74	-3.094e+01	2.2526	5.800e-01	-.4909	-5.7951	-5.4916
3.8051	-137.07	-2.736e+01	2.3296	6.150e-01	-.5131	-5.8301	-5.4863
4.1686	-137.46	-2.409e+01	2.4068	6.539e-01	-.5376	-5.8697	-5.4805
4.5667	-137.91	-2.108e+01	2.4856	6.959e-01	-.5645	-5.9142	-5.4739
5.0029	-138.44	-1.833e+01	2.5651	7.429e-01	-.5942	-5.9643	-5.4665
5.4808	-139.05	-1.580e+01	2.6458	7.946e-01	-.6269	-6.0208	-5.4583
6.0045	-139.77	-1.348e+01	2.7278	8.513e-01	-.6627	-6.0842	-5.4489
6.5784	-140.59	-1.135e+01	2.8123	9.136e-01	-.7021	-6.1556	-5.4380
7.2072	-141.54	-9.384e+00	2.8978	9.821e-01	-.7454	-6.2359	-5.4257
7.8958	-142.64	-7.582e+00	2.9843	1.058e+00	-.7929	-6.3260	-5.4120
8.6503	-143.91	-5.925e+00	3.0728	1.140e+00	-.8452	-6.4273	-5.3963
9.4770	-145.36	-4.399e+00	3.1655	1.231e+00	-.9028	-6.5413	-5.3776
10.3830	-147.03	-2.993e+00	3.2615	1.321e+00	-.9660	-6.6694	-5.3558

n= .4364e-01 ang**-2 or n/nc= .6855

T	u	Ln(P3D)	S/Nk	B	-P2d=W	F	E
.0753	-130.23	-1.731e+03	.5380	3.556e-01	-.0510	-5.7341	-5.7323
.0825	-130.25	-1.580e+03	.5582	3.510e-01	-.0502	-5.7345	-5.7325
.0904	-130.28	-1.442e+03	.5757	3.465e-01	-.0496	-5.7351	-5.7328
.0990	-130.31	-1.317e+03	.5982	3.416e-01	-.0490	-5.7358	-5.7332
.1085	-130.35	-1.202e+03	.6139	3.366e-01	-.0483	-5.7366	-5.7337
.1188	-130.38	-1.097e+03	.6368	3.320e-01	-.0477	-5.7376	-5.7343
.1302	-130.42	-1.001e+03	.6517	3.263e-01	-.0472	-5.7387	-5.7350
.1426	-130.46	-9.144e+02	.6744	3.209e-01	-.0468	-5.7400	-5.7358
.1562	-130.50	-8.348e+02	.6928	3.162e-01	-.0466	-5.7415	-5.7368
.1712	-130.54	-7.616e+02	.7088	3.108e-01	-.0464	-5.7433	-5.7380
.1875	-130.59	-6.953e+02	.7273	3.057e-01	-.0464	-5.7452	-5.7393
.2054	-130.64	-6.346e+02	.7444	2.995e-01	-.0466	-5.7475	-5.7409
.2250	-130.69	-5.792e+02	.7613	2.948e-01	-.0470	-5.7502	-5.7427
.2465	-130.74	-5.286e+02	.7790	2.893e-01	-.0477	-5.7532	-5.7448
.2701	-130.80	-4.822e+02	.7913	2.838e-01	-.0487	-5.7567	-5.7473
.2959	-130.85	-4.400e+02	.8088	2.791e-01	-.0501	-5.7606	-5.7501
.3242	-130.91	-4.013e+02	.8250	2.740e-01	-.0519	-5.7650	-5.7533
.3551	-130.98	-3.661e+02	.8510	2.684e-01	-.0542	-5.7700	-5.7568
.3890	-131.04	-3.339e+02	.8693	2.636e-01	-.0572	-5.7759	-5.7611
.4262	-131.11	-3.044e+02	.8793	2.592e-01	-.0610	-5.7825	-5.7661
.4669	-131.17	-2.775e+02	.9046	2.541e-01	-.0655	-5.7899	-5.7715
.5115	-131.24	-2.529e+02	.9261	2.513e-01	-.0712	-5.7985	-5.7778
.5604	-131.30	-2.304e+02	.9530	2.498e-01	-.0782	-5.8082	-5.7849
.6139	-131.37	-2.099e+02	.9824	2.503e-01	-.0864	-5.8193	-5.7930
.6725	-131.44	-1.911e+02	1.0066	2.495e-01	-.0959	-5.8319	-5.8024
.7367	-131.51	-1.740e+02	1.0379	2.476e-01	-.1069	-5.8462	-5.8129
.8071	-131.59	-1.583e+02	1.0623	2.458e-01	-.1196	-5.8624	-5.8250
.8842	-131.68	-1.439e+02	1.0997	2.434e-01	-.1341	-5.8806	-5.8382
.9687	-131.77	-1.306e+02	1.1432	2.465e-01	-.1512	-5.9015	-5.8532
1.0612	-131.87	-1.188e+02	1.1914	2.563e-01	-.1708	-5.9254	-5.8703
1.1625	-131.97	-1.078e+02	1.2617	2.724e-01	-.1939	-5.9531	-5.8891

1.2736	-132.09	-9.779e+01	1.2959	2.966e-01	-.2201	-5.9546	-5.9126
1.3952	-132.22	-8.862e+01	1.3710	3.309e-01	-.2504	-6.0207	-5.9372
1.5285	-132.38	-8.023e+01	1.4172	3.714e-01	-.2652	-6.0621	-5.9676
1.6745	-132.57	-7.256e+01	1.4661	4.177e-01	-.3235	-6.1086	-6.0015
1.8344	-132.86	-6.559e+01	1.5332	4.566e-01	-.3623	-6.1604	-6.0377
2.0097	-133.35	-5.929e+01	1.5879	4.747e-01	-.3978	-6.2170	-6.0777
2.2016	-133.95	-5.355e+01	1.6941	5.018e-01	-.4362	-6.2815	-6.1168
2.4119	-134.71	-4.833e+01	1.8038	5.293e-01	-.4761	-6.3547	-6.1648
2.6421	-134.82	-4.325e+01	1.8756	5.785e-01	-.4948	-6.3786	-6.1623
2.8943	-134.96	-3.866e+01	1.9485	6.266e-01	-.5155	-6.4053	-6.1592
3.1707	-135.14	-3.442e+01	2.0225	6.742e-01	-.5382	-6.4355	-6.1557
3.4735	-135.34	-3.053e+01	2.0971	7.233e-01	-.5632	-6.4695	-6.1516
3.8051	-135.59	-2.695e+01	2.1729	7.748e-01	-.5907	-6.5078	-6.1470
4.1686	-135.88	-2.371e+01	2.2491	8.311e-01	-.6210	-6.5510	-6.1418
4.5667	-136.24	-2.072e+01	2.3267	8.925e-01	-.6542	-6.5998	-6.1359
5.0029	-136.65	-1.797e+01	2.4053	9.585e-01	-.6908	-6.6543	-6.1292
5.4808	-137.14	-1.545e+01	2.4853	1.032e+00	-.7310	-6.7159	-6.1215
6.0045	-137.72	-1.314e+01	2.5667	1.112e+00	-.7752	-6.7853	-6.1127
6.5784	-138.40	-1.101e+01	2.6498	1.200e+00	-.8237	-6.8634	-6.1027
7.2072	-139.19	-9.057e+00	2.7344	1.296e+00	-.8770	-6.9512	-6.0912
7.8958	-140.11	-7.262e+00	2.8202	1.401e+00	-.9356	-7.0500	-6.0782
8.6503	-141.18	-5.610e+00	2.9077	1.516e+00	-.9998	-7.1610	-6.0634
9.4770	-142.43	-4.089e+00	2.9995	1.638e+00	-1.0702	-7.2857	-6.0452
10.3830	-143.87	-2.689e+00	3.0935	1.798e+00	-1.1479	-7.4255	-6.0248

n= .4848e-01 ang**-2 or n/nc= .7615

T	u	Ln(P3D)	S/Nk	B	-P2d=W	F	E
1.6745	-132.37	-7.245e+01	1.3409	3.400e-02	-.3577	-6.7752	-6.6663
1.8344	-132.45	-6.537e+01	1.4295	2.911e-01	-.4106	-6.8317	-6.7046
2.0097	-132.67	-5.895e+01	1.4913	6.292e-01	-.4628	-6.8946	-6.7493
2.2016	-132.94	-5.309e+01	1.5941	1.039e+00	-.5217	-6.9668	-6.7966
2.4119	-133.32	-4.776e+01	1.6575	1.533e+00	-.5861	-7.0493	-6.8555
2.6421	-133.36	-4.273e+01	1.7272	1.535e+00	-.6073	-7.0728	-6.8515
2.8943	-133.43	-3.813e+01	1.7984	1.547e+00	-.6309	-7.0997	-6.8474
3.1707	-133.53	-3.391e+01	1.8712	1.567e+00	-.6568	-7.1304	-6.8427
3.4735	-133.66	-3.005e+01	1.9450	1.592e+00	-.6854	-7.1653	-6.8378
3.8051	-133.83	-2.651e+01	2.0198	1.621e+00	-.7169	-7.2049	-6.8323
4.1686	-134.04	-2.327e+01	2.0952	1.651e+00	-.7515	-7.2496	-6.8262
4.5667	-134.29	-2.029e+01	2.1722	1.687e+00	-.7897	-7.3002	-6.8193
5.0029	-134.61	-1.756e+01	2.2506	1.727e+00	-.8317	-7.3574	-6.8115
5.4808	-134.98	-1.506e+01	2.3300	1.770e+00	-.8779	-7.4218	-6.8027
6.0045	-135.44	-1.276e+01	2.4110	1.818e+00	-.9286	-7.4945	-6.7927
6.5784	-135.98	-1.064e+01	2.4938	1.871e+00	-.9843	-7.5764	-6.7811
7.2072	-136.62	-8.701e+00	2.5780	1.927e+00	-1.0455	-7.6686	-6.7679
7.8958	-137.37	-6.915e+00	2.6636	1.990e+00	-1.1126	-7.7724	-6.7528
8.6503	-138.27	-5.273e+00	2.7512	2.059e+00	-1.1861	-7.8893	-6.7355
9.4770	-139.32	-3.761e+00	2.8429	2.145e+00	-1.2675	-8.0215	-6.7154
10.3830	-140.47	-2.361e+00	2.9373	2.289e+00	-1.3620	-8.1718	-6.6933

n= .5333e-01 ang**-2 or n/nc= .8377

T	u	Ln(P3D)	S/Nk	B	-P2d=W	F	E
2.4119	-131.21	-4.686e+01	1.5046	7.065e-01	-.6995	-7.6968	-7.5032
2.6421	-131.16	-4.190e+01	1.5784	9.606e-01	-.7295	-7.7244	-7.5020
2.8943	-131.16	-3.734e+01	1.6523	1.137e+00	-.7601	-7.7551	-7.5000
3.1707	-131.20	-3.318e+01	1.7265	1.266e+00	-.7929	-7.7900	-7.4981
3.4735	-131.28	-2.936e+01	1.8010	1.371e+00	-.8277	-7.8267	-7.4950
3.8051	-131.39	-2.587e+01	1.8759	1.467e+00	-.8652	-7.8721	-7.4914
4.1686	-131.54	-2.267e+01	1.9512	1.564e+00	-.9061	-7.9211	-7.4873
4.5667	-131.73	-1.973e+01	2.0276	1.661e+00	-.9505	-7.9759	-7.4821
5.0029	-131.98	-1.704e+01	2.1052	1.766e+00	-.9992	-8.0376	-7.4759
5.4808	-132.28	-1.456e+01	2.1839	1.880e+00	-1.0527	-8.1073	-7.4689
6.0045	-132.65	-1.229e+01	2.2643	2.008e+00	-1.1115	-8.1858	-7.4607
6.5784	-133.10	-1.021e+01	2.3465	2.150e+00	-1.1761	-8.2744	-7.4511
7.2072	-133.64	-8.288e+00	2.4301	2.310e+00	-1.2472	-8.3743	-7.4402
7.8958	-134.29	-6.524e+00	2.5152	2.488e+00	-1.3254	-8.4868	-7.4277
8.6503	-135.05	-4.901e+00	2.6021	2.687e+00	-1.4113	-8.6136	-7.4132
9.4770	-135.96	-3.407e+00	2.6931	2.878e+00	-1.5040	-8.7547	-7.3936
10.3830	-136.95	-2.022e+00	2.7867	3.006e+00	-1.6111	-8.9148	-7.3717

n= .5576e-01 ang**-2 or n/nc= .8759

T	u	Ln(P3D)	S/Nk	B	-P2d=W	F	E
2.4119	-130.96	-4.678e+01	1.4025	5.799e-01	-.7286	-8.0310	-7.8424
2.6421	-130.70	-4.172e+01	1.4914	1.055e+00	-.7750	-8.0627	-7.8430
2.8943	-130.54	-3.713e+01	1.5740	1.407e+00	-.8169	-8.0959	-7.8418
3.1707	-130.48	-3.295e+01	1.6526	1.580e+00	-.8561	-8.1317	-7.8395
3.4735	-130.48	-2.914e+01	1.7293	1.698e+00	-.8956	-8.1712	-7.8363
3.8051	-130.53	-2.565e+01	1.8051	1.792e+00	-.9372	-8.2154	-7.8324
4.1686	-130.61	-2.245e+01	1.8809	1.880e+00	-.9821	-8.2651	-7.8279
4.5667	-130.74	-1.951e+01	1.9573	1.979e+00	-1.0308	-8.3211	-7.8227
5.0029	-130.92	-1.683e+01	2.0347	2.093e+00	-1.0843	-8.3842	-7.8166
5.4808	-131.14	-1.436e+01	2.1131	2.216e+00	-1.1431	-8.4555	-7.8097
6.0045	-131.42	-1.209e+01	2.1933	2.353e+00	-1.2078	-8.5359	-7.8016
6.5784	-131.77	-1.000e+01	2.2752	2.507e+00	-1.2791	-8.6267	-7.7922
7.2072	-132.20	-8.088e+00	2.3585	2.678e+00	-1.3576	-8.7292	-7.7814
7.8958	-132.73	-6.327e+00	2.4430	2.862e+00	-1.4439	-8.8447	-7.7692
8.6503	-133.36	-4.705e+00	2.5300	3.067e+00	-1.5389	-8.9750	-7.7547
9.4770	-134.12	-3.213e+00	2.6204	3.355e+00	-1.6426	-9.1212	-7.7385
10.3830	-135.02	-1.837e+00	2.7134	3.520e+00	-1.7561	-9.2851	-7.7141

n= .5818e-01 ang**-2 or n/nc= .9139

T	u	Ln(P3D)	S/Nk	B	-P2d=W	F	E
2.4119	-130.62	-4.664e+01	1.2602	1.401e-01	-.7431	-8.3429	-8.1660
2.6421	-130.09	-4.149e+01	1.3742	5.967e-01	-.8103	-8.3792	-8.1679
2.8943	-129.68	-3.683e+01	1.4847	1.264e+00	-.8735	-8.4181	-8.1681
3.1707	-129.47	-3.263e+01	1.5757	1.743e+00	-.9256	-8.4582	-8.1676
3.4735	-129.40	-2.882e+01	1.6577	1.945e+00	-.9719	-8.5003	-8.1653
3.8051	-129.39	-2.535e+01	1.7359	2.112e+00	-1.0190	-8.5468	-8.1625
4.1666	-129.42	-2.216e+01	1.8122	2.274e+00	-1.0692	-8.5990	-8.1595
4.5667	-129.50	-1.924e+01	1.8865	2.419e+00	-1.1232	-8.6573	-8.1555
5.0029	-129.61	-1.657e+01	1.9657	2.552e+00	-1.1820	-8.7227	-8.1505
5.4808	-129.77	-1.411e+01	2.0439	2.697e+00	-1.2465	-8.7965	-8.1448
6.0045	-129.98	-1.185e+01	2.1234	2.854e+00	-1.3176	-8.8799	-8.1381
6.5784	-130.25	-9.773e+00	2.2049	3.028e+00	-1.3959	-8.9740	-8.1301
7.2072	-130.60	-7.865e+00	2.2877	3.217e+00	-1.4821	-9.0802	-8.1209
7.8958	-131.03	-6.111e+00	2.3719	3.421e+00	-1.5767	-9.1999	-8.1103
8.6503	-131.56	-4.497e+00	2.4586	3.629e+00	-1.6806	-9.3348	-8.0974
9.4770	-132.18	-3.008e+00	2.5489	3.831e+00	-1.7951	-9.4853	-8.0799
10.3830	-132.98	-1.640e+00	2.6417	4.052e+00	-1.9169	-9.6537	-8.0579

n= .6061e-01 ang**-2 or n/nc= .9521

T	u	Ln(P3D)	S/Nk	B	-P2d=W	F	E
1.0612	-139.22	-1.257e+02	.7969	9.783e+00	.3639	-8.0739	-8.0227
1.1625	-138.93	-1.138e+02	.8158	9.458e+00	.3136	-8.1071	-8.0496
1.2736	-138.56	-1.029e+02	.8230	9.024e+00	.2531	-8.1452	-8.0817
1.3952	-138.09	-9.282e+01	.8411	8.468e+00	.1805	-8.1891	-8.1179
1.5285	-137.46	-8.356e+01	.8601	7.795e+00	.0914	-8.2403	-8.1606
1.6745	-136.70	-7.503e+01	.8764	7.009e+00	-.0138	-8.2991	-8.2102
1.8344	-135.65	-6.711e+01	.9150	6.040e+00	-.1479	-8.3697	-8.2679
2.0097	-134.22	-5.972e+01	.9465	4.865e+00	-.3202	-8.4554	-8.3401
2.2016	-132.50	-5.289e+01	1.0028	3.502e+00	-.5250	-8.5556	-8.4218
2.4119	-130.41	-4.655e+01	1.0982	1.917e+00	-.7669	-8.6733	-8.5128
2.6421	-129.73	-4.135e+01	1.1951	2.016e+00	-.8496	-8.7125	-8.5211
2.8943	-128.97	-3.658e+01	1.3604	2.540e+00	-.9416	-8.7563	-8.5196
3.1707	-128.46	-3.231e+01	1.4885	3.099e+00	-1.0185	-8.8044	-8.5182
3.4735	-128.28	-2.850e+01	1.5824	3.234e+00	-1.0729	-8.8477	-8.5146
3.8051	-128.18	-2.503e+01	1.6642	3.303e+00	-1.1257	-8.8948	-8.5110
4.1666	-128.13	-2.185e+01	1.7420	3.371e+00	-1.1814	-8.9476	-8.5075
4.5667	-128.13	-1.894e+01	1.8186	3.438e+00	-1.2404	-9.0066	-8.5033
5.0029	-128.18	-1.628e+01	1.8957	3.511e+00	-1.3037	-9.0730	-8.4982
5.4808	-128.27	-1.383e+01	1.9735	3.599e+00	-1.3734	-9.1480	-8.4924
6.0045	-128.41	-1.159e+01	2.0528	3.701e+00	-1.4501	-9.2328	-8.4857
6.5784	-128.59	-9.521e+00	2.1339	3.819e+00	-1.5347	-9.3286	-8.4778
7.2072	-128.84	-7.621e+00	2.2165	3.954e+00	-1.6279	-9.4368	-8.4686
7.8958	-129.16	-5.875e+00	2.3008	4.107e+00	-1.7302	-9.5589	-8.4578
8.6503	-129.59	-4.270e+00	2.3873	4.281e+00	-1.8417	-9.6963	-8.4446
9.4770	-130.13	-2.792e+00	2.4776	4.486e+00	-1.9631	-9.8505	-8.4274
10.3830	-130.82	-1.432e+00	2.5708	4.605e+00	-2.0939	-10.0231	-8.4053

*n= .6303e-01 ang**-2 or n/nc= .9901*

T	u	Ln(P3D)	S/Nk	B	-P2d=W	F	E
.9687	-131.22	-1.302e+02	.7474	2.567e+01	-.3091	-8.5800	-8.5344
1.0612	-131.21	-1.182e+02	.7512	2.516e+01	-.3333	-8.6036	-8.5533
1.1625	-131.16	-1.071e+02	.7646	2.450e+01	-.3637	-8.6306	-8.5746
1.2736	-131.09	-9.701e+01	.7691	2.365e+01	-.3981	-8.6607	-8.5989
1.3952	-131.00	-8.774e+01	.7811	2.257e+01	-.4372	-8.6942	-8.6256
1.5285	-130.84	-7.922e+01	.7932	2.125e+01	-.4858	-8.7329	-8.6565
1.6745	-130.63	-7.141e+01	.8049	1.967e+01	-.5429	-8.7766	-8.6917
1.8344	-130.28	-6.418e+01	.8252	1.768e+01	-.6167	-8.8281	-8.7327
2.0097	-129.72	-5.748e+01	.8478	1.515e+01	-.7133	-8.8895	-8.7821
2.2016	-129.01	-5.131e+01	.8838	1.219e+01	-.8299	-8.9612	-8.8372
2.4119	-128.12	-4.560e+01	.9528	8.704e+00	-.9701	-9.0453	-8.9004
2.6421	-127.60	-4.055e+01	1.0212	7.641e+00	-1.0342	-9.0768	-8.9068
2.8943	-126.93	-3.588e+01	1.1525	6.339e+00	-1.1146	-9.1149	-8.9046
3.1707	-126.42	-3.167e+01	1.3900	5.457e+00	-1.1884	-9.1564	-8.8786
3.4735	-126.26	-2.792e+01	1.5015	5.200e+00	-1.2408	-9.1987	-8.8699
3.8051	-126.19	-2.451e+01	1.5878	5.034e+00	-1.2813	-9.2453	-8.8645
4.1686	-126.18	-2.138e+01	1.6668	4.887e+00	-1.3450	-9.2979	-8.8600
4.5667	-126.19	-1.852e+01	1.7495	4.801e+00	-1.4032	-9.3571	-8.8535
5.0029	-126.24	-1.589e+01	1.8261	4.785e+00	-1.4674	-9.4241	-8.8483
5.4808	-126.32	-1.348e+01	1.9034	4.777e+00	-1.5384	-9.5000	-8.8425
6.0045	-126.43	-1.126e+01	1.9823	4.780e+00	-1.6169	-9.5859	-8.8357
6.5784	-126.59	-9.217e+00	2.0628	4.795e+00	-1.7039	-9.6831	-8.8278
7.2072	-126.81	-7.340e+00	2.1449	4.820e+00	-1.7999	-9.7930	-8.8187
7.8958	-127.11	-5.615e+00	2.2286	4.852e+00	-1.9056	-9.9171	-8.8079
8.6503	-127.48	-4.026e+00	2.3172	4.969e+00	-2.0219	-10.0572	-8.7938
9.4770	-127.95	-2.562e+00	2.4077	5.131e+00	-2.1491	-10.2139	-8.7757
10.3830	-128.57	-1.215e+00	2.5017	5.233e+00	-2.2855	-10.3895	-8.7523

n= .6545e-01 ang**-2 or n/nc= 1.028

T	u	Ln(P3D)	S/Nk	B	-P2d=W	F	E
.9687	-119.11	-1.177e+02	.7319	2.691e+01	-1.3562	-9.1518	-9.1054
1.0612	-119.32	-1.070e+02	.7332	2.644e+01	-1.3610	-9.1706	-9.1197
1.1625	-119.56	-9.715e+01	.7458	2.582e+01	-1.3663	-9.1914	-9.1346
1.2736	-119.86	-8.819e+01	.7534	2.504e+01	-1.3683	-9.2134	-9.1506
1.3952	-120.25	-8.004e+01	.7640	2.406e+01	-1.3666	-9.2368	-9.1670
1.5285	-120.67	-7.257e+01	.7740	2.285e+01	-1.3650	-9.2628	-9.1854
1.6745	-121.15	-6.574e+01	.7846	2.142e+01	-1.3625	-9.2916	-9.2056
1.8344	-121.67	-5.949e+01	.7983	1.955e+01	-1.3603	-9.3238	-9.2280
2.0097	-122.24	-5.376e+01	.8172	1.723e+01	-1.3601	-9.3604	-9.2529
2.2016	-122.84	-4.850e+01	.8583	1.447e+01	-1.3633	-9.4030	-9.2793
2.4119	-123.50	-4.369e+01	.8649	1.120e+01	-1.3695	-9.4525	-9.3159
2.6421	-123.67	-3.906e+01	.9275	9.321e+00	-1.3732	-9.4675	-9.3071
2.8943	-123.89	-3.483e+01	1.0436	7.044e+00	-1.3782	-9.4835	-9.2888
3.1707	-124.01	-3.091e+01	1.3213	5.465e+00	-1.3992	-9.5156	-9.2414
3.4735	-124.00	-2.727e+01	1.4454	5.095e+00	-1.4385	-9.5546	-9.2260
3.8051	-124.01	-2.393e+01	1.5340	5.005e+00	-1.4834	-9.6000	-9.2179
4.1686	-124.04	-2.087e+01	1.6131	4.997e+00	-1.5335	-9.6519	-9.2118
4.5667	-124.08	-1.806e+01	1.6896	5.024e+00	-1.5901	-9.7109	-9.2059
5.0029	-124.12	-1.547e+01	1.7654	5.064e+00	-1.6545	-9.7781	-9.2000
5.4808	-124.19	-1.309e+01	1.8419	5.124e+00	-1.7261	-9.8543	-9.1936
6.0045	-124.29	-1.090e+01	1.9197	5.206e+00	-1.8059	-9.9409	-9.1865
6.5784	-124.44	-8.889e+00	1.9995	5.305e+00	-1.8945	-10.0390	-9.1781
7.2072	-124.63	-7.036e+00	2.0810	5.423e+00	-1.9928	-10.1501	-9.1685
7.8958	-124.90	-5.335e+00	2.1649	5.568e+00	-2.1013	-10.2758	-9.1570
8.6503	-125.20	-3.762e+00	2.2509	5.817e+00	-2.2247	-10.4169	-9.1445
9.4770	-125.60	-2.313e+00	2.3409	6.007e+00	-2.3586	-10.5768	-9.1268
10.3830	-126.16	-9.830e-01	2.4336	6.243e+00	-2.5009	-10.7580	-9.1042

n= .6788e-01 ang**-2 or n/nc= 1.066

T	u	Ln(P3D)	S/Nk	B	-P2d=W	F	E
.5115	-109.07	-2.096e+02	.7198	1.586e+01	-2.1758	-9.5793	-9.5543
.5604	-109.26	-1.911e+02	.7204	1.579e+01	-2.1710	-9.5873	-9.5599
.6139	-109.46	-1.742e+02	.7216	1.571e+01	-2.1659	-9.5960	-9.5660
.6725	-109.68	-1.588e+02	.7244	1.561e+01	-2.1610	-9.6059	-9.5728
.7367	-109.91	-1.446e+02	.7266	1.549e+01	-2.1562	-9.6168	-9.5805
.8071	-110.17	-1.317e+02	.7283	1.535e+01	-2.1508	-9.6288	-9.5889
.8842	-110.45	-1.199e+02	.7308	1.516e+01	-2.1444	-9.6419	-9.5981
.9687	-110.77	-1.091e+02	.7346	1.494e+01	-2.1372	-9.6562	-9.6079
1.0612	-111.13	-9.925e+01	.7368	1.467e+01	-2.1281	-9.6716	-9.6185
1.1625	-111.55	-9.027e+01	.7516	1.433e+01	-2.1156	-9.6879	-9.6286
1.2736	-112.09	-8.209e+01	.7661	1.392e+01	-2.0957	-9.7045	-9.6383
1.3952	-112.76	-7.467e+01	.7786	1.344e+01	-2.0669	-9.7212	-9.6474
1.5285	-113.54	-6.790e+01	.7901	1.284e+01	-2.0319	-9.7388	-9.6559
1.6745	-114.44	-6.174e+01	.8025	1.212e+01	-1.9894	-9.7574	-9.6632
1.8344	-115.51	-5.613e+01	.8188	1.118e+01	-1.9357	-9.7763	-9.6743
2.0097	-116.76	-5.104e+01	.8383	9.974e+00	-1.8696	-9.7955	-9.6812
2.2016	-118.19	-4.639e+01	.8788	8.537e+00	-1.7950	-9.8175	-9.6862
2.4119	-119.82	-4.216e+01	.9363	6.830e+00	-1.7090	-9.8424	-9.6891
2.6421	-120.55	-3.788e+01	1.0038	6.357e+00	-1.6645	-9.8474	-9.6674
2.8943	-121.35	-3.395e+01	1.1360	6.115e+00	-1.6180	-9.8551	-9.6319
3.1707	-121.85	-3.023e+01	1.2890	6.011e+00	-1.6049	-9.8758	-9.5984
3.4735	-121.95	-2.668e+01	1.3934	5.829e+00	-1.6336	-9.9117	-9.5831
3.8051	-121.97	-2.340e+01	1.4780	5.764e+00	-1.6762	-9.9558	-9.5740
4.1686	-121.98	-2.038e+01	1.5551	5.781e+00	-1.7271	-10.0072	-9.5672
4.5667	-121.99	-1.760e+01	1.6300	5.824e+00	-1.7855	-10.0662	-9.5610
5.0029	-122.01	-1.505e+01	1.7045	5.870e+00	-1.8517	-10.1338	-9.5550
5.4808	-122.05	-1.270e+01	1.7797	5.950e+00	-1.9262	-10.2108	-9.5487
6.0045	-122.11	-1.054e+01	1.8565	6.057e+00	-2.0098	-10.2984	-9.5417
6.5784	-122.20	-8.549e+00	1.9355	6.197e+00	-2.1032	-10.3978	-9.5336
7.2072	-122.33	-6.718e+00	2.0161	6.365e+00	-2.2071	-10.5106	-9.5243
7.8958	-122.51	-5.033e+00	2.0991	6.573e+00	-2.3224	-10.6383	-9.5132

8.6503	-122.72	-3.475e+00	2.1847	6.720e+00	-2.4527	-10.7628	-9.4999
9.4770	-123.03	-2.043e+00	2.2747	6.910e+00	-2.5937	-10.9452	-9.4819
10.3830	-123.48	-7.240e-01	2.3665	7.200e+00	-2.7462	-11.1277	-9.4598

n= .7030e-01 ang**-2 or n/nc= 1.104

T	u	Ln(P3D)	S/Nk	B	-P2d=W	F	E
.1562	-103.61	-6.627e+02	.7329	5.883e+00	-2.5993	-9.8834	-9.8754
.1712	-103.69	-6.047e+02	.7326	5.899e+00	-2.5965	-9.8857	-9.8769
.1875	-103.76	-5.523e+02	.7319	5.916e+00	-2.5934	-9.8880	-9.8784
.2054	-103.85	-5.042e+02	.7313	5.933e+00	-2.5900	-9.8907	-9.8801
.2250	-103.94	-4.604e+02	.7309	5.949e+00	-2.5865	-9.8936	-9.8820
.2465	-104.04	-4.203e+02	.7305	5.968e+00	-2.5826	-9.8968	-9.8841
.2701	-104.15	-3.836e+02	.7302	5.984e+00	-2.5786	-9.9004	-9.8866
.2959	-104.27	-3.501e+02	.7300	6.002e+00	-2.5742	-9.9043	-9.8892
.3242	-104.40	-3.195e+02	.7295	6.016e+00	-2.5697	-9.9087	-9.8921
.3551	-104.53	-2.916e+02	.7295	6.034e+00	-2.5649	-9.9135	-9.8953
.3890	-104.68	-2.661e+02	.7298	6.046e+00	-2.5597	-9.9188	-9.8989
.4262	-104.84	-2.428e+02	.7298	6.056e+00	-2.5544	-9.9248	-9.9029
.4669	-105.01	-2.215e+02	.7300	6.067e+00	-2.5488	-9.9314	-9.9074
.5115	-105.20	-2.020e+02	.7306	6.072e+00	-2.5431	-9.9387	-9.9124
.5604	-105.40	-1.842e+02	.7313	6.071e+00	-2.5372	-9.9468	-9.9180
.6139	-105.62	-1.680e+02	.7320	6.066e+00	-2.5305	-9.9557	-9.9241
.6725	-105.86	-1.531e+02	.7340	6.051e+00	-2.5237	-9.9655	-9.9308
.7367	-106.12	-1.395e+02	.7362	6.024e+00	-2.5162	-9.9764	-9.9383
.8071	-106.41	-1.271e+02	.7385	5.984e+00	-2.5075	-9.9882	-9.9463
.8842	-106.74	-1.157e+02	.7420	5.935e+00	-2.4971	-10.0010	-9.9548
.9687	-107.11	-1.053e+02	.7464	5.871e+00	-2.4849	-10.0148	-9.9639
1.0612	-107.54	-9.587e+01	.7513	5.789e+00	-2.4695	-10.0295	-9.9734
1.1625	-108.04	-8.725e+01	.7691	5.692e+00	-2.4493	-10.0449	-9.9820
1.2736	-108.67	-7.940e+01	.7909	5.642e+00	-2.4213	-10.0608	-9.9900
1.3952	-109.43	-7.229e+01	.8065	5.634e+00	-2.3839	-10.0769	-9.9978
1.5285	-110.33	-6.580e+01	.8217	5.603e+00	-2.3377	-10.0937	-10.0054
1.6745	-111.37	-5.991e+01	.8373	5.547e+00	-2.2814	-10.1111	-10.0125
1.8344	-112.64	-5.457e+01	.8607	5.445e+00	-2.2093	-10.1280	-10.0170
2.0097	-114.16	-4.974e+01	.8825	5.297e+00	-2.1193	-10.1444	-10.0198
2.2016	-115.89	-4.535e+01	.9253	5.089e+00	-2.0157	-10.1627	-10.0195
2.4119	-117.90	-4.136e+01	1.0151	4.829e+00	-1.8950	-10.1830	-10.0109

2.6421	-118.48	-3.710e+01	1.0909	5.706e+00	-1.8613	-10.1902	-9.9576
2.8943	-119.01	-3.315e+01	1.1803	6.769e+00	-1.8352	-10.2019	-9.9618
3.1707	-119.35	-2.944e+01	1.2704	7.381e+00	-1.8354	-10.2254	-9.9422
3.4735	-119.48	-2.597e+01	1.3533	7.384e+00	-1.8613	-10.2610	-9.9305
3.8051	-119.54	-2.276e+01	1.4298	7.306e+00	-1.9012	-10.3050	-9.9226
4.1686	-119.57	-1.980e+01	1.5029	7.241e+00	-1.9513	-10.3570	-9.9165
4.5667	-119.58	-1.707e+01	1.5752	7.207e+00	-2.0100	-10.4166	-9.9109
5.0029	-119.60	-1.456e+01	1.6476	7.211e+00	-2.0772	-10.4847	-9.9052
5.4808	-119.61	-1.225e+01	1.7212	7.239e+00	-2.1537	-10.5625	-9.8994
6.0045	-119.64	-1.013e+01	1.7965	7.286e+00	-2.2402	-10.6512	-9.8929
6.5784	-119.70	-8.168e+00	1.8740	7.355e+00	-2.3374	-10.7520	-9.8854
7.2072	-119.78	-6.364e+00	1.9537	7.452e+00	-2.4463	-10.8666	-9.8768
7.8958	-119.90	-4.702e+00	2.0357	7.568e+00	-2.5681	-10.9971	-9.8671
8.6503	-120.05	-3.167e+00	2.1206	7.874e+00	-2.7075	-11.1472	-9.8576
9.4770	-120.31	-1.756e+00	2.2100	8.014e+00	-2.8542	-11.3121	-9.8597
10.3830	-120.67	-4.540e-01	2.3008	8.212e+00	-3.0153	-11.4954	-9.8190

n= .7273e-01 ang**-2 or n/nc= 1.142

T	u	Ln(P3D)	S/Nk	B	-P2d=W	F	E
1.0612	-106.54	-9.493e+01	.7677	3.850e-02	-2.5713	-10.3197	-10.2605
1.1625	-107.02	-8.637e+01	.7878	2.827e-01	-2.5533	-10.3371	-10.2705
1.2736	-107.59	-7.855e+01	.8141	7.238e-01	-2.5316	-10.3564	-10.2810
1.3952	-108.25	-7.144e+01	.8329	1.363e+00	-2.5043	-10.3774	-10.2929
1.5285	-109.03	-6.496e+01	.8518	2.108e+00	-2.4697	-10.3997	-10.3050
1.6745	-109.95	-5.906e+01	.8709	2.970e+00	-2.4265	-10.4234	-10.3173
1.8344	-111.07	-5.372e+01	.9018	4.011e+00	-2.3695	-10.4479	-10.3275
2.0097	-112.41	-4.887e+01	.9260	5.314e+00	-2.2979	-10.4734	-10.3381
2.2016	-113.95	-4.447e+01	.9721	6.777e+00	-2.2144	-10.5016	-10.3462
2.4119	-115.73	-4.047e+01	1.0414	8.483e+00	-2.1168	-10.5339	-10.3512
2.6421	-116.04	-3.617e+01	1.1059	9.081e+00	-2.1112	-10.5505	-10.3380
2.8943	-116.29	-3.221e+01	1.1758	9.602e+00	-2.1147	-10.5728	-10.3253
3.1707	-116.48	-2.853e+01	1.2470	9.853e+00	-2.1307	-10.6025	-10.3149
3.4735	-116.60	-2.514e+01	1.3173	9.916e+00	-2.1578	-10.6384	-10.3056
3.8051	-116.68	-2.200e+01	1.3861	9.892e+00	-2.1958	-10.6816	-10.2980
4.1686	-116.72	-1.911e+01	1.4543	9.840e+00	-2.2435	-10.7324	-10.2915
4.5667	-116.74	-1.645e+01	1.5231	9.787e+00	-2.3003	-10.7911	-10.2853
5.0029	-116.76	-1.400e+01	1.5929	9.741e+00	-2.3666	-10.8587	-10.2791
5.4808	-116.78	-1.174e+01	1.6642	9.712e+00	-2.4429	-10.9362	-10.2728
6.0045	-116.80	-9.654e+00	1.7375	9.707e+00	-2.5298	-11.0248	-10.2661
6.5784	-116.84	-7.734e+00	1.8135	9.711e+00	-2.6280	-11.1259	-10.2582
7.2072	-116.90	-5.965e+00	1.8919	9.736e+00	-2.7386	-11.2409	-10.2492
7.8958	-117.03	-4.338e+00	1.9727	9.533e+00	-2.8583	-11.3696	-10.2367
8.6503	-117.11	-2.827e+00	2.0567	9.213e+00	-2.9973	-11.5149	-10.2209
9.4770	-117.32	-1.440e+00	2.1470	9.354e+00	-3.1488	-11.6816	-10.2017
10.3830	-117.61	-1.590e-01	2.2358	9.596e+00	-3.3169	-11.8706	-10.1822

n= .7515e-01 ang**-2 or n/nc= 1.180

T	u	Ln(P3D)	S/Nk	B	-P2d=W	F	E
1.8344	-110.16	-5.322e+01	.9221	6.672e-01	-2.4427	-10.7215	-10.5944
2.0097	-110.88	-4.811e+01	.9472	2.984e+00	-2.4342	-10.7671	-10.6241
2.2016	-111.72	-4.346e+01	.9963	5.641e+00	-2.4223	-10.8183	-10.6535
2.4119	-112.69	-3.920e+01	1.0419	8.759e+00	-2.4084	-10.8770	-10.6882
2.6421	-112.87	-3.497e+01	1.0983	9.069e+00	-2.4167	-10.8966	-10.6805
2.8943	-113.02	-3.108e+01	1.1590	9.323e+00	-2.4310	-10.9244	-10.6723
3.1707	-113.14	-2.748e+01	1.2213	9.528e+00	-2.4533	-10.9561	-10.6550
3.4735	-113.24	-2.417e+01	1.2843	9.662e+00	-2.4837	-10.9936	-10.6553
3.8051	-113.31	-2.112e+01	1.3475	9.741e+00	-2.5225	-11.0377	-10.6523
4.1686	-113.36	-1.831e+01	1.4114	9.799e+00	-2.5702	-11.0881	-10.6470
4.5667	-113.39	-1.572e+01	1.4765	9.852e+00	-2.6268	-11.1484	-10.6417
5.0029	-113.42	-1.333e+01	1.5435	9.911e+00	-2.6930	-11.2165	-10.6362
5.4808	-113.44	-1.113e+01	1.6125	9.968e+00	-2.7695	-11.2946	-10.6304
6.0045	-113.46	-9.098e+00	1.6840	1.002e+01	-2.8569	-11.3837	-10.6238
6.5784	-113.50	-7.226e+00	1.7582	1.010e+01	-2.9563	-11.4855	-10.6163
7.2072	-113.54	-5.499e+00	1.8351	1.021e+01	-3.0688	-11.6016	-10.6077
7.8958	-113.71	-3.919e+00	1.9150	1.044e+01	-3.1873	-11.7329	-10.5986
8.6503	-113.93	-2.460e+00	1.9982	1.067e+01	-3.3222	-11.8844	-10.5854
9.4770	-114.10	-1.100e+00	2.0858	1.080e+01	-3.4781	-12.0527	-10.5672
10.3830	-114.30	1.590e-01	2.1725	1.106e+01	-3.6547	-12.2445	-10.5493

*n= .7758e-01 ang**-2 or n/nc= 1.219*

T	u	Ln(P3D)	S/Nk	B	-P2d=W	F	E
.6139	-107.93	-1.717e+02	.7445	6.190e-02	-2.3074	-10.6803	-10.6449
.6725	-108.06	-1.564e+02	.7475	1.357e-01	-2.3109	-10.6943	-10.6553
.7367	-108.22	-1.423e+02	.7506	2.227e-01	-2.3143	-10.7097	-10.6668
.8071	-108.39	-1.295e+02	.7548	3.279e-01	-2.3180	-10.7265	-10.6793
.8842	-108.57	-1.178e+02	.7603	4.560e-01	-2.3222	-10.7451	-10.6930
.9687	-108.77	-1.071e+02	.7665	6.160e-01	-2.3270	-10.7657	-10.7081
1.0612	-109.00	-9.725e+01	.7771	8.355e-01	-2.3325	-10.7885	-10.7245
1.1625	-109.23	-8.826e+01	.7942	1.131e+00	-2.3407	-10.8144	-10.7428
1.2736	-109.39	-7.997e+01	.8123	1.508e+00	-2.3597	-10.8460	-10.7657
1.3952	-109.49	-7.233e+01	.8321	1.984e+00	-2.3859	-10.8833	-10.7933
1.5285	-109.61	-6.533e+01	.8537	2.612e+00	-2.4219	-10.9253	-10.8241
1.6745	-109.74	-5.893e+01	.8766	3.425e+00	-2.4558	-10.9724	-10.8565
1.8344	-109.87	-5.306e+01	.9108	4.518e+00	-2.5020	-11.0251	-10.8865
2.0097	-109.97	-4.766e+01	.9343	5.903e+00	-2.5564	-11.0881	-10.9424
2.2016	-110.08	-4.271e+01	.9847	7.590e+00	-2.6182	-11.1586	-10.9904
2.4119	-110.19	-3.817e+01	1.0291	9.633e+00	-2.6917	-11.2402	-11.0476
2.6421	-110.28	-3.399e+01	1.0801	9.860e+00	-2.7083	-11.2637	-11.0423
2.8943	-110.35	-3.015e+01	1.1351	1.011e+01	-2.7311	-11.2921	-11.0373
3.1707	-110.41	-2.662e+01	1.1924	1.031e+01	-2.7601	-11.3256	-11.0323
3.4735	-110.45	-2.337e+01	1.2508	1.047e+01	-2.7953	-11.3642	-11.0271
3.8051	-110.48	-2.038e+01	1.3099	1.060e+01	-2.8379	-11.4091	-11.0224
4.1686	-110.50	-1.762e+01	1.3703	1.070e+01	-2.8855	-11.4610	-11.0178
4.5667	-110.50	-1.506e+01	1.4322	1.079e+01	-2.9480	-11.5205	-11.0131
5.0029	-110.49	-1.274e+01	1.4963	1.088e+01	-3.0171	-11.5890	-11.0082
5.4808	-110.48	-1.059e+01	1.5626	1.098e+01	-3.0935	-11.6674	-11.0030
6.0045	-110.47	-8.600e+00	1.6318	1.109e+01	-3.1867	-11.7571	-10.9969
6.5784	-110.46	-6.765e+00	1.7040	1.123e+01	-3.2898	-11.8596	-10.9899
7.2072	-110.46	-5.072e+00	1.7793	1.138e+01	-3.4066	-11.9764	-10.9815
7.8958	-110.48	-3.509e+00	1.8579	1.185e+01	-3.5379	-12.1086	-10.9706
8.6503	-110.46	-2.058e+00	1.9401	1.237e+01	-3.6880	-12.2576	-10.9556
9.4770	-110.59	-7.290e-01	2.0261	1.253e+01	-3.8483	-12.4277	-10.9380

10.3830 -110.72 5.040e-01 2.1104 1.275e+01 -4.0324 -12.6219 -10.8220

n= .8000e-01 ang**-2 or n/nc= 1.257

T	u	Ln(P3D)	S/Nx	B	-P2d=W	F	E
.8071	-106.24	-1.268e+02	.7499	1.186e+01	-2.5191	-11.0182	-10.9698
.8842	-106.41	-1.153e+02	.7550	1.186e+01	-2.5249	-11.0380	-10.9846
.9687	-106.60	-1.048e+02	.7606	1.187e+01	-2.5320	-11.0600	-11.0010
1.0612	-106.79	-9.517e+01	.7705	1.190e+01	-2.5411	-11.0847	-11.0193
1.1625	-106.98	-8.633e+01	.7836	1.197e+01	-2.5544	-11.1180	-11.0402
1.2736	-107.11	-7.818e+01	.7938	1.194e+01	-2.5778	-11.1470	-11.0662
1.3952	-107.20	-7.068e+01	.8116	1.182e+01	-2.6114	-11.1671	-11.0965
1.5285	-107.26	-6.380e+01	.8315	1.178e+01	-2.6521	-11.2329	-11.1312
1.6745	-107.30	-5.747e+01	.8534	1.185e+01	-2.7012	-11.2852	-11.1708
1.8344	-107.29	-5.165e+01	.8834	1.207e+01	-2.7651	-11.3459	-11.2163
2.0097	-107.19	-4.628e+01	.9042	1.235e+01	-2.8412	-11.4167	-11.2713
2.2016	-107.05	-4.133e+01	.9530	1.284e+01	-2.9344	-11.4983	-11.3304
2.4119	-106.82	-3.677e+01	1.0051	1.351e+01	-3.0476	-11.5934	-11.3995
2.6421	-106.65	-3.270e+01	1.0521	1.381e+01	-3.0711	-11.6191	-11.3958
2.8943	-106.87	-2.895e+01	1.1036	1.390e+01	-3.0983	-11.6481	-11.3925
3.1707	-106.69	-2.551e+01	1.1577	1.402e+01	-3.1323	-11.6832	-11.3895
3.4735	-106.69	-2.234e+01	1.2133	1.414e+01	-3.1718	-11.7234	-11.3863
3.8051	-106.90	-1.944e+01	1.2697	1.419e+01	-3.2169	-11.7689	-11.3824
4.1686	-106.90	-1.676e+01	1.3273	1.420e+01	-3.2692	-11.8215	-11.3788
4.5667	-106.90	-1.429e+01	1.3864	1.419e+01	-3.3298	-11.8816	-11.3751
5.0029	-106.68	-1.202e+01	1.4479	1.415e+01	-3.3997	-11.9503	-11.3708
5.4808	-106.66	-9.927e+00	1.5139	1.415e+01	-3.4804	-12.0292	-11.3654
6.0045	-106.63	-7.993e+00	1.5808	1.421e+01	-3.5734	-12.1197	-11.3603
6.5784	-106.79	-6.207e+00	1.6510	1.425e+01	-3.6800	-12.2233	-11.3544
7.2072	-106.75	-4.557e+00	1.7245	1.444e+01	-3.8017	-12.3419	-11.3476
7.8958	-106.70	-3.031e+00	1.8011	1.455e+01	-3.9423	-12.4786	-11.3409
8.6503	-106.70	-1.624e+00	1.8831	1.434e+01	-4.0973	-12.6335	-11.3304
9.4770	-106.77	-3.270e-01	1.9682	1.455e+01	-4.2635	-12.8054	-11.3132
10.3830	-106.85	8.770e-01	2.0505	1.475e+01	-4.4544	-13.0020	-11.2987

n= .8242e-01 ang**-2 or n/nc= 1.295

T	u	Ln(P3D)	S/Nk	B	-P2d=W	F	E
.9687	-103.24	-1.013e+02	.7545	1.305e+01	-2.9207	-11.4283	-11.3691
1.0612	-103.42	-9.199e+01	.7627	1.306e+01	-2.9303	-11.4544	-11.3877
1.1625	-103.60	-8.342e+01	.7724	1.309e+01	-2.9447	-11.4832	-11.4092
1.2736	-103.74	-7.553e+01	.7777	1.303e+01	-2.9661	-11.5165	-11.4349
1.3952	-103.86	-6.829e+01	.7931	1.290e+01	-2.9952	-11.5549	-11.4637
1.5285	-103.93	-6.162e+01	.8098	1.282e+01	-3.0331	-11.5983	-11.4973
1.6745	-103.96	-5.548e+01	.8287	1.281e+01	-3.0823	-11.6509	-11.5385
1.8344	-103.91	-4.981e+01	.8534	1.290e+01	-3.1475	-11.7115	-11.5825
2.0097	-103.76	-4.457e+01	.8712	1.301e+01	-3.2301	-11.7820	-11.6377
2.2016	-103.51	-3.973e+01	.9155	1.326e+01	-3.3328	-11.8644	-11.6983
2.4119	-103.14	-3.525e+01	.9771	1.364e+01	-3.4601	-11.9613	-11.7670
2.6421	-103.03	-3.125e+01	1.0227	1.449e+01	-3.5010	-11.9928	-11.7700
2.8943	-102.98	-2.761e+01	1.0720	1.521e+01	-3.5384	-12.0282	-11.7705
3.1707	-102.95	-2.427e+01	1.1245	1.553e+01	-3.5772	-12.0621	-11.7683
3.4735	-102.92	-2.120e+01	1.1786	1.568e+01	-3.6200	-12.1026	-11.7652
3.8051	-102.90	-1.838e+01	1.2337	1.590e+01	-3.6691	-12.1501	-11.7632
4.1666	-102.89	-1.580e+01	1.2896	1.606e+01	-3.7236	-12.2035	-11.7604
4.5667	-102.87	-1.341e+01	1.3468	1.617e+01	-3.7850	-12.2639	-11.7569
5.0029	-102.86	-1.122e+01	1.4059	1.626e+01	-3.8551	-12.3330	-11.7533
5.4808	-102.83	-9.192e+00	1.4676	1.632e+01	-3.9366	-12.4123	-11.7493
6.0045	-102.79	-7.321e+00	1.5322	1.637e+01	-4.0310	-12.5031	-11.7449
6.5784	-102.74	-5.591e+00	1.6002	1.639e+01	-4.1386	-12.6067	-11.7391
7.2072	-102.66	-3.989e+00	1.6717	1.652e+01	-4.2647	-12.7258	-11.7328
7.8958	-102.59	-2.510e+00	1.7470	1.653e+01	-4.4064	-12.8617	-11.7248
8.6503	-102.60	-1.149e+00	1.8288	1.659e+01	-4.5574	-13.0134	-11.7096
9.4770	-102.62	1.110e-01	1.9120	1.670e+01	-4.7266	-13.1867	-11.6932
10.3830	-102.65	1.281e+00	1.9930	1.674e+01	-4.9233	-13.3839	-11.6784

n= .8485e-01 ang**-2 or n/nc= 1.333

T	u	Ln(P3D)	S/Nk	B	-P2d=W	F	E
.8842	-99.59	-1.076e+02	.7450	1.518e+01	-3.3135	-11.7634	-11.7075
.9687	-99.78	-9.776e+01	.7487	1.516e+01	-3.3202	-11.7661	-11.7245
1.0612	-99.96	-8.873e+01	.7547	1.515e+01	-3.3299	-11.8117	-11.7438
1.1625	-100.14	-8.045e+01	.7617	1.513e+01	-3.3445	-11.8411	-11.7660
1.2736	-100.30	-7.283e+01	.7644	1.504e+01	-3.3640	-11.8744	-11.7918
1.3952	-100.45	-6.585e+01	.7770	1.488e+01	-3.3893	-11.9123	-11.8203
1.5285	-100.56	-5.941e+01	.7900	1.474e+01	-3.4242	-11.9553	-11.8539
1.6745	-100.60	-5.347e+01	.8050	1.462e+01	-3.4719	-12.0078	-11.8934
1.8344	-100.55	-4.798e+01	.8239	1.452e+01	-3.5372	-12.0686	-11.9403
2.0097	-100.40	-4.290e+01	.8387	1.440e+01	-3.6203	-12.1391	-11.9961
2.2016	-100.13	-3.819e+01	.8764	1.435e+01	-3.7264	-12.2222	-12.0585
2.4119	-99.71	-3.382e+01	.9041	1.436e+01	-3.8601	-12.3203	-12.1353
2.6421	-99.39	-2.967e+01	.9783	1.470e+01	-3.9218	-12.3551	-12.1358
2.8943	-99.07	-2.626e+01	1.0324	1.578e+01	-3.9687	-12.3951	-12.1416
3.1707	-98.86	-2.298e+01	1.0855	1.703e+01	-4.0505	-12.4390	-12.1470
3.4735	-98.74	-2.000e+01	1.1396	1.783e+01	-4.1050	-12.4833	-12.1474
3.8051	-98.65	-1.727e+01	1.1945	1.807e+01	-4.1587	-12.5301	-12.1444
4.1666	-98.57	-1.476e+01	1.2496	1.832e+01	-4.2207	-12.5848	-12.1428
4.5667	-98.51	-1.246e+01	1.3057	1.857e+01	-4.2878	-12.6467	-12.1408
5.0029	-98.46	-1.034e+01	1.3633	1.874e+01	-4.3619	-12.7162	-12.1375
5.4808	-98.40	-8.384e+00	1.4229	1.885e+01	-4.4460	-12.7956	-12.1339
6.0045	-98.35	-6.580e+00	1.4856	1.892e+01	-4.5419	-12.8866	-12.1297
6.5784	-98.28	-4.913e+00	1.5517	1.906e+01	-4.6517	-12.9910	-12.1249
7.2072	-98.18	-3.367e+00	1.6217	1.918e+01	-4.7813	-13.1115	-12.1198
7.8958	-98.12	-1.944e+00	1.6957	1.905e+01	-4.9215	-13.2473	-12.1112
8.6503	-98.12	-6.310e-01	1.7768	1.909e+01	-5.0753	-13.4005	-12.0963
9.4770	-98.13	5.850e-01	1.8581	1.909e+01	-5.2476	-13.5741	-12.0799
10.3830	-98.18	1.712e+00	1.9391	1.899e+01	-5.4419	-13.7722	-12.0639

n= .8727e-01 ang**-2 or n/nc= 1.371

T	u	Ln(P3D)	S/Nk	B	-P2d=W	F	E
.8642	-95.43	-1.029e+02	.7410	2.026e+01	-3.8064	-12.1349	-12.0777
.9687	-95.63	-9.348e+01	.7436	2.023e+01	-3.8123	-12.1578	-12.0949
1.0612	-95.82	-8.483e+01	.7475	2.018e+01	-3.8211	-12.1836	-12.1144
1.1625	-96.01	-7.689e+01	.7523	2.011e+01	-3.8344	-12.2130	-12.1387
1.2736	-96.20	-6.961e+01	.7540	1.998e+01	-3.8509	-12.2459	-12.1621
1.3952	-96.38	-6.293e+01	.7640	1.981e+01	-3.8715	-12.2825	-12.1898
1.5285	-96.53	-5.678e+01	.7731	1.961e+01	-3.9016	-12.3256	-12.2226
1.6745	-96.62	-5.109e+01	.7838	1.937e+01	-3.9441	-12.3759	-12.2614
1.8344	-96.61	-4.583e+01	.7971	1.908e+01	-4.0039	-12.4351	-12.3075
2.0097	-96.52	-4.096e+01	.8092	1.873e+01	-4.0804	-12.5035	-12.3616
2.2016	-96.30	-3.645e+01	.8396	1.836e+01	-4.1806	-12.5843	-12.4260
2.4119	-95.92	-3.225e+01	.8506	1.798e+01	-4.3090	-12.6800	-12.5009
2.6421	-95.68	-2.847e+01	.8848	1.711e+01	-4.3625	-12.7126	-12.5065
2.8943	-95.25	-2.494e+01	.9541	1.668e+01	-4.4405	-12.7537	-12.5127
3.1707	-94.73	-2.167e+01	1.0357	1.744e+01	-4.5364	-12.8036	-12.5170
3.4735	-94.31	-1.872e+01	1.0951	1.908e+01	-4.6278	-12.8582	-12.5282
3.8051	-94.08	-1.607e+01	1.1521	2.049e+01	-4.7035	-12.9187	-12.5311
4.1686	-93.92	-1.365e+01	1.2084	2.105e+01	-4.7731	-12.9698	-12.5302
4.5667	-93.81	-1.143e+01	1.2545	2.123e+01	-4.8456	-13.0323	-12.5284
5.0029	-93.72	-9.390e+00	1.3214	2.146e+01	-4.9255	-13.1041	-12.5272
5.4808	-93.64	-7.514e+00	1.3797	2.160e+01	-5.0139	-13.1854	-12.5255
6.0045	-93.56	-5.783e+00	1.4408	2.170e+01	-5.1125	-13.2773	-12.5223
6.5784	-93.44	-4.176e+00	1.5051	2.194e+01	-5.2276	-13.3826	-12.5185
7.2072	-93.31	-2.692e+00	1.5733	2.196e+01	-5.3597	-13.5026	-12.5133
7.8958	-93.29	-1.332e+00	1.6480	2.180e+01	-5.4954	-13.6369	-12.5014
8.6503	-93.29	-7.300e-02	1.7276	2.174e+01	-5.6486	-13.7895	-12.4854
9.4770	-93.30	1.094e+00	1.8078	2.171e+01	-5.8212	-13.9636	-12.4687
10.3830	-93.40	2.173e+00	1.8892	2.130e+01	-6.0075	-14.1582	-12.4464

n= .8970e-01 ang**-2 or n/nc= 1.409

T	u	Ln(P3D)	S/Nk	B	-P2d=W	F	E
.8842	-90.21	-9.702e+01	.7378	2.620e+01	-4.4476	-12.5397	-12.4812
.9687	-90.42	-8.810e+01	.7394	2.614e+01	-4.4523	-12.5627	-12.4985
1.0612	-90.63	-7.994e+01	.7415	2.605e+01	-4.4582	-12.5885	-12.5180
1.1625	-90.84	-7.244e+01	.7448	2.592e+01	-4.4687	-12.6177	-12.5400
1.2736	-91.06	-6.557e+01	.7465	2.575e+01	-4.4821	-12.6499	-12.5646
1.3952	-91.29	-5.928e+01	.7539	2.554e+01	-4.4974	-12.6859	-12.5915
1.5285	-91.49	-5.348e+01	.7596	2.527e+01	-4.5211	-12.7275	-12.6233
1.6745	-91.64	-4.812e+01	.7663	2.486e+01	-4.5551	-12.7755	-12.6604
1.8344	-91.72	-4.317e+01	.7750	2.435e+01	-4.6036	-12.8316	-12.7041
2.0097	-91.74	-3.859e+01	.7844	2.370e+01	-4.6666	-12.8980	-12.7546
2.2016	-91.65	-3.434e+01	.8076	2.294e+01	-4.7514	-12.9720	-12.8125
2.4119	-91.41	-3.038e+01	.8235	2.207e+01	-4.8627	-13.0619	-12.8838
2.6421	-91.38	-2.684e+01	.8448	2.139e+01	-4.8921	-13.0864	-12.8882
2.8943	-91.19	-2.353e+01	.8746	2.020e+01	-4.9441	-13.1236	-12.8966
3.1707	-90.73	-2.041e+01	.9237	1.889e+01	-5.0315	-13.1702	-12.9075
3.4735	-90.04	-1.749e+01	1.0301	1.693e+01	-5.1512	-13.2252	-12.9072
3.8051	-89.36	-1.483e+01	1.1024	2.084e+01	-5.2789	-13.2949	-12.9166
4.1686	-88.93	-1.245e+01	1.1638	2.315e+01	-5.3877	-13.3645	-12.9293
4.5667	-88.70	-1.031e+01	1.2221	2.437e+01	-5.4750	-13.4314	-12.9307
5.0029	-88.54	-8.356e+00	1.2795	2.467e+01	-5.5606	-13.5028	-12.9286
5.4808	-88.42	-6.562e+00	1.3377	2.464e+01	-5.6508	-13.5821	-12.9245
6.0045	-88.32	-4.911e+00	1.3978	2.491e+01	-5.7508	-13.6733	-12.9205
6.5784	-88.16	-3.374e+00	1.4610	2.511e+01	-5.8726	-13.7605	-12.9154
7.2072	-88.04	-1.961e+00	1.5280	2.494e+01	-6.0028	-13.9004	-12.9126
7.8958	-88.06	-6.680e-01	1.6034	2.486e+01	-6.1353	-14.0341	-12.8985
8.6503	-88.07	5.300e-01	1.6815	2.474e+01	-6.2667	-14.1671	-12.8823
9.4770	-88.15	1.638e+00	1.7617	2.411e+01	-6.4510	-14.3577	-12.8601
10.3830	-88.37	2.657e+00	1.8441	2.350e+01	-6.6267	-14.5535	-12.8360

*n= .9212e-01 ang**-2 or n/nc= 1.447*

T	u	Ln(P3D)	S/Nk	B	-P2d=W	F	E
.8842	-84.16	-9.018e+01	.7358	3.029e+01	-5.1960	-12.8492	-12.8892
.9687	-84.38	-8.187e+01	.7367	3.021e+01	-5.1987	-12.8722	-12.9064
1.0612	-84.62	-7.427e+01	.7375	3.010e+01	-5.2029	-12.8978	-12.9257
1.1625	-84.86	-6.730e+01	.7398	2.992e+01	-5.2092	-13.0263	-12.9471
1.2736	-85.12	-6.091e+01	.7416	2.972e+01	-5.2166	-13.0577	-12.9707
1.3952	-85.39	-5.506e+01	.7471	2.951e+01	-5.2262	-13.0925	-12.9967
1.5285	-85.66	-4.966e+01	.7503	2.918e+01	-5.2416	-13.1326	-13.0270
1.6745	-85.91	-4.470e+01	.7541	2.871e+01	-5.2640	-13.1780	-13.0617
1.8344	-86.13	-4.012e+01	.7593	2.802e+01	-5.2962	-13.2300	-13.1017
2.0097	-86.31	-3.588e+01	.7664	2.715e+01	-5.3386	-13.2892	-13.1473
2.2016	-86.41	-3.196e+01	.7835	2.613e+01	-5.3986	-13.3565	-13.1995
2.4119	-86.40	-2.830e+01	.8071	2.492e+01	-5.4814	-13.4404	-13.2611
2.6421	-86.44	-2.497e+01	.8223	2.475e+01	-5.5004	-13.4630	-13.2628
2.8943	-86.43	-2.189e+01	.8420	2.427e+01	-5.5269	-13.4906	-13.2661
3.1707	-86.31	-1.902e+01	.8693	2.306e+01	-5.5779	-13.5283	-13.2744
3.4735	-85.87	-1.629e+01	.9105	2.118e+01	-5.6695	-13.5796	-13.2882
3.8051	-85.04	-1.369e+01	1.0022	2.012e+01	-5.8124	-13.6466	-13.2953
4.1686	-84.08	-1.128e+01	1.1074	2.164e+01	-5.9818	-13.7270	-13.3017
4.5667	-83.38	-9.143e+00	1.1752	2.483e+01	-6.1319	-13.8125	-13.3181
5.0029	-83.04	-7.256e+00	1.2364	2.682e+01	-6.2426	-13.8923	-13.3225
5.4808	-82.83	-5.542e+00	1.2959	2.783e+01	-6.3529	-13.9828	-13.3285
6.0045	-82.67	-3.970e+00	1.3563	2.850e+01	-6.4622	-14.0780	-13.3278
6.5784	-82.48	-2.512e+00	1.4196	2.848e+01	-6.5567	-14.1650	-13.3247
7.2072	-82.42	-1.180e+00	1.4864	2.818e+01	-6.7103	-14.3024	-13.3156
7.8958	-82.46	4.000e-02	1.5624	2.788e+01	-6.8382	-14.4342	-13.2978
8.6503	-82.54	1.170e+00	1.6404	2.718e+01	-6.9795	-14.5830	-13.2758
9.4770	-82.81	2.202e+00	1.7230	2.620e+01	-7.1211	-14.7496	-13.2454
10.3830	-83.22	3.153e+00	1.8076	2.466e+01	-7.2589	-14.9253	-13.1963

n= .9454e-01 ang**-2 or n/nc= 1.485

T	u	Ln(P3D)	S/Nk	B	-P2d=W	F	E
.8842	-77.53	-8.267e+01	.7349	3.714e+01	-6.0760	-13.4055	-13.3440
.9687	-77.76	-7.504e+01	.7355	3.706e+01	-6.0767	-13.4285	-13.3611
1.0612	-78.02	-6.806e+01	.7358	3.695e+01	-6.0778	-13.4538	-13.3800
1.1625	-78.30	-6.166e+01	.7375	3.679e+01	-6.0797	-13.4818	-13.4007
1.2736	-78.60	-5.579e+01	.7393	3.661e+01	-6.0820	-13.5125	-13.4235
1.3952	-78.91	-5.041e+01	.7433	3.642e+01	-6.0862	-13.5468	-13.4487
1.5285	-79.24	-4.547e+01	.7453	3.612e+01	-6.0935	-13.5852	-13.4775
1.6745	-79.58	-4.092e+01	.7474	3.570e+01	-6.1040	-13.6279	-13.5096
1.8344	-79.93	-3.674e+01	.7507	3.509e+01	-6.1188	-13.6759	-13.5457
2.0087	-80.28	-3.289e+01	.7559	3.432e+01	-6.1389	-13.7299	-13.5863
2.2016	-80.59	-2.932e+01	.7685	3.337e+01	-6.1734	-13.7924	-13.6325
2.4119	-80.82	-2.599e+01	.7944	3.224e+01	-6.2250	-13.8661	-13.6850
2.6421	-80.90	-2.287e+01	.8062	3.205e+01	-6.2400	-13.8881	-13.6987
2.8943	-80.95	-1.999e+01	.8210	3.180e+01	-6.2605	-13.9132	-13.7185
3.1707	-80.95	-1.733e+01	.8398	3.142e+01	-6.2894	-13.9425	-13.7408
3.4735	-80.86	-1.485e+01	.8656	3.020e+01	-6.3367	-13.9810	-13.7768
3.8051	-80.48	-1.249e+01	.9031	2.778e+01	-6.4272	-14.0360	-13.7111
4.1686	-79.61	-1.021e+01	.9745	2.536e+01	-6.5847	-14.1110	-13.7270
4.5667	-78.39	-8.050e+00	1.1086	2.590e+01	-6.7834	-14.2040	-13.7254
5.0029	-77.42	-6.132e+00	1.1861	2.972e+01	-6.9892	-14.3081	-13.7471
5.4808	-76.95	-4.469e+00	1.2512	3.067e+01	-7.1093	-14.3839	-13.7355
6.0045	-76.63	-2.963e+00	1.3141	3.120e+01	-7.2382	-14.4824	-13.7364
6.5784	-76.46	-1.597e+00	1.3787	3.103e+01	-7.3591	-14.5881	-13.7306
7.2072	-76.46	-3.540e-01	1.4494	3.071e+01	-7.4753	-14.7043	-13.7167
7.8958	-76.61	7.810e-01	1.5274	3.004e+01	-7.5911	-14.8338	-13.6937
8.6503	-76.91	1.820e+00	1.6079	2.876e+01	-7.7071	-14.9781	-13.6631
9.4770	-77.40	2.772e+00	1.6922	2.721e+01	-7.8191	-15.1368	-13.6207
10.3830	-78.11	3.645e+00	1.7779	2.684e+01	-7.9594	-15.3440	-13.5988

n= .9697e-01 ang**-2 or n/nc= 1.523

T	u	Ln(P3D)	S/Nk	B	-P2d=W	F	E
.8842	-70.17	-7.435e+01	.7351	3.532e+01	-7.0055	-13.8127	-13.7497
.9687	-70.42	-6.746e+01	.7356	3.526e+01	-7.0075	-13.8358	-13.7667
1.0612	-70.69	-6.115e+01	.7360	3.517e+01	-7.0060	-13.8611	-13.7854
1.1625	-71.00	-5.538e+01	.7373	3.504e+01	-7.0042	-13.8887	-13.8056
1.2736	-71.33	-5.008e+01	.7391	3.490e+01	-7.0026	-13.9191	-13.8278
1.3952	-71.68	-4.522e+01	.7421	3.474e+01	-7.0022	-13.9529	-13.8525
1.5285	-72.06	-4.076e+01	.7436	3.452e+01	-7.0029	-13.9903	-13.8801
1.6745	-72.47	-3.667e+01	.7453	3.419e+01	-7.0038	-14.0314	-13.9104
1.8344	-72.92	-3.292e+01	.7478	3.375e+01	-7.0053	-14.0765	-13.9435
2.0097	-73.40	-2.946e+01	.7515	3.317e+01	-7.0083	-14.1267	-13.9803
2.2016	-73.87	-2.626e+01	.7610	3.245e+01	-7.0215	-14.1842	-14.0218
2.4119	-74.29	-2.328e+01	.7850	3.156e+01	-7.0474	-14.2515	-14.0679
2.6421	-74.40	-2.041e+01	.7946	3.149e+01	-7.0584	-14.2727	-14.0691
2.8943	-74.49	-1.776e+01	.8063	3.136e+01	-7.0737	-14.2971	-14.0709
3.1707	-74.57	-1.531e+01	.8208	3.113e+01	-7.0956	-14.3263	-14.0739
3.4735	-74.60	-1.305e+01	.8394	3.084e+01	-7.1250	-14.3587	-14.0760
3.8051	-74.54	-1.093e+01	.8643	2.992e+01	-7.1707	-14.3958	-14.0789
4.1686	-74.25	-8.926e+00	.8999	2.745e+01	-7.2558	-14.4563	-14.0825
4.5667	-73.39	-6.956e+00	.9612	2.410e+01	-7.4240	-14.5406	-14.1150
5.0029	-72.03	-5.055e+00	1.1073	2.244e+01	-7.6563	-14.6407	-14.1035
5.4808	-70.89	-3.363e+00	1.2002	3.190e+01	-7.9208	-14.7947	-14.1568
6.0045	-70.44	-1.932e+00	1.2723	3.351e+01	-8.0590	-14.8695	-14.1487
6.5784	-70.31	-9.610e-01	1.3420	3.337e+01	-8.1783	-14.9959	-14.1398
7.2072	-70.40	4.860e-01	1.4184	3.255e+01	-8.2801	-15.1064	-14.1151
7.8958	-70.73	1.526e+00	1.5005	3.108e+01	-8.3705	-15.2258	-14.0789
8.6503	-71.32	2.466e+00	1.5849	2.898e+01	-8.4433	-15.3595	-14.0301
9.4770	-72.22	3.319e+00	1.6730	2.656e+01	-8.4957	-15.4987	-13.9612
10.3830	-73.21	4.117e+00	1.7575	2.087e+01	-8.4808	-15.5796	-13.8101

*n= .9939e-01 ang**-2 or n/nc= 1.561*

T	u	Ln(P3D)	S/Nk	B	-P2d=W	F	E
.8842	-64.05	-6.743e+01	.7360	3.707e+01	-7.8780	-14.2451	-14.1805
.9687	-64.31	-6.115e+01	.7366	3.702e+01	-7.8765	-14.2685	-14.1976
1.0612	-64.60	-5.541e+01	.7375	3.695e+01	-7.8731	-14.2939	-14.2161
1.1625	-64.93	-5.016e+01	.7388	3.686e+01	-7.8687	-14.3215	-14.2362
1.2736	-65.28	-4.533e+01	.7402	3.676e+01	-7.8641	-14.3520	-14.2583
1.3952	-65.66	-4.091e+01	.7427	3.664e+01	-7.8601	-14.3857	-14.2827
1.5285	-66.07	-3.685e+01	.7443	3.647e+01	-7.8560	-14.4227	-14.3097
1.6745	-66.53	-3.313e+01	.7462	3.626e+01	-7.8502	-14.4630	-14.3398
1.8344	-67.05	-2.972e+01	.7487	3.596e+01	-7.8425	-14.5068	-14.3703
2.0097	-67.61	-2.658e+01	.7512	3.559e+01	-7.8348	-14.5551	-14.4050
2.2016	-68.20	-2.368e+01	.7589	3.507e+01	-7.8317	-14.6087	-14.4436
2.4119	-68.76	-2.099e+01	.7794	3.442e+01	-7.8386	-14.6729	-14.4861
2.6421	-68.86	-1.832e+01	.7874	3.450e+01	-7.8503	-14.6946	-14.4878
2.8943	-68.96	-1.585e+01	.7970	3.458e+01	-7.8653	-14.7190	-14.4898
3.1707	-69.04	-1.357e+01	.8088	3.461e+01	-7.8850	-14.7472	-14.4923
3.4735	-69.11	-1.147e+01	.8234	3.453e+01	-7.9113	-14.7798	-14.4955
3.8051	-69.13	-9.509e+00	.8422	3.436e+01	-7.9467	-14.8173	-14.4998
4.1686	-69.07	-7.682e+00	.8671	3.390e+01	-7.9980	-14.8626	-14.5033
4.5667	-68.81	-5.953e+00	.9025	3.112e+01	-8.0823	-14.9212	-14.5116
5.0029	-68.22	-4.294e+00	.9752	2.694e+01	-8.2285	-15.0101	-14.5252
5.4808	-65.60	-2.398e+00	1.1104	2.364e+01	-8.6044	-15.1241	-14.5193
6.0045	-64.26	-9.060e-01	1.2268	3.315e+01	-8.8988	-15.2871	-14.5550
6.5784	-64.13	2.780e-01	1.3113	3.365e+01	-9.0063	-15.3823	-14.5250
7.2072	-64.43	1.316e+00	1.3970	3.241e+01	-9.0669	-15.4904	-14.4896
7.8958	-65.14	2.234e+00	1.4863	2.976e+01	-9.1248	-15.5989	-14.4325
8.6503	-66.17	3.062e+00	1.5744	2.756e+01	-9.1431	-15.7197	-14.3661
9.4770	-67.41	3.827e+00	1.6628	2.689e+01	-9.1783	-15.8777	-14.3115
10.3830	-68.71	4.550e+00	1.7517	4.003e+01	-9.4456	-16.2749	-14.4672

n= .1018 ang**-2 or n/nc= 1.599

T	u	Ln(P3D)	S/Nk	B	-P2d=W	F	E
.8842	-56.62	-5.903e+01	.7376	4.691e+01	-8.8666	-14.6528	-14.5864
.9687	-56.89	-5.349e+01	.7384	4.686e+01	-8.8850	-14.6764	-14.6036
1.0612	-57.19	-4.843e+01	.7396	4.681e+01	-8.8801	-14.7022	-14.6223
1.1625	-57.53	-4.379e+01	.7411	4.677e+01	-8.8741	-14.7302	-14.6425
1.2736	-57.89	-3.953e+01	.7423	4.671e+01	-8.8676	-14.7609	-14.6647
1.3952	-58.29	-3.563e+01	.7444	4.664e+01	-8.8613	-14.7950	-14.6892
1.5285	-58.72	-3.204e+01	.7465	4.655e+01	-8.8542	-14.8322	-14.7160
1.6745	-59.21	-2.876e+01	.7487	4.645e+01	-8.8446	-14.8726	-14.7450
1.8344	-59.77	-2.575e+01	.7517	4.635e+01	-8.8321	-14.9165	-14.7761
2.0087	-60.38	-2.298e+01	.7536	4.620e+01	-8.8182	-14.9645	-14.8103
2.2016	-61.02	-2.043e+01	.7599	4.595e+01	-8.8059	-15.0181	-14.8478
2.4119	-61.68	-1.806e+01	.7695	4.558e+01	-8.8004	-15.0785	-14.8906
2.6421	-61.76	-1.564e+01	.7764	4.544e+01	-8.8118	-15.1008	-14.8920
2.8943	-61.87	-1.340e+01	.7846	4.527e+01	-8.8260	-15.1248	-14.8935
3.1707	-61.97	-1.134e+01	.7945	4.505e+01	-8.8443	-15.1525	-14.8960
3.4735	-62.05	-9.434e+00	.8068	4.474e+01	-8.8662	-15.1851	-14.8978
3.8051	-62.12	-7.668e+00	.8222	4.426e+01	-8.8943	-15.2182	-14.8998
4.1686	-62.16	-6.025e+00	.8421	4.312e+01	-8.9294	-15.2573	-14.9000
4.5667	-62.22	-4.510e+00	.8690	4.211e+01	-8.9705	-15.3045	-14.9005
5.0029	-62.08	-3.065e+00	.9079	4.011e+01	-9.0423	-15.3615	-14.8991
5.4808	-61.66	-1.680e+00	.8769	2.877e+01	-9.2036	-15.4809	-14.9359
6.0045	-59.24	-6.800e-02	1.1416	2.295e+01	-9.5734	-15.6043	-14.9065
6.5784	-58.54	1.128e+00	1.2842	3.107e+01	-9.7958	-15.7550	-14.8950
7.2072	-59.10	2.055e+00	1.3890	2.879e+01	-9.8268	-15.8434	-14.8243
7.8958	-60.26	2.851e+00	1.4855	2.675e+01	-9.8055	-15.9403	-14.7462
8.6503	-61.62	3.588e+00	1.5761	2.490e+01	-9.7747	-16.0474	-14.6594
9.4770	-63.13	4.278e+00	1.6649	1.958e+01	-9.6820	-16.1092	-14.5029

n= .1042 ang**-2 or n/nc= 1.637

T	u	Ln(P3D)	S/Nk	B	-P2d=W	F	E
.7367	-48.41	-6.116e+01	.7383	4.620e+01	-9.9940	-15.0384	-14.9817
.8071	-48.64	-5.548e+01	.7390	4.616e+01	-9.9903	-15.0584	-14.9962
.8842	-48.89	-5.028e+01	.7397	4.612e+01	-9.9861	-15.0803	-15.0122
.9687	-49.17	-4.552e+01	.7407	4.608e+01	-9.9812	-15.1043	-15.0296
1.0612	-49.47	-4.115e+01	.7422	4.607e+01	-9.9757	-15.1305	-15.0485
1.1625	-49.81	-3.715e+01	.7437	4.607e+01	-9.9691	-15.1592	-15.0691
1.2736	-50.18	-3.348e+01	.7449	4.606e+01	-9.9617	-15.1906	-15.0917
1.3952	-50.58	-3.011e+01	.7467	4.604e+01	-9.9544	-15.2252	-15.1167
1.5285	-51.03	-2.701e+01	.7492	4.603e+01	-9.9459	-15.2631	-15.1438
1.6745	-51.52	-2.416e+01	.7517	4.607e+01	-9.9356	-15.3044	-15.1732
1.8344	-52.08	-2.156e+01	.7553	4.618e+01	-9.9229	-15.3493	-15.2049
2.0097	-52.69	-1.916e+01	.7568	4.627e+01	-9.9080	-15.3983	-15.2399
2.2016	-53.36	-1.694e+01	.7625	4.631e+01	-9.8928	-15.4525	-15.2776
2.4119	-54.05	-1.489e+01	.7637	4.624e+01	-9.8819	-15.5138	-15.3219
2.6421	-54.19	-1.276e+01	.7698	4.600e+01	-9.8891	-15.5353	-15.3233
2.8943	-54.33	-1.080e+01	.7771	4.566e+01	-9.8975	-15.5590	-15.3247
3.1707	-54.49	-8.984e+00	.7860	4.516e+01	-9.9078	-15.5857	-15.3260
3.4735	-54.67	-7.307e+00	.7970	4.447e+01	-9.9188	-15.6149	-15.3265
3.8051	-54.86	-5.759e+00	.8111	4.355e+01	-9.9311	-15.6473	-15.3257
4.1686	-55.12	-4.337e+00	.8293	4.256e+01	-9.9411	-15.6849	-15.3247
4.5667	-55.33	-3.002e+00	.8535	4.110e+01	-9.9583	-15.7240	-15.3179
5.0029	-55.58	-1.767e+00	.8865	3.839e+01	-9.9803	-15.7719	-15.3097
5.4808	-55.87	-6.230e-01	.9330	3.642e+01	-9.9795	-15.8008	-15.2680
6.0045	-55.88	4.920e-01	1.0614	2.361e+01	-10.0902	-15.9133	-15.2492
6.5784	-54.05	1.810e+00	1.2333	2.141e+01	-10.4134	-16.0455	-15.2001
7.2072	-54.81	2.650e+00	1.3924	2.347e+01	-10.4354	-16.1465	-15.1008
7.8958	-56.21	3.365e+00	1.4976	2.223e+01	-10.3764	-16.2329	-15.0008
8.6503	-57.84	4.025e+00	1.5860	2.105e+01	-10.3100	-16.3369	-14.9073
9.4770	-59.65	4.646e+00	1.6760	3.251e+01	-10.4152	-16.6303	-14.9752

n= .1067 ang**-2 or n/nc= 1.676

T	u	Ln(P3D)	S/Nk	B	-P2d=W	F	E
.5115	-40.24	-7.504e+01	.7390	4.679e+01	-11.1106	-15.4046	-15.3643
.5604	-40.40	-6.823e+01	.7392	4.677e+01	-11.1076	-15.4188	-15.3746
.6139	-40.58	-6.201e+01	.7396	4.674e+01	-11.1043	-15.4343	-15.3858
.6725	-40.77	-5.631e+01	.7402	4.672e+01	-11.1006	-15.4512	-15.3981
.7367	-40.99	-5.108e+01	.7408	4.668e+01	-11.0965	-15.4698	-15.4116
.8071	-41.22	-4.629e+01	.7415	4.665e+01	-11.0918	-15.4902	-15.4264
.8842	-41.48	-4.190e+01	.7423	4.661e+01	-11.0867	-15.5125	-15.4425
.9687	-41.76	-3.787e+01	.7433	4.658e+01	-11.0810	-15.5369	-15.4601
1.0612	-42.07	-3.417e+01	.7449	4.660e+01	-11.0755	-15.5641	-15.4797
1.1625	-42.40	-3.078e+01	.7464	4.667e+01	-11.0699	-15.5939	-15.5013
1.2736	-42.77	-2.766e+01	.7475	4.675e+01	-11.0634	-15.6265	-15.5250
1.3952	-43.17	-2.479e+01	.7492	4.680e+01	-11.0564	-15.6624	-15.5509
1.5285	-43.60	-2.215e+01	.7518	4.692e+01	-11.0493	-15.7020	-15.5794
1.6745	-44.08	-1.972e+01	.7543	4.719e+01	-11.0429	-15.7460	-15.6112
1.8344	-44.59	-1.747e+01	.7579	4.763e+01	-11.0371	-15.7948	-15.6464
2.0097	-45.16	-1.541e+01	.7596	4.814e+01	-11.0298	-15.8480	-15.6851
2.2016	-45.78	-1.351e+01	.7649	4.863e+01	-11.0213	-15.9064	-15.7267
2.4119	-46.46	-1.174e+01	.7614	4.903e+01	-11.0146	-15.9713	-15.7754
2.6421	-46.65	-9.912e+00	.7674	4.823e+01	-11.0105	-15.9886	-15.7723
2.8943	-46.89	-8.227e+00	.7748	4.720e+01	-11.0036	-16.0069	-15.7676
3.1707	-47.17	-6.676e+00	.7839	4.591e+01	-10.9935	-16.0270	-15.7617
3.4735	-47.52	-5.250e+00	.7958	4.422e+01	-10.9766	-16.0469	-15.7519
3.8051	-47.93	-3.936e+00	.8114	4.224e+01	-10.9547	-16.0680	-15.7386
4.1686	-48.36	-2.715e+00	.8313	4.004e+01	-10.9287	-16.0887	-15.7190
4.5667	-48.95	-1.606e+00	.8573	3.702e+01	-10.8909	-16.1142	-15.6935
5.0029	-49.67	-5.860e-01	.8913	3.404e+01	-10.8415	-16.1414	-15.6656
5.4808	-50.49	3.570e-01	.9342	3.055e+01	-10.7936	-16.1814	-15.6351
6.0045	-51.31	1.254e+00	1.0062	2.843e+01	-10.7209	-16.1956	-15.5509
6.5784	-51.30	2.229e+00	1.1947	1.611e+01	-10.8403	-16.3136	-15.4750
7.2072	-51.34	3.131e+00	1.3941	1.971e+01	-10.9443	-16.4227	-15.3506
7.8958	-52.92	3.781e+00	1.5121	1.910e+01	-10.8636	-16.5100	-15.2361

8.6503 -54.67 4.392e+00 1.6012 1.848e+01 -10.7769 -16.6097 -15.1318

n= .1091 ang**-2 or n/nc= 1.714

T	u	Ln(P3D)	S/Nk	B	-P2d=W	F	E
.3551	-32.93	-9.001e+01	.7406	4.024e+01	-12.1008	-15.6938	-15.6651
.3890	-33.05	-8.200e+01	.7408	4.022e+01	-12.0985	-15.7038	-15.6724
.4262	-33.17	-7.464e+01	.7409	4.022e+01	-12.0959	-15.7148	-15.6803
.4669	-33.31	-6.792e+01	.7411	4.021e+01	-12.0933	-15.7269	-15.6891
.5115	-33.45	-6.176e+01	.7415	4.020e+01	-12.0904	-15.7401	-15.6987
.5604	-33.62	-5.612e+01	.7418	4.019e+01	-12.0869	-15.7545	-15.7092
.6139	-33.80	-5.096e+01	.7422	4.018e+01	-12.0831	-15.7704	-15.7207
.6725	-33.99	-4.622e+01	.7430	4.016e+01	-12.0791	-15.7877	-15.7332
.7367	-34.21	-4.188e+01	.7435	4.014e+01	-12.0743	-15.8067	-15.7470
.8071	-34.45	-3.790e+01	.7443	4.013e+01	-12.0691	-15.8275	-15.7620
.8842	-34.71	-3.425e+01	.7451	4.011e+01	-12.0634	-15.8503	-15.7785
.9687	-35.00	-3.089e+01	.7459	4.010e+01	-12.0572	-15.8753	-15.7965
1.0612	-35.30	-2.780e+01	.7468	4.012e+01	-12.0522	-15.9032	-15.8167
1.1625	-35.62	-2.495e+01	.7483	4.017e+01	-12.0481	-15.9341	-15.8392
1.2736	-35.97	-2.232e+01	.7495	4.022e+01	-12.0432	-15.9679	-15.8637
1.3952	-36.37	-1.991e+01	.7511	4.027e+01	-12.0374	-16.0049	-15.8905
1.5285	-36.78	-1.769e+01	.7530	4.036e+01	-12.0330	-16.0459	-15.9203
1.6745	-37.21	-1.562e+01	.7549	4.054e+01	-12.0321	-16.0919	-15.9540
1.8344	-37.65	-1.369e+01	.7580	4.084e+01	-12.0354	-16.1433	-15.9916
2.0097	-38.14	-1.192e+01	.7603	4.118e+01	-12.0384	-16.1996	-16.0329
2.2016	-38.69	-1.028e+01	.7652	4.152e+01	-12.0403	-16.2611	-16.0774
2.4119	-39.29	-8.771e+00	.7665	4.183e+01	-12.0425	-16.3289	-16.1272
2.6421	-39.67	-7.269e+00	.7750	4.035e+01	-12.0126	-16.3409	-16.1175
2.8943	-40.13	-5.891e+00	.7856	3.870e+01	-11.9749	-16.3530	-16.1050
3.1707	-40.67	-4.624e+00	.7986	3.681e+01	-11.9285	-16.3655	-16.0892
3.4735	-41.32	-3.466e+00	.8144	3.483e+01	-11.8690	-16.3773	-16.0687
3.8051	-42.08	-2.400e+00	.8335	3.267e+01	-11.7989	-16.3895	-16.0435
4.1686	-42.96	-1.420e+00	.8566	3.012e+01	-11.7165	-16.4038	-16.0142
4.5667	-43.98	-5.160e-01	.8860	2.806e+01	-11.6187	-16.4167	-15.9752
5.0029	-45.09	3.290e-01	.9184	2.612e+01	-11.5134	-16.4329	-15.9316
5.4808	-46.31	1.122e+00	.9593	2.438e+01	-11.3986	-16.4504	-15.8768

6.0045	-47.56	1.878e+00	1.0195	2.190e+01	-11.2914	-16.4604	-15.6125
6.5784	-48.66	2.630e+00	1.1788	1.813e+01	-11.2164	-16.5249	-15.6789
7.2072	-48.59	3.513e+00	1.3669	1.669e+01	-11.3478	-16.6494	-15.5573
7.8958	-50.19	4.125e+00	1.5313	1.658e+01	-11.2601	-16.7364	-15.4172
8.6503	-52.06	4.694e+00	1.6212	1.587e+01	-11.1590	-16.8382	-15.3082

n= .1115 ang**-2 or n/nc= 1.751

T	u	Ln(P3D)	S/Nk	B	-P2d=W	F	E
2.4119	-34.34	-6.719e+00	.7981	3.105e+01	-12.8389	-16.6676	-16.4530
2.6421	-34.94	-5.478e+00	.8098	2.951e+01	-12.7751	-16.6708	-16.4323
2.8943	-35.62	-4.333e+00	.8231	2.795e+01	-12.7016	-16.6734	-16.4078
3.1707	-36.42	-3.285e+00	.8384	2.615e+01	-12.6138	-16.6751	-16.3787
3.4735	-37.31	-2.311e+00	.8558	2.471e+01	-12.5160	-16.6760	-16.3446
3.8051	-38.31	-1.409e+00	.8758	2.325e+01	-12.4054	-16.6765	-16.3049
4.1686	-39.40	-5.660e-01	.8993	2.233e+01	-12.2824	-16.6756	-16.2576
4.5667	-40.59	2.260e-01	.9278	2.154e+01	-12.1540	-16.6797	-16.2072
5.0029	-41.88	9.710e-01	.9586	2.065e+01	-12.0182	-16.6877	-16.1530
5.4808	-43.26	1.677e+00	.9969	1.972e+01	-11.8788	-16.7028	-16.0936
6.0045	-44.71	2.353e+00	1.0502	1.899e+01	-11.7267	-16.7118	-16.0087
6.5784	-46.12	3.015e+00	1.1789	1.752e+01	-11.6116	-16.7544	-15.8897
7.2072	-46.40	3.816e+00	1.3880	1.463e+01	-11.6880	-16.8621	-15.7467
7.8958	-48.05	4.398e+00	1.5511	1.424e+01	-11.5951	-16.9534	-15.5879
8.6503	-49.99	4.933e+00	0.0000	1.376e+01	-11.4812	-17.0549	-17.0549
10.3830	0.00	0.000e+00	0.0000	3.178e+01	-18.5682	-18.5682	-18.5682